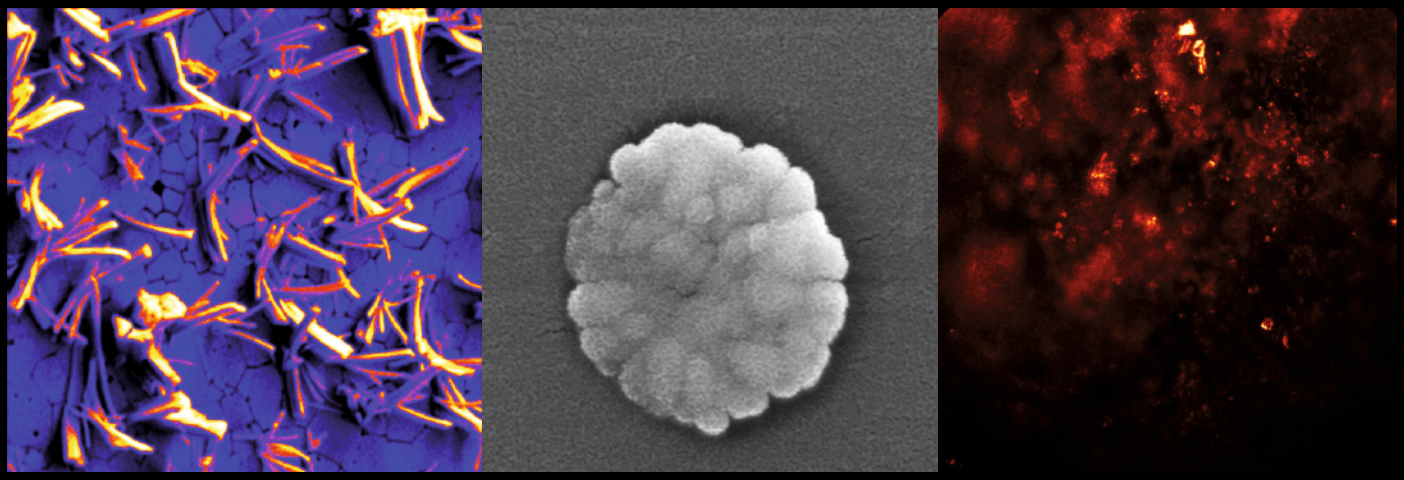

KIT SCIENTIFIC REPORTS 7600

Annual Report 2010

Institute for Nuclear Waste Disposal
Institut für Nukleare Entsorgung

H. Geckeis, T. Stumpf (eds.)

KIT Scientific Publishing

H. Geckeis, T. Stumpf (eds.)

Annual Report 2010

Institute for Nuclear Waste Disposal
Institut für Nukleare Entsorgung

Karlsruhe Institute of Technology

KIT SCIENTIFIC REPORTS 7600

Cover illustration (from left to right):
SEM image of a polished UO2 surface with studtite crystals, uranyl peroxide hydrate, grown as secondary phase in water under γ-irradtiation (acquired energy dose 1.5 MGy). Artificial view with pseudocolors.
SEM image of a spherical crystalline molybdate particle formed on the surface of a simulated nuclear waste glass containing 5.5 wt% MoO_3.
Eu(III) fluorescence of calcite and clay containing sample after excitation at 394 nm.

Annual Report 2010

Institute for Nuclear Waste Disposal
Institut für Nukleare Entsorgung

H. Geckeis
T. Stumpf
(eds.)

KIT Scientific Publishing

Report-Nr. KIT-SR 7600

Impressum

Karlsruher Institut für Technologie (KIT)
KIT Scientific Publishing
Straße am Forum 2
D-76131 Karlsruhe
www.ksp.kit.edu

KIT – Universität des Landes Baden-Württemberg und nationales
Forschungszentrum in der Helmholtz-Gemeinschaft

KIT Scientific Publishing 2011
Print on Demand

ISSN 1869-9669

Table of contents

1 Introduction to the Institut f r Nukleare Entsorgung

R&D at the Institut für Nukleare Entsorgung, INE, (**Institute for Nuclear Waste Disposal**) deals with the long-term safety assessment for final disposal of nuclear waste, the separation of minor actinides from high-level waste (partitioning) and the immobilization of high-level liquid waste by vitrification. All activities are integrated into the programme Nuclear Safety Research within the Energy Center of the Karlsruhe Institute of Technology, KIT. INE contributes to the German provident research for the safety of nuclear waste disposal, which is in the responsibility of the federal government.

Based on the scheduled operation times for nuclear power plants in Germany, about 17.000 tons of spent nuclear fuel will be generated. About 6200 tons have been shipped to France and UK before 2005 for reprocessing to recover plutonium and uranium. Therefore two types of high level, heat producing radioactive waste have to be disposed of safely, namely spent fuel and vitrified high level waste from reprocessing.

There is an international consensus that storage in deep geological formations is the safest way to dispose of high level heat producing radioactive waste. It ensures the effective protection of the population and the biosphere against radiation exposure over very long periods of time. The isolation and immobilization of nuclear waste in a repository is accomplished by the appropriate combination of redundant barriers (multi-barrier system).

INE research focuses on the geochemical aspects of nuclear waste disposal. Special emphasis is given to actinides and long-lived fission products because of their significant contribution to the radiotoxicity for long periods of time.

Relevant scenarios for the geological long-term behaviour of nuclear waste disposal have to take into account possible radionuclide transport via the groundwater pathway. Thermomechanical studies are performed at INE in order to describe the evolution of the repository after closure. The possible groundwater access to emplacement caverns is assumed to cause waste form corrosion. Radionuclide mobility is then determined by the various geochemical reactions in the complex aquatic systems: i.e. dissolution of the nuclear waste form (high-level waste glass, spent fuel), radiolysis phenomena, redox reactions, complexation with inorganic and organic ligands, colloid formation, surface sorption reactions at mineral surfaces, precipitation of pure solid phases and solid solutions. Prediction and quantification of all these processes require availability of thermodynamic data and a comprehensive understanding of these processes at a molecular scale.

Relevant radionuclide concentrations in natural groundwater lie in the nano-molar range, which is infinitesimally small in relation to the main groundwater components. Quantification of chemical reactions occurring in these systems calls for the application and development of new sophisticated methods and experimental approaches, which provide insight into the chemical speciation of radionuclides at very low concentrations. Innovative laser and X-ray spectroscopic techniques are continuously developed and applied. A theoretical group performs quantum chemical calculations on actinide complexes as an additional tool to support experimental results.

The long term safety assessment of a repository for nuclear waste has to be demonstrated by application of modelling tools on real natural systems over geological time scales. The experimental research programme at INE aims to acquire fundamental knowledge on model subsystems and to derive model parameters. Geochemical models and thermodynamic databases are developed as a basis for the description of radionuclide geochemical behaviour in complex natural aquatic systems. The prediction of radionuclide migration in the geosphere necessitates a coupled modelling of geochemistry and transport. Transferability and applicability of model predictions are examined by designing dedicated laboratory experiments, field studies in underground laboratories and by studying natural analogue systems. This strategy allows to identify and to analyse key uncertainties related to the accuracy and the relevance of the developed models.

The Partitioning & Transmutation (P&T) strategy is pursued in many international research programmes. The objective is to reduce the time horizon for safe disposal of high level waste from some hundred thousand to less than thousand years by significant reduction of the radiotoxicity and heat inventory. The aim of R&D at INE in P&T is to develop efficient processes for long-lived minor actinide separation from high active nuclear waste for subsequent transmutation into short-lived or stable fission products. INE develops highly selective extracting agents and performs experiments to derive kinetic and thermodynamic data for the extraction reaction. R&D spans theoretical and experimental work dedicated to a mechanistic understanding of extraction ligand selectivity on a molecular scale, to development of extraction processes.

Within the third R&D topic at INE, the vitrification of high level waste, INE contributes to the decommissioning of nuclear facilities. The core process technology for the Vitrification Plant (VEK) on the site of the former Karlsruhe Reprocessing Plant (WAK) located at the KIT Campus North has been developed by INE. Design of core process components, including the glass melting furnace and the off-gas cleaning system, comprises this development. Moreover, INE was involved in functional testing of major process systems, preparation of qualification records and certification of product quality, as well as in the performance of the cold test operation. INE also played a leading role in hot operation of the VEK plant which started in September 2009 and was completed in November 2010.

INE laboratories are equipped with the entire infrastructure necessary to perform radionuclide/actinide research, including hot cells, alpha glove boxes, inert gas alpha glove boxes and radionuclide laboratories. State-of-the-art analytical devices and methods are applied for analysis and speciation of radionuclides and radioactive materials. α–, β–, γ–spectroscopy instruments exist for the sensitive detection and analysis of radionuclides. Trace element and isotope analysis is made by instrumental analytical techniques such as X-ray fluorescence spectrometry (XRF), atomic absorption spectrometry (AAS), ICP-atomic emission spectrometry (ICP-AES) and ICP-mass spectrometry (Quadrupole-ICP-MS and high resolution ICP-MS). Surface sensitive analysis and characterisation of solid samples is done by X-ray diffraction (XRD), scanning electron microscopy (SEM), photoelectron spectroscopy (XPS), atomic force microscopy (AFM) and laser-ablation coupled with ICP-MS. INE scientists also have direct access to a TEM instrument at a nearby institute (Institute for Applied Science) on the KIT Campus North site. Laser spectroscopic techniques are developed and applied for sensitive actinide and fission product speciation such as time-resolved laser fluorescence spectroscopy (TRLFS), laser photoacoustic spectroscopy (LPAS), sum frequency infrared spectroscopy, laser-induced breakdown detection (LIBD) and Raman spectroscopy. Recently a tunable optical parametric oscillator (OPO) laser system with TRLFS-detection was installed for high resolution spectroscopy at liquid helium temperature. Speciation of actinide-ion complexation and polymerization products in solution is facilitated by nano electrospray time-of-flight mass-spectrometry (ESI TOF MS). Structural insight into actinide species is obtained by extended X-ray fine structure (EXAFS) spectroscopy at the INE-Beamline at the Karlsruhe synchrotron source ANKA. The INE-Beamline, in the direct vicinity of INE hot laboratories and in combination with the other analytic methods, represents a world-wide unique experimental and analytic infrastructure, which both profits from and contributes to INE's expertise in the field of chemistry and spectroscopy of the actinides. A new 400 MHz-NMR spectrometer was installed and adapted to measuring radioactive liquid samples. The first NMR-spectrum of an Pu(III)-complex was measured in October 2010.

Quantum chemical calculations are performed on INE's computing cluster, which is equipped with 17 nodes and 76 processors.

Additional facilities at INE include a non-radioactive vitrification test facility (1:1 mock-up of the VEK plant) used to investigate and to simulate vitrification processes for hot plants. The INE CAD workstations enable construction and planning of hardware components, process layout and flowsheets. The institute workshop is equipped with modern machine tools to manufacture components for specific experimental and analytical devices in hot laboratories.

2 Highlights

Contributions collected in this report provide a representative overview of the scientific outcome of INE research activities in 2010. The structure of the report follows widely the organisation of the institute according to research topics: (1) basic research towards understanding geochemical reactions of radionuclides on a molecular scale and (2) applied studies on radionuclide retention in multi-barrier system under 'real' repository conditions. Both these topics are strongly linked together and cover a broad range of chemical aspects for long term safety assessment of a repository for nuclear waste. The third research topic (3) supports these two areas by developing speciation methods and analytical techniques in order to obtain detailed chemical information on radionuclide speciation and structures. In addition to spectroscopic methods, quantum chemical calculations are increasingly implemented as an additional tool to gain insight into the molecular and electronic structure of radionuclide species. These experimental and theoretical tools are applied to geochemical studies and also to achieve mechanistic understanding of solvent extraction processes developed for separation of minor actinides from fission lanthanides, which is indispensible for P&T.

Research dedicated to the immobilisation of high-level radioactive liquid waste is much more technically and application oriented. In this field, a vitrification plant on the WAK site using INE technology was in hot operation from September 2009 to November 2010. In parallel, the Vitrification Project China (VPC) based on KIT-INE's technology was launched between Chinese organizations and a German consortium.

Important achievements of the research activities in 2010 are listed below:

In 2010, several research activities were focused upon the **aquatic redox-chemistry of actinides and long-lived fission products**. The solubility and speciation of actinides depend strongly on redox conditions and accordingly have to be analysed within this context to allow for quantitative predictions of solubility limits. Our work on Pu, Np and Tc has contributed to a better understanding of redox transformation processes and to constraining the stability fields of dominant oxidation states. Studies on Pu and Tc interaction with mineral surfaces yield new insight into relevant mechanistic and kinetic processes under reducing conditions towards improved schemes for thermodynamic modeling. Further studies on Pu and Np chemistry focus upon oxidising conditions of penta- or hexa-valent redox states, similarly aim at a **comprehensive thermodynamic description**. Experimental studies were complemented by the final report on the joint ReCosy Intercomparison Exercise (EU FP project, coordinated by KIT-INE), summarizing the present state-of-art in redox determination methods in the context of nuclear waste disposal. (Chapter 5.1)

Currently, there is a considerable lack of knowledge with respect to the alteration of actinide bearing cement products in saline solutions. Thus we studied the **alteration of hydrated ordinary portland cement (OPC) in chloride-rich brine** using batch-type experiments and by means of thermodynamic equilibrium calculations. The results of this study are important in particular for the safety assessment of final disposal of low/intermediate level active waste in rock salt. Since most experiments were conducted with high cement to brine ratios, reflecting disposal conditions, aqueous phase analyses were rather challenging. The calculated solution composition is in good agreement with the experimental results for a wide range of cement / brine ratios (0.01 to 1.0 kg cement / L solution). **Am(III) sorption in the cement / brine systems** was quantified from experiments with equilibrated solutions and cement corrosion products. Relatively high values of apparent sorption coefficients, R_s, for weakly alkaline ($3000 < R_s < 6000$ ml g^{-1}) and highly alkaline conditions ($R_s = 10000$ ml g^{-1}) demonstrate strong Am(III) retention by cement corrosion products (Chapter 6.2).

The focus of research within the **international Colloid Formation and Migration (CFM) project** is to understand formation of the bentonite gel layer, erosion of bentonite buffer/backfill material, generation of bentonite colloids and their impact on radionuclide transport in a shear zone under near-natural flow conditions. To overcome the high hydraulic gradient towards the tunnel surface in the underground laboratory, a sophisticated mega-packer system counteracting the hydraulic heads of the shear zone was constructed and installed at the end of 2009. Consecutively performed **colloid migration experiments** in 2010 **under near-natural flow conditions** with increasing residence time **demonstrate the slow bentonite colloid RN sorption reversibility,** especially for the tetravalent elements. Furthermore, these experiments demonstrated the sensitivity of colloid transport on flow path geometry/heterogeneity of the fracture/shear zone lending predictions based on correlations such as e.g. colloid recovery

versus residence time a very high uncertainty (Chapter 6.3).

The separation of americium and curium from the chemically similar fission lanthanides is essential to the **partitioning & transmutation strategy.** BTP and BTBP directly and selectively extract americium and curium from aqueous nitric acid solutions, as required for a possible industrial separation process. However, neither BTP nor BTBP are fully suitable for an industrial application, thus requiring further optimisation.

A **sulphonated hydrophilic BTP, SO_3-Ph-BTP**, was synthesised and successfully tested for the complexation of trivalent actinides in acidic solutions. SO_3-Ph-BTP can be used to selectively strip trivalent actinides from an organic solvent phase containing trivalent actinides and lanthanides. In contrast to other compounds previously applied (such as, e.g., DTPA), SO_3-Ph-BTP does not require any buffers or salting out agents. In combination with TODGA (an extracting agent co-extracting trivalent actinides and lanthanides), **SO_3-Ph-BTP has a selectivity for Eu(III) over Am(III) of up to 1000**. SO_3-Ph-BTP has triggered development of greatly improved actinide separation processes in the framework of the ACSEPT project (Chapter 7).

Based on **KIT-INE s vitrification technology,** the VEK vitrification plant was constructed to immobilize approximately 60 m^3 of HLLW with a total activity of $7.7 \cdot 10^{17}$ Bq stored on site of the former WAK pilot reprocessing plant. In September 2009 hot operation commenced with a one week hot test with reduced radioactivity level. Start-up of routine processing of the stored HLLW immediately followed the initial radioactive test and was completed in June 2010. Within a considerably short nine months operation **VEK immobili ed the existing 56 m^3 of highly radioactive waste solution, containing more than 400 kg of noble metals,** in 50 metric tons of glass. The glass was poured into 123 canisters, which all met the approved set of quality parameters. Operation could be maintained at a **time availability of 97 %**. Difficulties arising from melter off-gas pipe clogging and a single noble metals-related event were solved without severe impact on the time availability. During a rinsing program to reduce the level of activity remaining in the HLLW storage tanks and in the VEK installations following vitrification operation, 17 additional canisters have been produced. Emptying and shut down of the melter in November 2010 marks the ending of the rinsing program. Transportation of the 140 glass canisters inside five CASTOR casks from WAK to the intermediate storage facility ZLN near Lubmin took place in February 2011 (Chapter 8.1).

In summer 2009 the **Vitrification Project China** (VPC) contract between the Chinese organizations involved and the German industry consortium concerning construction of a vitrification plant on the basis of KIT-INE's vitrification technology was signed. In 2010 main project activities were dedicated to elaboration of the **basic design of the vitrification plant** and the intermediate storage building for waste glass canisters. The scope of the basic design carried out by INE covered the core process (HLLW reception, HLLW and glass frit feeding, glass melting, electric power supply for the melter including melter instrumentation and control and wet off-gas treatment system). Two editions of the basic design documentation (BDD) were delivered to China by December 2010 according to the project schedule (Chapter 8.2).

The **INE-Beamline for actinide research** at the KIT synchrotron source ANKA celebrated its five years of official operation in October 2010, marking successful application of this dedicated instrumentation for X-ray spectroscopic characterization of actinide samples and other radioactive materials. R&D work at the beamline focuses on various aspects of nuclear waste disposal within INE's mission to provide the scientific basis for assessing long-term safety of a final high level waste repository. The INE-Beamline is accessible for the actinide and radiochemistry community through the ANKA proposal system and the European Union Integrated Infrastructure Initiative ACTINET-I3. The modular beamline design enables sufficient flexibility to adapt sample environments and detection systems to many specific scientific questions and **in 2010 the portfolio available at the beamline has been increased**. Well established bulk techniques such as XAFS spectroscopy in transmission and fluorescence mode have been augmented by advanced methods including (confocal) XAFS/XRF with a microfocused beam or a combination of μ-XAFS and μ-XRD. Additional instrumentation for high energy resolution X-ray emission (HRXES) spectroscopy has been developed and initial results have already been obtained (Chapter 9.1).

A **high energy resolution X-ray absorption near-edge structure (XANES) spectroscopy study on U^{4+} (UO_2), U^{5+} ($[UO_2Py_5][KI_2Py_2]$), and U^{6+} $[UO_2(NO_3)_2(H_2O)_6]$** has been performed using high resolution X-ray emission (HRXES) spectrometer at the ESFR experimental station ID26. The measurements demonstrate the potential of this experimental technique for qualitative/semiqualitative and quantitative actinide speciation investigations. For the first time a pre-edge feature with

quadrupole nature (transitions involving 5f-like final states) is observed in a U *L*3 edge partial fluorescence yield-XANES spectrum. This feature is a tool for characterizing the participation of 5*f* orbitals in U-O bonding. The origin of the feature is explained by performing calculations with the finite difference method near-edge structure code (FDMNS) based on the multiple scattering theory and the finite difference method (Chapter 9.1).

The **structure of water near the corundum (001) surface was determined by means of Monte Carlo (MC) simulations,** which give direct information about the water species and their orientation close to the surface and thus help to better understand sum frequency spectroscopy results. These MC calculations are complemented by theoretical efforts using density functional theory at the corundum (001) and (110) surface. The sorption of trivalent lanthanides and actinides and the formation of inner-sphere complexes on the corundum (110) surface was investigated. Theoretical results confirm the experimental observed trend, of more water bonds to the (110) surface compared to the (001) surface (Chapter 9.6).

In order **to describe solvation effects** on a theoretical level, molecular dynamics provides a common tool. Therefore **we have extended the TCPEp force field and obtained new parameters for actinides,** water and counterions based on highly accurate state-of-the-art quantum-chemical calculations. As a result coordination numbers, bond distances, resident times, simulated EXAFS spectra, as well as thermodynamic data are obtained, which can be compared directly to experimental data. This project is a European collaboration with CEA / Saclay und Université Lille1.

3 Education and Training

Teaching

Teaching of students and promotion of young scientists is of fundamental importance to ensure high level competence and to maintain a leading international position in the field of nuclear and radiochemistry. INE scientists are strongly involved in teaching at KIT-Campus South and the Universities of Heidelberg, Berlin, Jena and Mainz.

Prof. Dr. Horst Geckeis, director of INE, holds a chair of radiochemistry at KIT Campus South, Department Chemistry and Biosciences. He teaches fundamental and applied radiochemistry for chemistry students in master and diploma courses. A radiochemistry module consisting of basic and advanced lectures on nuclear chemistry topics and laboratory courses has been set up for master students in Karlsruhe.

Prof. Dr. Petra Panak, heading a working group on actinide speciation at INE, holds a professorship of radiochemistry at the University of Heidelberg. A basic course in radiochemistry is offered for bachelor and/or master students. An advanced course is comprised of chemistry of f-elements and medical applications of radionuclides. The advanced radiochemistry lectures are supplemented by a scientific internship at the INE radioactive laboratories.

About 50 students from Karlsruhe and Heidelberg participated in two 3-week radiochemistry laboratory courses in 2010 held at KIT-CN in the FTU radiochemistry and hot laboratories at INE. Some students started to extend their knowledge in nuclear/radiochemistry topics within scientific internships at INE. It is obvious that the students became interested in nuclear chemistry topics and appreciate the various semester courses.

Dr. Andreas Bauer is lecturing Clay Mineralogy at the University of Jena. His lecture deals with mineralogical characterization of these fine materials and the importance of quantifying surface reactions. In the second part of the lectures sound, practical advice on powder X-ray diffraction in general is provided, as well as a useful set of step-by step instructions for the novice.

Lectures and practical units taught by Dr. Thorsten Schäfer at the Freie Universität Berlin, Institute of Geological Sciences, Department of Earth Sciences, focused in 2010 on a master degree course on laboratory and field methods in hydrogeology, including performance and analysis of tracer tests, pumping tests and permeability determination (Applied Hydrogeology III), as well as a special topic course on “Environmental radioactivity”.

Dr. Thorsten Stumpf gave lectures at the KIT Campus South, Department Chemistry and Biosciences, in the field of chemistry of f-elements and inorganic chemistry.

The lecture of Dr. Clemens Walther at the University of Mainz deals with electric power generation. All currently applied major techniques for electricity generation are presented with a focus on nuclear energy and the scientific basics of nuclear fission. Advantages and drawbacks of each technique are compared and present resources, sustainability and technical development are discussed.

Through this close cooperation with universities, students are educated in the field of nuclear and actinide chemistry, which most universities can no longer offer. Hence, INE makes a vital contribution to the intermediate and long-perspective of maintaining nuclear science competence.

PhD-students

In 2010 thirteen PhD students worked at INE on their dissertations. Five of them were awarded their doctoral degree. Topics of their theses are:

- Structural study on Cm(III) and Eu(III) complexes with ligands relevant to partitioning
- Spectroscopic and thermodynamic studies on the complexation of Cm(III) with inorganic ligands at elevated temperatures
- Interaction of trivalent lanthanides and actinides on various aluminium oxides/hydroxides minerals at the water interface
- Sorption of Ln(III)/An(III) and U(VI) onto monomineralic clays and natural claystones
- Co-precipitation of actinides with calcite - interfacial reactions and kinetics
- Influence of colloids on radionuclide mobility
- Study on the complexation behaviour of actinides by ESI-MS
- Separation of trivalent actinide from lanthanide ions by N-donor ligands
- Development, implementation and application of force-field interaction terms to aqueous actinide complexes

- Study on the speciation of Cm(III)/Eu(III) complexes relevant for partitioning
- Impact of kinetics and flow path heterogeneity on nanoparticle /radionuclide migration
- Incorporation of elements with low solubility in alkaline borosilicate glasses for the immoblisation of high-radioactive liquid waste
- Influence of pore clogging on the diffusion properties of porous media during geochemical perturbation: experiments and modelling

4 National and international cooperation

INE R&D involves a number of national and international cooperations and projects. These are described in the following.

The EURATOM FP7 Collaborative Project (CP) “Redox Controlling Systems” (ReCosy) started in April 2008. Main objectives of ReCosy are the sound understanding of redox phenomena controlling the long-term release/retention of radionuclides in nuclear waste disposal and providing tools to apply the results to performance assessment/safety case. The project is coordinated by INE, with Amphos 21 as the coordination secretariat and 32 institutions from 13 European countries contributing to the four-years CP. The international interest in the project is large, and organizations from the Finland, Japan, Korea, UK and USA have signed associated group agreements.

In June 2010 an additional FP7 Collaborative Project (CP) started, namely “Cation diffusion in clayrocks” (CatClay). The aim of CatClay is to improve understanding of the phenomena governing migration of radionuclides in clayrocks as potential host rocks for the deep geological disposal of nuclear waste. The project focuses on the diffusion-driven transport of cationic species, Sr^{2+}, Zn^{2+} and Eu^{3+}, which are more or less strongly sorbed on clay mineral surfaces. CatClay coordinated by CEA combines model and experimental developments from the partners ANDRA, BRGM, CEA, SCK·CEN, PSI-LES, Appelo Hydrochemical Consultant and KIT-INE.

The EURATOM FP7 CP “Actinide Recycling by Separation and Transmutation” (ACSEPT) is dedicated to the development of actinide separation processes. It is a four year project (2008–2012) coordinated by CEA. KIT-INE leads the “Hydrometallurgy” Domain. The consortium consists of 34 members from Europe, Japan and Australia. ACSEPT is a continuation of previous FP4, FP5 and FP6 partitioning projects in which KIT-INE also participated.

INE was one of the core members of the European "Network of Excellence for Actinide Sciences” (ACTINET-6) within the 6th FP of the EC which ended 2008. The negotiations for the follow up project ACTINET-I3 dragged on for over a year and the contract for the three year new project was finally signed by the Commission in January 2010. ACTINET-I3 is an Integrated Infrastructure Initiative. In contrast to the former ACTINET, the consortium has only eight members. These are the leading European actinide laboratories: CEA, JRC-ITU and KIT-INE, as well as FZD, PSI, CNRS, KTH and UNIMAN. The objectives of ACTINET-I3 are: (i) to establish and strengthen a network of actinide facilities across the EU and to foster their joint development in terms of capacity and performance; (ii) to support and manage jointly a programme of access to appropriate infrastructures for training and associated research projects making use of the proposed facilities; (iii) to conduct on a limited scale a set of Joint Research Activities (JRA) involving consortium member organisations, with an objective to improve the performance of infrastructures by developing new relevant instrumentations and/or data of common interest. Further, these activities will be complemented by a virtual infrastructure, the Theoretical User Lab, providing a limited support in theoretical and computational chemistry and modelling, with a focus on the complementarities between theory and experiment. Open access to the actinide laboratories and the integrated beam lines for outside scientist to perform experimental work within well defined joint research projects was very successful in ACTINET-6. This instrument will be continued in ACTINET-I3; the 1st Call for proposals was launched in February 2010.

With funding from the EU 7th Framework EURATOM program as a coordination and support action the project “Towards a European Competence Center for Nuclear Magnetic Resonance (NMR) on Actinides” began in autumn 2009. At the end of January 2010, a workshop "EURACT-NMR – European Radioactive Nuclear Magnetic Resonance" was held in Karlsruhe, to build competence and identify future trends and promising application fields in NMR actinide research. An expert round table was established with the aim of specifying required NMR instrumentation and infrastructure in the “European Competence Centre for NMR on Actinides” to be established as a joint initiative of JRC-ITU and KIT-INE together with partners from the University of Cambridge and CEA Marcoule to meet the experimental needs of research in this field.

Two international projects focus on the stability of the bentonite buffer/backfill in contact with water conducting features and the influence of colloids on radionuclide migration in crystalline host rock: the Colloid Formation and Migration (CFM) experiment, coordinated by NAGRA (National Cooperative for the Disposal of Radioactive Waste, Switzerland), and the Colloid Project, initiated by SKB (Swedish Nuclear Fuel and Waste Management Co., Sweden). Both projects are currently jointly

working together using the experimental set-up at the Grimsel Test Site (Switzerland). Additional partners involved are from Japan (JAEA, AIST, CRIEPI), South Korea (KAERI), Finland (POSIVA Oy), Switzerland (NAGRA, PSI-LES), and Spain (CIEMAT). INE plays a decisive role in the laboratory program of both projects and is also mainly carrying out the field activities.

INE is involved in various bi- and multilateral cooperations with national universities on different topics. Scientific cooperation with various German universities, research institutions and industrial partners is partly supported by the German Federal Ministry for Economics and Technology (BMWi), the geoscientific research and development program GEOTECHNOLOGIEN funded by the Federal Ministry for Education and Research (BMBF) and the German Research Foundation (DFG) and the Federal Ministry for the Environment, Nature Conservation and Nuclear Safety (BMU). These research programs are dedicated to actinide and long-lived fission product geochemistry and, specifically, the impact of reactive surfaces, colloidal and natural organic matter. The BMWi funded collaborative projects VESPA, THEREDA, HATT, KOLLORADO-2 and the BMBF/DFG funded project RECAWA should be specifically mentioned here.

Primary goal within the collaborative project VESPA coordinated by GRS with partners FZD-IRC and FZJ-IEF is to reduce the conservativeness in the assumptions currently made in performance assessment calculations concerning the radionuclides ^{14}C, ^{79}Se, ^{129}I and ^{99}Tc. There is reasonable evidence that sorption values for radionuclides on organics, clay surfaces, layered double hydroxides or steel corrosion products are significantly higher than currently used in modelling approaches. This could, in “what if” scenarios, lead to significantly lower radionuclide release rates than currently predicted. The project VESPA focuses on the reduction of these uncertainties.

Within the THEREDA project INE generates a centrally managed and administered database of evaluated thermodynamic parameters in cooperation with the Gesellschaft für Anlagen- und Reaktorsicherheit (GRS) mbH, Braunschweig, Forschungszentrum Dresden-Rossendorf, Institut für Radiochemie (FZD-IRC), Technische Universität Bergakademie Freiberg, Institut für Anorganische Chemie (TU-BAF) and AF-Colenco AG, Baden (Schweiz). Thermodynamic data are required for environmental applications in general and radiochemical issues in particular. This database is to be developed to a national (reference) standard and will be the basis for performance assessment calculations for a national nuclear waste repository.

The HATT project focus on the migration of radionuclides in natural clay formations and in bentonite considered as technical barrier. Within this project not only the mechanism of radionuclide sorption onto clay is studied, but also the influence of organic matter naturally occurring in the clay stone on the radionuclide migration. Parallel to the characterization of clay organic compounds, the interaction of actinides with humic substances, kerogen-like compounds and small organic molecules are examined. Besides INE, the members of this collaborative project are GRS, FZD-IRC, University of Mainz, University of Potsdam, University of Munich and University of Saarland.

The bilateral GRS-INE project KOLLORADO-2 started mid-2009 as successor of the KOLLORADO project focusing on the erosion stability of compacted bentonite barrier as a function of the contact water chemistry/ hydraulics and the formation of near-field colloids/nanoparticles as potential carriers for actinides/radionuclides. Both a detailed experimental program investigating the influence of surface roughness/charge heterogeneity on nanoparticle mobility and actinide bentonite nanoparticle sorption reversibility, as well as approaches to implement the acquired process understanding in reactive transport modeling codes comprise the project activities.

In the BMBF/DFG funded joint research project RECAWA with partners from KIT (Institute of Reinforced Concrete Structure and Building Materials; KIT-IfMB, Institut of Mineralogy and Geochemistry; KIT-IMG), the University Frankfurt (Institute of Geoscience, UniFaM-IfG) and industrial partners (Rheinkalk Akdolit, Lafarge Cement and Schäfer Kalk), basic understanding of processes with regard to the reactivity and dynamics of calcite mineral surfaces during crystal growth in aquatic systems will be developed. INE focuses on the immobilization of environmentally relevant anionic trace elements (Se, U) on calcite surfaces using an integrated approach on the basis of batch sorption and co-precipitation experiments with molecular calculations and spectro-microscopic information.

The BMBF funded in the framework of the funding concept ‘Basic research Energy 2020+’ entitled "Grundlegende Untersuchungen zur Entwicklung und Optimierung von Prozessen zur Abtrennung langlebiger Radionuklide (Partitioning)“ continued in 2010. This is a cooperative project between KIT (both Campus North and South), Forschungszentrum Jülich and the Universities of Erlangen and Heidelberg aimed at understanding the differing reactivity

between 4f and 5f elements with the ultimate goal of using this information to optimize their separation in partitioning.

In 2010 activities in the Helmholtz – Russia Joint Research Group (HRJRG) entitled “Actinide Nano-Particles: Formation, Stability, and Properties Relevant to the Safety of Nuclear Waste Disposal” continued for their third and final year. This HRJRG is a cooperative effort between KIT-INE and the Chemistry Department of Lomonosov Moscow State University, with the goal of developing a molecular-level understanding of the formation, stability, and properties of nano-sized actinide containing colloids relevant to safe spent nuclear fuel (SNF) and high level radioactive waste (HLW) disposal, thereby filling conceptual gaps in the source term and transport models used in long-term assessment for deep geological repositories.

The Helmholtz University Young Scientist Group (HHNG) “Elucidation of Geochemical Reaction Mechanisms at the Water/Mineral Phases Interface” has been supported by HGF and KIT since 2006. The partner of the HHNG is the Faculty of Chemistry and Geosciences of the University of Heidelberg. The project was funded over five years with a 1.25 million Euro volume, including funding for personnel as well as for non-personnel items. The leader of the working group has teaching functions at the Heidelberg University. The HHNG was evaluated successfully and finished at the end of 2010.

The Virtual Institute (VI) “Advanced Solid-Aqueous Radio-Geochemistry“ supported by the HGF and coordinated by INE began in March 2008. The work is focused on the elucidation of reaction mechanisms, which are responsible for the migration and/or retardation of radionuclides. The investigations range over a broad scale of complexity, from a thorough study of a model system for the formation of solid solutions (calcite, powellite), up to monitoring the complex interaction of cations and anions with cementious material under repository conditions. Experimental work, modern spectroscopy and Monte Carlo simulations, as well as quantum mechanical calculations are performed to achieve a process understanding on a molecular level. Members of the VI are KIT, the Universities of Frankfurt (Germany) and Oviedo (Spain), the Research Center Jülich and the Paul Scherrer Institut (PSI) in Switzerland.

In May 2010, INE hosted the NEA symposium “‘From Thermodynamics to the Safety Case" which was organised jointly by the NEA TDB and Sorption Projects. The objective of the symposium was to present and discuss the principal outcomes of these two projects with interested communities (academic institutions, technical support organisations, waste management organisations, regulatory bodies). Emphasis was placed on illustrating and discussing the successful use and key challenges when applying thermodynamic models and underlying databases to problems of interest to the waste management community as a whole. The symposium was attended by 75 delegates from 16 countries.

5 Fundamental Studies: Process understanding on a molecular scale

In the following section recent achievements are presented on basic actinide chemistry in aqueous solution which are relevant to the migration of actinides and long-lived fission products in the near- and far-field of a nuclear repository in deep geological formations. This includes provision of reliable thermodynamic data and models but also fundamental understanding of relevant processes. The reported studies deal with the chemistry of actinides in aqueous solution, their interaction with mineral/water interfaces and the formation of actinide containing solid solution phases. Whereas the first topic is oriented to derive realistic solubility data, both last topics are aimed at the elucidation of retention/ retardation mechanism and their thermodynamic quantification. These fundamental studies are strongly linked to applied studies on natural systems relevant for safety assessment.

5.1 Chemistry and thermodynamic of actinides in aqueous solution

M. Altmaier, K. Dardenne, D. Fellhauer[b], X. Gaona, S. Höhne, S. Hofmann T. Kobayashi, Ch. Marquardt, P.J. Panak, A. Skerencak

In co-operation with:

L. Charlet[a], Th. Fanghänel[b], R. Kirsch[c], A. Rossberg[c], A. Scheinost[c], J. Tits[d], E. Wieland[d]

[a] ISTerre, Grenoble, France; [b] JRC-ITU, European Commission, Karlsruhe, Germany, [c] IRC-HZDR, Dresden, Germany; [d] PSI-LES, Villigen, Switzerland

Introduction

In order to assess the long-term safety of a nuclear waste repository, it is essential to have a reliable understanding of the chemical effects controlling both radionuclide retention and mobilization. For the last decades, a correct and reliable quantitative description of actinide solubility and speciation within robust chemical and thermodynamic models has been at the centre of successful research activities at INE. In addition to these investigations mainly using redox stable radionuclides, the similarly important investigation of actinide redox chemistry has recently received increasing attention, as aqueous actinide chemistry is strongly depending on the actinide oxidation state and thus directly correlated to redox processes. The following studies highlight current research activities at KIT-INE focussing on different aspects of redox controlled aqueous actinide and technetium chemistry. In addition, new studies on Cm(III) – propionate complexation (at 25-90°C) are presented, reflecting experimental programs at INE focussing on actinide chemistry at elevated temperature conditions.

The ReCosy Intercomparison Exercise on redox determination methods

Redox conditions in aqueous systems are usually characterised and reported by the redox potential (E_h or pe) in solution. Reliable measurements of redox potentials are therefore essential requirements for reliable investigations and predictions of redox related processes. Within the EURATOM FP7 Collaborative Project “Redox phenomena controlling systems” (CP ReCosy), an InterComparison Exercise (ICE) on redox determination methods was performed at KIT-INE in 2009/2010. More than 40 scientists working on different topics related to redox chemistry from 20 ReCosy partner organisations and associated groups contributed to ReCosy ICE, thus providing a broad scientific basis.

The main conclusion of RECOSY ICE is that the redox state of an aqueous system can be determined by the existing experimental techniques, although the degree of confidence strongly depends of the kind of aqueous system investigated and the degree of optimisation of the experimental equipment and handling protocols. In how far the available experimental accuracy and precision is sufficient to adequately characterise the sample must be assessed in each case and cannot be generalised. Based on the outcome of the ICE, the partners have agreed upon a list of recommendations. The central argument is that it is strongly recommended to use a combination of several experimental approaches to identify and assess systematic errors as there is no single “best method” to determine the redox state of a given system. This is especially true for the analysis of (intrinsically highly complex) natural systems. Further recommendations, e.g. concerning non-conventional techniques, instrumentation, sampling and improved handling protocols have been derived and are

reported in the final ReCosy ICE report. In addition, several topics have been identified beyond the present state-of-the-art that may provide significant input for future research activities related to redox phenomena in aqueous systems.

The report on ReCosy ICE [1] and additional supporting information is available from the authors and can be downloaded via the ReCosy project webpage www.recosy.eu or at http://digbib.ubka.uni-karlsruhe.de/volltexte/1000021898.

Plutonium Redox Behavior in Aqueous Solutions and on Nanocrystalline Iron Phases

Plutonium chemistry in aqueous solution is strongly determined by its oxidation state; either Pu(V) / Pu(VI) under oxidizing conditions or Pu(III) / Pu(IV) under reducing conditions. Since secondary iron mineral phases may be formed in a nuclear waste repository via canister corrosion and are ubiquitous in the environment, the interaction of iron minerals with Pu and the impact on Pu oxidation state distribution requires a detailed understanding.

Redox processes of Pu(V) and Pu(III) in presence of heterogeneous iron mineral suspensions have been investigated using advanced XANES/EXAFS spectroscopy to identify surface complexes [2] and determine the Pu redox state distribution on the mineral surface after reaction. The results from spectroscopic in-situ investigations are compared to the calculated Pu redox state distribution based on macroscopic thermodynamic constants. Complementary experiments in homogeneous solutions with similar redox conditions as in the heterogeneous systems were also performed.

Aliquots of electrochemically prepared ^{242}Pu(V) or ^{242}Pu(III) stock solution were added to suspensions of synthetic Maghemite (γ-Fe_2O_3), Magnetite (Fe_3O_4), Mackinawite (FeS), Hematite (α-Fe_2O_3), Goethite (FeOOH) and Siderite ($FeCO_3$) in 0.1 M NaCl at pH 6-8.5. Within few minutes the initial Pu concentration ($1.3\pm0.1\cdot10^{-5}$ M) decreased by more than 90 % in all experiments indicating fast sorption of Pu onto the mineral phases. XANES and EXAFS analysis (ROBL at ESRF) after 40 days revealed that in all samples with initial Pu(V) a combination of sorption and reduction to Pu(IV) and Pu(III) had occurred. No changes in the initial Pu oxidation state were observed for the experiments with additions of Pu(III) except the sample Pu(III)+Maghemite, where partial oxidation to Pu(IV) occurred.

After 6 months, a second experimental series with longer equilibrations times were performed. The results from the 40 days experiments with initial Pu(V) were confirmed: reduction to Pu(IV) and Pu(III) occurred in all cases. Deviations from the previous findings were, however, observed for the experiments with initial Pu(III). In 5 of 6 samples Pu(IV) was the predominant oxidation state after 6 month although redox conditions were comparable in both series. A redox transformation of Pu(III) to Pu(IV) occurs under the given experimental conditions on a rather long time scale.

The observations can be analysed by comparing the experimental (E_H + pH) values with the predicted stability fields for different Pu oxidation states in the Pu Pourbaix diagram (see Fig. 1). The fast reduction of initial Pu(V) agrees with the predictions since the experimental conditions (E_H + pH) in the corresponding samples are several orders of magnitude below the stability field of Pu(V). The metastability of initial Pu(III) (with the tendency towards slow transformation into Pu(IV)) is also not surprising as the measured (E_H + pH) values lie close to the borderline calculated for the equilibrium Pu(III) ⇔ Pu(IV).

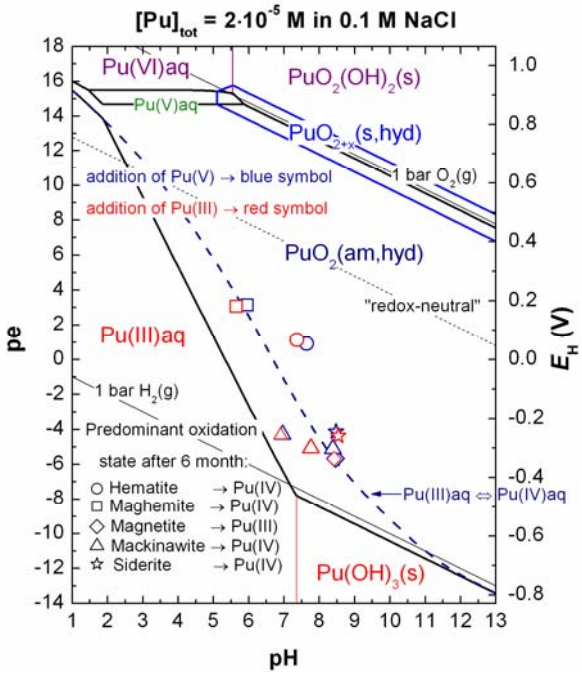

Fig. 1: *Comparison of experimental data with the calculated Pourbaix diagram of Plutonium for ($[Pu]_{tot} = 2\cdot10^{-5}$ M and 0.1 M NaCl.*

Pu(V) redox experiments in homogeneous solution with similar redox conditions and similar $[Pu]_{tot}$ as in the iron mineral suspensions confirm the observations made for the heterogeneous systems. Fast reduction of Pu(V) to Pu(IV) occurred in samples where the (E_H + pH) values are in the stability field of Pu(IV)

while mixtures of Pu(IV) / Pu(III) were obtained when redox conditions are close to the borderline Pu(III) ⇔ Pu(IV).

The results of our experiments indicate that the redox chemistry of Pu is strongly related to the "solution parameters" pH and pe both in homogeneous solutions and heterogeneous suspensions. The assessment of predominant Pu redox states based upon thermodynamic modeling has a remarkable predictive capability, even considering the presently still rather high uncertainties related to experimental data, e.g. pe measurements, and thermodynamic modeling. The present work underlines the advantages of combining information from advanced spectroscopic in-situ techniques like EXAFS and geochemical model calculations based upon macroscopic thermodynamic data. Using these complementary approaches, improved chemical and thermodynamic models can be derived and a comprehensive picture of the complex redox behavior of plutonium under conditions relevant for nuclear waste disposal obtained.

Redox processes of Tc(VII)/(IV) in 0.1 M NaCl under various redox conditions

The amount of Technetium potentially mobilized from a nuclear waste repository to the environment is strongly related to Tc redox processes. In the heptavalent Tc(VII) oxidation state, stable under non-reducing conditions, Tc exists as a highly soluble TcO_4^- anion. On the other hand, reduced tetravalent Tc(IV) is easily hydrolyzed to form sparingly soluble oxyhydroxide solid phases. For a reliable prediction of Tc chemistry under near field and far field conditions, it is essential to predict the Tc redox state distribution and respective stability fields as function of basic geochemical parameter (E_h, pH, ionic strength). Based upon a consistent understanding of Tc redox behavior, related processes influencing Tc mobilization can be assessed, e.g. by systematic studies on Tc(IV) solubility and speciation as function of different geochemical boundary conditions. The systematization of Tc redox processes in homogenous and heterogenous systems within the established E_h/pH concept offers a robust approach and furthermore allows conclusions on main reaction mechanisms.

The redox behavior of the Tc(VII)/Tc(IV) couple in 0.1 M NaCl/NaOH solutions was investigated in various homogeneous and heterogeneous reducing systems. TcO_4^- stock solution was added to 0.1 M NaCl/NaOH solutions pre-equilibrated with different reducing agents to a final concentration of $[TcO_4^-]_{init} = 1 \cdot 10^{-5}$ M. After given periods, pH and E_h were measured and Tc concentrations in solution determined after 10 kD (2-3 nm) ultrafiltration using Liquid Scintillation Counting.

In the systems with $Na_2S_2O_4$, Sn(II), Lawsone, Fe powder (neutral pH), or AQDS/AH_2QDS (acidic pH), the initial Tc concentration decreased quickly within a few days or weeks, indicating the reduction of Tc(VII) and the formation of the expected sparingly soluble Tc(IV) solid phases. On the other hand, in the systems with AQDS/AH_2QDS (alkaline pH), hydroquinone, Fe(II)/Fe(III) (acidic pH) or Fe powder (alkaline pH), Tc(VII) was not reduced and the concentration constant at the initial Tc level. The results are summarized quantitatively in the E_h-pH diagram shown in Fig. 2.

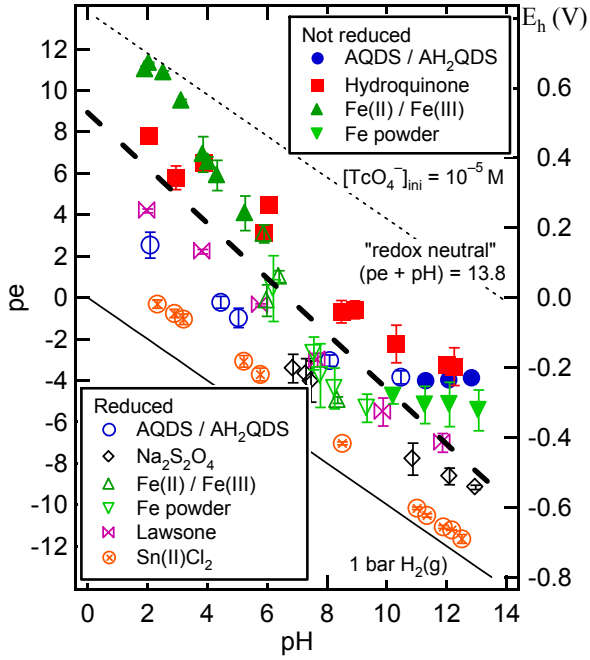

Fig. 2: *Reduction of Tc(VII) in 0.1 M NaCl/NaOH solutions. Open symbols indicate Tc(VII)-(IV) reduction, filled symbols indicate no Tc(VII) reduction within up to 1.5 months.*

A clear and systematic trend regarding E_h/pH conditions and Tc(VII)/Tc(IV) redox behavior is apparent as expected from thermodynamic calculations [3]. The dashed line in Fig. 2 represents the experimental borderline for the reduction, which was found to be independent of the reducing chemicals or the presence of iron solid phases. The work indicates that Tc redox processes in the investigated systems can be systematized and predicted using experimental data (E_h, pH, [Tc]) and thermodynamic model calculations, e.g. E_h/pH predominance diagrams. Well defined stability fields for the respective Tc(VII) and Tc(IV) species can be established for the given experimental parameters indicating E_h and pH conditions clearly

favoring the tetravalent Tc(IV) redox state and thus Tc retention. For a more detailed discussion of this work please refer to [4].

This work is part of an ongoing extended experimental program on Tc(IV) chemistry at KIT-INE to derive improved solubility data, aqueous speciation schemes and activity models (SIT, Pitzer) required for geochemical modeling at intermediate and high ionic strength conditions.

Redox chemistry of Np(V/VI) under hyperalkaline conditions: aqueous speciation and solid phase formation

The redox chemistry of the Np(V/VI) couple under alkaline conditions remains largely unknown and the stability fields and thermodynamics of Np(VI) species rather ill-defined. In the aqueous phase, the formation of hexavalent anionic species (*e.g.* $NpO_2(OH)_3^-$ and $NpO_2(OH)_4^{2-}$) has been proposed, although no thermodynamic data are currently selected in the NEA reviews [5]. In analogy to the U(VI) system, the precipitation of Na- and Ca-neptunate solids can be expected. The formation of these aqueous Np(VI) species and solid compounds may significantly limit the stability field of Np(V) in favour of hexavalent Np species in cementitious and saline environments, and therefore deserves detailed investigation.

In a first step, aqueous Np speciation and solid phase formation were investigated in tetramethylammonium hydroxide (TMA-OH) solutions, in order to limit the precipitation of solid phases and maintain Np in solution for EXAFS/XANES analysis. However, the high total Np concentration ($[Np]_{tot}$ ~ $2\cdot10^{-3}$M) gave rise to the precipitation of solid Np phases in some of the samples. Carbonate concentration (as impurity of TMA-OH) was $2\text{-}3\cdot10^{-3}$M. Redox conditions were defined by the absence or presence of ClO^- as oxidizing agent (Na-salt, $5\cdot10^{-3}$M and $5\cdot10^{-2}$M), whereas pH ranged between 9 and 13.5. In Fig. 3, a summary of the samples prepared is plotted in the predominance diagram of Np for 8<pH<14 and -1V<E_H<+1V. Thermodynamic calculations in the figure were conducted consistently with the NEA reviews [5], except for $NpO_2(OH)_3^-$ and $NpO_2(OH)_4^{2-}$ (in analogy to U(VI)), and $NpO_2(OH)_2(CO_3)^{3-}$ (as reported in [6]).

UV spectra obtained from the supernatant in TMA-OH solutions and in absence of ClO^- showed very clear Np(V) features, identified as NpO_2^+, $NpO_2(CO_3)^-$ and $NpO_2(OH)_2(CO_3)^{3-}$. XANES of these samples confirmed the predominance of Np(V). No UV features were observed within 800-1300 nm for samples with ClO^-, even though Np(VI) is expected to occur.

This different behaviour could be explained by the lower Np concentration in some of the samples, but is also indicative of the possible formation of centrosymmetric Np(VI) species (*e.g.* $NpO_2(OH)_4^{2-}$) with lower absorptivity coefficients. XANES of this second set of samples confirmed the predominance of Np(VI), in accordance with reference spectra [7]. A similar Np redox distribution was observed for the solid phases based on XANES and EXAFS measurements. EXAFS spectra indicative of $Np^VO_2OH(s)$ and $Np^{VI}O_3\cdot xH_2O(s)$ were obtained for samples Np-1/Np-2 and Np-5/Np-9, respectively. The formation of a Na-Np(VI) solid phase in $5\cdot10^{-2}$M ClO^- and pH~12 (sample Np-8) was indicated from both EXAFS and chemical analysis.

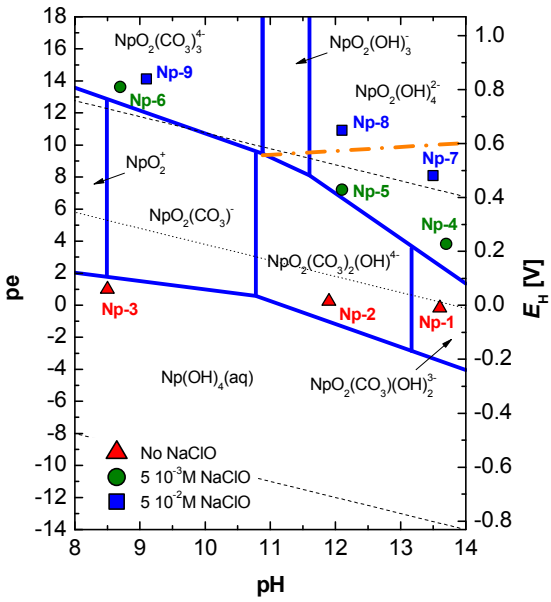

Fig. 3: *Predominance diagram of Np aqueous species including measured experimental pH and E_H conditions. Calculations for $[Np]_{tot}$ = $1\cdot10^{-4}$ M; $[CO_3]_{tot}$ = $2.5\cdot10^{-3}$M; I = 0.6M. The orange line indicates the Np(V)/Np(VI) border calculated with NEA-TDB.*

The results of this study confirm the relevance of Np(VI) in hyperalkaline systems even under mildly oxidizing conditions. Anionic species analogous to U(VI) are expected to form in the pH range 10-14. Indications of a Na-neptunate formation at [Na] = 0.01M highlight the potential relevance of Na-Np(VI) (and Ca-Np(VI)) solid phases in cementitious and saline environments. For a more detailed description to this work see [8]. Additional experimental series in alkaline carbonate free NaCl and $CaCl_2$ systems are in progress to identify solubility limiting solid phases, determine the stoichiometry and stability of aqueous Np(VI) species and derive an improved and comprehensive thermodynamic description.

Thermodynamic and spectroscopic studies on the complexation of Cm(III) with propionate at T = 25 90 C

The prediction of actinide chemistry at higher temperatures is a key topic required for the assessment of repositories for heat producing highly radioactive waste, operating under elevated temperature conditions for several thousand years after closure. Cm(III) is an excellent analogue for other actinides potentially present in the trivalent oxidation state under reducing conditions (Am, Pu) and ideal analytical probe for speciation studies at trace level concentrations owing to very advantageous spectroscopic properties. The present ligand system is studied, because increased concentrations of low molecular weight organic acids (LMWOA, f.e. propionate) are found in the pore water of different natural clay formations. Hence, the thermodynamic characterization of the interaction of trivalent actinides with LMWOA at increased temperatures is of importance for a comprehensive long term safety assessment.

The formation of $Cm(Prop)_n^{3-n}$ (n = 0, 1, 2) complexes was investigated by time resolved laser fluorescence spectroscopy (TRLFS) and UV/Vis spectroscopy in the temperature range from 25 to 90°C. The experiments were performed in a quartz cuvette embedded in a temperature controlled copper block. Two sets of samples were prepared using the molal (mol/kg H_2O) concentration scale. The first set contains samples at constant ionic strength in $NaClO_4$ media at I_m = 2.0 and varying propionate concentration ($[Prop^-]_{tot} = (0.1–3.0)\cdot10^{-2}$ m. The second set of samples was prepared at a constant total ligand concentration and different ionic strengths ($[Prop^-]_{tot} = 0.5\cdot10^{-2}$ m, I_m = 0.1–4.0 ($NaClO_4$)). The proton concentration in all samples was fixed with $HClO_4$ at $[H^+]_{tot} = 1.287\cdot10^{-4}$ m.

The temperature dependent species distribution as function of ligand concentration and temperature is determined by deconvolution of the TRLFS emission spectra. A detailed speciation at T = 25 and 90°C is given in Fig. 4.

At room temperature, the speciation of the samples is defined by the molar fractions of the aquo ion and the $[Cm(Prop)^{2+}]$ complex. The $[Cm(Prop)_2^+]$ complex is formed only up to 20%. An increase in the temperature results in a general shift of the species distribution towards the complexed species.

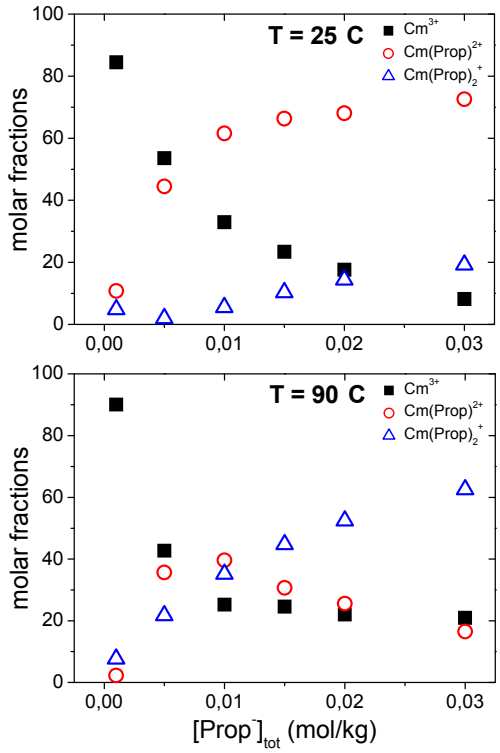

Fig. 4: Speciation of the Cm(III) propionate system as function of the total propionate concentration ($[Prop^-]_{tot}$) at T = 25 and 90°C.

The temperature dependent conditional log $K'_n(T)$ values are calculated using the spectroscopically determined speciation and pK'_a(T) values of HProp, measured with UV/Vis absorption spectroscopy.

The calculated log K'_n values are extrapolated to zero ionic strength with the SIT approach (specific ion interaction theory) [5]. The complex formation constants in the standard state and corresponding log $K^0_n(T)$ values are displayed in Fig. 5 as function of the reciprocal temperature. The log K^0_1(25°C) value is about 0.4 order of magnitude higher compared to

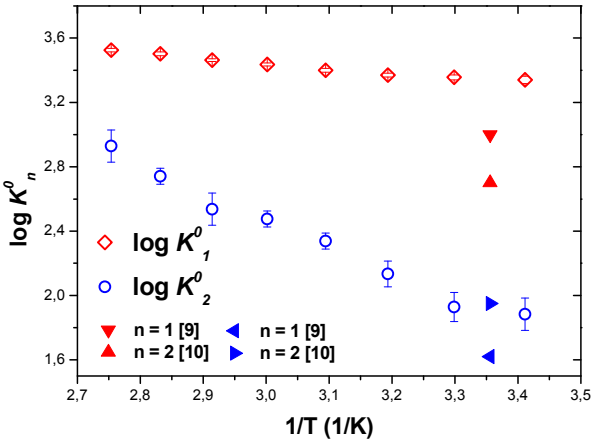

Fig. 5: Stability constants at zero ionic strength for $Cm(Prop)^{2+}$ and $Cm(Prop)_2^+$ (log K^0_1, log K^0_2) plotted as function of the reciprocal temperature (T^{-1}).

agreement with the literature [9,10]. The stabil lty constants show a linear correlation with the [9,10], while the log K^0_2(25°C) value is in good reciprocal temperature. Hence, constant $\Delta_r H^0_m$ of the individual, stepwise reactions are assumed and the linear Van't Hoff approach is used to model the temperature dependency of the stability constants. The thermodynamic constants ($\Delta_r G^0_m$, $\Delta_r H^0_m$, $\Delta_r S^0_m$) for the stepwise formation of the complexed species are summarized in Table 1.

	n = 1	n = 2
$\Delta_r G^0_{m,(25°C)}$ [kJ/mol]	-19.03 ± 1.0	-10.85 ± 0.25
$\Delta_r H^0_m$ [kJ/mol]	5.76 ± 1.1	30.40 ± 2.3
$\Delta_r S^0_m$ [J/mol·K]	83.16 ± 0.4	138.34 ± 7.9

Tab. 1: *Thermodynamic data for the stepwise formation of* $[Cm(Prop)_n]^{3-n}$ *(n = 1, 2)*

The results show, that the driving force of the complexation reaction of Cm(III) and propionate is the increase in the entropy of reaction, explaining the observed increase of the stability constants with increasing temperature. The studies are part of ongoing research activities at KIT-INE on the field o high temperatures actinide chemistry, relevant for a comprehensive long term safety assessment of a nuclear waste repository.

References

[1] Intercomparison of Redox Determination Methods on Designed and Near-Natural Aqueous Systems (2010). M. Altmaier, X. Gaona, D. Fellhauer, G. Buckau (eds.). FP 7 EURATOM Collaborative Project "Redox Phenomena Controlling Systems", Karlsruhe Institute of Technology KIT SR 7572 - ISSN 1869-9669, (2011).

[2] R. Kirsch, D. Fellhauer, M. Altmaier, V. Neck, A. Rossberg, T. Fanghaenel, L. Charlet, A.C. Scheinost. Oxidation state and local structure of plutonium reacted with magnetite, mackinawite and siderite. Environ. Sci. Technol. (submitted).

[3] J. Rard, M. Rand, G. Anderegg, H. Wanner. *Chemical Thermodynamics of Technetium*, NEA OECD, Elsevier (1999).

[4] T. Kobayashi, X. Gaona, D. Fellhauer, M. Altmaier (2011). Redox behavior of Tc(VII)/Tc(IV) couple in various reducing systems. In: 3rd Annual Workshop proceedings of the collaborative project "Redox Phenomena controlling systems" (7th EC FP CP REOSY), Balaruc-les-Bains, France.

[5] R. Guillaumont, T. Fanghänel, V. Neck, J. Fuger, D.A. Palmer, I. Grenthe, M.H. Rand (2003) Chemical Thermodynamics 5. Update on the Chemical Thermodynamics of Uranium, Neptunium, Plutonium, Americium and Technetium. NEA OECD, Elsevier.

[6] V. Neck, T. Fanghänel, TJ.I. Kim (1997). Mixed hydroxo-carbonate complexes of Neptunium(V). Radiochimica Acta, 77, 167-175.

[7] V. Liu, N.L. Banik, B. Brendebach, K. Dardenne, J. Rothe, C.M: Marquardt, M.A. Denecke (2009). Neptunium redox speciation in perchloric acid by in situ XANES/EXAFS using a newly developed spectro-electrochemical cell. ANKA - Annual Report 2009. Karlsruhe Institute of Technology

[8] X. Gaona, J. Tits, K. Dardenne, E. Wieland, M. Altmaier (2011). XAFS investigations of Np(V/VI) redox speciation in hyperalkaline TMA-OH solutions. In: 3rd Annual Workshop proceedings of the collaborative project "Redox Phenomena controlling systems" (7th EC FP CP REOSY), Balaruc-les-Bains, France.

[9] G.R. Chopping, A.J. Graffeo, Inorg. Chem., 4, 1254 - 1257, (1965).

[10] S.A. Wood, Eng. Geo., 34, 229 - 259, (1993).

5.2 Sorption of trivalent metal ions onto aluminium(hydr)oxides

*T. Kupcik, N. Huittinen, Th. Rabung, J. Lützenkirchen, H. Geckeis, Th. Fanghänel**

**Universität Heidelberg, Physikalisch-Chemisches Institut, Im Neunheimer Feld 253, D-69120 Heidelberg*

Introduction

Migration of actinide species in the near- and far-field of a nuclear waste repository in deep geological formations strongly depends on reactions at solution-mineral-interfaces, e.g. inner- and outer-sphere adsorption, ion exchange, and structural incorporation (solid solution formation). For a long-term safety analysis, a sound understanding of the involved processes is required. This includes the identification and characterization of the formed surface species. Aluminium oxides/hydroxides themselves are of minor direct importance in the context of nuclear waste disposal, but can conveniently be used as isomorphous model phases for trivalent iron oxides/hydroxides. The latter phases occur both as natural minerals in various types of rocks in the far-field and as corrosion products in the near-field of a nuclear waste repository and do exhibit strong sorption capacity. In contrast to iron oxides/hydroxides, aluminium oxides/hydroxides show no absorption in the visible light region, thus allowing TRLFS experiments, which in turns yields direct information about the surface speciation. In addition, natural alumosilicate minerals like clays exhibit surface aluminol sites as do the aluminium hydroxides. Furthermore, Gibbsite, as an alteration product of alumosilicate minerals, is by far the most common crystalline aluminum(hydr)oxide in soil environments.

In TRLFS studies on the interaction of Cm(III) with γ–Al_2O_3, three different Cm(III) surface species were distinguished between pH 3 and 13 and assigned to the surface complexes γ-$Al_2O_3\cdots Cm(OH)_x(H_2O)_{5-x}$ (x = 0, 1, 2) [1]. As the undefined structure of the γ-Al_2O_3 particles inhibits an assignment to the reactive surface sites, Cm(III) sorption studies were extended to sapphire (α-Al_2O_3) single crystals, for which information about the reactive surface sites, their distribution and concentration is available [2]. TRLFS results at pH values of 4.5 and 5.1 show differences in peak position and fluorescence lifetime for Cm(III) bound to the (001) α-Al_2O_3 surface compared to the (018), (104), (012) and (110) crystal planes. This indicates a clear influence of the nature of the aluminol groups present at the mineral surface, their acidity and the way Cm(III) is bound to these surface groups. As pure Al-oxide surfaces are not thermodynamically stable in water and undergo (surface) phase transformations into the hydroxides [3], [4], the investigations were further extended to a pure aluminiumhydroxide, gibbsite (α-$Al(OH)_3$). From the Cm(III) emission spectra two Cm(III) surface species could be distinguished [5]. In addition, a third Cm(III) species could be observed at pH 6-11. This species is assigned to an incorporated Cm(III) species, possibly forming as a consequence of precipitation of $Al(OH)_3$ from an oversaturated solution. In that case, formation of an incorporated Cm(III) species should be inhibited by using a suspension equilibrated at the gibbsite solubility minimum.

The aim of this work is to study trivalent metal ion sorption onto α-Al_2O_3 (corundum) powder and a second aluminiumhydroxide, bayerite (β-$Al(OH)_3$). In continuation of the experiments by Rabung et al. [2], Cm(III) sorption onto sapphire single crystals is extended to higher pH.

Experimental

Gibbsite used in this study was prepared at KIT-INE and is described in the literature [5]. The mineral suspension was equilibrated at the solubility minimum (pH = 6.2) for four months prior to the Cm(III) sorption study. Starting the Cm(III) sorption experiments with this suspension from the solubility minimum and increasing and decreasing the pH in two separate sets of experiments should minimize the formation of an incorporated Cm(III) species between pH 5 and 9. Bayerite microrods were synthesized by titration of an aluminate solution with HCl to pH 9 at elevated temperatures [6]. α-Al_2O_3 powder was supplied by Taimicron, Japan (TM-DAR). Cm(III) TRLFS measurements were performed with 0.5 g/L solid content and $2x10^{-7}$ M Cm(III) in 0.1 M $NaClO_4$. After addition of the acidic Cm(III) stock solution, the desired pH was adjusted in small steps for corundum and bayerite. For gibbsite, Cm(III) was diluted in 0.1 M $NaClO_4$ and the pH was increased to pH ~ 6 prior to the gibbsite addition to avoid changes in the initial state of the gibbsite suspension. The suspensions were shaken periodically for 2-3 days to reach sorption equilibrium. The α-Al_2O_3 single crystals with the surfaces (001), (110) and (012) were obtained from MaTecK, Jülich. The samples were subjected to a standard cleaning procedure before use to eliminate the organic carbon and minimizing inorganic contamination [2]. Streaming potential measurements with Eu(III) sorbed onto sapphire (001), (110) and (012) single crystals

were carried out with one side polished samples with a dimension of 2 x 1 cm. For the Cm(III) sorption experiments, both sides polished (001) and (110) single crystals with a dimension 1 x 1 cm were used. Two Cm(III) solutions were prepared in 0.1 M $NaClO_4$. A Cm(III) concentration of $1 \cdot 10^{-6}$ M was used for the sapphire (001) surface, while a concentration of $3 \cdot 10^{-6}$ M was adjusted in case of the (110) single crystals due to a lower Cm(III) uptake of the latter surface [2]. The pH was adjusted to 5 and 6. To inhibit hydrolysis of Cm(III), the studies at pH > 6 were carried out in a Cm(III) free 0.1 M $NaClO_4$ solution, i.e the samples equilibrated at lower pH in the presence of Cm(III) were exposed to this new solution. Prior to the TRLFS study, the crystals were removed from the solutions and dried under Ar.

Results and discussion

Cm(III) sorption onto corundum and bayerite

Based on time resolved laser fluorescence spectroscopy (TRLFS) results on the interaction of Cm(III) with bayerite and corundum between pH 3 and 13, three different Cm(III) surface species for both minerals can be distinguished by peak deconvolution (Fig. 1).

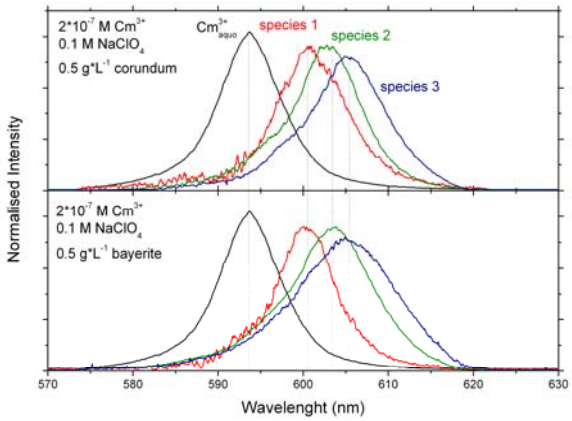

Fig. 1: *TRLFS single component spectra for the interaction of Cm(III) with corundum (**top**) and bayerite (**bottom**).*

For corundum, the Cm(III) species exhibit emission peak maxima at λ_{max} = 600.7, 603.0 and 605.0 nm. For bayerite, the single component spectra show peak maxima at λ_{max} = 600.6, 603.6 and 605.9 nm. In addition, a fluorescence lifetime of τ = 110 ± 10 µs can be observed for all Cm(III) species, which suggests the presence of ~ 5 H_2O/OH^- ligands in the first Cm(III) coordination sphere [7]. Based on the almost similar TRLFS results obtained for the interaction of Cm(III) with γ-Al_2O_3 particles [1], the three Cm(III) surface species can be assigned to the complexes $[surface \cdots Cm(OH)_x(H_2O)_{5-x}]^{3-x}$ (x = 0, 1, 2). In the case of corundum these similarities can be related to the formation of hydroxidic structures on the aluminium oxide surface and consequently to the presence of similar aluminol groups on both minerals in the presence of water. This assumption can be further extended to the γ-Al_2O_3 surface, which is known to transform to bayerite with time. Consequently, very similar pH dependent species distributions in the pH range between pH 3 to 13 are observed for Cm(III) interacting with corundum and bayerite (Fig. 2). At low pH values (pH < 4.0), the only species present is Cm^{3+}_{aquo}. Increasing the pH leads to the formation of the first Cm(III) surface species. This surface complex is only observed in a narrow pH range with a maximal abundance of ~ 50 %. At pH = 6.0 the second Cm(III) surface species is formed by hydrolysis of the first one, thus leading to a ternary surface complex. It is the predominant Cm(III) species in a broad pH range (6.5 < pH < 10.5). At pH ≥ 9 the third Cm(III) species is being formed, its abundance increasing with increasing pH up to pH = 13.

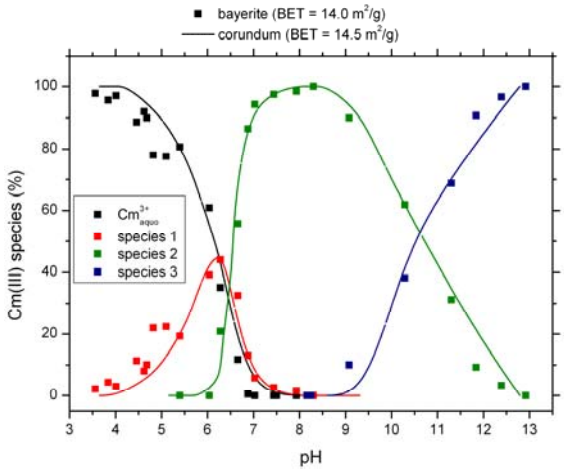

Fig. 2: *Cm(III) species distribution for Cm(III) sorption onto corundum and bayerite.*

Cm(III) sorption onto gibbsite

To avoid the formation of an incorporated Cm(III) species as a consequence of $Al(OH)_3$ precipitation which has been previously reported [5], a new suspension, equilibrated in the gibbsite solubility minimum was used and the pH dependent TRLFS experiments were started at pH = 6.2. In two separate sets of experiments the pH was increased (alkaline branch) and decreased (acidic branch), respectively. The results for the acidic branch show the formation of two Cm(III) surface species with λ_{max} = 603.5 and 605.6 nm (Fig. 3). Compared to the systems

Cm(III)/corundum and Cm(III)/bayerite the red-shifted emission spectra for the first Cm(III) species can be attributed to the direct formation of a ternary Cm(III) surface complex ($[gibbsite\cdots Cm(OH)(H_2O)_4]^{2+}$. This different Cm(III) speciation is due to different acid-base-properties of gibbsite compared to corundum and bayerite, leading to a higher isoelectric point for gibbsite and therefore a sorption edge, which is shifted to higher pH values. For the second Cm(III) species further hydrolysis and the formation of a surface complex $gibbsite\cdots Cm(OH)_2(H_2O)_3$ is most likely.

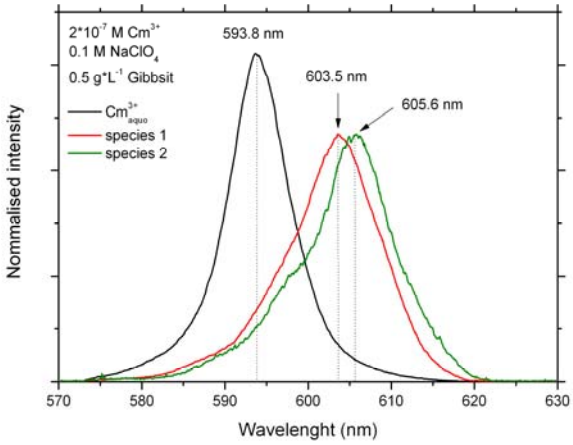

Fig. 3: *TRLFS single component spectra for the interaction of Cm(III) with gibbsite.*

In addition to these Cm(III) surface complexes, the existence of an incorporated Cm(III) species is observed at pH values near the gibbsite solubility minimum (5 < pH < 7). Although this Cm(III) species couldn't be excluded, its formation could be significantly suppressed under the conditions applied.

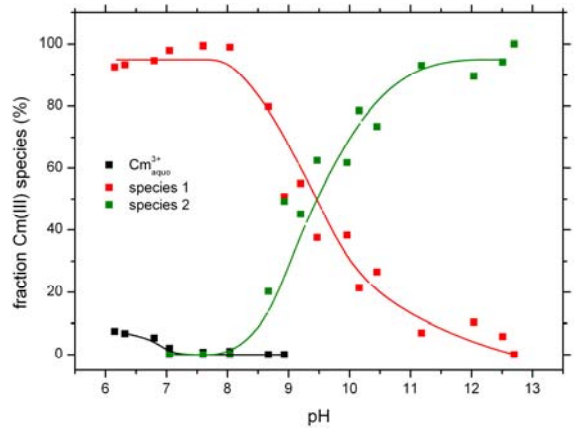

Fig. 4: *Cm(III) species distribution for Cm(III) sorption onto gibbsite for pH ≥ 6.2..*

The pH dependent species distribution for the alkaline branch is shown in Fig. 4. At pH = 6.2, the Cm^{3+}_{aquo} ion is only present in small quantities. The first visible Cm(III) complex is the predominant Cm(III) species up to pH = 9. The second Cm(III) surface complex is formed at pH ≥ 8.5 being the predominate Cm(III) species from pH = 9.5 up to pH = 13.

M(III) sorption onto sapphire single crystals

Cm(III) TRLFS study

For the sapphire single crystals, a higher Cm(III) uptake on the (001) surface compared to the (110) surface is observed at pH = 5 and 6 by α-spectrometry. This result is in agreement with previous results [2]. The deviations for the two crystal surfaces have to be attributed to the presence of different reactive aluminol groups. On the (001) surface, all oxygen atoms of the terminal layer are bound to two Al atoms in the bulk structure (doubly coordinated aluminol groups), while for the (110) surface, singly, doubly and triply coordinated aluminol groups are present. The different reactive surface groups also lead to a different Cm(III) speciation behaviour in the pH range between 5 and 13. For the (001) surface the pH dependent TRLFS results show the formation of three different Cm(III) surface species with emission peak maxima at λ_{max} = 601.5, 605.3 and 607.5 nm (Fig. 5). Up to pH = 12 a constant Cm(III) fluorescence lifetime of τ = 140 ± 10 µs is observed, which can be related to ~ 4 H_2O/OH^- molecules in the first Cm(III) coordination sphere [7]. Based on the results obtained for the Cm(III) interaction with corundum, bayerite and γ-Al_2O_3 [1], the single component spectra can thus be attributed to the Cm(III) species $[sapphire\text{-}(001)\cdots Cm(OH)_x(H_2O)_{4-x}]^{3-x}$ with x = 0, 1, 2.

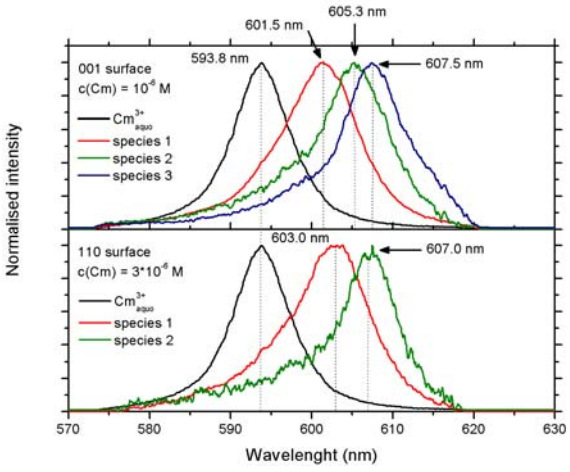

Fig. 5: *TRLFS single component spectra for the interaction of Cm(III) with the sapphire (001) (**top**) and sapphire (110) surface (**bottom**).*

The first Cm(III) species (x = 0) is the predominant species up to pH = 9.5 (Fig. 6). The second surface complex (x = 1) is formed at pH ~ 8, and its abundance increases up to pH = 11. Above this pH, its fraction decreases with further increasing pH. Simultaneously, the third Cm(III) species is formed, which predominates above pH = 11.5.

On the (110) surface two Cm(III) surface species were derived by peak deconvolution with λ_{max} = 603.0 and 607.0 nm (Fig. 5). Together with a significantly higher fluorescence lifetime of τ = 190 ± 40 µs (2 -3 H_2O/OH^- ligands) this result indicates a higher Cm(III) coordination onto the (110) surface compared to the (001) crystal surface. As the same emission peak maximum for the first Cm(III) surface species is observed at pH = 4.5 [2], a ternary Cm(III) surface complex can be ruled out. The two Cm(III) species can therefore be assigned to the complexes $[\textit{sapphire-(110)}\cdots Cm(OH)_x(H_2O)_{(2-3)-x}]^{3-x}$ with x = 0, 1. In contrast to the (001) surface, the decrease of the fraction of the first Cm(III) surface species (x = 0) and accordingly the increase of the percentage of the second Cm(III) surface complex (x = 1) is observed over a broader pH range (Fig. 6). At pH = 10.5, both Cm(III) surface species appear in similar quantities. At higher pH values, the second surface complex is the predominant Cm(III) species, its abundance increasing up to pH = 13.

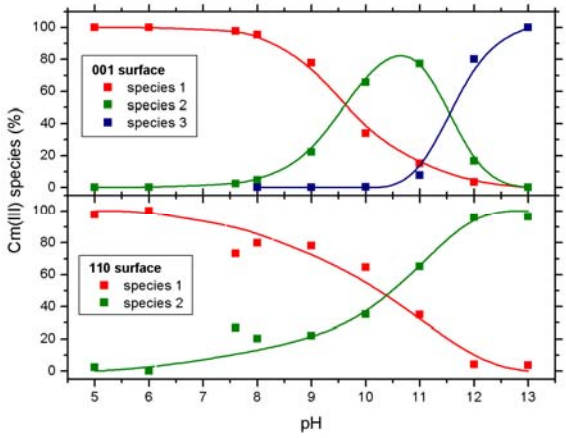

Fig. 6: *Cm(III) species distribution for Cm(III) sorption onto the sapphire (001) (**top**) and sapphire (110) surface (**bottom**).*

Zeta-Potential measurements with Eu(III)

The higher Cm(III) uptake on the (001) surface is *a priori* unexpected since the ideal (001) plane consists of doubly coordinated hydroxyl groups only. These hydroxyl groups are considered within surface complexation models as rather inert compared to singly coordinated groups, which in turn occur on the (110) or (012) surface. The zeta-potential measurements were designed to study, with an independent method, these single crystal systems (i) to verify the trend previously found and (ii) to investigate, in more detail, the concomitant dependence of Eu(III) adsorption to different cuts as a function of europium concentration and pH. Eu(III) was chosen as a non-radioactive lanthanide homologue to Cm(III). Streaming potential measurements were carried out on sapphire (001), (110) and (012) single crystal surfaces with two identical samples in a flow channel of about 100 µm width.

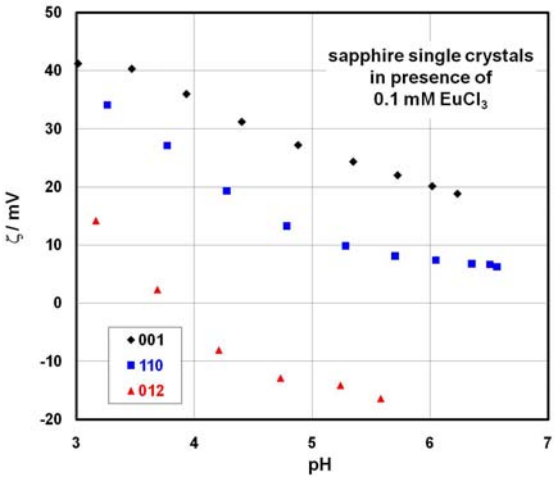

Fig. 7: *Zeta-potential as a function of pH at a total Eu(III) concentration of 0.1 mM for three different cuts of α-Al_2O_3.*

In the absence of Eu(III) similar zeta-potential vs. pH curves are obtained with an isoelectric point around pH = 4 for all three crystal planes studied. In 0.1 mM Eu(III), distinct differences occur in the zeta-potential vs. pH curves (Fig. 7) for the different planes. The strongest effect is found for the (001) plane in the presence of europium, whereas the (012) plane is not affected at all by these relatively high Eu(III) concentrations. The isoelectric point of the (012) plane does not shift, while the (001) and (110) planes show isoelectric points at pH > 6.5. The strong impact on the (001) plane agrees with the observations mentioned before and the results obtained by Rabung et al. [2] and confirmed as reported in the previous section. However, based on the results by Rabung et al., it would be expected that the (110) and (012) planes should behave similar, which is not supported by the streaming potential measurements under the chosen conditions. However, it is to be noted that the work by Rabung et al. [2] had been carried out at significantly lower M(III) concentrations.

To study possible effects of the total M(III) concentration on the behaviour, zeta-potentials at pH = 5 (within the range of pH studied by Rabung et al. [2]) were determined as a function of the total europium content in the system. The results are shown in Fig. 8.

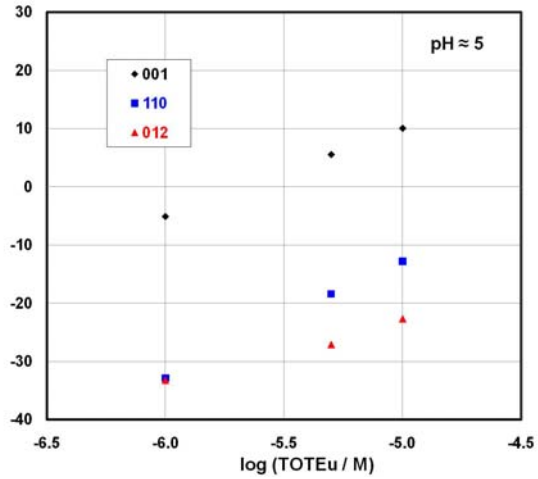

Fig. 8: *Zeta-potential at pH = 5 as a function of the total Eu(III) concentration for three different cuts of* α*-*Al_2O_3*.*

As observed in the pH dependence study, the Eu(III) interaction with the (001) plane is obviously quite strong compared to the two other cuts. In the latter, singly coordinated hydroxyl groups are present, on which stronger adsorption would *a priori* be expected compared to the (001) plane which only contains doubly coordinated groups. As can be seen from Fig. 8 for the (110) and (012) planes, similar behavior for a total Eu(III) concentration of about 1 µM is obtained. Since the studies by Rabung et al. [2] had been carried out at low concentrations, the streaming potential measurements confirm the results of the previously published uptake and spectroscopic studies both with respect to the observed differences in affinity and the unexpectedly strong interaction of the trivalent ions on the (001) plane. Increasing the Eu(III) concentration then results in a stronger effect on the (110) plane compared to the (012) plane, which in turn is in agreement with the results of the pH-dependent study (Fig. 7). The results of the streaming-potential study therefore appear to be self-consistent. However, it is not clear why the (012) plane shows a rather unusual effect of total europium concentration at constant pH.

The rather strong affinity of the trivalent ions for the (001) plane agrees with previous spectroscopic studies by Bargar et al. [8], [9] for divalent ions. Both Pb(II) and Co(II) could be adsorbed on this plane in sufficient amounts to allow EXAFS (extended x-ray absorption fine structure) measurements. The structural assignment of the surface complexes was such that a tridentate surface complex within the six-ring structure of the sapphire (001) plane was postulated. This assignment to the (Al-OH-Al)-six rings for the divalent ions agrees well with theoretical results for trivalent ions [10]. However, some disagreement exists with respect to the kind of the surface complex formed. Whereas for Pb(II) Bargar et al. [8] postulated a structure that involved rather outer-sphere coordination based on their EXAFS-data, it has been found that adsorption of Co(II) and the trivalent ions occurs via a inner-sphere coordination on the (001) surface [2][9], [10].

Conclusions

The pH dependent TRLFS results on the Cm(III) interaction with aluminium(hydr)oxides suggest the presence of different Cm(III) surface complexes. Since the Al_2O_3 surfaces are hydrated in aqueous solution, comparable Cm(III) species can be observed for Al_2O_3 and β-$Al(OH)_3$. Besides Cm(III) adsorption onto the mineral surfaces, an incorporation process for gibbsite could be verified. For the sapphire single crystals, a higher Cm(III) uptake on the (001) surface compared to the (110) surface is observed. This result is verified by zeta-potential measurements with Eu(III) and can be related to the different aluminol groups present on the crystal surfaces.

Since a combination of different spectroscopic methods is necessary to investigate processes occurring at the water-mineral-surface, an EXAFS investigations on the Gd(III) sorption onto gibbsite, bayerite and corundum should give further information about the sorption environment and the way the metal ion is bound to the mineral surfaces.

References

[1] Th. Rabung, H. Geckeis, X.K. Wang, J. Rothe, M.A. Denecke, R. Klenze, Th. Fanghänel, Radiochim. Acta, 94, 609-618 (2006).

[2] Th. Rabung, D. Schild, H. Geckeis, R. Klenze, Th. Fanghänel, J. Phys. Chem. B, 108, 17160-17165 (2004).

[3] D.H. Lee and R.A. Condrate Sr., Mater. Lett., 23, 241-246 (1995).

[4] E. Laiti, P. Persson, L.-O. Öhman, Langmuir, 14, 825-831 (1998).

[5] N. Huittinen, Th. Rabung, J. Lützenkirchen, S.C. Mitchell, B.R. Bickmore, J. Letho, H.

Geckeis, J. Colloid Interface Sci., 332, 158-164 (2009).

[6] G. Lefèvre and M. Fédoroff, Mater. Lett., 56, 978-983 (2002).

[7] T. Kimura and G.R. Choppin, J. Alloys Comp., 213/214, 313-317 (1994).

[8] J.R. Bargar, G.E. Brown Jr., G.A. Parks, Geochim. Cosmochim. Acta, 61, 2617-2637 (1997).; 61, 2639-2652 (1997).

[9] J.R. Bargar, S.N. Towle, G.E. Brown Jr., G.A. Parks, J. Colloid Interface Sci.,185 473-492 (1997).; S.N. Towle, J.R. Bargar, G.E. Brown Jr., G.A. Parks, J. Colloid Interface Sci., 217, 312-321 (1999).

[10] R. Polly, B. Schimmelpfennig, Th. Rabung, M. Floersheimer, R. Klenze, H. Geckeis, Radiochim. Acta, 98, 627-634 (2010).

5.3 Retention of radionuclides by secondary phase formation

F. Heberling, T. Stumpf, K. Holliday, N. Finck, S. Heck, M. L. Schlegel, K. Dardenne, J. Rothe, T. Schäfer, D. Bosbach***

**CEA Saclay, France.*
*** FZJ, Germany.*

Secondary phases may form during the geochemical evolution of a High Level nuclear Waste (HLW) repository system upon alteration of the waste matrix in contact with groundwater. The neoformation of such phases represents a significant retention potential for radiotoxic long-lived radionuclides (RN) in aqueous systems. Besides reactions at the mineral / solution interface, RN binding may occur by incorporation into the bulk structure (coprecipitation), resulting in long-term immobilization, especially if (meta)stable solid-solutions are formed. The mechanism of RN incorporation in selected mineral phases, relevant for the disposal of HLW in deep repositories, is investigated at INE. Most of the activities in this field are related to the retention of actinides, but also to a lesser extent to the binding of long-lived fission products. Molecular-scale information about incorporation processes is obtained by using various complementary spectroscopic techniques. This information is important for the safety assessment of HLW repositories.

Ln(III)/An(III) phosphate bearing mineral phases

Experimental

A 0.6 M La solution doped with Eu was made by dissolving the oxides in a minimal amount of 10 M HNO_3 and diluting with water (18 MΩ). A 4 mL aliquot of the prepared La solution was added to 8 mL of 1 M NaOH. To the well-stirred suspension, 8 mL of $(NH_4)_2HPO_4$ solution (0.27 M) was added. The pH was then adjusted to 12.5 with 4 M NaOH and the solution transferred to a Teflon-lined steel autoclave (Parr Instruments). The autoclave was then heated to 200°C for 2 hours in a box furnace. Once cool, the suspension was centrifuged and supernatant discarded. The solid was suspended with stirring in 25 mL of 0.1 M HNO_3 for 3 days in order to dissolve $La(OH)_3$ created by excess La under hydrothermal treatment. The resulting pure $LaPO_4$ solid was then recovered by centrifugation and dried at 90°C overnight.

TRLFS was performed using a pulsed (20 Hz) XeCl-eximer laser (Lambda Physics, EMG, 308 nm) pumped dye laser (Lambda Scanmate). High resolution fluorescence measurements were recorded by an Andor spectrometer consisting of a polychrometer with 2400 lines/mm holographic grating (Shamrock) and intensified, gated CCD camera (I-Star). The measurements on this system had a maximum resolution of 0.013 nm. The samples were cooled to 4 K by a helium refrigerated cryostat (CTI-cryogenics) to improve resolution.

Results and discussion

The results of site-selective time resolved laser fluorescence measurements of Eu and Cm doped $LaPO_4$ as prepared by hydrothermal synthesis and subsequent sintering are presented here. The major site before and after sintering was found to be the same despite the lower temperature synthesis method. The emission spectra from the major Eu site shows a resolved and fully degenerate 5-fold splitting of the F_2 transition, confirming previously calculated data and proving that Eu was incorporated in the La site through isomorphic substitution (Fig. 1).

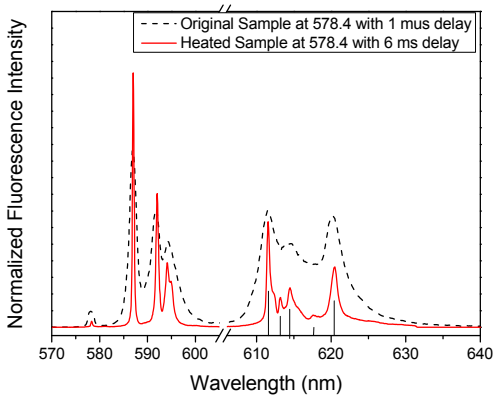

Fig. 1: *Emission spectra of the major Eu species from direct excitation at 578.4 nm before and after sintering $LaPO_4$. The sintered sample confirms previously calculated peak positions (indicated with lines) between 605 and 625 nm.*

This was compared to Cm spectroscopic data to conclude that the major site in Cm:$LaPO_4$ is also Cm substituted on the La site of $LaPO_4$. High resolution direct excitation time resolved laser fluorescence spectroscopy was used to show that this single site of Cm was actually four slightly different environments or satellites as can be seen in Fig. 2. This was concluded to be a difference in the four La sites within a $LaPO_4$ unit cell due to a deviation from the ideal structure which breaks their equivalence.

A minor site was identified in both Eu and Cm samples. The fluorescence lifetime and emission data suggests that the minor site is coordinated to a single hydroxide interstitial. This minor site persisted in the Eu doped sample after sintering, however, the fluorescence lifetime and emission spectra changed. This change in spectra was attributed to a change in the hydroxide interstitial due to heat treatment.

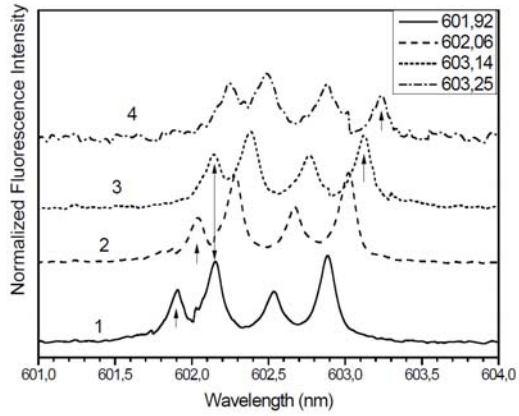

Fig. 2: *High resolution emission spectra from direct excitation of Cm in sintered $LaPO_4$. Single arrows indicate wavelength of direct excitation used to obtain that emission spectrum as listed in the legend. Double arrow indicates position of direct excitation that would excite multiple Cm species yielding more than the maximum four peaks allowed by the ground state splitting of a single species.*

Ln(III)/An(III) clay minerals

Clay minerals may form as secondary phases upon alteration of the HLW waste matrix in the presence of groundwater [1]. For example, the magnesian smectite hectorite is frequently observed in HLW glass corrosion experiments. These minerals have a high affinity for trivalent f-elements. Various distinct molecular-scale binding mechanisms have been identified, but information on the retention by incorporation in the bulk structure is limited. Hectorite was precipitated in the presence of Eu(III) and X-ray absorption spectroscopy (XAS) was used to characterized Eu(III) species during various synthesis steps to track the incorporation mechanism.

Experimental

Hectorite was coprecipitated in the presence of Eu(III) (Eu-Hectorite) following a multi-step synthesis protocol [2]. Briefly, a freshly precipitated Eu(III)-containing brucite precursor was refluxed in the presence of LiF. After 30 minutes a silica sol was added and the suspension reacted for additional 48 hours. The resulting hectorite was washed to remove any remaining precursor phase. Separately, a Eu(III)-containing brucite (Eu-Brucite) was freshly precipitated under identical experimental conditions, europium hydroxide and europium carbonate (Eu-carbonate) [3] were prepared as reference phase. Eu(III) was also sorbed on pre-existing Eu-free hectorite (Eu/Hectorite; m/V ~ 4 g/L; TotEu = 110 µM; pH = 7.0(1); *I* = 0.5 M $NaClO_4$) and on the starting silica sol (Eu/Silica; m/V ~ 4 g/L; TotEu = 100 µM; pH = 5.6(1); *I* = 0.5 M $NaClO_4$). Europium L_{III}-edge XAS data were collected at the ESRF (BM30B beamline) and at the ANKA (INE-Beamline). Conventional powder XAS data were collected for the hydroxide and carbonate reference phases, Eu/Hectorite and Eu/Silica. Polarized XAS [4] data were collected for Eu-Hectorite and Eu-Brucite considering various angles (α) between the electric field vector ***E*** of the X-ray beam and the layer plane.

Results and discussion

XRD – XRD data unambiguously identified the main phase in Eu-Hectorite and in the Eu-free hectorite as clay mineral, and in Eu-Brucite as brucite. The europium hydroxide was identified as $Eu(OH)_3$ and the data collected for the carbonate phase are identical to those reported for $NaEu(CO_3)_2.5H_2O$ [3].

Powder EXAFS – The Fourier transforms (FTs) of the powder EXAFS data (at 35° polarized and powder EXAFS data are identical) collected for all samples are shown Fig. 1. All FTs display a first peak originating from O atoms ligated to Eu(III). For Eu-hectorite, Eu-brucite and Eu/Hectorite, this contribution was modeled considering two subshells of ~2.5 and ~4.5 O atoms at 2.27 Å and 2.42-2.44 Å, respectively. All FTs display contributions at higher distances originating from the presence of next nearest atomic shells. For Eu-Brucite, ~2 Mg backscatterers were detected at 3.32 Å and higher distances O neighbors. These results can best be explained by Eu polyhedra (d(Eu-O) = 2.27 Å) sharing edges (d(O-O) = 2.78 Å) with Mg octahedra (d(Mg-O) = 2.10 Å) in brucite. Whether adsorbed to or coprecipitated with hectorite, successive Mg (3.27-3.28 Å) and Si (3.84-3.87 Å) shells were detected. However, lower Mg coordination numbers were obtained by fitting the data for Eu/Hectorite (~0.4 atom) compared to Eu-Hectorite (1.3 atom), suggesting distinct chemical environment. This shell can also best be explained by considering edge-sharing between Mg octahedra and Eu polyhedra. Finally, compelling formation of hydroxide and/or carbonate phases during the hectorite multi-step synthesis procedure may be ruled out by comparison with the corresponding FTs (Fig. 3).

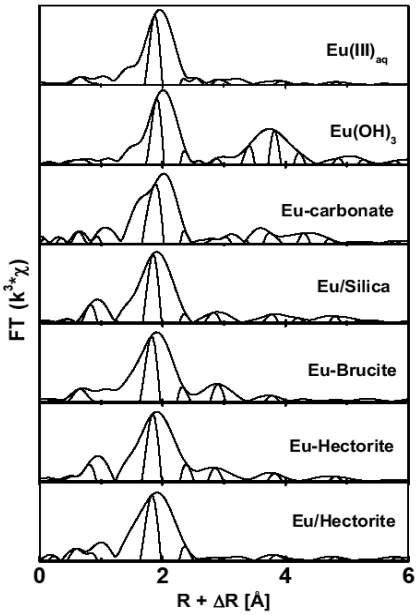

Fig. 3: *FTs of EXAFS data collected for the Eu-containing samples together with the Eu-Hectorite and Eu-Brucite.*

Polarized EXAFS – Polarized EXAFS data were collected for oriented samples of Eu-Brucite and Eu-Hectorite. In a polarized XAS experiment, the absorber-backscatterer pair parallel to ***E*** is probed preferentially. For α < 35°, the contribution of in-plane neighbors may be increased, whereas out-out-plane neighbors are probed preferentially at α > 35° [4].

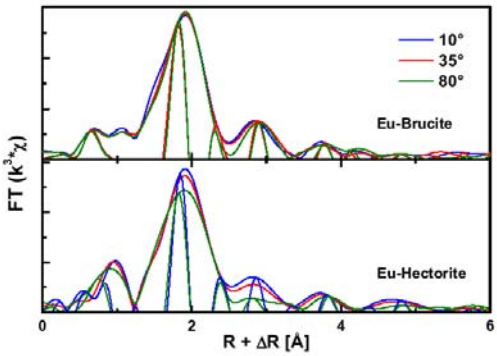

Fig. 4: *FTs of polarized EXAFS data collected for Eu-Brucite and Eu-Hectorite.*

The data collected for Eu-Brucite show weak angular dependence (Fig. 4), suggesting Eu to be located in an isotropic environment. In contrast, the data collected for Eu-Hectorite are clearly angular dependent, suggesting a local anisotropic environment surrounding Eu, and thus a structural association to the solid phase. Furthermore, the decreasing Mg coordination numbers (Fig. 5) with increasing α hints an in-plane orientation of the Mg neighbors.

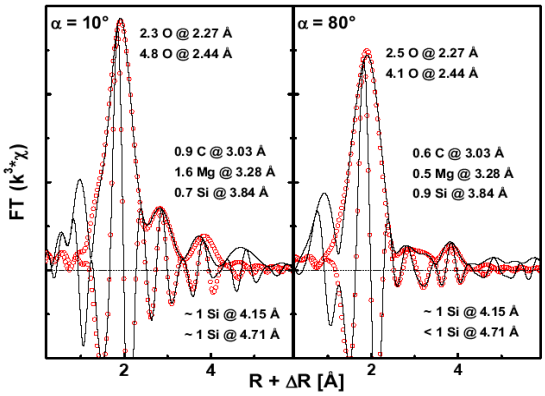

Fig. 5: *Experimental and modeled FTs of Eu-Hectorite EXAFS data collected at α = 10 and 80°.*

Comparison with literature data – These results contrast with previous findings on Lu coprecipitation with hectorite [5]. For Lu, the next nearest Mg and Si shell were detected at 3.12(2) and 3.35(2) Å, respectively. The Si shell is located at a distance that may suggest homovalent substitution of Lu(III) for Mg structural site, implying (nearly) complete crystallization of hectorite from the precursor phase. For Eu(III), at least part of the cations may be located in the brucite octahedral layer, but in a highly distorted site as evidenced from the split O shell. This geometrical constrain may prevent from clay crystallization in the close vicinity of Eu(III). This may best account for the very similar first coordination shell in Eu-Brucite and Eu-Hectorite, and the absence of close Si shell compared to undoped hectorite (3.25 Å [6]).

Incorporation of selenium in mineral phases

Selenium-79 is a long-lived fission product ($T_{1/2}$ ~ $3.27x10^5$ a) with a significant contribution to the long-term radiotoxicity of HLW. Its chemistry is similar to that of sulfur and its solubility is strongly dependent on the pH – Eh conditions. Under oxidizing conditions, the oxyanions selenate (SeO_4^{2-}) and selenite (SeO_3^{2-}) are the dominating species. They are expected to be highly mobile. In contrast, elemental selenium and selenide species (Se(-II)) occur as solids with low solubility [7]. Consequently, depending on the environmental conditions, different phases may account for effective Se immobilization.

Se(-II) – iron sulfides

Under reducing conditions, Se is expected to occur in low oxidations sate (0, -II). Under these conditions, mackinawite (FeS) is the first iron sulfide to form under ambient conditions. The retention of selenide by coprecipitation with FeS (Se-Mackinawite) was investigated. Separately, a Fe(II) solution was added to a Se(-II) solution (sample $FeSe_x$). The solid

phases could hardly be identified by XRD. Information on the Se oxidation state and on its chemical environment was obtained by collecting XAS data at ANKA (INE-Beamline). In the XANES region, the data point to the presence of Se(-II) species, as the *K*-edge position depends on the Se oxidation state (Fig. 6) [8]. In Se-Mackinawite, only Fe atoms were detected in the Se first coordination sphere, ruling out the presence of Se(0) (Fig 7). Only S and Fe atoms were needed to model next atomic shells, pointing to the presence of Se in a FeS-like environment and ruling out the formation of a FeSe-like phase.

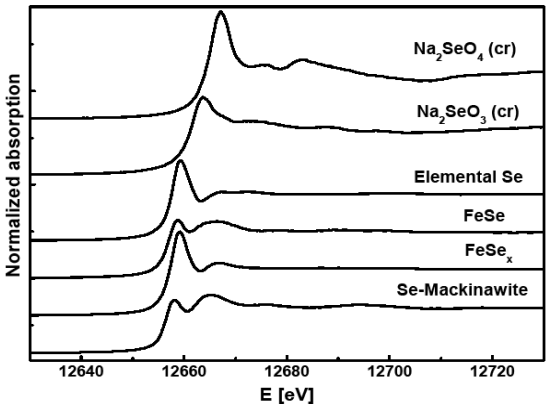

Fig. 6: *Se K-edge XANES region for references and both experimental samples.*

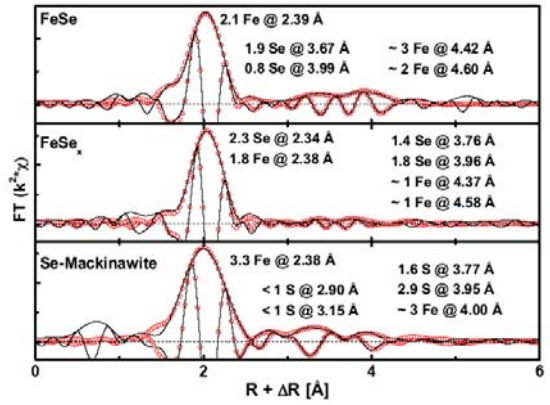

Fig. 7: *Experimental and modeled FTs of Se K-edge XAS data.*

Selenite-calcite interactions

The oxidized selenium species selenite $Se(IV)O_3^{2-}$ and selenate $Se(VI)O_4^{2-}$ are expected to be highly mobile in subsurface environments [9]. The question of how contaminant species migrate in groundwater aquivers is largely a question of how they interact with mineral surfaces. Here we investigate how selenite interacts with calcite surfaces and research its potential to be incorporated into the calcite crystal structure.

In batch-type adsorption experiments at calcite equilibrium conditions and trace Se concentrations (~10^{-13} mol/L) very limited adsorption of Se(IV) at the calcite surface is observed. Below pH 9, K_D values are in the range 1-2*10^{-3} L/g. Above pH 9 no adsorption is observed. These results contradict previously published experimental adsorption data [10], where at comparable reactive surface area and much higher Se concentrations (10^{-7} – 10^{-6} mol/L) higher relative adsorption (~7 * 10^{-3} L/g) is reported. The reason for this discrepancy is not yet known. Grazing incidence Se K-edge EXAFS spectra measured in-situ at the calcite(104) surface in contact to a calcite equilibrated solutions at pH 7.5 and 8.3 containing 10^{-3} mol/L Se(IV) are not significantly different from EXAFS spectra of aqueous Se(IV).

Upon coprecipitation with calcite in mixed flow reactor (MFR) experiments considerable amounts of Se(IV) can be incorporated into the calcite crystal structure. Se(IV) doped calcite crystals grown at room temperature at surface controlled growth conditions, slow growth rates (~10^{-9} – 10^{-8} mol/(m^2s)), and low calcite supersaturations (SI(calcite): ~0.7 – 1.0) can contain up to ~6 % selenium. Se K-edge EXAFS analyses (see k^3-weighted k- and R-space EXAFS data and models in Fig. 8 a and b) reveal that Se(IV) in calcite occupies a slightly distorted carbonate lattice site. This result is in perfect agreement with previously published data [11].

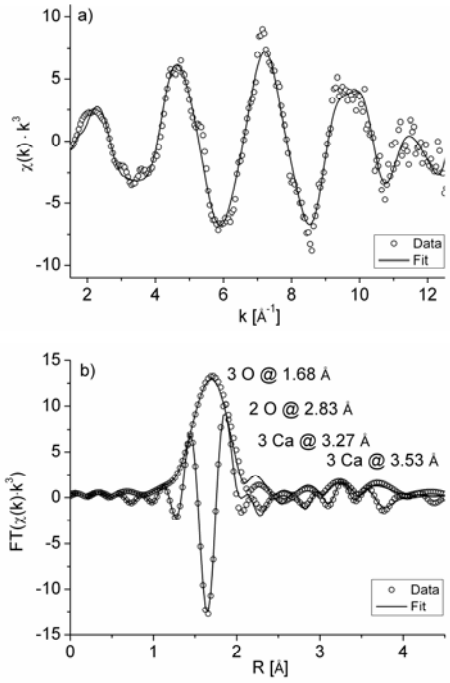

Fig. 8: *K- and R-space data and modelled Se K-edge EXAFS spectra of Se(IV) doped calcite.*

An interesting effect is observed in polarization dependent grazing incidence Se K-edge

XANES spectra measured at the calcite(104) surface in contact to a Se(IV) containing solution. The difference between this sample and the pure adsorption samples described above, where no interaction between Se(IV) and calcite could be detected, is, that starting from an equilibrated solution with pH 7.5 the pH was in this case increased to pH ~ 8 by addition of NaOH in order to achieve an SI(cacite) ~ 0.6. With the increasing SI, calcite precipitation starts and selenite is coprecipitated with calcite. As selenite substitutes for carbonate in the freshly grown calcite it becomes ordered with respect to the calcite substrate. This ordering is observable in the polarization dependent grazing incidence XANES spectra shown in Fig 9. The two spectra are measured on the same sample the blue curve corresponds to measurements where the polarization vector, ε, of the incoming x-rays is parallel to the crystallographic [010] direction of calcite (named b) while the purple curve corresponds to measurements where the polarization vector, ε, of the incoming x-rays is parallel to the crystallographic [42-1] direction of calcite (named a). Following the hypothesis that selenite substitutes for carbonate in calcite, this means that the predominant pre-edge feature observable in the blue spectrum originates from the preferred excitation to bound states (Se-O bonds) in the selenite molecule.

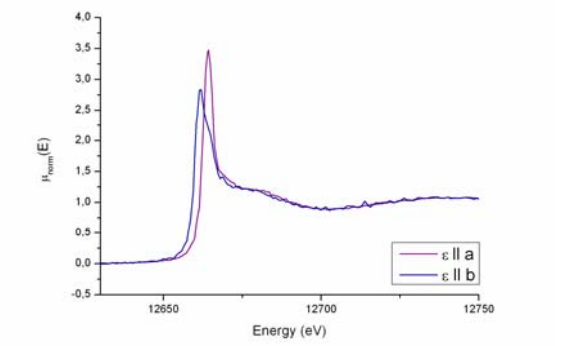

Fig. 9: *Polarization dependent grazing incidence XANES spectra of Se(IV) coprecipitated with a (104) oriented calcite single crystal surface.*

References

[1] A. Abdelouas, J.-L. Crovisier, W. Lutze, B. Grambow, C.-J. Dran, R. Müller, Surface layers on a borosilicate nuclear waste glass corroded in $MgCl_2$ solution. Journal of Nuclear Materials, 240, (2) 100-111 (1997).

[2] K.A. Carrado, P. Thiyagarajan, K. Song, A study of organo-hectorite clay crystallization. Clay Minerals, 32, (1) 29-40, (1997).

[3] V. Philippini, T. Vercouter, A. Chaussé, P. Vitorge, Precipitation of $ALn(CO_3)_2{,}xH_2O$ and $Dy_2(CO_3)_3xH_2O$ compounds from aqueous solutions, Journal of Solid State Chemistry, 181, (9) 2143-2154 (2008).

[4] M.L. Schlegel, A. Manceau, D. Chateigner, L. Charlet, Sorption of Metal Ions on Clay Minerals: I. Polarized EXAFS Evidence for the Adsorption of Co on the Edges of Hectorite Particles. Journal of Colloid and Interface Science, 215, (1) 140-158 (1999).

[5] N. Finck, M.L. Schlegel, D. Bosbach, Sites of Lu(III) Sorbed to and Coprecipitated with Hectorite. Environmental Science & Technology, 43, (23) 8807-8812 (2009).

[6] W. Seidl, J. Breu, Single crystal structure refinement of tetramethylammonium-hectorite. Z. Kristall., 220, (2-3) 169-176 (2005).

[7] M.A. Elrashidi, D.C. Adriano, S.M. Workman, W.L. Lindsay, CHEMICAL-EQUILIBRIA OF SELENIUM IN SOILS - A THEORETICAL DEVELOPMENT. Soil Sci., 144, (2) 141-152 (1987).

[8] I.J. Pickering, G.E. Brown, T.K. Tokunaga, Quantitative Speciation of Selenium in Soils Using X-ray Absorption Spectroscopy. Environmental Science & Technology, 29, (9) 2456-2459 (1995).

[9] P.H. Masscheleyn, R.D. Delaune, W.H. Patrick, Transformations of selenium as affected by sediment oxidation-reduction potential and pH. Environmental Science & Technology, 24, (1) 91-96 (1990).

[10] C.E. Cowan, J.M. Zachara, C.T. Resch, Solution ion effects on the surface exchange of selenite on calcite. Geochimica et Cosmochimica Acta, 54, (8) 2223-2234 (1990).

[11] G. Aurelio, A. Fernandez-Martinez, G.J. Cuello, G. Roman-Ross, I. Alliot, L. Charlet, Structural study of selenium(IV) substitutions in calcite. Chem. Geol., 270, (1-4) 249-256 (2010).

6. Applied Studies: Radionuclide retention in the multi-barrier system

The multi-barrier system of a nuclear waste disposal consists of a variety of components with specific characteristics and properties. Investigation and quantification of their respective retention functions require different approaches, methods, analytical techniques and models. A series of studies on subsystems of the multi-barrier system are performed in the scope of international co-operations. In the shielded cells of INE, the behaviour of spent nuclear fuel in high pH solutions was investigated and new studies with glass samples from the vitrification process at VEK are in preparation. For cemented low level and intermediate level wastes (LLW/ILW), sorption studies with Am onto corroded cement phases were completed showing extremely high retention even in high saline solutions relevant for LLW/ILW disposal in rock salt (e.g. Asse II salt mine). The impact of colloids onto the radionuclide migration was studies covering the FEBEX bentonite colloid stability in Grimsel ground water as well as migration experiments (CFM) under near-natural flow conditions using Eu, Tb, Hf and Th as chemical homologues. Concerning argillaceous host rocks, organic matter was extracted from the Callovo-Oxfordian (COx) formation, clay – organic matter model substances were synthesized and the influence of the preparation procedure on the metal-humic acid complex formation was quantified. The modelling activities covered thermodynamic equilibrium calculations on cement corrosion in $MgCl_2$ solutions, the migration of nano-particles in a natural granite fracture by means of a comparison between experimental results and 3D CFD models based on µCT data and the 3D simulation for the long-term behaviour of a real underground structure in rock salt.

6.1 Key processes influencing corrosion of highly active waste forms

A. Loida, E. Bohnert, C. Bube, E. Janata, M. Kelm, B. Kienzler, V. Metz, N. M ller and E. Soballa*

* Helmholtz-Zentrum Berlin für Materialien und Energie, Solar Energy, Berlin

Corrosion behaviour of spent nuclear fuel in high pH solutions

Introduction

Boom clay is presently considered as site for disposal of high level wastes in Belgium. In the underground host rock laboratory HADES, the thermo-mechanical, hydraulic and geochemical properties of this host rock are under investigation for 30 years. The Boom clay site is situated at a depth of ~200 m. It has a low degree of induration, about 40 wt.% of swelling clay minerals and a water content of $\geq$ 20 wt%. For disposal of spent nuclear fuel (SNF), a specific disposal concept was developed. In the context of this concept, corrosion studies with SNF under the expected geochemical conditions have been conducted.

The Belgian "Supercontainer Design"

In Belgium, the Supercontainer design is investigated as a possible option for the deep disposal of spent nuclear fuel (SNF). It comprises the encapsulation in a carbon steel overpack surrounded by concrete buffer called "supercontainer" [1]. After re-saturation of the engineered barriers, the pore water composition will alter by interactions with concrete. The altered pore water is simulated by an "Evolved Cement Water" (ECW) which represents an advanced degree of concrete alteration. The ECW is characterized by a high pH value (pH 12.5), the main constituents NaOH, $Ca(OH)_2$, KOH and virtually the absence of carbonate. Due to the slow corrosion rate of the canister materials [2] under highly alkaline conditions, the SNF could come in contact with the evolved highly alkaline solution.

Recently, the corrosion behaviour of SNF in an ECW-type solution (16 mM NaOH, 14 mM $Ca(OH)_2$, 0.2 mM KOH) was studied experimentally at INE [3]. In this study, concentrations of U were found close to 10^{-9} M in the leachant. Concentrations of Tc, Pu, Am and Np were close to or below the detection limit after > 450 days of experimental duration. Based on the release rates of Sr, dissolution rates of the SNF matrix were calculated in the range of 10^{-7}/d [3]. The experimental observations indicate strong retention effects of the actinides. The aim of the present work is to study the behaviour of SNF (i) under the influence of H_2 overpressure resulting from the corrosion of the Fe based canister, and (ii) in a different type of pore water, i.e. "Young Cement Water with Ca" (YCWCa). YCWCa solution is dominated by KOH and NaOH, whereas Ca, Al, Si, sulphate and dissolved inorganic carbon are minor components or

present in trace concentrations. The pH of the YCWCa (pH = 13.5) is unit more alkaline than the pH of the "ECW" solution [4]. In the present study, a YCWCa-type solution with 370 mM KOH, 136 mM NaOH, 2.0 mM Na_2SO_4, 0.4 mM $Ca(OH)_2$ and 0.3 mM $CaCO_3$ was used. Compositions of ECW-type and YCWCa-type solutions were defined by SCK·CEN [4].

Experimental approach

High burnup LWR-UO_2 SNF from the PWR power plant Gösgen, Switzerland (burnup 50400 MWd/tHM) was used for the experiments. More details are given in reference [3]. Two SNF slices, denoted "2K11a" and "2K11b", were prepared for the corrosion experiments. Sample 2K11a was exposed to ECW-type solution and sample 2K11b to YCWCa-type solution, respectively.

Both experiments were performed in 250 ml Ti lined stainless steel autoclaves. The experiments under H_2 overpressure were started after a 4 days cleaning procedure with DIW and wash cycles over 21 days in ECW-type or YCWCa-type solutions. The experiments were started at 1 bar pH_2 for the first 253 days. Then pH_2 of 3.2 bars was applied for the following 173 days. The release of radionuclides was measured by sampling and analyzing the free gas phases and the solutions during the cleaning and wash cycles, and 58 d, 181 d, 253 d, 343 d and 426 d after start of the experiments under H_2 over-pressure. Detailed descriptions of the sampling and analytical procedures are given in [5]. After termination of both experiments, the solid materials (fuel and Ti samples) were recovered for further studies.

Results

Figure 1 shows the releases of various radionuclides during the entire experiment "2K11a" in ECW-type solution in terms of FIAP or FIGP[1] values as functions of time. Due to pH_2 application the ^{99}Tc concentration changed: From $4.3x10^{-8}$ M ($FIAP_{Tc-99}$ $2.5x10^{-4}$) after the wash cycle without H_2 to $<10^{-9}$ M (detection limit) in the first interval of the corrosion experiment at 1 bar pH_2.

Special attention is attributed to the release of ^{90}Sr. In the first observation interval of 58 days after the end of the wash cycles and application of H_2 overpressure, the ^{90}Sr concentration in Fig. 1 shows a slight decrease. After 181 days, the ^{90}Sr concentration increases by a factor 3 ($FIAP_{Sr-90}$ $1.1x10^{-5}$ to $3.8x10^{-5}$), and remains on this level ($FIAP_{Sr-90}$ $4.1x10^{-5}$) until the end of the experiment. This finding is interpreted as a decreasing matrix dissolution rate (~10^{-8}/day). The ^{137}Cs release shows similar time dependence as ^{90}Sr, however, at a higher concentration level. The concentration remains at a constant level of $FIAP_{Cs-137}$ ~10^{-3} from 253 days until the end of the experiment. The initial concentration of ^{238}U in solution under H_2 overpressure is found to be low ~$1.9x10^{-10}$ M, the calculated $FIAP_U$ is ~$6.3x10^{-9}$. Concentrations of Tc, Np, Pu and Am are found to be below their detection limit.

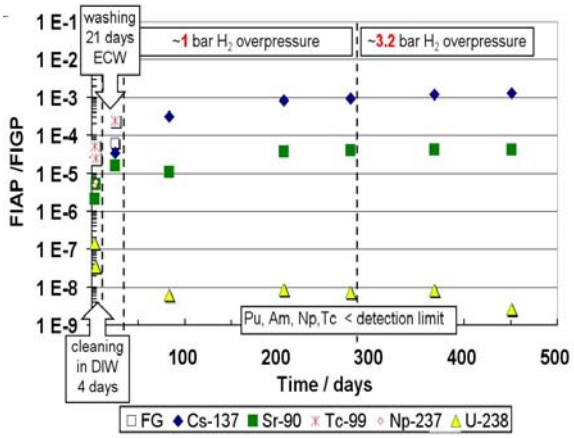

Fig. 1: *Release of radionuclides during the consecutive steps of the experiment in ECW-type solution (SNF sample 2K11a, externally applied H_2).*

The release of radionuclides from SNF sample 2K11b in contact with YCWCa-type solution at pH 13.5 is shown in Figure 2. Due to pH_2 application ^{99}Tc concentration drops from $8.2x10^{-8}$ M ($FIAP_{Tc-99}$ $4.8x10^{-4}$) to $6.9x10^{-9}$ M after the first 58 days and below detection limit during following the static stage of the test. A significant decrease of the ^{238}U concentration from $4x10^{-7}$ to $1.5x10^{-9}$ M is found under H_2 overpressure in the course of this experiment.

^{90}Sr concentration also decreases under these conditions from $1.2x10^{-9}$ to $1.4x10^{-10}$ M over the static period. The decrease of the ^{90}Sr concentrations with time is not yet understood. After the washing cycles, the leachants are replaced, so, a lower concentration of ^{90}Sr at the next sampling can be explained. However, the ^{90}Sr behaviour during the static experiment after the first sampling is interpreted with a different reaction process, such as precipitation or sorption. For this reason, ^{90}Sr release cannot be used to estimate reliably the matrix dissolution rate in the experiment with YCWCa-type solution.

The solution concentrations of radionuclides at the end of both experiments after 426 days are summarized in Table 1.

[1] FIAP or FIGP: Fraction of the inventory in the aqueous (gas) phase

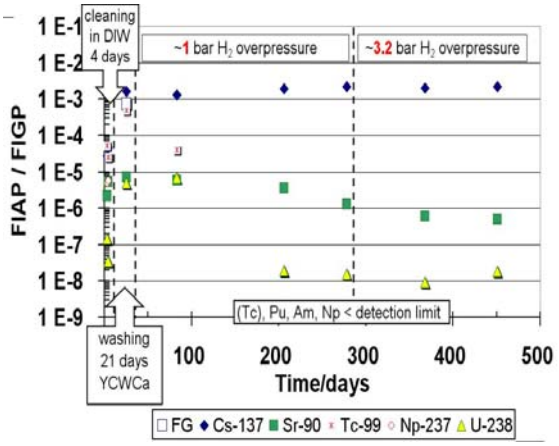

Fig. 2: *Release of radionuclides during the consecutive steps of the experiment in YCWCa-type solution (SNF sample 2K11b, externally applied H_2).*

	2K11a (ECW)	2K11b (YCWCa)
Cs	$8.0x10^{-7}$	$1.4x10^{-6}$
Sr	$1.2x10^{-8}$	$1.4x10^{-10}$
Am	$<1x10^{-10}$	$<1x10^{-10}$
Pu	$<3x10^{-10}$	$<3x10^{-10}$
Np	$<3x10^{-11}$	$<3x10^{-11}$
U	$2.1x10^{-10}$	$1.5x10^{-9}$

Tab. 1: *Solution concentrations in mol/L of radioelements at the end of spent fuel corrosion in ECW-type solution at pH 12.5 and YCWCa-type solution at pH 13.5 (total time since start of the static stage: 426 days).*

Summary and concluding remarks

Due to the external H_2 overpressure during 426 days of the SNF corrosion experiments in ECW-type and YCWCa-type solution, a fast decrease of ^{99}Tc concentrations in both experiments below detection limit is observed. ^{238}U concentrations decreased distinctly to $1.5x10^{-9}$ (in YCWCa-type solution), and to $2.1x10^{-10}$ M (in ECW-type solution). An explanation for the higher uranium concentration in the YCWCa-type solution may be attributed to the presence of U(IV) carbonato complexes [6,7]. In contrast to ECW-type solution, the YCWCa-type solution contains CO_3^{2-} in trace concentration.

The release of ^{90}Sr in ECW-type solution is relatively low ($FIAP_{Sr\text{-}90}$ ~10^{-8}/day) over the whole test duration. ^{90}Sr concentrations in YCWCa-type solution decrease significantly, probably caused more by redox-insenstive precipitation or sorption phenomena rather than by an effect of H_2 overpressure on the SNF corrosion. In the experiment with YCWCa-type solution, the ^{90}Sr cannot be used as matrix degradation indicator. The release of ^{137}Cs from SNF in ECW-type solution is similar to the ^{137}Cs release in YCWCa-type solution. The overall results indicate that the matrix dissolution rates are similar in both SNF corrosion experiments.

Planned studies on real HLW glass from the VEK

Since more than 30 years, leaching and corrosion studies have been performed using mainly simulated borosilicate glasses in the institute. The investigations covered the mobilization of radionuclides but also the influence of radiation on the stability of HLW glass. Meanwhile a huge database exists which covers the interactions and release of nuclides. Unfortunately, most of the investigations have been performed with simulated glasses and the verification of the existing data by test with real HLW glasses is still pending.

In 2010, the vitrification process of liquid high-level waste was completed at the Verglasungseinrichtung Karlsruhe (VEK) and the glass canisters were ready for transportation [8]. During the vitrification process, VEK was required to save retain samples which had to be disposed of into the last canister. In order to get access to this rarely available material, it was decided to transfer some samples in the INE lab and to initiate an investigation program.

Transfer of HLW glass samples to INE

It was intended to get representative sample, which are typical products arising from reprocessing of spent nuclear fuel. Therefore, samples were selected for which a constant course of the vitrification took place without any interventions such as replacement of the off-gas tubes or agitation with N_2. Sample from the glass canisters # 23, # 57 und # 71 were chosen. Sample # 71 is shown in Fig. 3.

The samples were prepared at VEK, transferred to the on-site WAK reprocessing plant and transported in shielded casks to INE. The dose rate of each sample was ~500 mSv/h in contact (see Tab. 2).

In a first step, the characteristics of the solid glass samples will be investigated by Raman, SEM-EDX and XPS. Afterwards, long-term leaching/corrosion tests will be conducted.

Fig. 3: *Photo of the HLW glass sample #71*

Sample	Mass / g	Dose rate mSv/h
# 23 (3 fragments)	0.4365	450
# 57 (1 big, 2 small fragments and particles)	1.033	500
# 71 (1 fragment)	0.750	500

Tab. 2: *Mass and dose rate of the HLW glass samples.*

Interaction of hydrogen with radiolysis products in NaCl solution

Hydrogen effect on radiolytic enhanced spent nuclear fuel corrosion

Radiolysis studies and leaching experiments with spent nuclear fuel and UO_2(s) indicate that molecular hydrogen both impedes radiolytic decomposition of the studied formation water simulates and considerably inhibits corrosion of the UO_2(s) matrix of spent nuclear fuel ([9, 10, 11, 12] and references therein). Still, there is insufficient knowledge about the molecular mechanisms of the protective hydrogen effect on SNF corrosion. A recent international benchmark study on modeling of spent nuclear fuel corrosion shows that model uncertainties are still very large, especially regarding the effect of hydrogen as well as the respective parameters of the radiolytic reactions [13].

Various research studies have been dedicated to examine the influence of molecular hydrogen on the radiolysis of pure water (e.g. [14, 15, 16, 17]). To the present knowledge, a single reaction accounts for the influence of molecular hydrogen on radiolysis of aqueous solution:

$$^{\bullet}OH + H_2 = H_2O + H^{\bullet} \qquad (1)$$

Ultimately, this reaction converts oxidizing $^{\bullet}OH$ radicals into reducing $H^{\bullet}$ radicals. The aim of our study is to examine the effect of molecular hydrogen in NaCl solution.

Pulse radiolysis study on hydrogen effect in NaCl solutions

In pulse radiolysis experiments at 22 °C production and decay of $Cl_2^{\bullet-}$ radicals were studied in 0.1 and 1.0 molar NaCl solutions by observing its optical absorption over a time span of 20 ms. In addition to experiments with NaCl solutions equilibrated with N_2O at ambient pressure, a series of experiments were conducted with NaCl solutions equilibrated at 10 MPa hydrogen partial pressure and 0.1 MPa N_2O partial pressure.

The results of the pulse radiolysis experiments were compared to model predictions. To improve the accuracy of the simulations, we screened the widely used reaction scheme of Sunder and Christensen [18] and revised the rate constants of reactions, which are strongly affected by the presence of hydrogen in NaCl solutions. Finally, we took into account 31 reactions of primary radiolysis products and consecutive reactions between these products. These reactions are the basis for radiolysis reactions in chloride bearing groundwater.

In the presence of hydrogen, the $Cl_2^{\bullet-}$ yield was significantly reduced compared to that in hydrogen free experiments. The effect of hydrogen on the radiolytic yield is more pronounced in 0.1 molar NaCl solution (Fig. 4) than in the relatively concentrated NaCl solution.

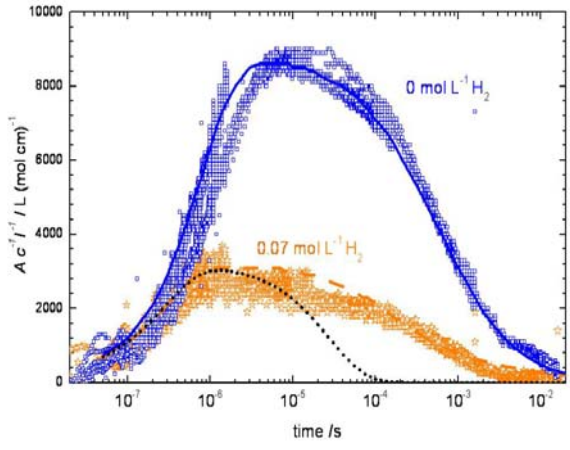

Fig. 4: *Effect of H_2 on normalized absorbance ($A \cdot c^{-1} \cdot l^{-1}$) in 0.1 molar NaCl solution. The continuous and the dashed lines denote simulations with the revised reaction scheme of Kelm et al. [19]; the dotted line denotes the simulation taking into account reaction (2) (see text).*

Comparing measured and simulated absorption of $Cl_2^{\bullet-}$ as a function of time, the

rate constant of reaction $Cl_2^{\bullet-}$ + $Cl_2^{\bullet-}$ = Cl^- + Cl_3^-, is determined as k = 5.2(±0.8)·10^8 dm^3 mol^{-1} s^{-1} at zero ionic strength. This value is within the range of published rate constants for the $Cl_2^{\bullet-}$ disproportionation reaction (Fig. 5).

In order to estimate whether reaction

$Cl_2^{\bullet-} + H_2 = H^{\bullet} + HCl + Cl$ (2)

postulated by Kelm and Bohnert [20], affects the radiolysis of aqueous chloride solution in the presence of hydrogen, we simulated the experiments with k_2 in the range of 0 dm^3 mol^{-1} s^{-1} (value of the revised data-set) to 4.3·10^5 dm^3 mol^{-1} s^{-1} (value proposed by Kelm and Bohnert).

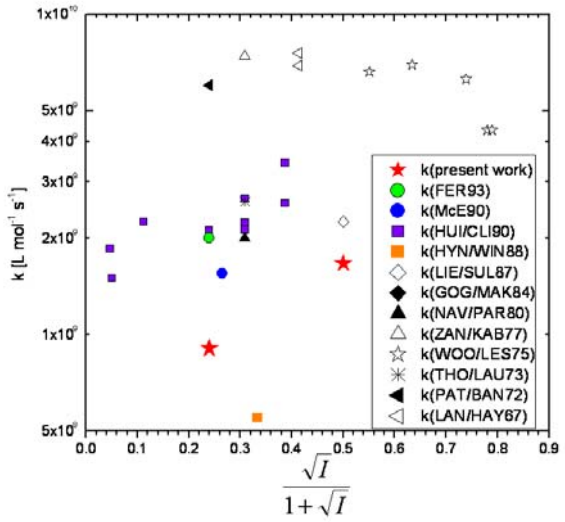

Fig. 5: *Rate constants for reaction* $Cl_2^{\bullet-}$ + $Cl_2^{\bullet-}$ = Cl^- + Cl_3^- *as function of I = ionic strength). Filled stars denote rate constants determined in the present work, other symbols denote rate constants determined in previous studies. Abbreviations and references of publications are given in Kelm et al. (2011) [19].*

When considering the postulated reaction (2), the simulations for 0.1 and 1.0 molar NaCl solution show considerable discrepancies from the measured data with respect to the decay of the normalized absorbance for $k_2 \geq 1 \cdot 10^4$ dm^3 mol^{-1} s^{-1} (e.g. see dotted line in Fig. 4; experiment with 0.1 molar NaCl). At lower k_2 values, the simulations are within error the same as for k_2 = 0 dm^3 mol^{-1} s^{-1}. Consequently, reaction (2) is too slow to significantly affect the decay of $Cl_2^{\bullet-}$. This finding is in agreement with the observed decay of $Cl_2^{\bullet-}$ in experiments with hydrogen in 0.1 and 1.0 molar NaCl solution, which is controlled by a second order reaction (Fig. 4). In case reaction (2) took effect on the $Cl_2^{\bullet-}$ concentration, the decrease in absorption would follow a pseudo first order rate law. It is concluded that H_2 interacts radiation chemically solely with the $^{\bullet}OH$ radical via reaction (1) even in a solution containing 1.0 mol/L chloride.

Acknowledgement

The financing of the spent nuclear fuel corrosion experiments by ONDRAF/NIRAS, Brussels (B) is gratefully acknowledged.

References

[1] R. Gens, J. Bel, A. Pourbaix, M. Hélie, S.Wickham and D. Bennett, Journal de Physique IV (Proceedings), 136, 13-23 (2006).

[2] B. Kursten et al., Sixth International Conference on the Management and Disposal of Radioactive Waste, Luxembourg, pp. 428-453 (2004).

[3] A. Loida, R. Gens, V. Metz, K. Lemmens, C. Cachoir, T. Mennecart, B. Kienzler, Mat. Res. Soc. Symp. Proc. 1193, 597-604 (2010).

[4] C. Cachoir, Preparation of Evolved Cement Water (ECW) and Young Cement Waters (YCW and YCWCa) for the Supercontainer experiments, SCK·CEN Work Instruction IW.W&D.0009 (2006).

[5] B. Grambow, A. Loida, P. Dressler, H. Geckeis, J.Gago, I. Casas, I., J. de Pablo, J.Gimenez, M.E. Torrero, Forschungszentrum FZKA report 5702 (1996).

[6] I. Grenthe, J. Fuger, R.J.M. Konings, R.J. Lemire, A.B. Muller, C. Nguyen-Trung, H. Wanner, Chemical thermodynamics of uranium. Elsevier Science Publ., Amsterdam, Netherlands (1992).

[7] R. Guillaumont, T. Fanghänel, J. Fuger, I. Grenthe, V. Neck, P.D. Palmer; M.H. Rand, Update on the chemical thermodynamics of uranium, neptunium, plutonium, americium and technetium. Elsevier Science Publ., Amsterdam, Netherlands (2003).

[8] J. Fleisch, W. Grünewald, G. Roth, F. J. Schmitz, W. Tobie, M. Weishaupt, Waste Management Conference WM-2011, Phoenix, USA (2011).

[9] J. Bruno and R. Ewing, Elements 2, 343-349 (2006).

[10] P. Carbol et al., Geochimica et Cosmochimica Acta, 73, 4366-4375 (2009).

[11] Fors, P., Ph. D. thesis, Chalmers University of Technology, Göteborg, Sweden (2009).

[12] D. Cui, E. Ekeroth, P. Fors, K. Spahiu, Mat. Res. Soc. Symp. Proc. 1104, 87-99 (2008).

[13] J. Bruno, J. Merino, A. Tamayo, C. Ferry, J. Quinones, E. Iglesias, N. Rodriguez Villagra, J. M. Nieto, A. Martínez-Esparza, A. Loida, V. Metz, M. Jonsson, and E. Ekeroth, MICADO, Deliverable 3.1. European Commission, Brussels (2009).

[14] D. Bunn, F.S. Dainton, G.A. Salmon, T.J. Hardwick, Transactions of the Faraday Society 55, 1760-1767, 1959.

[15] H. Christensen and K. Sehested, Journal of Physical Chemistry 87, 118-120 (1983).

[16] K.H. Schmidt, Journal of Physical Chemistry 81, 1257–1263 (1977).

[17] J.K. Thomas, Transactions of the Faraday Society 61, 702-707 (1965).

[18] S. Sunder and H. Christensen, Nuclear Technology 104, 403-417 (1993).

[19] M. Kelm, V. Metz, E. Bohnert, E. Janata, C. Bube, Radiation Physics and Chemistry 80, 426-434 (2011).

[20] M. Kelm and E. Bohnert, Journal of Nuclear Materials 346, 1-4 (2005).

6.2 Actinide retention in cemented nuclear waste forms

C. Bube, E. Bohnert, B. Kienzler, V. Metz, M. Plaschke, D. Schild, M. Schlieker and E. Soballa.

Introduction

Cementation is a common method to treat and solidify low and intermediate radioactive waste (LLW/ILW). Alteration of actinide bearing cement products in diluted aqueous solutions has been studied quite extensively. Yet, in chloride-rich solutions, which are relevant for final LLW/ILW disposal in rock salt, there is still a lack of thermodynamic data and understanding with respect to both cement corrosion and radionuclide behaviour. In the present work, alteration of hydrated Ordinary Portland Cement (OPC) in $MgCl_2$-rich brine has been studied experimentally and by using thermodynamic equilibrium calculations. In addition, Am(III) retention by cement corrosion products has been quantified from experiments with equilibrated cement corrosion products.

Experimental Materials and Methods

OPC CEM I 32,5R was used to produce hardened cement paste with a water / cement ratio of W/C = 0.4. In a series of radionuclide-free ("inactive") batch experiments, powder aliquots of the cement paste were leached in so-called R-brine for 200 to 1327 days. The composition of R-brine in mol (kg H_2O)$^{-1}$ is as follows: Mg^{2+}: 4.9, Na^{+}: 0.2, K^{+}: 0.1, Cl^{-}: 10.0, SO_4^{2-}: 0.4. Cement brine equilibration was studied in four binary systems, having ratios of cement paste mass to brine volume of m/V = 0.45, 0.65, 0.75 and 1.00 g mL^{-1}. Approaching equilibrium was monitored by probing the compositions of both the altered solution and the altered solid. After equilibration of the systems with m/V = 0.45 and 1.00 g mL^{-1}, they were doped with small quantities of acidic ^{241}Am(III) and ^{243}Am(III) solutions (10^{-9}, 10^{-8} and 10^{-7} mol (kg H_2O)$^{-1}$). Am concentrations and solution composition were monitored for 1000 days in these "active" batch experiments. Cement alteration and sorption experiments were carried out in glove boxes under Argon flow at room temperature (pO_2 < 5 ppm, pCO_2 < 5 ppm).

Modeling

Thermodynamic equilibrium calculations were performed using the software code "The Geochemist`s Workbench" (GWB) [1]. The applied thermodynamic database was based on the "HMW84" dataset provided by Harvie et al. (1984) for the Na-K-Mg-Ca-H-Cl-SO_4-OH-HCO_3-CO_3-CO_2-H_2O system [2]. The HMW84 data set was extended for aqueous Al [3] and Si [4] data as well as for a number of solid phases, which are relevant in cementitious environments (data of [4], [5], [6], [7], [8]). Pitzer-parameters are taken from Harvie et al. (1984) [2] and Reardon (1990) [9].

Results and discussion

Due to dissolution of portlandite, ettringite and other solid cement phases, the initially $MgCl_2$-rich solution altered to alkaline $CaCl_2$-rich solutions. Mg^{2+} from the solution was exchanged against Ca^{2+} from the solid phase. Besides reprecipitation of gypsum, formation of hydrotalcite phases, Mg-Ca-Al hydroxochloride and brucite was observed. Compositions of the altered solution and solid phases depend strongly on the cement / brine ratio (Fig. 1 and 2).

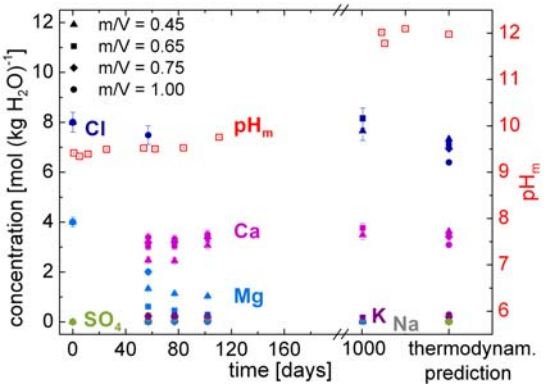

Fig. 1: *Change of solution composition in binary cement / R-brine systems as function of time.*

In all systems, a distinct increase in measured pH_c (i.e., -log(m_{H+})) was observed within the first 102 days (Fig. 1). In the systems with a cement / brine ratio of 0.45 ≤ m/V ≤ 0.75 g mL^{-1}, pH_c measured after 102 days was still about one unit lower than at a later stage (1000 days). Fastest cement alteration kinetics was found in the system with the highest initial cement mass relative to the brine volume (m/V = 1.0 g mL^{-1}), where measured pH_c attains a constant level within the first three months of the experiment. In the long term, the equilibrated solutions were strongly alkaline $CaCl_2$-rich solutions that reached pH_c values of ~11.5 at the higher ratios of cement / brine (≥ 0.65 g mL^{-1}), while at the lowest ratio (0.45 g mL^{-1}), final pH_c values were ~10 (Fig. 2). At the end of the inactive experiments, the solids were composed of alteration products; primary clincer phases and cement hydration phases (e.g. portlandite and ettringite) were absent in the final solid samples.

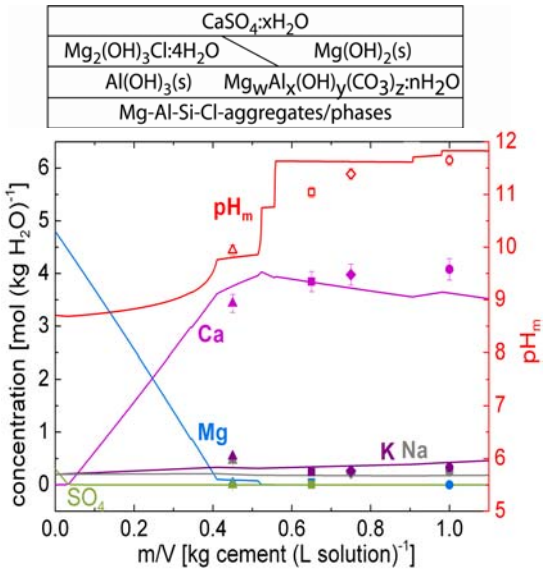

Fig. 2: *Solution compositions from equilibrium calculations for different cement / brine ratios (lines) compared to solution compositions measured at the end of inactive batch experiments (symbols). Above the diagram, major solid phases are shown.*

In the non-agitated experiments with the Am / cement / brine systems, Am concentration decreased considerably with time. Within six months sorption equilibria were achieved, demonstrating strong retention of Am(III) by the corroded cement products (Fig. 3). Data of equilibrated systems indicate linear sorption isotherms, which allow determining apparent sorption coefficients, R_s. A coefficient of R_s = 3060 ml g^{-1} is derived from the experiments in weakly alkaline $CaCl_2$ systems (-log(m_{H+}) ~ 9.0), whereas in highly alkaline $CaCl_2$ systems (-log(m_{H+}) ~ 11.5) R_s = 10000 ml g^{-1} is observed (Fig. 4). A similar apparent Am sorption coefficient is reported for a binary system of cement altered in initially $MgCl_2$ rich brine (m/V < 0.1 g mL^{-1}, weakly alkaline $MgCl_2$-$CaCl_2$ solution after equilibration) [10].

In the present study we use the Freundlich-isotherm to describe sorption. This isotherm is given by the equation

$$q = K_F \cdot C^n \text{ or } \log(q) = \log(K_F) + n \cdot \log(C)$$

where *q* is the amount of Am adsorbed (e.g. in mol g^{-1} also called loading), *C* is the dissolved Am concentration (in mol L^{-1}) and K_F and *n* are fitting parameters. In Fig. 4 the fits to the Freundlich-isotherms are shown in double-logarithmic isotherm plots. Such fits to the mean adsorption data yield statistically better results for the weakly alkaline and strongly alkaline cement / brine systems than the linear isotherm ($\log q = 0.8 + (1.04) \cdot \log C$ with R^2 = 0.97 and $\log q = 3.3 + (1.25) \cdot \log C$ with R^2 = 0.82). Due to the limited number of data points and the analytical errors, linear isotherm would give an adequate representation of the data (Fig. 4).

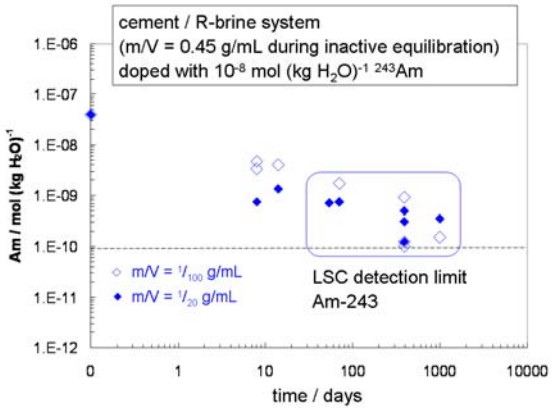

Fig. 3: *Observed Am sorption kinetics in the system Portland cement corroded in initially $MgCl_2$-rich brine.*

By means of thermodynamic simulations, equilibrium compositions of the inactive systems were calculated with the modified database and compared to the measurements. Fig. 2 shows the calculated solution compositions as a function of cement / brine ratio and the final compositions measured in the experiments. The calculated solution composition is in good agreement with the experimental results. The Mg/Ca exchange reactions between solids and solution that have been observed in the experiments are also predicted in the calculations. In the upper part of Fig. 2, the solid phase assemblage is shown. Most of the solids that are detected by solid phase analyses are also calculated for the equilibrium composition, e.g. brucite, anhydrite/gypsum, Al-hydroxide. Some secondary phases present are weakly crystalline and are characterized by less defined or heterogeneous compositions, e.g. hydrotalcite phases and Mg-Ca-Al hydroxochloride. Since ideally crystalline end-member phases are used as proxies for these phases in the thermodynamic calculations, the simulated solid composition differs to some extent from the distribution of phases detected in the equilibrated solid. Morevover, most of the literature data on cementitious environments deals with low ionic strength systems. There is a lack of thermodynamic data for the alteration of cementitious phases in chloride-rich media, which should be addressed in the future.

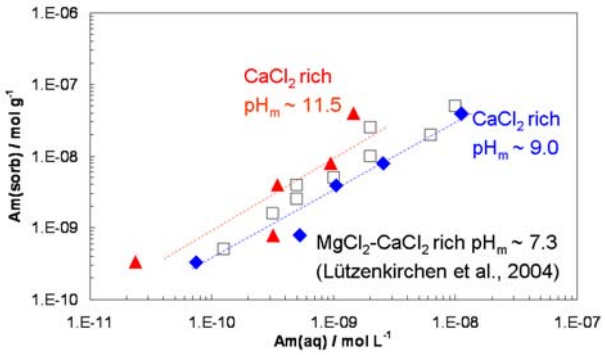

Fig. 4: *Isotherm plot (log Am loading vs. log aqueous Am concentration) for Portland cement corroded in initially $MgCl_2$-rich brine.*

Conclusions

Alteration of hydrated OPC in $MgCl_2$-rich brine results in weakly to strongly alkaline $CaCl_2$ enriched solutions, formation of secondary Mg-Ca-Al (chloro-) hydroxides and reprecipitation of $CaSO_4$. The solution composition at equilibrium can be predicted well with thermodynamic calculations. Since the thermodynamic database that is used in the simulations relies on ideal end-member phases, the predicted mineral assemblage is in agreement with crystalline phases identified in the cement alteration products. Amorphous Mg-Ca-Al-Si-rich phases, characterized by heterogeneous compositions, are represented in the thermodynamic calculations by proxy minerals, e.g. nontronite or Ca-montmorillonite. The retention of radionuclides on cement alteration products has often been claimed not only for dilute solutions, but also for saline brines. This work enables to quantify the retention of Am and thus corroborates previous estimations with experimental data.

References

[1] C.M. Bethke and S. Yeakel, The Geochmist`s Workbench, Urbana, University of Illinois (2009)

[2] C.E. Harvie, N. Møller, N., J.H. Weare, Geochim. Cosmochim. Acta, 48, 723-751 (1984).

[3] V. A. Pokrovskii and H. C. Helgeson, Am. J. Sci., 295, 1255 (1995)

[4] E.J. Reardon, Waste Management, 12, 221-239 (1992).

[5] L. De Windt, F. Marsal, E. Tinseau, D. Pellegrini, Phys. Chem. Earth, 33, 295-305 (2008)

[6] T.J. Wolery, "EQ3/6, A software package for geochemical modeling of aqueous systems," in UCRL-MA-110662 University of California: Lawrence Livermore National Laboratory, (1992).

[7] T. Matschei, B. Lothenbach, F.P. Glasser, Cem. Concr. Res., 37, 1379-1410 (2007).

[8] R.A. Robie and B.S. Hemingway, US Geol. Survey Bulletin 2131 (1995).

[9] E.J. Reardon, Cem. Concr. Res., 20, 175-192 (1990).

[10] J. Lützenkirchen, P. Vejmelka, B. Kienzler, G. Lösch, M. Schlieker, V. Metz, FZK-INE 015/03, Forschungszentrum Karlsruhe (2003).

6.3 Colloid impact on radionuclide migration

M. Bouby, G. Buckau, A. Chai, H. Geckeis, R. Götz, W. Hauser, P. Höss, F. Huber, C. M. Marquardt, T. Schäfer, L. Truche, C. Walther*

**now Université Henri Poincaré, Nancy, France*

Introduction

For the disposal of radioactive waste in deep geological formations a thorough knowledge of the chemical processes possibly occurring in the engineered (EBS) and the geological (host rock) barrier are prerequisite. Inorganic and organic colloids can occur in the near- and far-field of a deep geological repository. Colloids or nanoparticles (< 1 µm in size) are characterized by a high surface area and the ability to remain suspended in water therefore potentially being mobile in groundwater systems. Accordingly, colloids are discussed as a potential pathway for the radionuclide release from a nuclear waste repository. Insight into the possible colloid generation mechanisms, their stability and mobility under given groundwater conditions is required to assess the colloid relevance on radionuclide migration. Other key questions are the mechanisms of radionuclide interaction with colloids and notably the reversibility of the radionuclide-colloid binding.

In most repository designs, the massive metal canisters, in which the waste is packed, are surrounded by a large volume of bentonite clay functioning as geo-engineered barrier (buffer and backfill material) confining the waste. Although bentonite is expected to act as a colloid filter, the contact zone (gel layer) to water conducting features in crystalline host rock formations may act itself as a colloids source due to erosion by advective transport. Once released from the compacted bentonite, the colloids have to be stable under the specific geochemical conditions to effect the radionuclide mobility in the host rock formation.
Experimental evidence of laboratory and field studies suggests colloid instability in saline ground waters with time [1]. Ground waters of low ionic strength and high pH are thought to enhance bentonite colloid stability, as demonstrated in various laboratory and field experiment over short observation periods (few months) [2].

Once formed, if they are mobile and stable under the specific conditions, bentonite colloids might transport associated radionuclides along shear zones as demonstrated in studies within the CRR/CFM project. Experiments performed in the framework of the BMWi project KOLLORADO-2 (duration 2009-2012) are closely related to the CFM (Colloid Formation and Migration) project performed in the Grimsel Test Site (GTS) in the frame of the Phase VI (www.grimsel.com/gts-phase-vi/cfm-section).
Research on the stability of the geotechnical barrier under glacial melt water conditions and the potential release of bentonite colloids constitutes the scientific goal of the CFM project. In 2009, under highly demanding engineered-technological efforts, a tunnel mega-packer system was constructed. This mega-packer minimizes the gradient and groundwater flow in the MI shear zone intersecting the tunnel and enables the work under near-natural hydraulic conditions similar to the post-closure situation of a deep geological repository. In this chapter, we report on:

- *The FEBEX bentonite colloid stability under Grimsel ground water (GGW) conditions over a 3 years observation period and*
- *The CFM migration experiments performed during the year 2010.*

In addition to inorganic nanoparticles, the presence of organic colloids naturally present or artificially introduced during the excavation process [3] might have an impact on the migration of radionuclides in the geosphere. Research on their generation, mobility and interaction with radionuclide has been conducted. In this chapter, we report:

- *On a protocol to extract rock mineral associated organic matter in the Callovo-Oxfordian (COx) formation,*
- *On the synthesis and characterization of a hybrid clay-based material (HCM) montmorillonite- melanoidin via Maillard reaction as a potential clay- humic substance model, and*
- *On the influence of the preparation procedure to the metal-humic acid (HA) complexes formation.*

FEBEX bentonite colloid stability under Grimsel ground water conditions (high pH, low ionic strength, IS)

FEBEX bentonite blocks are crushed and sieved. The < 63 µm fraction is homoionized by washing with LiCl 1M during 4 days. The colloid stock suspension is prepared by 4 centrifugation-collection-resuspension in fresh GGW cycles. The colloid concentration in the stock solution is 1.23 g/L.
The Flow Field-Flow Fractionation coupled to ICP-MS [4] is used to characterize over time

the clay colloids batch samples (further diluted in GGW down to 20 mg/L) by looking at the evolution of the Al fractogram (size, recovery), Al being used as tracer for the bentonite colloids (see Figure 1).

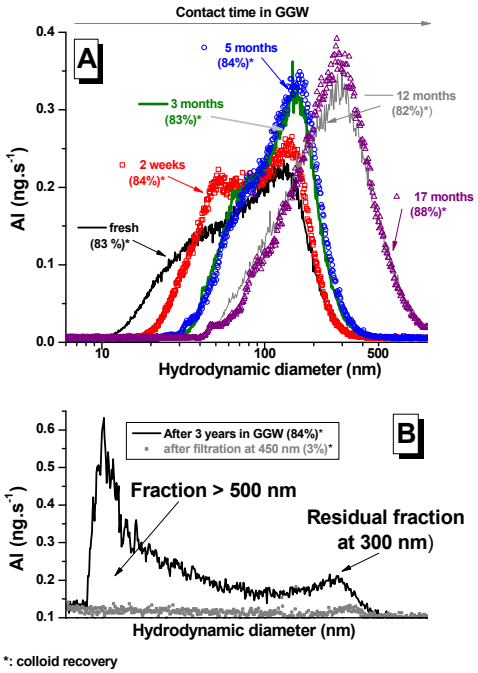

Fig. 1: *Bentonite clay colloids size evolution in Grimsel ground water over a period of 3 years.*

Over 3 years, a slow agglomeration process, reproducible, is clearly evidenced and representative of the sample with more than 80 % Al (bentonite colloids) recovered. The explanation lies in the $[Li^+]$ / $[Ca^{2+}]$ concentration ratio changes after the homoionization process and the batch preparation in GGW. The Ca^{2+} ions are considered responsible of the clay platelets induced agglomeration. This agrees with the critical coagulation concentration (CCC) value of 10^{-3} M determined in $CaCl_2$ system [1].
In conclusion, even the low IS and high pH conditions of the GGW do not seem to be sufficient to stabilize the bentonite clay colloids for long time periods (years) under room temperature conditions.

In-situ migration experiments (CFM project) at the Grimsel Test Site (GTS)

As mentioned above, the Colloid Formation and Migration (CFM) project aims on the detailed process understanding of bentonite backfill/buffer material stability in contact with a water conducting feature in a crystalline host rock. Focus of the research within this international collaboration is to understand the formation of the bentonite gel layer, the erosion of the bentonite buffer/backfill material, the generation of bentonite colloids and their impact on radionuclide transport in a natural shear zone. The field investigations are accompanied by an extensive laboratory program to assess the influence of parameters as *inter alia* ionic strength, pH, contact water cation composition; fracture aperture and bentonite dry density on the formation of colloidal phases. Earlier field colloid migration tests at the GTS conducted within the CRR (Colloid and Radionuclide Retention) experiment suffered from relatively short residence times (60-80min)/ high flow velocity of the tracer in the fracture [5,6]. CFM field migration experiments have been conducted throughout the years 2008 to 2010 reducing successively the flow velocity to near-natural flow conditions and therefore establishing higher tracer residence times in order to quantify retention/sorption reversibility of colloid-bound radionuclides. To overcome the high natural gradient towards the tunnel surface the migration (MI) shear zone was hydraulically isolated by installing a sophisticated mega-packer system (see Figure 2) counteracting the hydraulic heads of the shear zone.

Fig. 2: *The mega-packer system of the CFM experiment at the GTS. The shear zone is sealed with resin layer and surface packers are installed at outflow points on shear zone intersection. Pressurised water in annulus provides mechanical support to resin layer to counteract hydraulic head in the shear zone.*

Three migration experiments using Eu, Tb, Hf and Th as chemical homologues for the tri- and tetravalent actinides have been conducted in a 6.08m dipole with a conservative tracer (uranine) added under variation of the fracture residence time ranging from 230min to ~6000min (peak arrival). Colloid analysis included laser-induced breakdown detection (LIBD), single particle counting (SPC), photon correlation spectroscopy (PCS), AFM and colloid quantification via Al analysis by ICP-MS.
The results showed a surprisingly high recovery of both the bentonite colloids (injection concentration 22-31 $mg \cdot L^{-1}$) and the colloid associated tri- and tetravalent elements, not expected from previous experiments conducted within the CRR project in the same

shear zone, but another dipole. Recovery of tetravalent elements (Th, Hf) decreased from 78-93% down to 30-32% and trivalent elements (Tb, Eu) from 56% down to 7-14% with a residence time increase from 230min to 2250min (peak arrival time). In parallel, the colloid recovery decreased from 95-100% down to 47-64% (Fig. 3). The magnitude of metal ion retention/recovery observed in the field experiments is consistent with laboratory determined bentonite sorption reversibility kinetic data obtained in the ternary system fracture filling material – bentonite colloids – radionuclides with a desorption rate k_3 ~0.01h^{-1} [7]. A further experiment (CFM Run 10-03) at lower flow velocity with a peak arrival time of 5962 min (1st peak) using a higher colloid cocktail concentration of 105mg·L^{-1} and 2L injection volume resulted in a colloid recovery of 40 ± 10% quantified via the ICP-MS Al signal. The element recoveries with 43 ± 10% (Th), 46 ± 6% (Hf), 14 ± 2% (Tb), and 6 ± 2% (Th) are very comparable to the previously performed experiment (CFM Run 10-01).

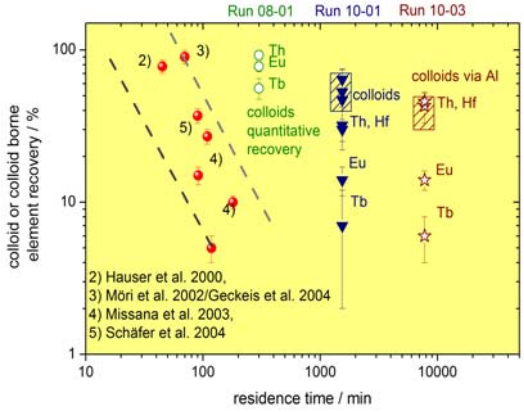

Fig. 3: *Comparison of colloid (shaded area for Run 10-01 and 10-03) and element recovery of field and laboratory migration experiments within the CRR project (red symbols) and the new data obtained within the CFM project (Run 08-01, 10-01 and 10-03).*

Size distribution analysis by LIBD and SPC showed for all experiments no size chromatography effect in the colloid breakthrough. This lack of size exclusion phenomena in combination with high colloid recovery indicates a broad channel („highway“) as flow path for the CFM experiments. Overall, the CRR and CFM project results obtained so far clearly demonstrate the sensitivity of colloid transport on flow path geometry/heterogeneity of the fracture/shear zone giving predictions based on correlations as e.g. colloid recovery versus residence time (Fig. 3) a very high uncertainty, but demonstrate the slow bentonite colloid sorption reversibility especially for the tetravalent elements.

Extraction of rock mineral associated organic matter from the Callovo-Oxfordian (COx) formation.

One site under consideration in France for the disposal of medium and high level, long lived radioactive waste is in the eastern part of the Paris Basin (Meuse/Haute Marne, France), where the National Radioactive Waste Management Agency (ANDRA) operates an underground laboratory. The sedimentary host formation is a 130 m thick, clay-rich Callovo-Oxfordian deposit ca. 350–550 m below ground in the selected area. The major fraction (>95%) of the organic matter (OM) present is associated with minerals and might be a source of organic colloids in geochemical disturbed systems (e.g. alkaline plume). In order to better understand the importance of OM on the chemistry of this formation, a protocol has been developed allowing extraction/fractionation of organic compounds in the rocks. The protocol is based on classical methods currently used for the isolation of humic substances from soils and for the separation of kerogen in ancient sediments using sequential extraction with solvents and water at different pH value. This allows to remove a large part of the minerals and to suspend almost all (>90%) of the OM (associated with residual recalcitrant minerals) in water. The OM can then be analysed via spectroscopic methods, such as mass spectrometry (MS), Fourier transform infrared spectroscopy (FTIR), or C (1s) near-edge X-ray absorption fine structure (NEXAFS) spectroscopy. The molecular composition of the solvent-soluble, directly-extractable part shows the OM to be thermally immature. The solvent-soluble fractions obtained after acid and alkaline treatments are mostly polar in nature and have a high degree of aliphaticity. C(1s) NEXAFS analysis of water soluble organic fractions indicate a progressive increase in aliphaticity and a decrease in carboxylic/carbonyl groups with consecutive extraction steps providing evidence for increasing hydrophobicity and a more kerogen like structure of the later extracts [8].

Synthesis and characteri ation of hybrid clay-based material (HCM) montmorillonite- melanoidin via Maillard reaction as a potential clay organic matter model.

The study of the interactions among metals, minerals, and humic substances is essential in understanding the migration of inorganic pollutants in the geosphere. A considerable amount of organic matter in the environment is associated with clay minerals. To understand

the role of organic matter in the environment and its association with clay minerals, a hybrid clay-based material (HCM), montmorillonite (STx-1) – melanoidin, was prepared from l-tyrosine and l-glutamic acid by the Maillard reaction. The HCM was characterized by elemental analysis, nuclear magnetic resonance, x-ray photoelectron spectroscopy (XPS), scanning transmission x-ray microscopy (STXM), and thermal analysis. The presence of organic materials on the surface was confirmed by XPS and STXM. The STXM results showed the presence of organic spots on the surface of the STx-1 montmorillonite and the characterization of the functional groups present in those spots. Thermal analysis confirmed the existence of organic materials in the montmorillonite interlayer, indicating the formation of a composite of melanoidin and montmorillonite. The melanoidin appeared to be located partially between the layers of montmorillonite and partially at the surface, forming a structure that reminds on the geometry of a cork sealing a champagne bottle [9].

Influence of the preparation procedure to the metal-humic acid (HA) complexes formation.

To understand the actinide (An) - humic/fulvic acids (HA/FA) interaction mechanisms the metal-HA/FA complexes have to be formed and further analyzed.

The present study focuses on the interaction of the Th(IV) ions at trace concentrations ([Th(IV)] = 10^{-7} M) with HA (purified HA, extracted from Gorleben ground water Gohy-573, [HA] = 0.75 mg·L^{-1}; [$NaClO_4$] = 10^{-2} M; pH = 9.5) by using the Flow Field-Flow Fractionation coupled to ICP-MS [4]. Under those conditions, the nominal loading of the HA carboxylate groups with metal ions (An(IV)) is < 10 %. Th(IV)-HA complexes are prepared by three different procedures: MODE 1: titration of the acidic Th(IV) solution with HA solution (pH = 9.5); MODE 2: spiking Th(IV) directly to a HA solution (pH = 9.5) and MODE 3: mixing of all components at pH = 3 and increasing the pH to 9.5 by slow NaOH addition. According to Neck et al. [10], this means that the Th(IV) solubility curve is crossed over three different ways (Figure 4).

AsFlFFF-ICP-MS studies demonstrate the appearance of different colloid types depending on the preparation mode (Figure 5).

Following the preparation MODE 1 leads to the formation of large Th-oxide/hydroxide colloids or Th-HA agglomerates (size ~ 100 nm). Following the preparation MODE 2 leads to the formation of relatively small HA-coated Th-(oxy)hydroxide colloids or Th-HA agglomerates (size ~ 12 nm).

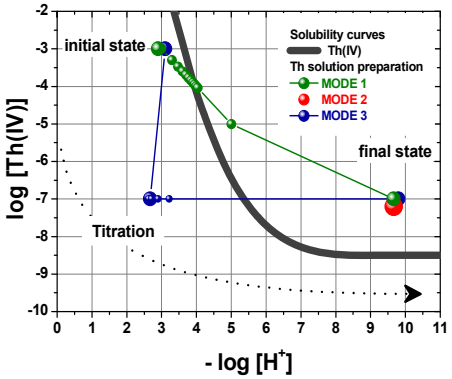

Fig. 4: *Th(IV) solubility curves, from [10] and summary of the different preparation modes.*

Following the preparation MODE 3 leads to the initial formation of the Th(IV)-HA complexes (size ~3 nm) while a metal induced HA agglomeration develops with time (not shown here) consequently, even at low metal concentrations. At a first glance, results can be explained according to the experimental protocol used showing its influence on the final resulting product. Nevertheless, according to thermodynamic data, whatever the mode of preparation, identical complexes have to form with time. This point has to be checked and calls for further and deeper investigations.

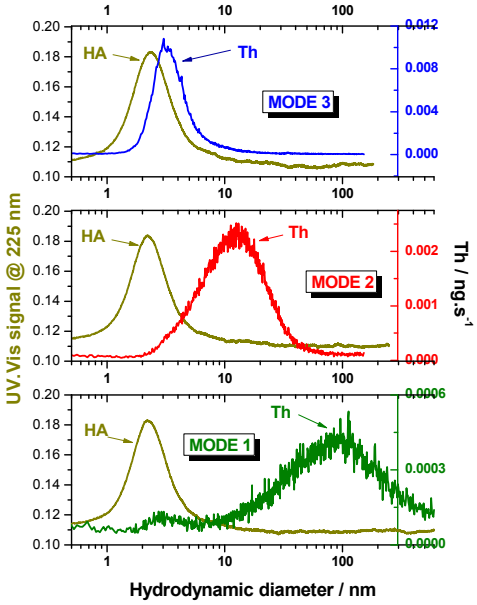

Fig. 5: *Gohy-HA-573 UV-fractogram and Th-ICP-MS-fractogram obtained after injection of a HA-Th(IV) solution prepared according to the Mode 1, 2 or 3.*

[1] M. Bouby, A. Filby, H. Geckeis, F. Geyer, R. Götz, W. Hauser, F. Huber, B. Kienzler, P. Kunze, M. Küntzel, J. Lützenkirchen, U. Noseck, M. Plaschke, A. Pudewills, T. Schäfer, H. Seher, C. Walther, C., T. Schäfer, U. Noseck, (Eds). Wissenschaftliche Berichte/

Forschungszentrum Karlsruhe, FZKA 7515 (2010).

[2] T. Missana, U. Alonso, M.J. Turrero, J. Cont. Hydrol., 61, 17-31 (2003).

[3] Hallbeck, L., SKB Technical Report, TR-10-19, (2010).

[4] M. Bouby, H. Geckeis, F. Geyer, Anal. Bioanal. Chem., 392, 1447-1457 (2008).

[5] H. Geckeis, T. Schäfer, W. Hauser, T. Rabung, T. Missana, C. Degueldre, A. Möri, J. Eikenberg, T. Fierz, W. R. Alexander, Radiochim. Acta, 92, 765-774 (2004).

[6] A. Möri, W. R. Alexander, H. Geckeis, W. Hauser, T. Schäfer, J. Eikenberg, T. Fierz, C. Degueldre, T. Missana, Colloids Surf. A, 217, 33-47 (2003).

[7] F. Huber, P. Kunze, H. Geckeis, T. Schäfer, Appl. Geochem., in review, (2011).

[8] L. Grasset, J. Brevet, T. Schäfer, F. Claret, E. C. Gaucher, A. Albrecht, A. Amblès, Org. Geochem., 41, 221-233 (2010).

[9] V.V. Vilas, B. Mathiasch, J. Huth, J.V. Kratz, S. Rubert de la Rosa, P. Michel, T. Schäfer, Soil Sci. Soc. Am. J., 74, 2239-2245 (2010).

[10] V. Neck, J.I. Kim, Radiochim. Acta, 89, 1-16 (2001).

6.4 Numerical simulation studies

Nanoparticle migration in a CT scanned natural granite fracture: Experiments and 3D CFD modeling.

F. Huber, F. Enzmann[1], A. Wenka[2], M. Bouby, M. Dentz[3], T. Schäfer

[1]Institute for Geosciences. Johannes Gutenberg University, 55099 Mainz, Germany; [2]Karlsruhe Institute of Technology, Institute of Micro Process Engineering (IMVT), P.O. Box 3640, 76021 Karlsruhe, Germany; [3]Department of Geosciences, Institute of Environmental Assessment and Water Research (IDAEA-CSIC), Barcelona, Spain

Introduction

In contrast to porous media, fluid flow through fractured rocks is bound to discrete roughly shaped planes, which act as main flow paths. As a consequence this issue has been extensively studied in the past by several authors [1-4]. Both experimental and theoretical approaches have been applied to shed light on the processes governing flow and transport in single fractures as well as fracture networks. In most cases, fractures were treated with the parallel plate model or the streaming tube approach, where real natural fracture geometries are replaced by simplified and abstracted geometries. These simplifications have been made because of a more easily mathematical description resulting in a lesser computational effort. Besides, random fractures have been generated virtually by means of statistical and mathematical methods [5]. The governing equations describing fluid flow are the Navier-Stokes equations which represent a nonlinear system of partial differential equations, only to be solved numerically in 3D. Modern laboratory techniques, like e.g. computer tomography can serve as a non-destructive tool for characterization of natural fractures in drill cores providing geometrical information which can be used directly in numerical codes to conduct flow and mass transport simulations on the measured scale. This more realistic approach has been applied in our study.

Materials and Methods

The 3D model applied in this study is generated using the µCT measurements. The µCT scan resulted in 1691 stacked 2D slices transformed into a 3D model representation of the drill core. The obtained µCT dataset was pre-processed using different computational tools for data artifact reduction facilitating the segmentation of the fracture planes. Care was taken to accurately capture the fracture geometry. Subsequently, 3D triangulated surfaces of the fracture were produced out of the full resolution segmented raw µCT data. The final 3D mesh of the fracture consists of ~ 10.5 Mio. elements (3156334 nodes).

Flow and solute transport simulations on basis of the Navier-Stokes equation and the advection-diffusion-equation, respectively were modeled using the finite volume CFD software FLUENT©. A molecular diffusion coefficient for HTO of 2.5×10^{-9} $m^2\cdot s^{-1}$ was applied. The molecular diffusion coefficient of 4.2×10^{-11} $m^2\cdot s^{-1}$ for the nanoparticles (quantum dots; QD) was calculated based on their hydrodynamic diameter (12 nm) using the Stokes-Einstein equation. Quantum dots were used in this study as a monodisperse reference material for the smallest clay colloid size fraction. Calculations were carried out on the KIT high performance cluster HP XC3000.

Results and discussion

Figure 1 shows exemplarily a volume rendering plot of the simulated normalized velocity magnitude for the core. Generally speaking, the simulated 3D flow field reflects the spatial complexity of the overall geometry of the fracture. The resulting flow field is a combination of four spatial fracture characteristics: (a) the wedge-shaped nature of the fracture, (b) the aperture variability, (c) the asperities and (d) the irregular right fracture boundary. The influence of the asperities leads to channeling of the flow which is obvious e.g. in the upper third domain of the model where the fracture is closed to a high extent. Here, flow velocities strongly increase as a result of the narrowing of the flow cross sectional area. In consequence, the highest flow velocities occur in this region. The fastest flow velocities (red colors in Figure 1) always occur in the vicinity of asperities indicating their high impact on the flow velocity distribution. The very irregular right fracture boundary causes a splitting of the flow velocity distribution into low velocity areas near the right fracture side (blue colors in Figure 1) in contrast to the middle and left side part of the fracture where the apertures are higher and thus higher flow velocities can be observed (green and yellow colors in Figure 1).

Migrations experiments using HTO and engineered nanoparticles (QD) have been conducted for two different fluxes. Figure 2

shows the experimental breakthrough curves for both runs in conjunction with the results for the mass transport simulations. In the following Run#1 represents the higher velocity experiment (Reynolds number Re = 0.026) and Run#2 the lower velocity experiments (Re = 0.0058), respectively.

Run#1. In general, both the experimental HTO and QD BTC show a pronounced tailing (Figure 2a,b). The shapes of both BTCs differ from each other in such that QD show a Δt between first arrival and peak maximum of 470 s compared to a Δt of 600 s for HTO indicating a sharper increase for the QD´s.

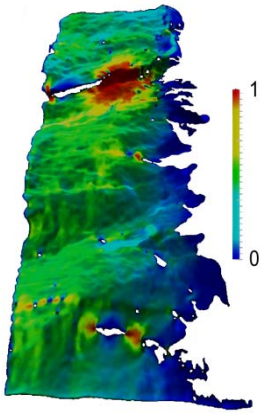

Fig. 1: *Normalized volume rendering plot of the flow field as calculated on basis of the µCT data. Note the complex flow velocity distribution due to fracture geometry.*

The tailing of the HTO BTC can be approximated fairly well by fitting to a power law of $t^{-3/2}$. This type of power law is often referred to as matrix diffusion and has been observed both in field and laboratory studies.[6] Considering the Re numbers prevailing, the occurrence of matrix diffusion seems reasonably to some extent. In contrast to the HTO BTC, the QD residence time distribution is much more broadened but also characterized by a pronounced tailing. As expected for colloidal transport, the QD peak maximum arrives faster than the HTO peak maximum which is a frequent observation in both field and laboratory experiments [7,8]. The calculated experimental retardation factor (R_f) for the QD peak is 0.94 based on the positions of the peak maximum time of HTO and QD (Table 1). This finding can be explained by the different chemical properties and physical transport behavior of the colloids compared to solutes. In consequence, the QD BTC tailing cannot be described by the empirical matrix diffusion power law. This observation can be expected since the diffusion coefficient of the QD is almost two orders of magnitude lower than it is the case for HTO which is further reflected in the Peclet number Pe of 607 for the QD and only 10 for HTO, respectively. This indicates that the QD are more strongly influenced by advection whereas HTO exhibits a much higher impact of molecular diffusion facilitating matrix diffusion. Matrix diffusion coefficients for colloids range between 7×10^{-18} $m^2\cdot s^{-1}$ for 2nm to 1.5×10^{-18} $m^2\cdot s^{-1}$ for 100 nm colloids, respectively [9]. Moreover, the QD are likely to be effectively hindered to diffuse into a possible porous fracture wall matrix due to other processes like e.g. size exclusion effects.

Tab. 1: *Comparison of the experimental and simulated breakthrough curve data.*

	Run #1	***Run #2***
Flux ($\mu l\cdot min^{-1}$)	66.8	14.2
Re [-]	0.026	0.0058
Pe HTO[-]	10	53
Pe QD [-]	607	135
max. velocity magnitude [$m\cdot s^{-1}$]	0.0013	0.00029
volume averaged velocity magnitude [$m\cdot s^{-1}$]	$5.67\cdot10^{-5}$	$1.26\cdot10^{-5}$
R_p (Peak max. exp. HTO) [min]	51	129
R_p (Peak max. exp. QD) [min]	48	128
R_p (Peak max. model. HTO) [min]	50	161
R_p (Peak max. model. QD) [min]	49	159
R_f exp. [-]	0.94	0.99
R_f model [-]	0.98	0.99
Recovery HTO	96%	99%
Recovery QD	88%	68%

R_p = peak elution time; R_f = retardation factor ($R_f = R_p$[QD]/ R_p[HTO])

Run#2. The HTO BTC is again characterized by a sharper increase in concentration and peak maximum compared to the QD BTC. The QD BTC shows a Δt between first arrival and peak maximum of 1740 s compared to a Δt of 1370 s for HTO indicating this time a sharper increase for the HTO compared to the QD BTC. The tailing of the HTO can be approximated by the empirical matrix diffusion power law in line with the BTC from Run#1. The Pe number for HTO in Run#2 is 2 indicating an even stronger impact of molecular diffusion on the transport behavior. Consequently, the prevailing flow and transport conditions even more facilitate a diffusion of the HTO into a possible core matrix. Recoveries of HTO are within analytical

uncertainty quantitative both for Run#1 and Run#2 and decrease for the QD with decreasing flow velocities from 88% in Run#1 to 68% in Run#2, respectively. This leads to the conclusion of a more pronounced interaction of the QD with the fracture surfaces in terms of sorption or filtration processes with decreasing flow velocity explaining the observed difference in the rising edge of the BTCs. Similar to Run#1, the QD BTC shows an earlier first arrival time than the HTO peak. The position of the peak maximum between the QD and HTO BTCs are almost identical (R_f QD = 0.99) showing that the mean residence times approach each other with decreasing flow velocity.

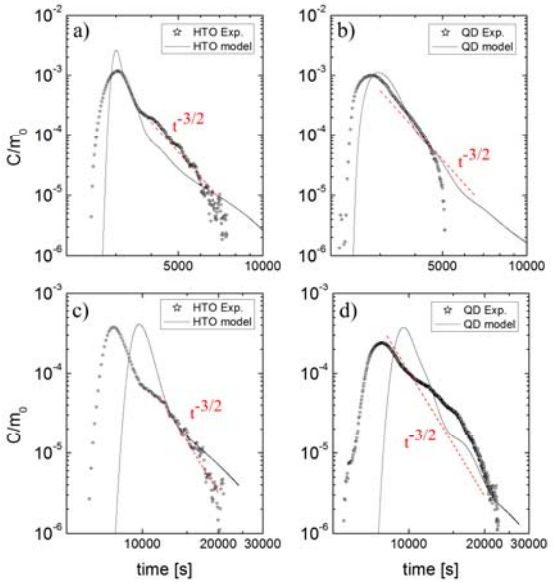

Fig. 2: *Experimentally derived BTCs (open stars) in comparison to simulated BTCs (black lines). a) HTO BTCS for Run#1 b) QD BTCs for Run#1 c) HTO BTCS for Run#2 and d) QD BTC's for Run#2. Red lines in a) and b) represent the empirical power law for matrix diffusion ($t^{-3/2}$).*

Transport modeling (Run#1 & Run#2). Regarding the first arrival of the modeled BTCs, the QD BTCs for both flow velocities show an earlier arrival times compared to the HTO BTCs in line with the experimental findings. Furthermore, the position of the QD peak maximum is also shifted to earlier times compared to the HTO BTC. Again, this observation fits to the experimental findings. The overall modeled BTC positions are shifted to later times for the lower flow velocity (Run#2) compared to the experimental BTCs, whereas for Run#1 the positions are almost comparable. Though, the Rf value of 0.98 for the simulated QD peak is slightly higher than the experimental QD Rf (0.94) in Run#1, whereas the QD Rf value of 0.99 is equal to the experimental QD Rf value (0.99). Concerning HTO, the modeled BTC (Run#1) describes the peak maximum position quite good though over-predicts the maximum normalized concentration. The modeled HTO BTC of Run#2 can reproduce the experimental maximum concentration very well and also the overall peak shape of the BTC fits satisfactorily to the experimental BTC though shifted to much later times. In contrast, the simulated QD BTC of Run#1 describes the normalized concentration of the experimental BTC very good, but is shifted to later times as stated above. The modeled QD BTC of Run#2 shows in addition to the time shift also a higher peak maximum and the agreement to the experimental BTC in terms of predicted maximum concentrations and overall peak shape is rather poor. Here, the model exhibits a much sharper peak shape than the experimental QD BTC. The deviation in Run#2 can be explained with the observed decrease in QD recovery (Table 1), which would dampen the peak maximum and influence through retardation the shape of the BTC tailing.

Overall, as in the case for the experimental BTCs, the simulated residence time distributions show pronounced tailings. Since the model does not include matrix diffusion the tailing cannot be fitted to a power law of $t^{-3/2}$. Generally speaking, the observed heavy tailings in the simulated breakthrough curves can be clearly attributed solely to dispersion due to the fracture geometry.

Conclusions

Our study clearly shows the mobility of the hydrophilic QD in a natural single fracture under natural Grimsel groundwater conditions. Concerning the core migration experiments, a decrease in QD recovery is observed with decreasing flow velocity indicating a possible sorption to the fracture wall or filtration effects. Experimental HTO BTCs show pronounced tailings which may be attributed to a combination of fracture heterogeneity and matrix diffusion. Simulated HTO and QD breakthrough curves exhibit heavy tailing reflecting the influence of fracture heterogeneity on flow velocity distributions and on mass transport. Generally speaking, the observed heavy tailings in the simulated breakthrough curves can be clearly attributed solely to dispersion due to the fracture geometry and confirms the proposal made by Kosakowski (2004) [10] that tailing of the colloids is mainly caused by the structure of the flow field and that for colloid/nanoparticle transport matrix diffusion is of minor importance.

Despite the higher computational and technical effort in creating a 3D model on basis of µCT data, the results provide a step forward towards a more fundamental understanding of the processes governing fluid flow and mass transport in real single fractures. Furthermore, this approach facilitates the interpretation and analysis of migration experiments which most often represent black box type experiments.

3D Simulation for long-term behaviour of a real underground structure in rock salt.

A. Pudewills

Introduction

In recent decades, a large and detailed experimental and theoretical knowledge base for the geomechanical behavior of rock salt has been compiled by several groups. On this basis, a number of elaborated and advanced constitutive models and procedures for the determination of characteristic salt type-specific parameter values and for the handling of numerical simulations have been developed [11, 12]. Between August 2007 and July 2010, the German Federal Ministry of Education and Research has funded a joint project within its research program “Improvement of tools for the safety assessment of underground repositories” [13]. The five project partners performed 3-D benchmark model calculations of a real underground structure in rock salt in the Angersdorf mine near Halle in Germany. The aim of the projects was to check the ability of the models to describe correctly the relevant deformation phenomena in rock salt under various influences, (i.e. transient and steady-state creep, the evolution of dilatancy and damage, short-term failure and long-term creep failure, post-failure behavior and residual strength) and to increase confidence in the results of numerical simulations and enhance the acceptance of the results. In addition, the work show needs for the further development and improvement of the models.

Model description

At the Institut für Nukleare Entsorgung (INE) the Finite Element Code ADINA is used to study the mechanical behaviour of rock salt under repository conditions [15]. A new viscoplastic constitutive model for rock salt that can describe the volumetric strain (dilatancy) and the damage of the rock has been proposed and implemented in this code. The material parameters for the numerical modelling have been evaluated on the available laboratory experiments [16]. The Angersdorf mine consists of a regular pattern of large rooms and pillars at a depth of about 530 m. Therefore, a 3-D vertical section with a half of a room and a half of the salt pillar was chosen as a representative calculation model (Fig. 3). The total dimension of the model in direction of x/y/z was 745 m/20 m/800 m.

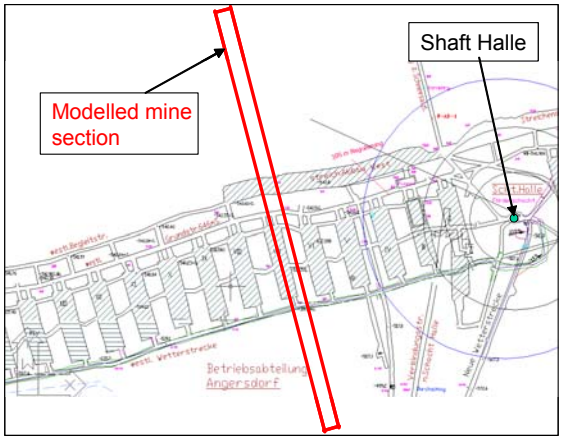

Fig. 3: *Angersdorf mine consists of a regular pattern of rooms and pillars at a depth of about 530 m [14] and the chosen mine section for model calculation.*

The selected Angersdorf mine section was modelled with the ADNA code [15] and in Fig. 4 is shown.

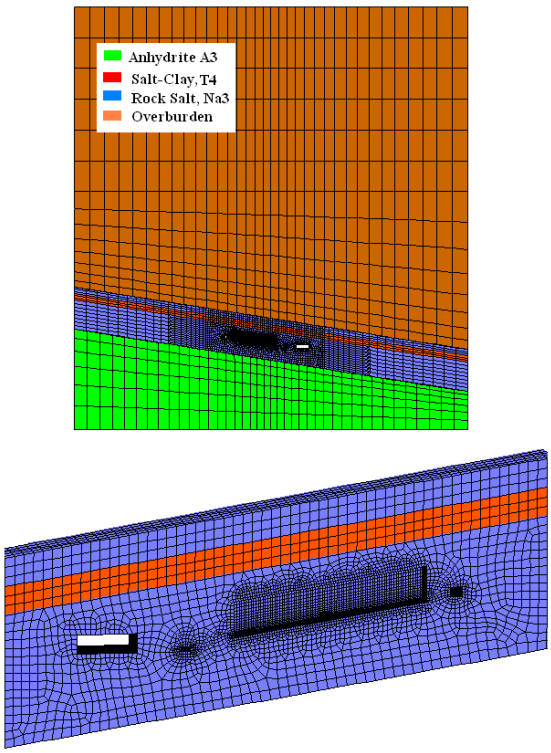

Fig. 4: *FE-model of the Angersdorf mine section that was indicated in red in Fig. 1. The rock layers and main room are inclined by 9° to the north. Bottom: Detail of the model with the underground openings.*

Calculation results

In the first step of the benchmark calculations, the initial state of stress taking into account the creep behaviour of the rock salt (NA3) and the clay (T3) has been determined. After excavation of the main room and different drifts the calculations have been continued over 120 years. Fig. 5 shows contour plots of the EDZ (i.e. the porosity of rock salt and the effective creep strain) in the near field of a connecting gallery.

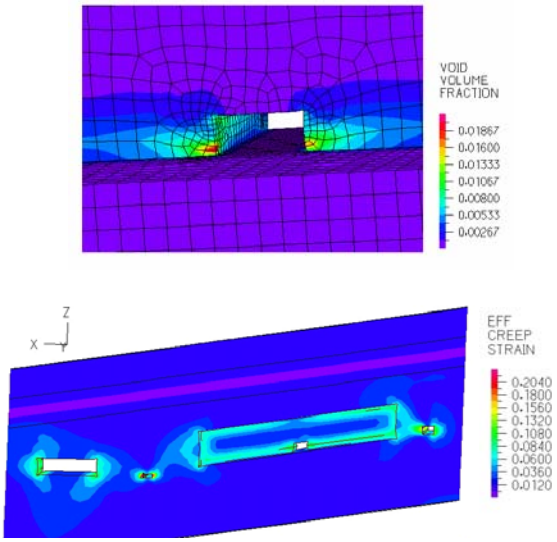

Fig 5: *Volumetric strain (porosity) around the connecting drift between room VIII and room IX and effective creep strain at time point t = 50 years.*

In Fig. 6 the simulation results inside the modelled pillar were compared with the in-situ data of the minimal principal stress. The simulation results 50 years after excavation (i.e. the actual situation) agree with in situ measurements.

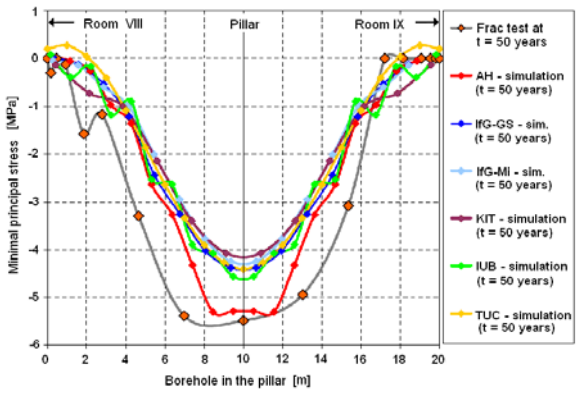

Fig. 6: *Simulation results of all project partners.*

were evaluated at t = 50 a and compare with the minimum principal stress measured in situ in the pillar with frac tests in a horizontal borehole.

Further calculation results provide a prediction of the geomechanical phenomena expected in rock salt as a barrier.

Conclusions

The benchmark calculations and comparisons of the results in the frame of the project have yielded the following results:

- The predictive capabilities of the constitutive model for rock salt developed originally for crushed salt have been increased to describe the dilatancy deformations. The model is able to describe the main behaviour of the rock salt such as transient creep, dilatancy and material damage.
- In addition, the work displayed possibilities for the further development and improvement of the constitutive models.
- The 3-D modelling of the complex section of the Angersdorf mine was also a crucial test of the numerical tools used by project partners

References

[1] L. Moreno, Y.W. Tsang, C.F. Tsang, F.V. Hale, I. Neretnieks, Water Resour. Res., 24, (12), 2033-2048 (1988).

[2] Y.W. Tsang, C.F. Tsang, I. Neretnieks, L. Moreno, *Water Resour. Res.*, *24*, (12), 2049-2060 (1988).

[3] P.M. Meier, A. Medina, J. Carrera, *Ground Water 39*, (1), 10-17 (2001).

[4] J. Carrera, *J. Contam. Hydrol. 13*, (1-4), 23-48 (1993).

[5] C.F. Tsang, C. Doughty, M. Uchida, *Water Resour. Res. 44*, (8) (2008).

[6] J. Carrera, X. Sánchez-Vila, I. Benet, A. Medina, G. Galarza, J. Guimerà, *Hydrogeology Journal 6*, (1), 178-190 (1998).

[7] H. Geckeis, T. Schäfer, W. Hauser, T. Rabung, T. Missana, C. Degueldre, A. Möri, J. Eikenberg, T. Fierz, W.R. Alexander, *Radiochimica Acta 92*, (9-11), 765-774 (2004).

[8] T. Schäfer, H. Geckeis, M. Bouby, T. Fanghänel, *Radiochimica Acta 92*, 731-737 (2004).

[9] U. Alonso, T. Missana, A. Patelli, V. Rigato, J. Ravagnan, *Earth. Planet. Sci. Lett. 259*, (3-4), 372-383 (2007).

[10] G. Kosakowski, *J. Contam. Hydrol. 72*, (1-4), 23-46 (2004).

[11] O. Schulz.: Eds. K.-H. Lux, W. Minkley, M. Wallner and H.R. Hardy, Jr., London: Taylor & Francis (Balkema), pp. 77-88 (2007).

[12] A. Hampel, Abschlußbericht zum BMBF-Verbundprojekt (FKZ 02C1004-1054), Projektträger Karlsruhe im Karlsruher Institut für Technologie (KIT), Wassertechnologie und Entsorgung (PTKA-WTE) (2007).

[13] A. Hampel, R.M. Günther, K. Salzer, W. Minkley, A. Pudewills, B. Leuger, D. Zapf, R. Rokahr, K. Herchen, R. Wolters, U. Düsterloh, Proc. 44th US Rock Mechanics Symposium (ARMA

2010), Salt Lake City/Utah/USA, 27.-30.06.2010, American Rock Mechanics Association (ARMA), (2010).

[14] IFG: Langzeitsicherheitsnachweis Grube Teutschenthal, Fortschreibung unter besonderer Berücksichtigung eines Sicherungs- und Verwahrungskonzeptes für das Grubenfeld Angersdorf. Institut für Gebirgsmechanik GmbH, Leipzig, (2006).

[15] ADINA R & D, Inc., Report ARD 01-9, Watertown, MA, US, www.adina.com, (2008).

[16] A. Pudewills, FZKA-7185, Karlsruhe: Forschungszentrum Karlsruhe (2005).

7. Separation of long-lived minor actinides

B. Beele, A. Bremer, A. Geist, U. Müllich, D. Magnusson, P.J. Panak, C. Ruff

Background

Plutonium and the minor actinides (neptunium, americium, and curium) are the major contributors to the long term radiotoxicity of used nuclear fuels. Alternatively to their direct final disposal in a deep geological repository, actinides could be separated from spent nuclear fuels and be recycled in advanced nuclear reactors – the Partitioning & Transmutation strategy [e.g. [1]). Partitioning involves chemical separation processes based on pyrometallurgy or hydrometallurgy.

Work at INE regards hydrometallurgical (i.e., based on chemical liquid-liquid extraction) actinide separation, with a focus on the separation of trivalent americium and curium from the chemically similar lanthanides.

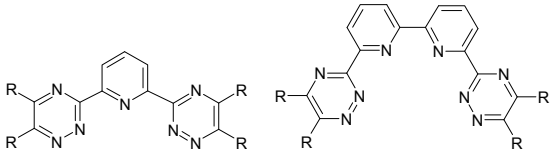

Fig. 1: *BTP and BTBP.*

This separation is possible using N-donor extracting agents such as alkylated bis-triazinyl-pyridines (BTP, **Fig. 1** left) [2, 3] and alkylated bis-triazinyl-bipyridines (BTBP, **Fig. 1** right) [4]. Nevertheless, these extracting agents require further optimisation towards a possible industrial application.

To support this development, we continue fundamental studies aimed at understanding selectivity and performance of such compounds. One of these studies is presented below.

We have also synthesised and tested a novel hydrophilic BTP suitable for what is called the innovative SANEX *(i*-SANEX) process. Liquid-liquid distribution data required for process development and complexation and speciation data were collected.

Complexation of Cm(III) and Eu(III) with C_5-*hemi*-BTP

Introduction

C_5-*hemi*-BTP (6-(5,6-dipentyl-1,2,4-triazin-3-yl)-2,2‘-bipyridine, **Fig. 2**) was developed and tested as a SANEX extracting agent in the European PARTNEW project [5]. Although this molecule did not qualify as a SANEX candidate [6] we use it within our fundamental studies of N-donor extracting agents.

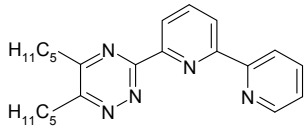

Fig. 2: *C_5-hemi-BTP.*

Results and discussion

Metal nitrates

The complexation of Cm(III) and Eu(III) (used as metal nitrates) with C_5-*hemi*-BTP in H_2O:2-PrOH is investigated by time-resolved laser fluorescence spectroscopy (TRLFS). Unfortunately, the kinetics of complex formation is extremely slow.

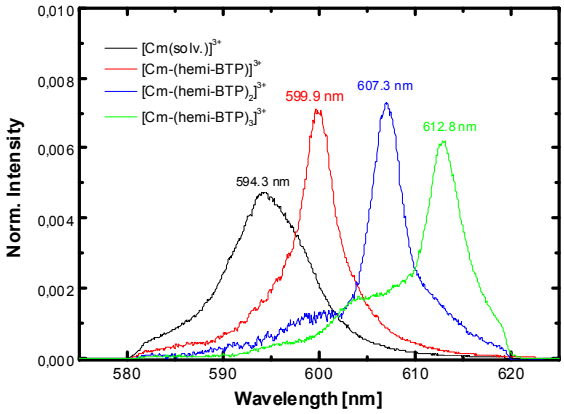

Fig. 3: *Fluorescence spectra of the [Cm(C_5-hemi-BTP)$_x$]$^{3+}$ complexes (x = 1,2,3).*

With Cm(III) three different species are found (**Fig. 3**); the 1:1, 1:2 and 1:3 complexes with emission bands at 599.9 nm, 607.3 nm, and 612.8 nm, respectively.

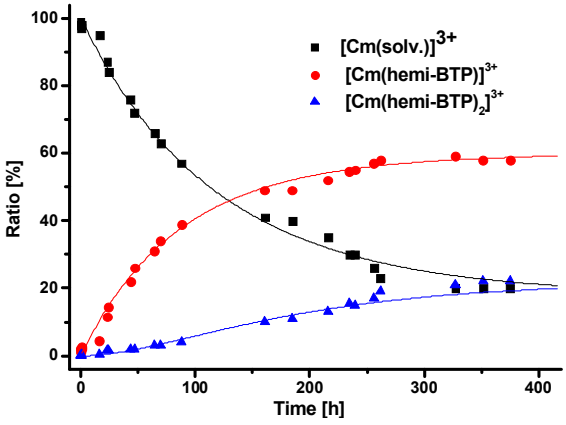

Fig. 4: *Species distribution of the [Cm(C_5-hemi-BTP)$_x$]$^{3+}$ complexes (x = 1,2) as a function of time.*

Fig. 4 shows the experimentally determined concentrations of $[Cm(solv)]^{3+}$, the 1:1, and 1:2 complexes as a function of time; equilibrium is attained only after approx. 400 h for [Cm] =

$2x10^{-7}$ mol/L and [C_5-*hemi*-BTP] = $1.3x10^{-4}$ mol/L. Fitting of the experimental data yields rate constants of k_1 = $1.5x10^{-2}$ s^{-1} and k_2 = $7x10^{-3}$ s^{-1} for the formation of the 1:1 and 1:2 complexes, respectively.

The equilibrium species distributions for various ligand concentrations are determined by peak deconvolution of the emission spectra. The following stepwise stability constants have been derived: logK_{01} = 4.4, logK_{12} = 3.5, and logK_{23} = 3.3, yielding a logβ_{03} = 11.2 for the formation of the 1:3 complex. The stability constant of $[Cm(C_5\text{-}hemi\text{-}BTP)_3]^{3+}$ is three orders of magnitude lower than logβ_{03} = 14.4 for $[Cm(n\text{-}Pr\text{-}BTP)_3]^{3+}$ [7].

Metal 2-bromocarboxylates

C_5-*hemi*-BTP does not extract An(III) nitrates; a lipophilic anion such as a 2-bromocarboxylic acid is required. We characterise the Cm(III) complexes formed in the presence of both C_5-*hemi*-BTP and 2-bromocarboxylic acid by TRLFS.

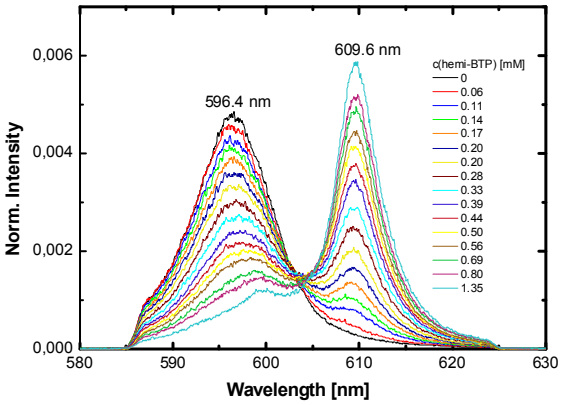

Fig. 5: *Fluorescence spectra of Cm(III) with increasing concentrations of C_5-*hemi*-BTP ([2-bromohexanoic acid] = 0.1 mol/L).*

Fig. 5 shows normalised Cm(III) fluorescence spectra at a constant 2-bromohexanoic acid concentration of 0.1 mol/L and increasing C_5-*hemi*-BTP concentrations. At lower ligand concentrations a 1:1 Cm-2-bromohexanoate species forms with an emission maximum at 596.4 nm. With increasing C_5-*hemi*-BTP concentration the emission band shifts to 609.6 nm, indicating the formation of a ternary Cm/2-bromohexanoate/C_5-*hemi*-BTP-complex.

The complex stoichiometry is identified by the peak position of the ternary species in comparison to the reference spectra (**Fig. 3**), slope analysis and the utilisation of deuterated solvents: Cm(III) is coordinated by two C_5-*hemi*-BTP, one 2-bromhexanoate, and 2 water molecules.

A complex prepared by extracting Cm(III) from an aqueous phase into a solution of C5-*hemi*-BTP + 0.5 mol/L 2-bromodecanoic acid in *tert*.-butyl benzene shows an identical fluorescence spectrum. Thus, the extracted complex is $[Cm(C_5\text{-}hemi\text{-}BTP)_2(2\text{-}Br\text{-}carboxylate)(H_2O)_2]^{2+}$. Charge balance is maintained by two additional 2-bromocarboxylates not present in the first coordination sphere.

i-SANEX process

Introduction

Following the separation of uranium and plutonium (and possibly neptunium) in the PUREX process, DIAMEX and SANEX processes would be required for separating americium and curium: the latter could be co-extracted with the lanthanides from the PUREX raffinate in the DIAMEX process, followed by separating them from the lanthanides in the SANEX process [1].

Each of these processes in their most basic design consists of an extraction/scrub section and a back extraction section plus a solvent regeneration section. Combining the DIAMEX and SANEX processes into a single process would make for an important simplification – the innovative SANEX process (*i*-SANEX). The French *i*-SANEX process [8] is based on a DIAMEX-like extraction/scrub section (generating an organic phase loaded with actinides(III) and lanthanides) and selective back extraction of actinides(III) from the loaded organic phase using DTPA [9]. The use of DTPA has two drawbacks:

1. DTPA does not work in acidic solutions; a buffer must be added to maintain pH at approx. 3.
2. To keep the lanthanides in the organic phase under such conditions, a nitrate salt must be added to the selective back extraction solution. Another option is adding a second extracting agent to keep lanthanides in the organic phase at low acidity.

This however generates additional secondary wastes.

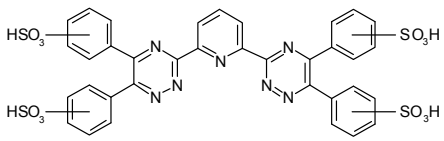

Fig. 6: *SO_3-Ph-BTP.*

Recent fundamental studies show that BTP remains selective in aqueous phase [7]. This means that a hydrophilised BTP should be useful as selective actinide(III) complexing agent for *i*-SANEX process development.

We have synthesised a hydrophilic BTP, 2,6-bis(5,6-di(sulphophenyl)-1,2,4-triazin-3-yl)-pyridine (SO_3-Ph-BTP, **Fig. 6** [10]). SO_3-Ph-BTP has excellent solubility in water or HNO_3;

no less than 0.5 mol/L is soluble in 0.5 mol/L HNO_3.

Liquid-liquid extraction tests

SO_3-Ph-BTP was tested for its ability of selectively masking actinides(III) in nitric acid solutions (thus also allowing for their selective back extraction). Tests were performed extracting Am(III) and Eu(III) from HNO_3 into a solution of TODGA [11] + 5% 1-octanol in kerosene (TODGA co-extracts actinides(III) and lanthanides from nitric acid).

Influence of HNO_3 concentration

While TODGA co-extracts Am(III) and Eu(III), addition of 10 mmol/L SO_3-Ph-BTP to the aqueous phase suppresses the extraction of Am(III) while it has little influence on the extraction of Eu(III), see **Fig. 7**. For 0.1 mol/L < $[HNO_3]$ < 0.6 mol/L, $D_{Am(III)} < 1$ and $D_{Eu(III)} > 1$ (meaning Am(III) largely remains in the aqueous phase whereas Eu(III) is extracted into the organic phase). The separation factor $SF_{Eu(III)/Am(III)} = D_{Eu(III)}/D_{Am(III)}$ is in the range of 250–1000, as compared to $SF_{Eu(III)/Am(III)} \approx 7$ without SO_3-Ph-BTP (being the selectivity of TODGA).

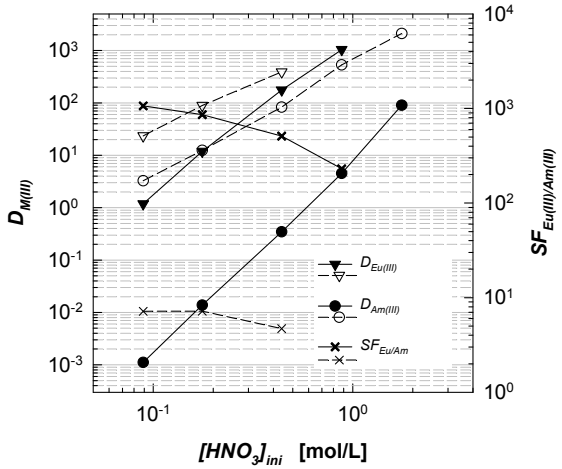

Fig. 7: *Effect of SO_3-Ph-BTP on the extraction of Am(III) and Eu(III) into TODGA. Organic phase, 0.2 mol/L TODGA + 5 % vol. 1-octanol in kerosene. Aqueous phase, ^{241}Am(III) + ^{152}Eu(III) in HNO_3, with (filled symbols, solid lines) or without (open symbols, dashed lines) 10 mmol/L SO_3-Ph-BTP.*

In a more realistic experiment, Am(III) + Eu(III) were extracted from a spiked PUREX raffinate surrogate into (0.2 mol/L TODGA + 5 % vol. 1-octanol in kerosene). The loaded phase was back extracted into

a) H_2O, resulting in $D_{Am(III)} = 23$; $D_{Eu(III)} = 180$; $SF_{Eu(III)/Am(III)} = 7.5$
b) 10 mmol/L SO_3-Ph-BTP in H_2O, resulting in $D_{Am(III)} = 0.059$; $D_{Eu(III)} = 49$; $SF_{Eu(III)/Am(III)} = 830$, demonstrating selective back-extraction of Am(III) from a loaded organic phase.

Influence of SO_3-Ph-BTP concentration

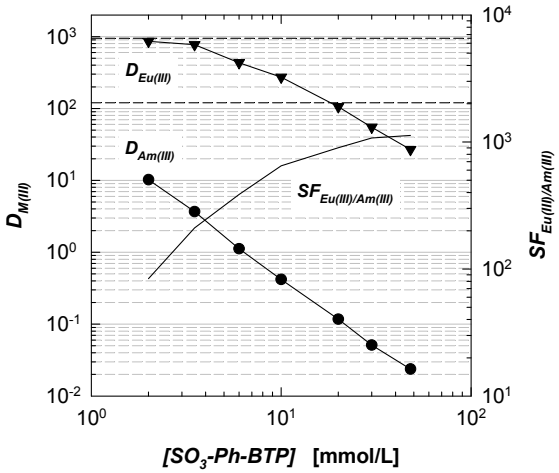

Fig. 8: *Extraction of Am(III) and Eu(III) into TODGA, influence of $[SO_3$-Ph-BTP$]$. Organic phase, 0.2 mol/L TODGA + 5 % vol. 1-octanol in kerosene. Aqueous phase, ^{241}Am(III) + ^{152}Eu(III) (1 kBq/mL each) + SO_3-Ph-BTP in 0.50 mol/L HNO_3.*

Fig. 8 shows the extraction of Am(III) and Eu(III) from 0.5 mol/L HNO_3 with varied concentrations of SO_3-Ph-BTP into a solution of (0.2 mol/L TODGA + 5 % vol. 1-octanol in kerosene). The horizontal dashed lines represent distribution ratios ($D_{Eu(III)}$ = 950, $D_{Am(III)}$ = 120) in the absence of SO_3-Ph-BTP. Adding increasing concentrations of SO_3-Ph-BTP increasingly suppresses the extraction of Am(III); the extraction of Eu(III) is less affected.

The separation factor $SF_{Eu(III)/Am(III)}$ has a value of 900 for e.g. 20 mmol/L SO_3-Ph-BTP; with increasing SO_3-Ph-BTP concentration it approaches a value of approx. 1200.

Back extraction kinetics

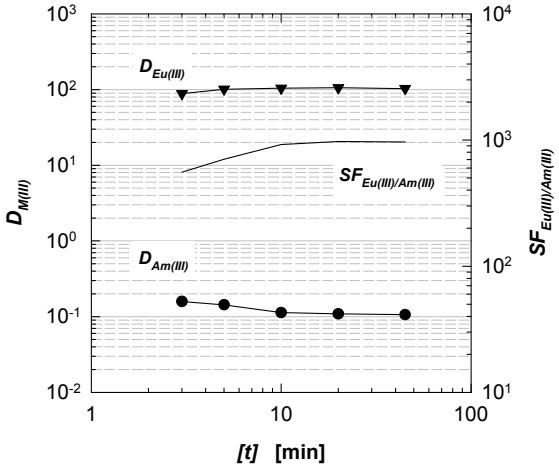

Fig. 9: *Am(III) and Eu(III) back extraction kinetics with SO_3-Ph-BTP. Organic phase, 0.2 mol/L TODGA + 5 % vol. 1-octanol in kerosene, loaded with ^{241}Am(III) + ^{152}Eu(III) (1 kBq/mL each) from 3 mol/L HNO_3. Aqueous phase, 20 mmol/L SO_3-Ph-BTP in 0.29 mol/L HNO_3.*

To test back extraction kinetics, Am(III) and Eu(III) were extracted from 3 mol/L HNO_3 into

an organic phase consisting of (0.2 mol/L TODGA + 5 % vol. 1-octanol in kerosene). Then the loaded solvent was contacted with a solution of SO_3-Ph-BTP in 0.29 mol/L HNO_3. The influence of contacting time on Am(III) and Eu(III) distribution ratios is shown in **Fig. 9**. Although the mechanical shaking device used for this experiment is not very efficient (oscillating at approx. 5 Hz), equilibrium was attained within 10 min. Within only 3 min distribution ratios were close to equilibrium. This indicates that the selective An(III) back extraction with SO_3-Ph-BTP is not impeded by slow kinetics.

Separation of An(III) from Ln(III)

TODGA is known to extract Am(III) and Cm(III) from HNO_3 with distribution ratios similar to those of the lighter lanthanides [11]. The effect of adding 20 mmol/L SO_3-Ph-BTP to the aqueous phase is shown in **Fig. 10** (although all Ln(III) except Pm(III) were measured, only data up to Dy(III) are shown as the heavier Ln(III) are not present in irradiated nuclear fuel). The extraction of Am(III) and Cm(III) is strongly suppressed. The extraction of the lightest lanthanides is virtually unchanged; the extraction of heavier lanthanides is increasingly suppressed but not to an extent as to interfere with An(III) extraction.

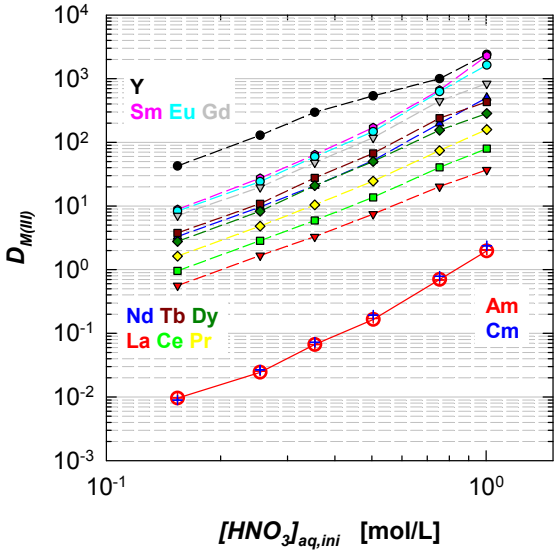

Fig. 10: *Effect of SO_3-Ph-BTP on the extraction of An(III) and Ln(III) into TODGA. Organic phase, 0.2 mol/L TODGA + 5 % vol. 1-octanol in kerosene. Aqueous phase, 20 mmol/L SO_3-Ph-BTP + ^{241}Am(III) + ^{244}Cm(III) (1 kBq/mL each) + (Y(III) + Ln(III), 20 mg/L each) in HNO_3.*

Clearly, an efficient separation of Am(III) and Cm(III) from all lanthanides is viable, the lowest selectivity (Cm(III) over La(III)) having a separation factor of approx. 50.

TRLFS complexation studies

Solutions of Cm(III) in water or HNO_3 were titrated with increasing concentrations of SO_3-Ph-BTP and fluorescence spectra were recorded.

Complexation in H_2O

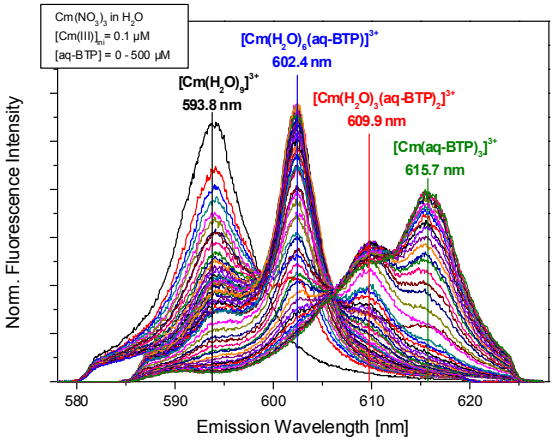

Fig. 11: *Titration of Cm(III) with SO_3-Ph-BTP in H_2O. Fluorescence spectra as a function of SO_3-Ph-BTP concentration. Initially $2 \cdot 10^{-7}$ mol/L Cm(III); 0–500 µmol/L SO_3-Ph-BTP in H_2O (pH = 2.7).*

When Cm(III) is titrated with SO_3-Ph-BTP in H_2O (pH = 2.7), three new complex species with emission maxima at 602.4 nm, 609.9 nm, and 615.7 nm form the Cm(III) aquo complex (see **Fig. 11**). Slope analysis identifies them as 1:1, 1:2, and 1:3 Cm(III)-BTP complexes. As is the case with other Cm(III)-BTP complexes, lifetimes cannot be linked quantitatively to hydration numbers with the *Kimura* equation, due to quenching by the coordinating BTP molecules [7].

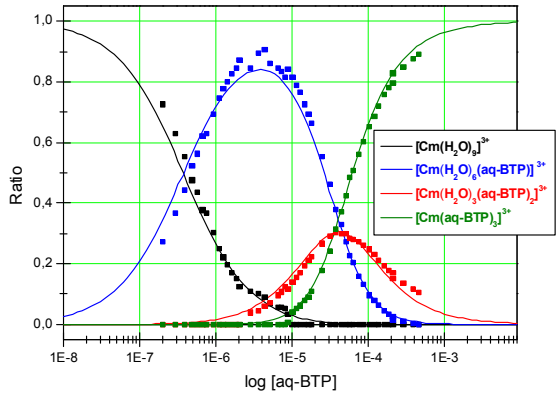

Fig. 12: *Species distribution derived from fluorescence spectra (**Fig. 11**). Symbols, experimental data. Lines, calculated with $\log\beta_1$ = 6.4; $\log\beta_2$ = 10.7; $\log\beta_3$ = 15.2.*

A speciation plot is shown in **Fig. 12**. Clearly, at *[SO_3-Ph-BTP]* > 1 mmol/L, only the 1:3 complex is present. The following stability constants are calculated, $\log\beta_1$ = 6.4; $\log\beta_2$ = 10.7; $\log\beta_3$ = 15.2. The $\log\beta_3$ value is slightly larger than $\log\beta_3$ = 14.4 for the [Cm(*n*-Pr-BTP)$_3$]$^{3+}$ complex in methanol/water [7].

Complexation in HNO_3

When Cm(III) is titrated with SO_3-Ph-BTP in (0.2 mol/L, 0.5 mol/L, 0.7 mol/L, 1.0 mol/L) HNO_3, formation of the 1:1 and 1:2 complexes is suppressed. The 1:3 complex directly forms from a mixture of the aquo species (593.8 nm) and the nitrato species (596.8 nm). This is shown in **Fig. 13** for 0.5 mol/L HNO_3, and is further supported from the results of slope analysis, see **Fig. 14** and **Tab. 1**.

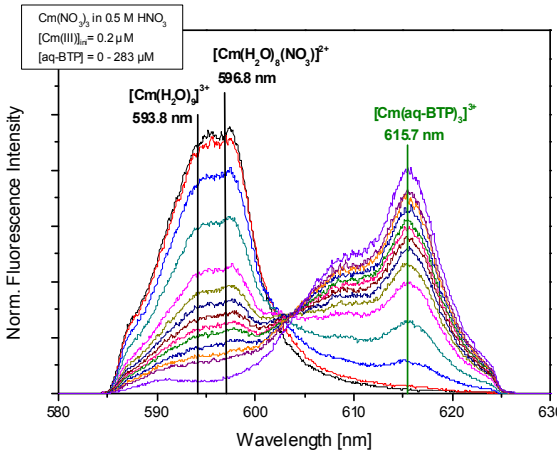

Fig. 13: *Titration of Cm(III) with SO_3-Ph-BTP in HNO_3. Fluorescence spectra as a function of SO_3-Ph-BTP concentration. Initially $2 \cdot 10^{-7}$ mol/L Cm(III); 0–283 µmol/L SO_3-Ph-BTP in 0.5 mol/L HNO_3.*

Stability constants $\log\beta_3$ for the 1:3 complex are summarised in **Tab. 1**. It is interesting to notice that both the slopes and the stability constants decrease with increasing HNO_3 concentration. However, it must be considered that stability constants were calculated with concentrations, not with activities. A meaningful discussion of these results is thus not yet possible. The required calculations are currently being performed.

Tab. 1: *Results from slope analysis and stability constants $\log\beta_3$ for the complexation of Cm(III) with SO_3-Ph-BTP in HNO_3. The stability constant in H_2O (pH = 2.7) is shown for comparison.*

[HNO_3] (mol/L)	0.2	0.5	0.7	1.0	(pH = 2.7)
slope	2.9	2.9	2.8	2.7	
$\log\beta_3$	13.7	13.3	12.9	12.6	15.2

Conclusions

SO_3-Ph-BTP was successfully tested as a hydrophilic complexing agent for actinides(III). This compound is highly efficient for the selective back etraction of An(III) from e.g. a loaded TODGA phase. HNO_3 can be used as salting out agent for the lanthanides in the selective back extraction section; no additional salts or buffering agents are required. The available data indicate that a flowsheet for a selective An(III) back extraction process would not require many stages.

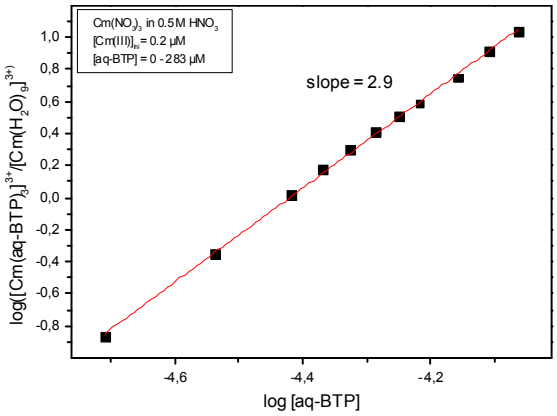

Fig. 14: *Double logarithmic plot of the concentration ratio ($[Cm(BTP)_3]^{3+}$ / Cm^{3+}_{aq}).*

References

[1] K. Gompper A. Geist and H. Geckeis, Nachr. Chem., 58, 1015-1019 (2010).

[2] Z. Kolarik, U. Müllich and F. Gassner, Solvent Extr. Ion Exch., 17, 1155-1170 (1999).

[3] S. Trumm, A. Geist, P.J. Panak and T. Fanghänel, Solvent Extr. Ion Exch., 29, 213-229 (2011).

[4] A. Geist, C. Hill, G. Modolo, M.R.S. Foreman, M. Weigl, K. Gompper, M.J. Hudsonand C. Madic, Solvent Extr. Ion Exch., 24, 463-483 (2006).

[5] C. Madic, F. Testard, M.J. Hudson, J.-O. Liljenzin, B. Christiansen, M. Ferrando, A. Facchini, A. Geist, G. Modolo, A.G. Espartero, and J. De Mendoza, CEA-R-6066, CEA, France, (2004).

[6] M.G.B. Drew, M.R.S. Foreman, A. Geist, M.J. Hudson, F. Marken, V. Norman and M. Weigl, Polyhedron, 25, 888-900 (2006).

[7] S. Trumm, P.J. Panak, A. Geist and T. Fanghänel, Eur. J. Inorg. Chem., 3022-3028 (2010).

[8] X. Hérès, C. Sorel, M. Miguirditchian, B. Camès, C. Hill, I. Bisel, D. Espinoux, C. Eysseric, P. Baron, and B. Lorrain, (2009) Proc. Internat. Conf. GLOBAL 2009, Paris, 6–11 September 2009, paper 9384.

[9] B. Weaver and F.A. Kappelmann, ORNL-3559, Oak Ridge Nat'l Laboratory, (1964).

[10] G.L. Traister and A.A. Schilt, Anal. Chem., 48, 1216-1220 (1976).

[11] Y. Sasaki, Y. Sugo, S. Suzuki and S. Tachimori, Solvent Extr. Ion Exch. 19, 91-103 (2001).

8. Vitrification of High-Level Radioactive Liquid Waste

H. Braun, W. Gr newald, K. Hardock, J. Knobloch, K. Meyer, G. Roth, A. Salimi, W. Tobie, S. Weisenburger, U. Weiler, K.-H. Weiß, M. Böttle, F. Geyer, A. Görtzen, K. Gompper, S. Heck, A. Kaufmann, T. Kisely, M. Lagos, M. Plaschke, A. Seither, C. Walschburger, A. Kutzer, P. Kaden, T. Vitova

8.1 VEK Project

Introduction

Fourteen years after its establishment the mission of the VEK project has been fulfilled by end of 2010. The VEK project has been founded to immobilize approx. 60 m³ of high-level liquid waste (HLLW) with a total radioactive inventory of 7.7E+17 Bq in the new VEK vitrification plant erected from 1999 to 2004 and equipped with INE's vitrification technology. Immobilization of the waste solution stored at the site of the former German WAK pilot reprocessing facility has been the prerequisite to further decommissioning and dismantling of the WAK facilities which have been underway since the mid-nineties. Within a minimum operation period of only 9 months from September 2009 until June 2010 the highly noble metals containing HLLW was successfully processed and the HLLW storage tanks of WAK were finally emptied. Subsequent to hot vitrification of the HLLW solution an extensive rinsing of the storage tanks and VEK plant components was performed. The resulting rinsing liquids were also vitrified. As a general outcome of the VEK operation it can be stated, that the vitrification technology designed by INE proved to be reliable and mature.

Vitrification of stored HLLW

Vitrification of genuine HLLW was started on September 16th, 2009 and terminated on June 21st, 2010. The HLLW had been transferred by 37 batches of about 1.5 m^3 each from the two storage tanks alternating into one of the two HLLW receipt tanks of VEK. The HLLW processing phase was terminated by emptying the melter completely and subsequent immediate refilling with start glass to keep the melter in idling conditions in preparation of following processing of liquids arising from rinsing of HLLW storage tanks and process components. The production data resulting from HLLW processing are given in the first data column of Table 1. Finally 55,5 m^3 of HLLW solution were immobilized in 48,9 metric tons of waste glass. The waste glass was poured by 478 batches into 123 canisters including one resulting from melter emptying at the end of the HLLW campaign. In total more than 400 kg of noble metals (in terms of elements) were vitrified.

Rinsing operation

Table 1 also contains major production data obtained from the vitrification of waste solutions generated during the plant rinsing program. This program was completed by November 24th, 2010 and followed by immediate shutdown of the waste glass melter. During a production period of 55 days 22 m^3 of rinsing solutions were processed in 13 batches to nearly 7 metric tons of waste glass poured into another 17 glass canisters. About 10 m^3 of the solution (8 batches) originating from HLLW storage tank rinsing were directly vitrified whereas another 5 batches were mixtures of different origin (rinsing liquids, scrub solution from dust scrubber, evaporator concentrate, HLLW simulate). To adhere to the guaranteed canister specification, chemicals (Na, Fe, La, Ni, Mn as nitrate solutions) were partly added to the rinsing solution mix prior to vitrification. The production data of the rinsing operation is also given in Table 1, which additionally contains an overview of the complete production data of the VEK operation compared to the design data. The comparison shows an increase of canisterized glass due to the additional rinsing program which was not included in the planning basis.

Plant availability

The comparison of the total production time of the VEK with the planned maximum operation time of 18 months (9 months net time for HLLW processing at the design HLLW throughput of 9 l/h at 100 % time availability) reveals a remarkably high availability of the complete vitrification process. During the processing of the HLLW solution as well as during the rinsing operation a time availability of about 97% was achieved (see table 1). Major operation troubles associated with an interruption of HLLW feeding were mainly due to:

- Exchange of the melter offgas pipe due to severe deposits – interruption of feeding for 22 hours

- Installation of an air bubbler to remobilize assumed noble metal built-up and exchange of the glass inventory - interruption of feeding for 35 hours

- Glass exchange with addition of solids deposits removed from the offgas pipe – interruption of feeding for 81 hours

Tab. 1: Main production data of VEK operation in comparison with planned values

Parameter	Production data HLLW operation	Production data rinsing operation	Total production data	Planning basis
Operation time	9 months	1.8 months	10.8 months	18 months
HLLW volume/ rinsing solution	55.5 m HLLW	22 m (including HLLW simulate)	77.5 m	60 m HLLW
Glass product	48.8 t	6,8 t	55.6 t	50 t
Glass pourings	478	65	543	500
Number of canisters (400 kg)	123	17	140	125
Plant availability	97%	99 %	98 %	50*)%

*) Calculation based on net operation time at design throughput of 9 l/h of HLLW

Apart from theses major interruptions during HLLW processing there were only a few minor problems that did not essentially reduce the productivity of the plant.

Melter operation and glass pouring

As already demonstrated during the cold test phase, the VEK melter proved to be a reliable component also under hot operation conditions. The design throughput of about 10 l/h was maintained with high precision during processing of HLLW and also of rinsing liquids. The sophisticated melter feed and process control ensured the maintenance of specified melting conditions required from safety as well as from glass quality assurance point of view. The accurate glass filling into the canisters during more than 540 glass pourings confirmed the reliability of the bottom drain system. The bottom drain system is one of the key features of the melter to ensure the processability of highly noble metals-containing HLLW solutions.

Noble metals behavior

A major concern of processing the HLLW from WAK was due to the high concentration of noble metals Ru, Rh, and Pd. In total, 408 kg noble metals (in terms of oxides) passed through the melter during vitrification operation. The melting process is greatly influenced by the behavior of the noble metals which are insoluble in the glass melt [1]. As the noble metals cannot be bound in the borosilicate glass matrix and tend to accumulate and form electrically conductive layers at the bottom of the melter. The discharge behavior is affected adversely by the high viscosities of those sediments. Accumulating noble metals may impact the operation of the directly heated melter by distortion of the electrical field. The design of the VEK melter with funnel-shaped walls at an angle of > 50° at the bottom largely prevents such sedimentations (see Fig. 1). The electric operation data (voltage, current, and power input) of the main electrodes are plotted in Fig. 2 versus operation time.

After about 7 months of smooth operation, a significant decrease in voltage and power occurred, that was attributed to the onset of noble metal deposition. Compensation of the power loss by increased current did not stop this trend. A later detailed analysis of electrical potential data revealed a nonsymmetrical accumulation near the bottom electrode. As countermeasure to recover the previous operability, an air bubbler was installed with the outlet close to the assumed noble metals

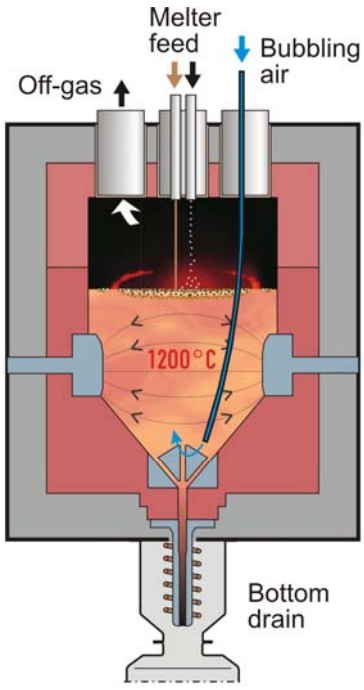

***Fig. 1:** Scheme of the noble metals compatible VEK melter design including arrangement of air bubbler*

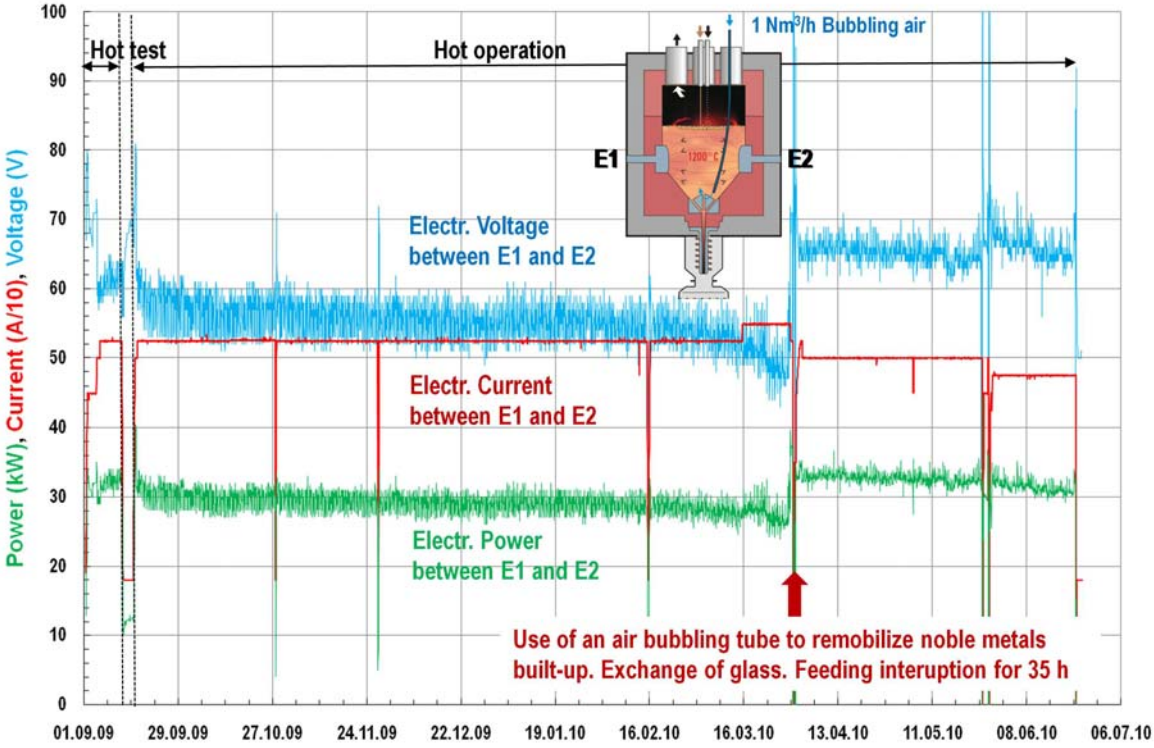

Fig. 2: *Electrical operation data of the VEK glass melter*

built-up in order to remobilize the sediments. Additionally a complete exchange of the glass inventory was performed. Both measures together were successful as they caused the operation parameters of the melter to return to normal values. The operation could then be continued without further noble metals induced incidents.

Melter emissions and off-gas treatment

In the course of the HLLW processing the melter emissions increasingly caused material deposits along the wall of the melter off-gas pipe. The properties of these deposits proved to be of a hard nature. As a result the periodical cleaning with pressurized air blasters was not effective enough to prevent long-term plugging of the off-gas pipe. The somewhat sintered material reflects a comparably high off-gas temperature due to non-optimized cold cap conditions in the melter.

Higher temperature conditions in the melter plenum also entail an increased volatility of elements like cesium and technetium. From balance calculations the Cs retention of the melter did not confirm the results known from the operation of the PAMELA plant and of inactive operation of the prototype test facility at INE. However, the emitted cesium was effectively retained in the off-gas treatment system, as there was no indication of increased radioactivity at the monitoring point at the stack.

Product specification

All of the 140 canisters produced by VEK have met the specified composition and quality parameters. For the canisters produced during HLLW processing, the waste glass loading was aimed at a target of 16.0 wt.%. After the initial phase of the rinsing operation the target waste glass loading was reduced to 15.0 wt.% to keep the quality parameters in the tolerated range. Figure 3 shows the values calculated from mass balance and used for product control. For canister declaration these values were corrected by taking into account the material loss of the stored HLLW caused by evaporation. The data range of the quality parameters for all canisters are compiled in Table 2 and compared with the guaranteed values.

Intermediate Storage of glass canisters

Five CASTOR casks have been available for the interim storage of the canisters. Directly

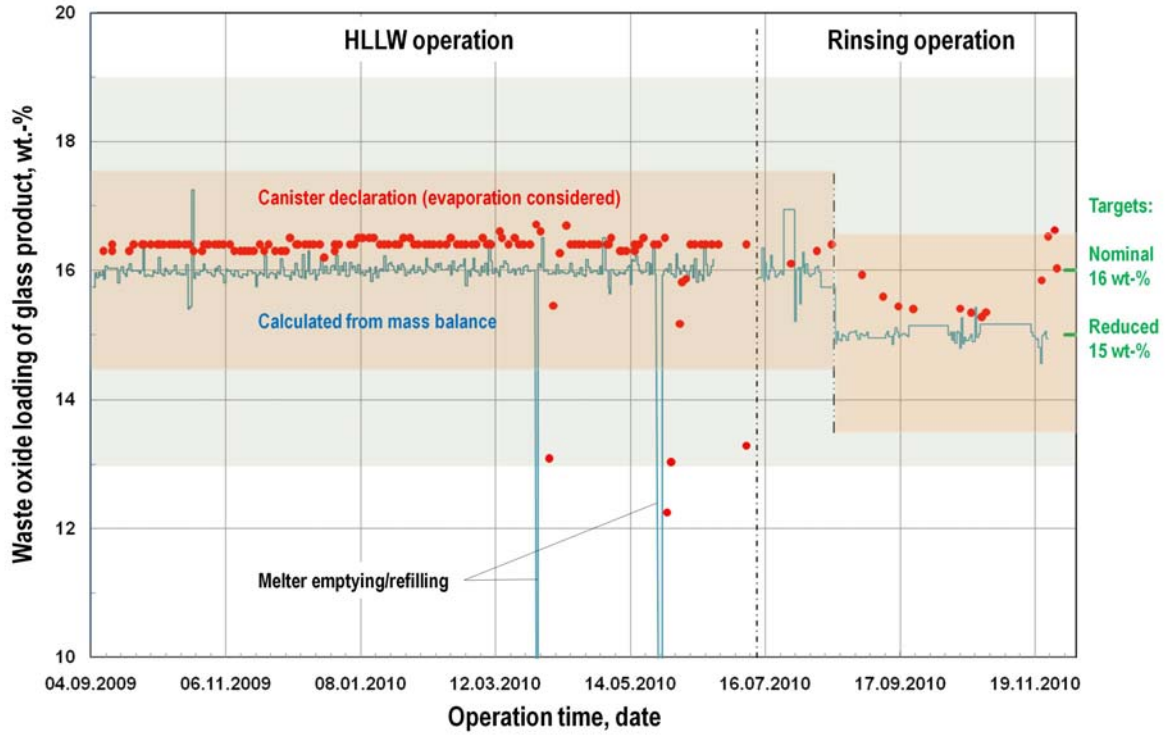

Fig. 3: *Waste glass loading achieved during HLLW processing and rinsing operation phases*

Tab. 2: *Specified canister data compared with guaranteed values*

Parameter	Guaranteed value	Average value	Data range
Waste oxide loading, wt.%	≤19	16.2	12.2 - 16.7
Total mass, kg	<550	496	466.1 - 497.9
Activity Sr-90/Y-90, Bq	<4.5 E15	1.98 E15	5.32 E13 - 51 E15
Activity Cs-137/ Ba-137, Bq	<5.1 E15	3.35 E15	6.46 E13 - 4.02 E15
α activity, Bq	<8.6 E13	4.54 E13	7.17 E11 - 6.42 E13
β/γ activity, Bq	<9.6 E15	6.89 E15	1.19 E14 - 8.67 E15
Mass U, g	<7200	3700	92 - 4730
Mass PU, kg	<210	128	3 - 162
Dose rate			
β/γ (surface), Gy/h	<440	183	2 - 225
β/γ (distance 1m) Gy/h	<35	14	0.2 - 18
Decay heat, W	<734	455	10 W - 548

after the production of a canister, contamination and dose rate measurements are performed to verify the radiological and inventory data, and the canister data are then transmitted to PKS (Produktkontrollstelle Jülich) for review. After each 28 canisters have been produced, all canister data are passed on to the supervisory authority of the state of Mecklenburg-West Pomerania responsible for interim storage. This ensures timely clearance for loading. By end of 2010 four CASTOR casks have been loaded according to schedule. No operation interruptions due to delayed review or cask preparation have occurred. Transportation of all CASTOR casks has been envisaged for early 2011.

Chemical analysis of HLLW solutions

The nuclear operation of VEK was accompanied by chemical process analysis under the guidelines of the VEK analysis handbook [2]. Sampling and sample preparation (i.e., filtration and dilution) is accomplished by WAK-VEK hot laboratory and sample transport is organized by WAK-HDB. At KIT-INE all samples were repacked due to elevated superficial contamination of sample tubes and further diluted. Samples from the receipt tank (HLLW), wet off-gas and secondary liquid waste treatment (i.e., dust scrubber, jet scrubber, condenser, NOx absorber and concentrate tank) are analyzed regularly. Multi-element and isotope analysis are performed by box-adapted inductively coupled plasma optical emission spectrometry (ICP-OES, Perkin Elmer Optima 4300) and mass spectrometry (ICP-MS, Perkin Elmer Elan 6100). Special measuring procedures were developed for all methods. As a matter of course quality control of chemical analysis including accurate documentation are assured.

Figure 4 demonstrates the chemical composition of receipt tank samples during the nuclear operation which can be sequenced as

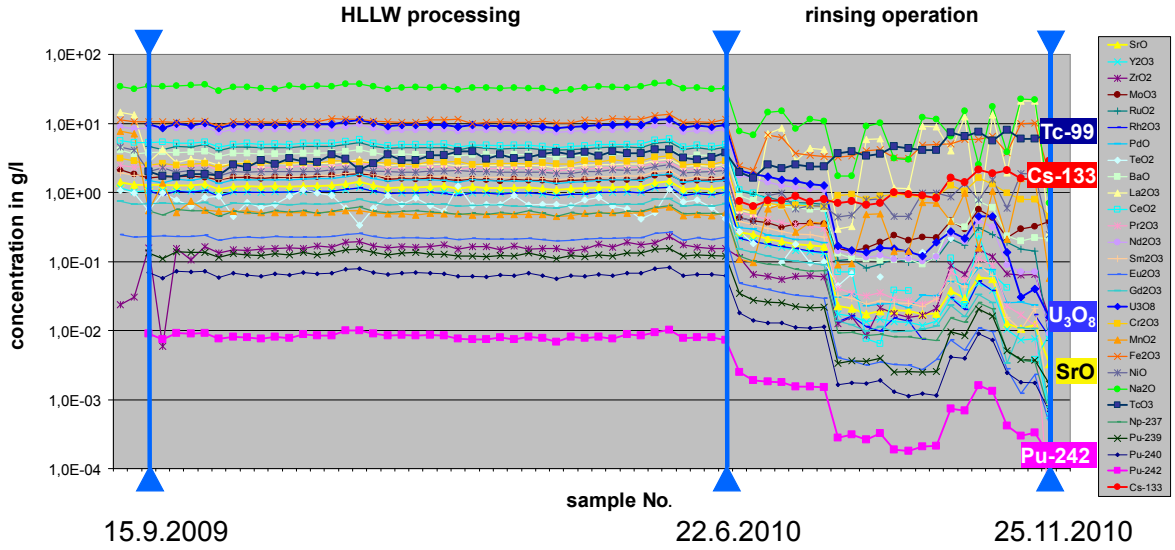

Fig. 4: *Elemental analysis of receipt tank samples during nuclear VEK operation*

follows: (1) nuclear test operation in September 2009, (2) nuclear operation (vitrification of HLLW) from September 2009 until June 2010 and (3) rinsing operation (vitrification of scrubbing solutions) from June 2010 until November 2010.

Samples from the receipt tanks (HLLW) are analyzed weekly and, as expected, provide a constant elemental composition during operation. A slight increase of the Tc-99 is observed during the process both in receipt tank and wet off-gas samples (not shown). Tc is among the volatile elements and is effectively retained (thereby enriched) by the off-gas treatment and recycled during the process.

In the course of the plant operation a solid condensed on the walls of the melters' off-gas pipe (see above). These pipe sections had to be exchanged once to maintain further operation. From the vertical and horizontal part of these pipe sections two highly active samples (each around 100 mg and 1 Sv/h dose rate) were taken, digested at JRC-ITU (Institute for Transuranium Elements) and analyzed at INE and ITU. Both labs found an elemental pattern correlating to HLLW with an enrichment of volatile elements, i.e. Cs and Tc.

During the rinsing operation the vitrification plant including the two storage tanks is extensively decontaminated by flushing with nitric acid. Scrubbing solutions from different plant components (optionally concentrated by evaporation) were finally merged in the receipt tanks and vitrified. Before that, simulant solutions containing Na, La, Fe, Mn and Ni must be added in order to assure constant process parameters and glass product quality (see Figure 4).

Tab. 3: *Sample statistics of VEK operation*

	3/2009	4/2009	1/2010	2/2010	3/2010	4/2010	Σ
receipt tank (HAWC)	4	14	13	12	13	8	64
dust scrubber	4	8	5	11	3	5	36
jet scrubber	7	13	3	3	3	3	32
condenser	6	10	4	3	3	3	29
NOx absorber	7	11	3	3	3	3	30
concentrate tank	2	6	10	10	8	1	37
solid samples				4	2		6
other samples	1	3		1	3		8
glas frit				7			7
Σ	31	65	38	54	38	23	**249**

In summary, around 250 highly radioactive samples were analyzed during nuclear operation of VEK (Table 3). Elaborated analytical procedures, application of management tools and good co-operation between the involved laboratories were the precondition for effective analytical work always staying on the tight time schedule of the vitrification process.

8.2 VPC Project

The VPC project has been founded to construct a HLLW vitrification plant in the Sichuan province of China on the basis of the technology developed by KIT-INE. Official start of the project had been December 1st, 2009. In 2010 the main part of the project was dedicated to elaboration of the basic design of the vitrification plant and the intermediate storage building to be used for waste glass canisters. The first edition of basic design documentation (BDD) had been delivered in September 2010. A second revised BDD edition was delivered in December 2010.

The scope of the basic design carried out by INE covered the core process (HLLW reception, HLLW and glass frit feeding, glass melting, electric power supply for melter including melter instrumentation and control and wet off-gas treatment system). Essential contributions comprehended the creation of a preliminary layout of the process building (PB), the arrangement of the melter and the other process components (feeding vessel, dust scrubber, condenser) in the melter cell V2 (3D design). Further contributions delivered were the elaboration of the process block diagram, the piping and instrumentation (P&I) flow sheets and the associated instrumentation and sampling (I&S) flow sheets along with the associated component drawing and lists.

Another part of planning dealt with the creation of the BDD of the glass melter and its subcomponents including the mean frequency heating system of the bottom drain system.

The BD activities were supplemented by an experimental program performed to design the airlift systems that will be applied in the VPC plant including the transfer of waste solution and the circulation of scrub solution in the dust scrubber. The results were used for dimensioning of the pipes, determination of the air flow rates, the submerge conditions and the geometrical arrangement.

8.3 Structural investigations of elements with low solubility in simulated HLW borosilicate glass

Introduction

Immobilization of high level radioactive liquid waste (HLW) by vitrification is a well established process that has been studied extensively over the last 50 years. Borosilicate glass is the preferred first generation waste form, due to extensive knowledge of its properties and manufacture. Its selection as preferred waste form is based on its flexibility for waste loading and its tolerance towards variations in waste stream composition, coupled with good glass-forming ability and acceptable thermal, mechanical, and chemical stability. However, the presence of certain critical elements in radioactive waste, like molybdenum or sulfur, can be particularly problematic due to their low solubility in borosilicate glass compositions that are currently used for immobilization of HLW [3,4]. Combined with other elements, molybdenum and sulfur tend to form complex 'yellow phases', which can incorporate significant amounts of radioactive isotopes. Furthermore, these phases may crystallize during melt glass cooling, thereby negatively affecting waste durability. One strategy to avoid such phase separation processes is to minimize waste loading, which has the detrimental effect of leading to an intolerable volume of waste glass. It is therefore important to develop glass compositions with an enhanced capacity of accommodating critical elements in its matrix. To this end, understanding the molecular mechanisms controlling such element's incorporation into the glass matrix is essential.

In this work fundamental structural investigations have been performed on two types of borosilicate glass compositions having varying Mo content: a simple low component system, as well as a complex multi-component glass composition simulating vitrified nuclear waste. Spectroscopic methods have been applied to obtain information of glass structure, in particular X-ray absorption near edge structure (XANES) and Magic Angle Spinning Nuclear Magnetic Resonance (MAS NMR) spectroscopy.

Experimental

Glass preparation:

Two glass systems were synthesized: A five component system (SiO_2-B_2O_3-Na_2O-Eu_2O_3-SO_3) representing a simple, model nuclear waste glass and a complex simulated 'VPC' nuclear waste glass system. The glasses were prepared from mixtures of stoichiometric amounts of SiO_2, B_2O_3, Na_2CO_3 and various additional components, depending on the glass composition. All samples were first decarbonized for 1 h at 800°C in air in Pt crucibles and then molten for 2 h at 1150, 1200 or 1250°C. Subsequently the glass melts were quenched as cylinders on a stainless steel plate without annealing.

MAS-NMR:

^{29}Si MAS NMR spectra were recorded at 79.50 MHz on a Bruker Avance III 400 spectrometer and ^{11}B MAS NMR spectra at 272.73 MHz on a Bruker Avance III 850 spectrometer. Powdered samples were spun at 15 kHz in a 4 mm MAS probe. Chemical shifts were determined relative to tetramethylsilane for ^{29}Si ($\delta(^{29}Si) = 0$) and liquid H_3BO_3 for ^{11}B ($\delta(^{11}B) = 0$).

XANES spectroscopy:

Mo K-edge XANES spectra were recorded at the INE-Beamline at ANKA. Pressed sample pellets of 13 mm diameter were prepared for measurements using a mixture of powder

samples diluted with microcrystalline cellulose. Energy calibration was performed by defining the first inflection point in the XANES of a Mo(0) foil measured in transmission mode simultaneously as 20.0 keV. All sample XANES spectra were measured in fluorescense mode.

Results and discussion

MAS NMR studies:

An example of a ^{29}Si MAS NMR spectrum recorded for the five component model waste glass is shown in Figure 5. The ^{29}Si MAS spectrum was fit with the DMFIT program [5], deconvoluting it into three Gaussian functions centered at -83.0, -89.6 and -97.1 ppm with relative proportions of 41.5, 35.6 and 22.9 %, attributed to Q_2, Q_3 and Q_4 units, respectively. The designation of Q_n units with n = 0 - 4 corresponds conventionally to tetrahedral [SiO_4] units with n bridging oxygen atoms. Individual peak intensities indicate the relative proportions of three different ^{29}Si unit environments, i.e. the degree of network polymerization in the glass, with Q_2 indicating chain polymerization, Q_3 two dimensional sheets and Q_4 the amount of [SiO_4] units building a three dimensional framework in the Si network. ^{29}Si MAS NMR spectra were obtained for various simplified nuclear waste glasses containing different amounts of sulfate. The spectra show that the incorporation of sulfate ions has an effect on the network polymerization; with increasing sulfate concentration, the proportions of the lower polymerized Si species, Q_2 as well as Q_3, increase. This effect has also been reported on a comparable system [6]. Further investigations on the influence of the incorporation of other critical components on the Si network of complex model nuclear waste glasses are currently underway.

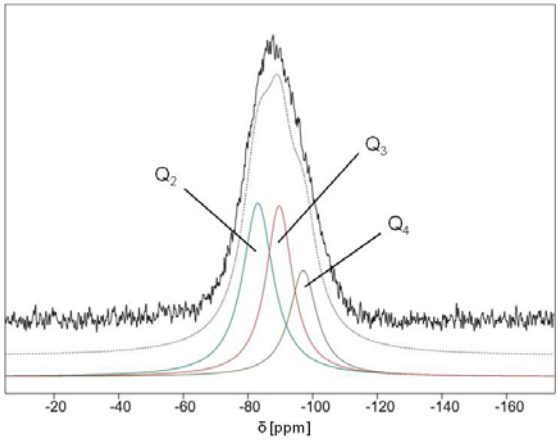

Fig. 5: *^{29}Si MAS NMR spectrum (black), fit (narrow black line) and Gaussian deconvolution (colored lines) of one of the simple model nuclear waste glasses studied. The individual peaks indicate the relative proportions of three different ^{29}Si environments, which indicate the degree of polymerization of the Si network.*

In Figure 6, an example of a ^{11}B MAS NMR spectrum recorded for an inactive 'VPC' nuclear waste glass is shown. ^{11}B signals corresponding to $BO_{3/2}$ ($^{[3]}$B) and $BO_{4/2}$ ($^{[4]}$B) species are centered around 12.5 and -2.5 ppm, respectively.

The use of a high magnetic field (20 T) allows good resolution between the trigonal planar $BO_{3/2}$ and the symmetric tetrahedral $BO_{4/2}$ species, because the line shape of the $BO_{3/2}$ signal is not affected by second order quadrupolar interactions, which are scaled inversely to the magnetic field strength. This is prerequisite for quantifying the different ^{11}B environments through deconvolution of individual signal components. Several ^{11}B MAS NMR spectra of inactive 'VPC' nuclear waste glasses with varying MoO_3 contents were obtained. The spectra indicate only a limited dependence of the different ^{11}B species distribution in the boron network on the incorporation of MoO_3.

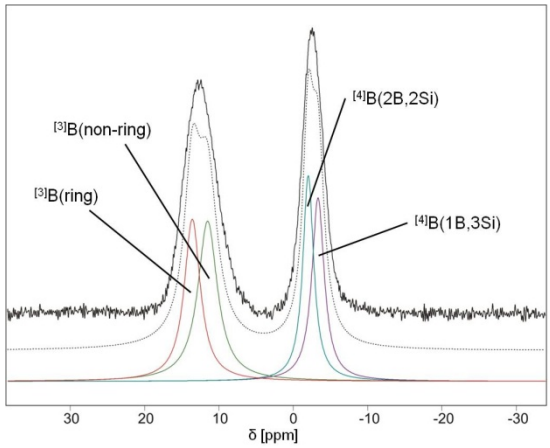

Fig. 6*: ^{11}B MAS NMR spectrum (black), fit (narrow black line) and Gaussian deconvolution (colored lines) of one of the inactive 'VPC' nuclear waste glasses showing the relative proportions of the different ^{11}B environments.*

Mo K-edge XAFS studies:

The Mo K-edge XANES spectra of inactive 'VPC' nuclear waste glasses containing different MoO_3 concentrations are shown in Figure 7. The shape of XANES spectral features (indicated by an arrow in Fig. 3) systematically changes as a function of the MoO_3 concentration. This suggests a systematic change in occupancies of Mo outer electronic states with changing glass loadings.

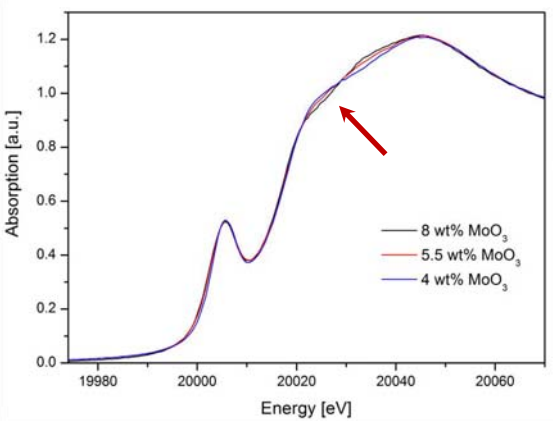

Fig. 7: *Mo K-edge XANES spectra of inactive 'VPC' nuclear waste glasses containing different MoO_3 concentrations.*

Work is underway to correlate the observed spectral trends with Mo outer orbital states and associated local structural changes by performing calculations with suitable codes, e.g., based on the multiple scattering theory (FEFF9, FDMNES) and comparing these to EXAFS results.

Outlook

Synthesis and spectroscopic characterization of further nuclear waste glass compositions are planned, including modifications of glass compositions aimed at enhancing incorporation of critical elements. Additional sample characterization will be performed with the aid of various spectroscopic methods including Raman spectroscopy, XRD and SEM/EDX. Further NMR spectroscopic investigations will be performed such as ^{11}B-MQMAS, ^{23}Na-, ^{29}Si- and ^{95}Mo MAS NMR spectroscopy. Moreover, Mo K-edge high resolution (HR) XANES, as well as µ-XAFS studies will be applied to gain insight into Mo atomic and electronic environment, as a function of differing glass composition.

Acknowledgements

The authors gratefully thank S. Wegner and Ch. Steffen from Bruker BioSpin GmbH for providing the opportunity to measure ^{11}B MAS NMR spectra on a 850 MHz Bruker Avance III NMR spectrometer. This work is supported by the WAK GmbH.

References

[1] W. Grünewald, G. Roth, W. Tobie, K.H. Weiß, S. Weisenburger, "The role of the platinum group elements ruthenium, rhodium and palladium in the vitrification of radioactive high level liquid waste using Joule-heated ceramic-lined waste glass melters", Glass Tech.: Eur. J. Glass Sci. Technol. A, December 49 (6), 266-278 (2008).

[2] M. Plaschke, K. Bender, M. Böttle, S. Heck, S. Hilpp, A. Kaufmann, T. Kisely, M. Lagos, A. Görtzen, H. Geckeis, F.W. Geyer, K. Gompper, A. Seither, C. Walschburger; "Prozessbegleitende Analytik zum Nuklearen Betrieb der Verglasungseinrichtung Karlsruhe (VEK)", 6. Workshop RCA & 23. SAAGAS, 6.-8.9.2010, Dresden-Rossendorf, Germany.

[3] W. Grünewald, G. Roth, W. Tobie, A. Salimi, S. Weisenburger, B. Brendebach, „Laboratory-scale Development Technical Demonstration of Borosilicate Glass Tailored for Vitrification of High Sulfur Bearing HLLW", Proceeding of Global 2009, Paris, France, Sept. 6-11, 2009, Paper 9260.

[4] W. Gong, W. Lutze, I.L. Pegg, Glass Technol.: Eur. J. Glass Sci. Technol. A, 50(3): 151 (2009).

[5] D. Massiot, F. Fayon, M. Capron, I. King, S. Le Calvé, B. Alonso, J.O. Durand, B. Bujoli, Z. Gan, G. Hoatson, Magn. Reson. Chem., 40: 70 (2002).

[6] R.K. Mishra, K.V. Sudarsan, P. Sengupta, R.K. Vatsa, A.K. Tyagi, C.P. Kaushik, D. Das, K. Rajz, J. Am. Ceram. Soc., 91(12): 3903 (2008).

9. Development of actinide speciation methods

INE continued in 2010 to make notable improvements in and developments of instrumentation and techniques available for actinide speciation. The INE-Beamline at ANKA, in addition to supporting in-house activities and hosting groups from all over Europe, was able to make improvements to the electronics and control systems, commission a new high temperature and pressure liquid sample cell and obtain first, modest results using the Johann spectrometer for high resolution X-ray emission spectroscopy. Laser spectroscopy developments included for the first time application of vibrational side band spectroscopy to study bonding and coordination in partitioning complexes. A new Sector field-ICP-MS at INE is a highly sensitive isotope specific instrument and has been combined with capillary electrophoresis for application to Np speciation at trace (potentially ultra-trace) concentration levels. In continuing TEM investigations of Np sorption onto green rust, INE scientists were successful for the first time to record Np-$O_{4,5}$ and Fe-$M_{2,3}$ electron energy loss spectra (EELS) at various sample locations and thereby identify a negative correlation between these two elements in the sample. Actinide EELS are rare and INE will be filling the paucity in the future. The newest addition to INE speciation portfolio is a 400 MHz NMR spectrometer, which was acquired in collaboration with Professor Breher at KIT Campus South in the framework of a BMBF funded partitioning project. In 2010 this instrument was commissioned and the first results for a radioactive sample, a plutonium solution complex, are presented in Chapter 9.5. This instrument will attract use by groups from all over Europe within the future EU FP7 project EURACT-NMR. Computational chemistry continued in 2010 to support experimental activities in a positive symbiosis. A new activity is aimed at using a special force-field molecular dynamic approach to characterize the coordination environment of actinide ions in aqueous solution.

9.1 R&D projects conducted at the INE-Beamline for Actinide Research at ANKA and at external SR sources

K. Dardenne, M. A. Denecke, R. Götz, W. Hauser, J. Rothe, A. Skerencak, T. Vitova

Introduction

The INE-Beamline for actinide research at the KIT synchrotron source ANKA celebrated its five years of official operation in October 2010, marking successful application of this dedicated instrumentation for X-ray spectroscopic characterization of actinide samples and other radioactive materials [1]. R&D work at the beamline focuses on various aspects of nuclear waste disposal within INE's mission to provide the scientific basis for assessing long-term safety of a final high level waste repository. The INE-Beamline is accessible for the actinide and radiochemistry community through the ANKA proposal system [2] and the European Union Integrated Infrastructure Initiative ACTINET-I3 [3]. The modular beamline design enables sufficient flexibility to adapt sample environments and detection systems to many specific scientific questions and in 2010 the portfolio available at the beamline has been increased. Well established bulk techniques like XAFS spectroscopy in transmission and fluorescence mode have been meanwhile augmented by advanced methods like (confocal) XAFS/XRF detection with a micro-focused beam or a combination of (micro-) XAFS and (micro-)XRD. Additional instrumentation for high energy resolution X-ray emission (HRXES) spectroscopy has been developed and initial results already obtained. In addition to conducting research projects at ANKA, INE scientists perform various experiments at external SR sources, which offer unique capabilities not - or not yet - available at KIT.

INE-Beamline user operation in 2010

In 2010 a total of 35 internal and external projects were granted beamtime at the INE-Beamline. As in the previous years the share available for INE in-house research amounts to ~50% of all available shifts (85 days). INE projects at the beamline cover a broad range of topics related to safe disposal of high level radioactive waste (HAW) and the reduction of HAW radiotoxicity. Many of these studies are presented in more detail elsewhere in this annual report or the ANKA 2009/2010 User Report [4]. In-house projects in 2010 include studies of the polymerization processes in Pu(V) chloride solutions, sorption of Ga ions onto Al-hydroxides, aqueous Np speciation at high salinity and high pH, stabilization of tetravalent protactinium in aqueous solution, Se(IV/VI) sorption onto calcite single crystals and incorporation into calcite secondary phases, investigation of selenide binding to iron sulfides, investigation of selenite reduction by sulfide species, Am(III) co-precipitation with and adsorption onto clay minerals, lanthanide incorporation into natural and synthetic clay minerals, sulfur speciation in Gorleben humic

acids, Pu complexation by partitioning model ligands, Np precipitate formation at high salinity, µ-XRF/XAS/XRD speciation of uranyl phases in corroded cement samples, characterization of Mo in simulated HAW glass, uranyl sorption onto Fe_2O_3 nanoparticles and redox speciation of Np(V), Pu(V) and Tc(VII) sorbed onto Opalinus clay and Callovo Oxfordian fracture filling material. In the context of the latter project Tc K-XAFS was measured for the first time at the INE-Beamline.

General user research projects provided with beamtime through the ANKA review committee (ARC) or through direct cooperation with INE were conducted by 15 groups in 2010, covering nearly 40% of the total available operation time. This includes two projects under the contractual cooperation with Bonn University. Researchers from the following institutions conducted experiments at the INE-Beamline in 2010:

- Uppsala University, Physics and Astronomy Dept., Sweden – start of an ACTINE-I3 long-term project
- JRC-Institute for Transuranium Elements, EU
- Institut für Kernchemie, Universität Mainz, Germany
- Natural History Museum, Department of Mineralogy and Petrology, Prague, Czech Republic
- Institute für Anorganische Chemie, Universität Erlangen, Germany
- KIT-Institut für Nanotechnologie, Karlsruhe, Germany
- KIT Campus Süd, Institut für Mineralogie und Geochemie, Karlsruhe, Germany
- ETH Zürich, Institut für Umweltwissenschaften, Switzerland
- Lomonosov Moscow State University, Chemistry Department, Radiochemistry Division, Russia
- HZD-Rossendorf, Institut für Radiochemie, Dresden, Germany
- Universität Bonn, Physikalisches Institut (PI-Bonn)
- Fachhochschule Niederrhein, Fachbereich Ökotrophologie

For the first time the setup enabling µ-XRF/XAS detection with a 30 µm spot size (cf. 2009 annual report) was externally requested in ANKA Call 16 (10/2010-03/2011) for the speciation of uranium bound to organic matter in a medieval mining dump at Jáchymov (Joachimsthal), Czech Republic.

As in the previous years, a significant percentage of in-house and ARC beamtime was used by PhD students to perform experiments in the framework of their theses (a total of 12 projects corresponding to ~30% of the available shifts). The long-term contractual cooperation between INE and PI-Bonn officially ran out at the end of December 2010. This cooperation - not solely dedicated to scientific

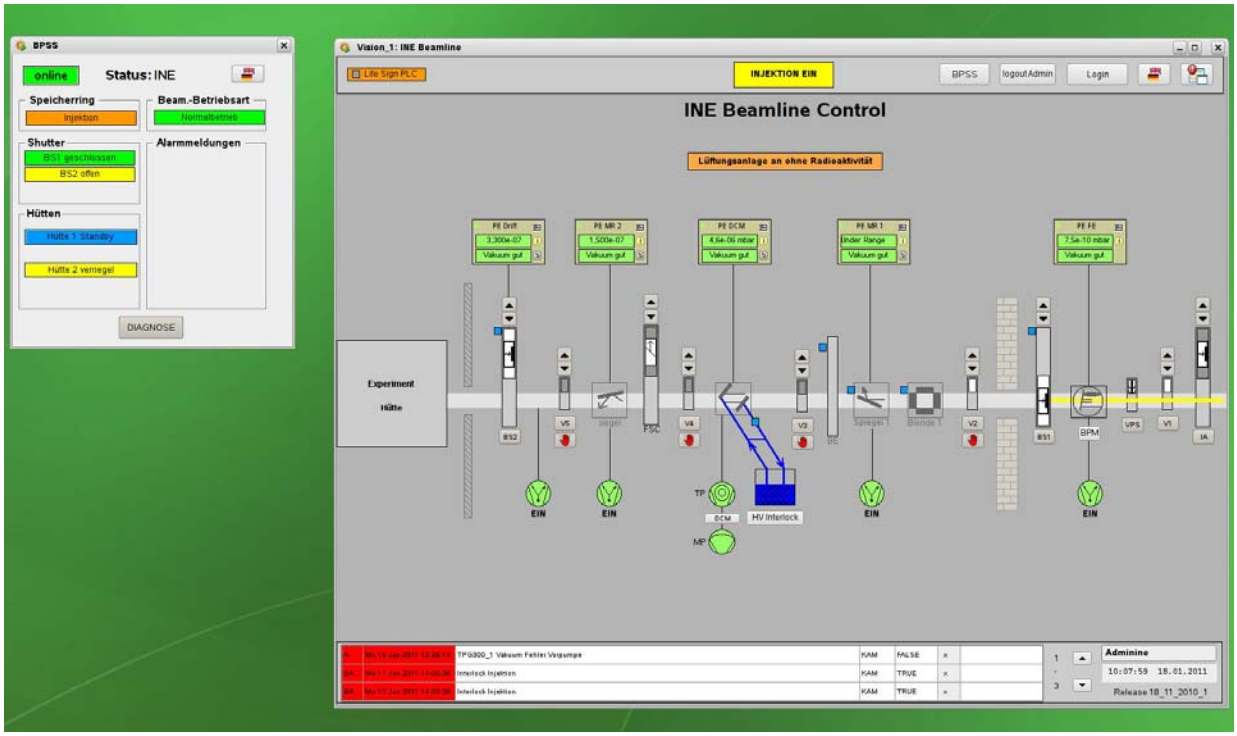

Fig. 1: *GUI of the new PVSS at the INE-Beamline.*

investigations by PhD and diploma students, but also to instrumental development at the beamline - will be continued on the basis of a mutual agreement.

INE-Beamline upgrades in 2010

Continuous maintenance and instrumental improvements are required to guarantee steady user operation in accordance with the ANKA beamtime calendar - and to reduce the time span necessary to switch between experimental setups. The major part of the experimental development in 2010 was dedicated to the installation of a new beamline control system ('personnel and vacuum safety system', PVSS), adhering to recently modernized ANKA standards. Commissioning of the new PVSS was completed in January 2011.

Upgrades of the beamline control system

The replacement of the initial PVSS ('RST-System') by a SPS (Siemens-S7) based system became necessary due to the phasing out of the VME computer based predecessor, which is no longer supported by the ANKA/ISS IT-group. Along with the PVSS installation the beamline LAN and most of the experimental hutch wiring were renewed or reorganized – including the setup of a new 19'' rack for motor and detector controllers. Critical devices are now addressed via GPIB-Ethernet communication, which guarantees a more stable command transmission compared to the previous serial connection. Most obvious for beamline users is the new graphical interface (GUI, cf. Fig. 1) running as a beamline-individual client of the central ANKA safety server on the Linux data acquisition PC.

High-T sample cell

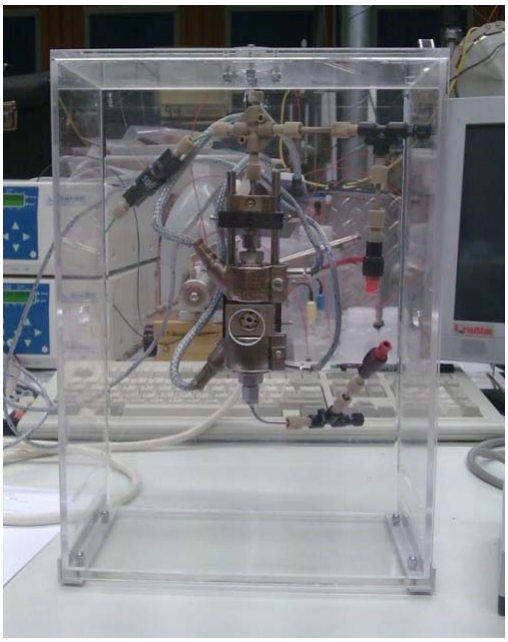

Fig. 2a: *High-T XAFS cell with secondary containment.*

The high temperature (high-T) sample cell developed at INE for laser spectroscopic actinide speciation studies in aqueous solution (e.g., for the determination of pK_a values) at elevated temperature up to 200°C was adapted for XAFS measurements in X-ray fluorescence detection mode. This required modifying the windows and mounting the cell in a safe secondary containment. The quartz windows at the cell entrance and pointing towards the fluorescence detector have been replaced by Kapton-passivated beryllium windows. The cell body can now be mounted into a plexiglass encasement with Kapton covered openings for the X-ray beam path (Fig. 2a). Initial tests ([243-Am(III)] = 1mM in I = 0.5M $NaNO_3/HNO_3$) at 200°C, corresponding to a pressure of ~20 bar, exhibit stable conditions for at least 10 h, which is sufficient to collect high quality Am L3-XAFS data (Fig. 2b). The RT EXAFS spectrum recorded with the high-T setup reproduces previously published results; the marginal temperature dependence of the EXAFS data at 200°C simply reflects thermal disorder. Future studies will focus on investigations of the speciation of Am with stronger binding ligands such as SO_4^{2-} using the high-T cell.

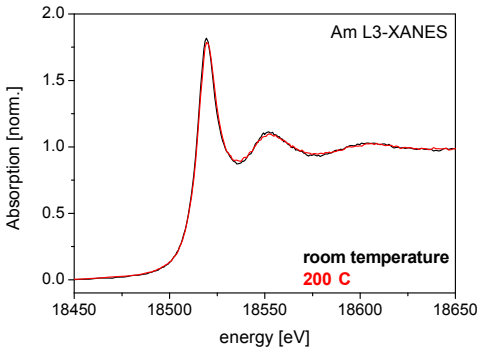

Fig. 2b: *Am L3-XANES of $Am(III)_{aq}$ nitrate complex at RT and 200°C.*

High-resolution X-ray emission (HRXE) spectroscopy

The first measurement of U Mα emission of a thin UO_2 layer as a function of the excitation energy across the U M5 edge with the INE HRXES spectrometer (cf. previous annual reports) is plotted in Fig. 3. Narrowing of the U M5 partial fluorescence yield X-ray absorption near edge (PFY-XANES) maximum (white line, WL) (Fig. 3b) is obtained by integrating the emission over a decreasing number of CCD detector pixels on either side of the Mα

emission line maximum. The signal-to-noise ratio of this spectrum will be improved during 2011 by integrating a pneumatic in-vacuo fast shutter/filter inserter required to enable defined irradiation intervals of the CCD camera. The An M5 edge WL describes 3d→5f-like electron transitions and thereby directly probes the number and energy distribution of An 5f valence electrons. The WL narrowing indicates reduced core-hole life-time spectral broadening, which has significant application potential for detection of minority An valence

XANES spectroscopy, performed for the first time at the INE-Beamline. Initial Pu M5-XANES spectra of as-prepared films and films exposed to water for 24 h show no significant differences (Fig. 4).

HRXES investigations were also carried out at external synchrotron sources. A high energy resolution XANES spectroscopy study performed at beamline id26, ESRF, on U^{4+} (UO_2), U^{5+} ($[UO_2Py_5][KI_2Py_2]$), and U^{6+} ($UO_2(NO_3)_2(H_2O)_6$) materials demonstrates the

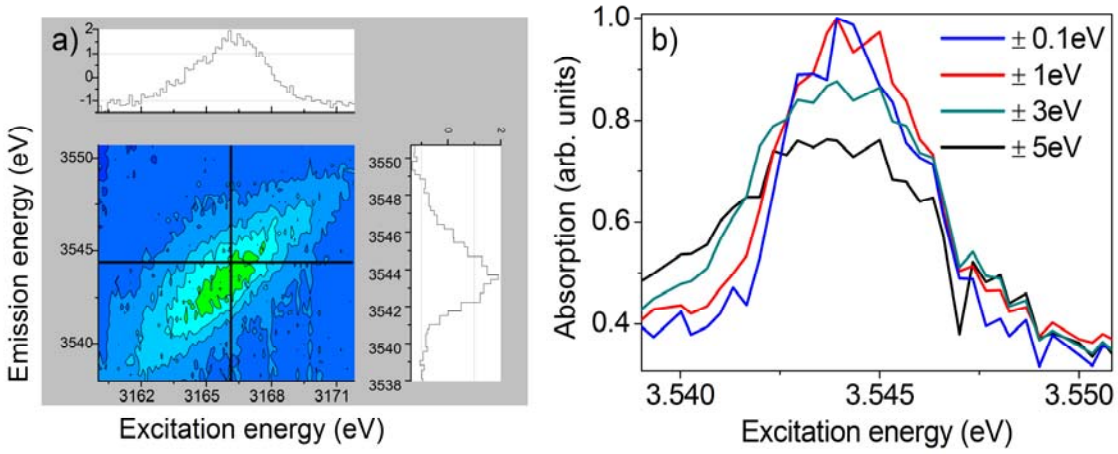

Fig. 3: a) *U Mα emission of UO_2 measured across the U M5 edge.* ***b)*** *U M5 edge UO_2 PFY-XANES spectra with varying energy resolution.*

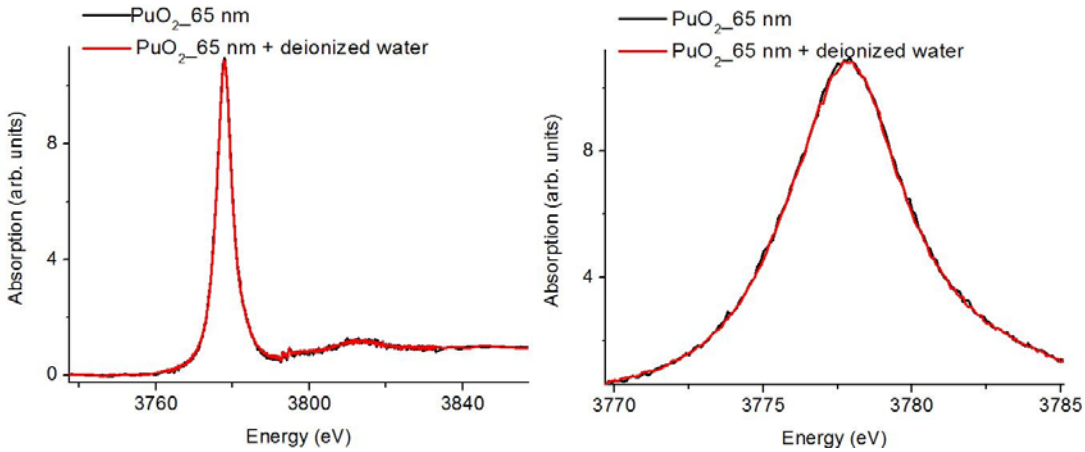

Fig. 4: *Conventional fluorescence mode Pu M5-XANES of a 65 nm PuO_2 film and this film exposed to deionized water.*

species in oxidation state mixtures.
This improved 5f electron characterization is especially useful for Pu speciation. In 2011, the spectrometer will be employed for the speciation of Pu with higher than +IV oxidation state (PuO_{2+x}) in a PuO_2 film with a thickness of 65-100 nm exposed to deionized water. These investigations are supported by ACTINE-I3 as long term collaboration between JRC-ITU, KIT-INE and Uppsala University, Sweden. The project started in 2010 with conventional fluorescence mode Pu M5-

potential of the HRXES experimental technique at the An L3 edge for qualitative and quantitative actinide speciation investigations. A pre-edge feature with quadrupolar nature in a U L3 edge PFY-XANES spectrum was observed, which can be potentially applied for characterization of 5*f* orbital participation in U-O bonding. We explained the origin of this feature by performing calculations with the finite difference method near-edge structure (FDMNES) code based on the multiple scattering theory and the finite difference

method [5]. The experimental and calculated spectra are shown in Fig. 5.

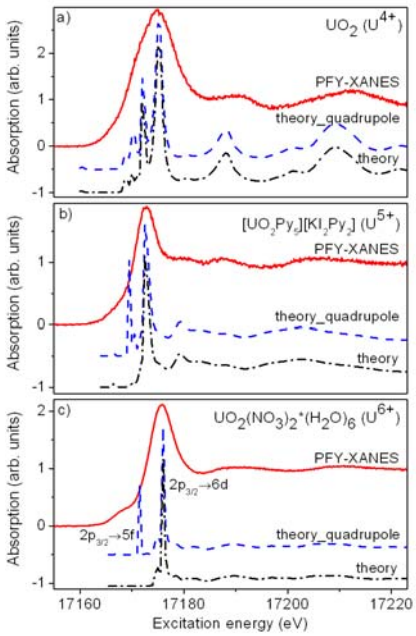

Fig. 5: *The U L3-PFY-XANES spectra of* ***a)*** UO_2 (U^{4+}), ***b)*** $[UO_2Py_5][KI_2Py_2]$ (U^{5+}), *and* ***c)*** $UO_2(NO_3)_2(H_2O)_6$ (U^{6+}) *compared to theoretical FDMNES calculations with (theory_ quadrupole) and without (theory)* $2p_{3/2}\rightarrow 5f$ *electronic transitions.*

Outlook for 2011

The following instrumentation upgrades at the INE-Beamline will be accomplished in 2011:

- Installation of a pneumatic in-vacuo fast shutter/filter inserter required to enable defined irradiation intervals for XRD (image plate) and HRXES (CCD) detection, which is presently impossible with beamline radiation protection shutter or gate valves;
- Design and construction of a new inert gas sample cell with improved geometry for measurements of liquid and solid samples in transmission and fluorescence detection mode. Additionally, the glove box in INE's controlled labs for EXAFS preparation will be equipped with a hand press for preparation of pellets for experiments and a device to seal wrapped samples.

Besides ongoing work at the INE-Beamline, efforts in 2011 will concentrate on two large projects, which will ultimately open complete new perspectives for synchrotron-based actinide research at KIT-INE/ANKA, i.e., the start of the Helmholtz Young Investigator Group 'Advanced synchrotron-based systematic investigations of actinide and lanthanide systems to understand and predict their reactivity' awarded to T. Vitova in July 2011 and the design of the new CAT-ACT wiggler beamline for catalysis and actinide research at ANKA. This new beamline will deliver more flux and offer a broader range of X-ray beam energies for investigations. It is intended to become operational in 2013.

Acknowledgement

Cooperation with W. Mexner and T. Spangenberg (ISS IT-group) for hardware and software implementation at the INE-Beamline is gratefully acknowledged. Part of the INE-Beamline development was a contractual cooperation between KIT-INE and PI-Bonn. We are grateful to H. Blank (PI-Bonn), A. Neumann, V. Krepper, J. Thomas and G. Christill (INE) for technical support.

References

[1] K. Dardenne et al., Journal of Physics: Conference Series 190, 012037 (2009).

[2] http://ankaweb.fzk.de/website.php?page=userinfo_main

[3] http://www.actinet-i3.eu

[4] Report of User Experiments at ANKA 2009/2010, KIT-ISS, October 2010.

[5] T. Vitova et al., PRB 82, 235118 (2010).

9.2 Laser Spectroscopy

S. Büchner, A. Chai, A. Geist, R. Götz, W. Hauser, P. Hoess, P. Lindqvist, T. Schäfer, M. Steppert and C. Walther

Vibrational Side Band Spectroscopy for probing nitrate complexation of $Eu^{(III)}(BTBP)_n$ in octanol

BTBP [6,6'-Bis-(5,6-dialkyl-1,2,4-triazin-3-yl)-2,2'-bipyridine] selectively extract Am(III) and Cm(III) from nitric acidic solutions with good selectivity over Ln(III) (see §7). The extraction properties are well understood and the structure of the complexes was investigated extensively in the past. The (typically eight- or nine-coordinate) Eu^{3+} ion coordinates with one or two BTBP ligands in tetradentate fashion. In the case of the one-to-one complex, solvent molecules (octanol in the present case) or anions (nitrate or perchlorate) coordinate directly to the metal center. The situation is different, however, in the case of the one-to-two complex, $Eu^{(III)}(BTBP)_2$. Previous studies applying conventional time-resolved laser-fluorescence spectroscopy (TRLFS) showed no evidence of perchlorate ions in the first coordination sphere of this 1:2 complex in octanol, but with nitrate the picture is not conclusive. To elucidate whether or not these anions coordinate to the metal center in the 1:1 and 1:2 complexes we apply vibrational sideband spectroscopy (VSBS), a method able to probe directly the energy transfer from Eu^{3+} to vibrational modes of the coordinating anion. Eu^{3+} is excited by photons of a pulsed tunable laser and subsequent fluorescence of the $^5D_0 \rightarrow {}^7F_J$ (J = 0, 1, 2) is observed. In addition to these pure electronic transitions, vibrational excitation of the nitrate ion is possible by energy transfer from the Eu^{3+} ion, leading to Stokes lines at lower energy in analogy to Raman spectroscopy (Fig.1 dashed and dotted lines). Contrary to Raman or IR spectroscopy, where all Raman and IR-active modes of the solvated complex and the bulk solvent add to the spectrum, VSBS monitor only vibrational modes in the close proximity of the fluorescent metal ion. Moreover, in cases where different Eu^{III} coordination environments occur, the laser wavelength may be tuned to excite selectively only one site at a time [1]. Each of which may exhibit a notably different fluorescence spectrum with accompanied VSBs; coordination of water or alcohol molecules significantly decrease the fluorescence lifetime.

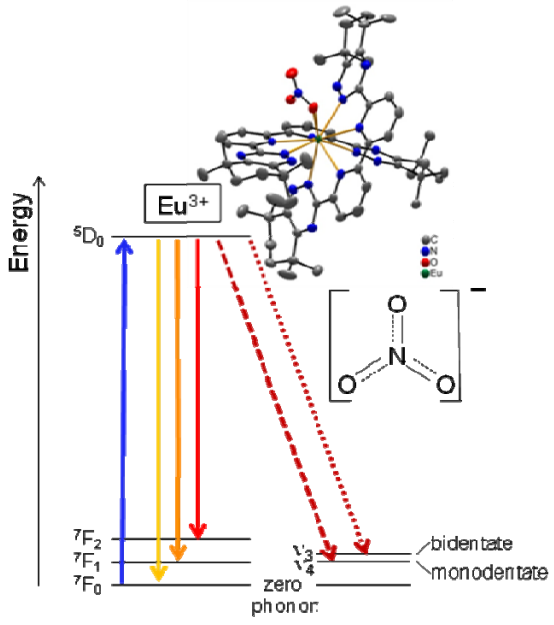

Fig. 1: *Top: The $[Eu(BTBP)_2(NO_3)]^{2+}$ ion in the crystal structure of $[Eu(BTBP)_2(NO_3)][Eu(NO_3)_5]$ (H atoms are omitted). Bottom: Principle of VSB. Part of the energy from the excited Eu^{3+} ion is transferred to vibrational excitation of the nitrate molecule allowing Raman-spectroscopy-like evaluation of the spectra.*

In a solution of $Eu(NO_3)_3$ in 1-octanol ([Eu]=10^{-4} M) two bands at 604.5 and 605.8 nm in the region between the $^5D_0 \rightarrow {}^7F_{1,2}$ transitions of the Eu^{3+} are recognized (Fig. 2). We assign these bands, with Stoke shifts at 704 and 740 cm^{-1} relative to the $^7F_0$ ground state, to the ν_5 and ν_3 vibrations of bidentate coordinated nitrate ions, respectively. This is in agreement with previous reported values of vibronic side bands of ν_5 and ν_3 modes of Eu(III) compounds with bidentate coordinated nitrate ions [2-4].

Titrations of $Eu(NO_3)_3$ octanol solutions ([Eu]=10^{-4} M) are performed with three different BTBP ligands, denoted t-Bu-C2-BTBP, C5-BTBP, and $CyMe_4$-BTBP. In the case of t-Bu-C2- and C5-BTBP a bathochromic shift of the zero phonon $^5D_0 \rightarrow {}^7F_0$ transition is observed with increasing ligand concentration, pointing to higher complexation strength. Likewise, the sidebands shift their position by the same values (for C5-BTBP, see Fig. 2, top). This shows that the vibronic sideband of the ν_3 transition originates from nitrate ions of $Eu(BTBP)_x(NO_3)_y$ complexes (x =1-2, y =1-3). For the C5-BTBP ligand the fluorescence intensity of the vibronic sideband follows a monoexponential decay function with τ = 900 µs. The VSB spectra of the complexes of all three ligands (L) at concentrations of

[L=1.3×10^{-3}M, [Eu]=10^{-4}M) are compared in Fig. 2 (bottom). Noticeably, with increasing ligand concentration the intensity of the ν_3 side band at about 607.0 nm (740 cm^{-1}) decreases, accompanied by the evolution of a much weaker band at 605.3 nm (685 cm^{-1}) correlated with vibronic transitions of the BTBP ligand. This indicates the replacement of one or more nitrate ions by a BTBP ligand to form a one-to-two complex. With a large excess of BTBP the ν_3 sideband at $\Delta\nu$= 740 cm^{-1} disappears, leaving a weaker band at 606.4 nm (720 cm^{-1}).

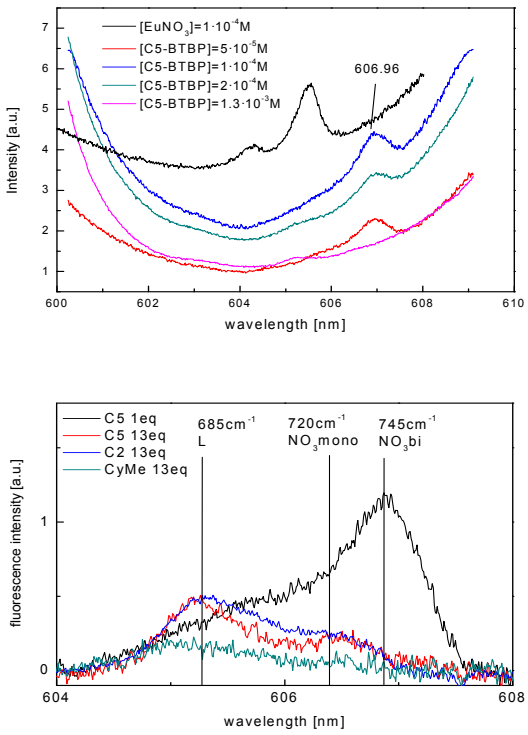

Fig. 2: *Top: Vibronic sideband region of the nitrate vibration transitions of Eu(NO$_3$)$_3$ during the titration with C5-BTBP ligand. Bottom: Vibronic sideband region for the different tested ligands for C5-BTBP with 1 and 13 equivalent and t-Bu-C2-BTBP and CyMe$_4$-BTBP after baseline correction. Note that the corresponding wavenumbers describe the shift by cm^{-1} from the respective zero phonon line (ZPL; in this case the respective $^5D_0 \rightarrow {}^7F_0$ transition)*

Because of steric reasons [5,6], this weaker sideband is likely due to a ν_4 vibration of a monodentately bound nitrate ion in a nine-coordinate complex, $[Eu(BTBP)_2NO_3]^{2+}$. The shift from 740 to 720 cm^{-1} in vibrational frequency is consistent with a change from a bidentate to a monodentate mode of the nitrate ion, as well as a change of its symmetry from C_{2v} to D_{3h}. This frequency shift is indeed observed for 1:2 complexes with C2- and C5-BTBP ligands but not for that with the bulkier and sterically more demanding CyMe$_4$-BTBP ligand. In the latter, apart from the weak vibronic sidebands of the ligand itself, no other sidebands are observed that would point to nitrate coordination. The absence of a nitrate ion in the first coordination sphere of CyMe$_4$-BTBP complexes is in agreement with a recent TRLFS study [7]. Nitrate anions may, however, interact with the solvated complex at a greater distance by forming an outer-sphere complex; however, due to the strong (r^{-6}) bond distance dependence of the energy transfer, vibrational modes of nitrate ions (or any other molecules) not directly bound to the metal center are too weak to be detected as VSBs.

The present interpretation is corroborated by ESI TOF MS measurements that indicate a hydrophobic character of $Eu(C5BTBP)_2(NO_3)^{2+}$ complexes due to the shielding of the nitrate ion by the BTBP molecules. Conventional TRLFS-lifetime measurements add further evidence: 1:2 complexes of C5- and *t*-Bu-C2-BTBP show significantly longer lifetimes in the nitrate system than in the perchlorate system indicating displacement of 1-octanol molecules (which act as florescence quenchers) by nitrate ions (non-quenching), while in the perchlorate system no such replacement seems to take place. On the other hand, due to the bulkiness of the CyMe$_4$-BTBP ligand, solvent molecules and anions are unlikely to directly coordinate to $[Eu(CyMe_4\text{-}BTBP)_2]^{3+}$ complexes in solution.

Colloid breakthrough quantification in the CFM experiment Run 10-03 at Grimsel Test Site using different laser-induced breakdown detection methods

There are two methods of the laser-induced breakdown detection (LIBD) developed in the INE for the quantification of colloids in aquatic systems. The 2d-optical detection LIBD with constant laser pulse energy (~1.3mJ) can be applied online with a typical measurement duration of 1-10min. It can be used in a robust, mobile system in field experiments with a pressurized flow-through detection cell (60 bar). With this method an average diameter between 20 and 1000nm and the concentration of the colloids are determined.

With the s-curve detection LIBD the breakdown events are recorded with a photoacoustic detector. With this method the laser pulse energy is varied from 0 to 5 mJ. For adequate accuracy the typical measurement duration is 0.5 to 1.5h. So most measurements are performed offline. This method is applied with a precise instrument in laboratory experiments. Compared to the method above particle concentrations are determined for eight particle size fractions in the range 15 to 1000nm.

The colloid formation and migration experiment (CFM) Run 10-03 has been performed in the

CRR-Tunnel of the Grimsel Test Site. A cocktail (volume 2L) of FEBEX bentonite colloids with a concentration of 105 mg/L, the homologues Eu, Tb, Hf, Th, and Grimsel groundwater was injected via borehole CFM 06.002 into a fracture zone with a flow path which was directed to the tunnel. From there the cocktail migrated along the fracture zone to the surface of the tunnel ("Pinkel"). At this point the groundwater was extracted by means of a surface packer with a flow rate of 10 mL/min.

After the start of the experiment 63 groundwater samples have been taken as a function of time. They were transported to the INE for analysis with ICP-MS, the 2d-optical detection LIBD, and the s-curve detection LIBD. The results are presented in Fig.3.

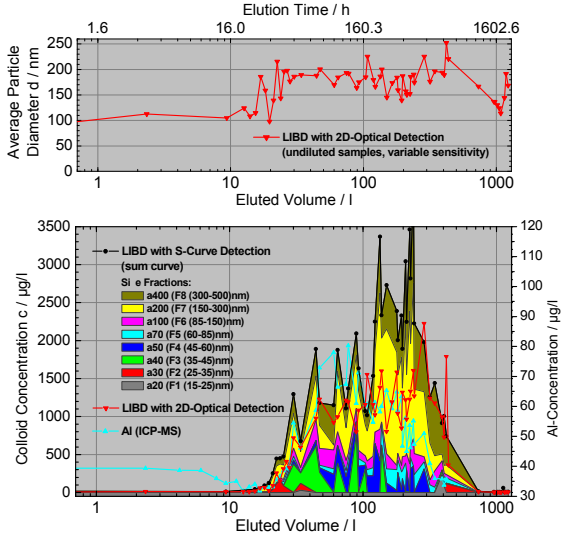

Fig. 3: *LIBD and ICP-MS detected breakthrough of bentonite colloid cocktail during the colloid migration experiment Run 10-03. Top: Average particle diameter determined with the 2d-optical detection LIBD. Bottom: Colloid concentrations including size fractions from the s-curve detection LIBD with Al (monitoring element for bentonite colloids).*

The breakthrough of the bentonite colloids starts after 20L eluted volume. The ICP-MS determined Al concentration (monitoring element for bentonite colloids) shows a maximum at ~80L eluted volume. Up to 100L elution volume the colloid concentrations of the 2d-optical detection LIBD as well as the s-curve detection LIBD correspond well with the Al. With both LIBD methods the same average particle diameter of ~180nm (main size fraction) in the breakthrough are detected.

Furthermore, it is significant that all data show almost the same scattering pattern of the concentration. A comparison of this data with data from online pressure and turbidity measurements in the eluted groundwater demonstrates that the scattering exactly corresponds with the period of the tides. In this experiment minor changes of the groundwater pressure (flow) cause a significant variation of the colloid concentration.

For elution volumes >100L the Al concentration decreases whereas both LIBD detected colloid concentrations are significantly higher. This big difference results in a recovery for the Al of ~40% (FEBEX bentonite colloids), which is consistent with the recovery of the homologues Hf, Th. The recovery calculated for the colloid concentrations detected with both LIBD methods is >100%. This means that additional colloids may have been created by artefacts (e.g. sampling) or by mobilization in the fracture zone. This will be verified by additional investigations.

References

[1] M. Schmidt *et al.*, Angew. Chem. Int. Ed. 47, 5846 (2008).

[2] V. Tsaryuk *et al.*, Spectrochimica Acta Part A: Molecular and Biomolecular Spectroscopy 56, 1149 (2000).

[3] V. Tsaryuk *et al.*, Journal of Applied Spectroscopy 60, 185 (1994).

[4] V. Tsaryuk *et al.*, Proceedings of the 4th International Spring Workshop on Spectroscopy, Structure and Synthesis of Rare Earth Systems 380, 418 (2004).

[5] S.V. Volkov, N.P. Evtushenko, and K. B. Yatsimirskii, Teoreticheskaya i Éksperimental'naya Khimiya 9, 273 (1973).

[6] I.S. Perelygin, and G. P. Mikhailov, Zhurnal Prikladnoi Spektroskopii 48, 766 (1988).

[7] T.H. Vu, in *CEA Rapport CEA-R-6229* (Commissariat à l'énergie atomique, Saclay, France, 2009).

9.3 Mass Spectrometry Methods

N. L. Banik, S. B chner, M. Fuss, F. Geyer, M. Lagos, C.M. Marquardt, J. Rothe, T. Sasaki, M. Steppert and C. Walther*

**Department of Nuclear Engineering, Kyoto University, Yoshida Honmachi, Sakyo, Kyoto 606-8501, Japan*

Speciation is a key property which has a strong influence on the mobility of actinide species in aqueous systems. It also plays an important role in the sorption behaviour of elements on mineral surfaces, which is an essential aspect when it comes to questions about the retention potential for actinides in the far field (i.e. the surrounding rocks) of a potential nuclear waste repository. Here, mass spectrometry is applied for speciation in aqueous solution.

Investigation of Zr (IV) polymerisation by electroyspray mass- spectrometry using isotopically pure ^{90}Zr

Zirconium plays an important role in nuclear technology, e.g. it serves as cladding material of uranium fuel rods, and in addition, Zr(IV) is a frequently used analogue for solubility investigations of tetravalent Pu(IV). One remarkable chemical similarity is the strong tendency of both metals to hydrolyse and form polynuclear species. In the case of Zr(IV) particularly the tetramer, $Zr_4(OH)_8^{8+}$, denominated (4,8) in the following, is well known [1]. For a correct prediction of Zr(IV) solubility the formation and stability of these polymers need to be known. Previous studies by LIBD, EXAFS and ESI TOF were carried out at rather high concentration. The large number of stable isotopes of Zr requires minimum concentrations of [Zr]=1.5×10^{-3}M in the case of ESI, since the time-of-flight signal distributes in a binomial fashion over a large number of peaks (see [2]). In the present work monoisotopoic $^{90}ZrCl_4$ was prepared at the University of Kyoto allowing to measure at concentrations as low as [Zr(IV)]= 10^{-5}M.

$^{90}ZrCl_4$ powder was dissolved in 0.1M HCl and samples of [Zr]=10^{-5}M – 10^{-3}M were prepared by appropriate dilution with HCl and deionized water. [H$^+$] was measured by use of glass combination electrodes (ROSS type) calibrated against HCl reference solutions. Zr concentration was determined by ICP MS. All samples were allowed to equilibrate for at least 24h before measurement by ESI TOF. Samples were stored in closed PE Eppendorf vials (no air exchange, but no inert gas either) without taking any further precautions. After 12 months the measurements were repeated. The measured species distribution (symbols) is compared to predictions (lines) using formation constants of [1] (Fig. *1*). In order to describe the present findings, a dimer (2,2) is introduced, the equilibrium constant for the tetramer (4,8) is taken from [3] and transition of (4,8) to (4,10) mimics the observed continuous hydrolysis of the polymers.

We refrain, however, from adding formation constants for the larger polymers and this includes the pentamer proposed in [2] since their long term stability is still controversially discussed. The NEA constants serve as operative basis for modeling solubility phenomena.

The [Zr]=10^{-3}M samples show a pronounced ageing effect. While large polymers form in the as prepared solutions even at low pH, mainly monomers and small species survive after 12 months ageing. For the higher pH samples this effect is less pronounced.

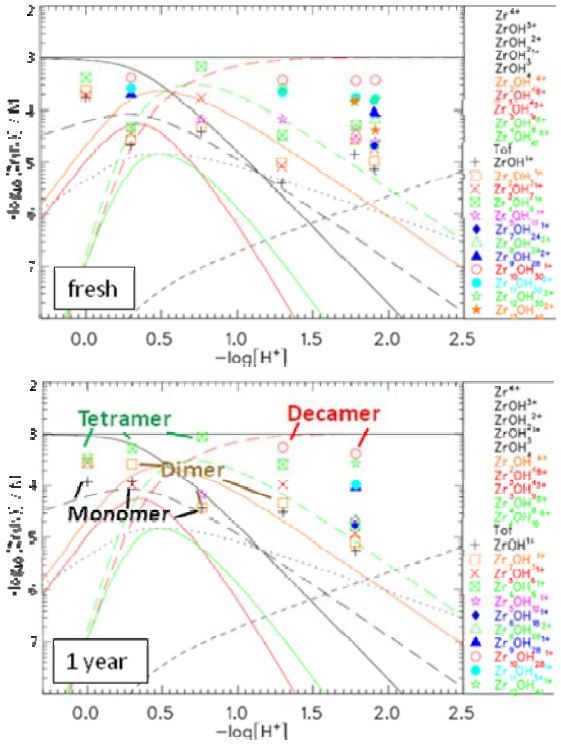

Fig. 1: *Species distribution in solutions of [Zr]=10^{-3}M as measured by ESI TOF MS. Top: Fresh solution. Bottom: After 12 months ageing*

The large scattering of the ESI data points for the as prepared samples is most likely due to slightly different conditions during preparation and/or different time spans between preparation and measurement (between 1h and several days). The species we found deviate rather strongly from what the equilibrium constants of [1] suggest. For the

aged solutions, however, the data show a better agreement and a systematic trend. The relative amount of monomeric species decreases and, except for the most acidic sample, agrees rather well with the sum of monomers predicted by the model. Dimeric species, not considered by NEA, are clearly stable for at least 12 months. Trimers (in red) are in agreement below pH 1 but strongly overestimated at higher pH. This is due to the fact that in the NEA database the (3,9) is the polymer with the lowest charge (z=3+) and consequently dominates at higher pH. Tetramers are more abundant than expected from the formation constant [3]. The same phenomena was reported already in [2]. At pH > 1.0 large polymers are stable and dominate the species distribution: Nonamer, decamer, undecamer, and dodecamer, in agreement with measurements by T. Sasaki at Kyoto. Comparing the results with those obtained in [2] it is clearly that Zr(IV) solutions do not equilibrate fast. A tendency for dissolution of larger polymers at low pH is observed and destabilization of tetramers and pentamers in favor of nonamers and larger ones takes place at higher pH.

Samples prepared at [Zr] =10^{-4}M evolve similarly as do the higher concentrated solutions. The data scatter of the as prepared solutions is less pronounced, probably due to the fact that the samples were produced by dilution of the samples at [Zr]=10^{-3}M being pre equilibrated for some days. Smaller polymers form and the total relative number of polymers is reduced as compared to the samples at [Zr]=10^{-3}M. However, also here the measured species distribution deviates from NEA equilibrium data.

In the case of the 10^{-3}M samples a solubility decrease was observed for the aged samples. At pH 2 only 30% of the $[Zr]_{tot}$ passed a 10kD filter after 12 months ageing. Though the systems are undersaturated with respect to freshly formed Zr hydroxide, ageing leads to a more condensed, partly crystalline, modification as observed previously by Neck, Altmaier, and Müller [4] with considerably lower solubility. This explains the formation of (large) polymers upon ageing. EXAFS measurements revealed no detectable Zr-Zr backscattering in the unfiltered samples suggesting the well known effect of destructive interference in the presence of many geometrically different species.

Redox speciation of Np in aqueous solution determined by Capillary Electrophoresis Sector Field ICP-MS (CE-SF-ICP-MS)

Capillary Electrophoresis (CE) as a species selective tool has been applied in combination with a new Sector field-ICP-MS (Element XR, Thermo Fisher Scientific, Bremen), which is a highly sensitive isotope specific detection system, to study the redox behaviour of Np in the aqueous phase of sorption experiments. The ability of modern SF-ICP-MS to detect actinides down to the sub-ppq level (~10^{-15} mol/l in conventional setup) with almost zero background has been successfully used to study the speciation of actinides even at concentrations as low as 10^{-12} mol/l [5] when using SF-ICP-MS together with capillary electrophoresis.

The CE measurements presented here were performed using a Beckmann P/ACE^{TM} MDQ instrument (Fullerton, USA) equipped with a 73 cm long uncoated fused silica capillary (50 μm ID). It was linked to SF-ICP-MS with a Mira Mist CE system (Burgener Research Inc.), an especially designed nebulizer and mini spray chamber for hyphenation of CE instruments to ICP-MS. The nebulizer works under low sample uptake rates typically below 10 μl/min. Extensive optimization of the CE measurements in the run-up of the Np redox species determinations have yielded an optimal uptake rate of 8 μl/min of the makeup

Fig. 2: *Set-up of capillary, nebulizer, and spray chamber (Mira Mist CE system) used for the CE-SF-ICP-MS measurements.*

solution (2 % HNO_3 with 10 % Ethanol) which is delivered by a syringe pump. The whole capillary-nebulizer-spray chamber set-up which generates a dry sample aerosol with excellent sensitivities is shown in Figure 2.

All separations were carried out with sample solutions from redox speciation experiments of neptunium in water suspensions of crushed Opalinus Clay (OPA) and Callovo-Oxfordian argillite (COx) rocks with a solid to liquid ratio of 50 at constant ionic strength (0.1 M NaCl), and with contact times of 7 months. The initial concentration of Np(V) in solution before sorption started, varied between 1.0×10^{-7} and 1.0×10^{-9} M. For the measurement filtrate (10 kD) supernatant solutions from clay suspension are taken in 2 mL glass vials under inert atmosphere then transported to the ICP-MS laboratory. However, the measurement

has been performed under air atmosphere and oxidation of Np species cannot be excluded. Separations are completed within 15-18 min. Sample injections are hydrodynamically carried out at 0.8 psi during 5 s. Separations are performed at 20 kV at a constant pressure of 0.2 psi (to avoid clogging of the capillary) using a 0.1 M acetic acid buffer solution which was routinely replaced after several runs to avoid any contamination or electrolytic dissociation of the background electrolyte. A comprehensive washing procedure at the end of each run comprising several rinse steps (with 1 M HCL, 1 M NaOH, MilliQ and buffer solution) ensured low memories and backgrounds during the course of the measurements. An extended washing procedure was also performed at the end of each day.

To understand the separation of neptunium oxidation states by CE-SF-ICP-MS, especially under air conditions, several mixtures of Np(V) and Np(IV) (~$3x10^{-7}$ M Np in 0.01 M $HClO_4$) are tested. The solutions were prepared by diluting Np solution with higher Np concentrations and with Np(V)/(IV) composition well characterized by UV-Vis spectroscopy. Figure 3 shows an electropherogram of a solution with Np(IV) only, which is partly oxidized by air, but gives two well separated peaks for tetravalent and pentavalent Np. It emphasizes that the impact of air must not be neglected by using the current sample injection system of the CE.

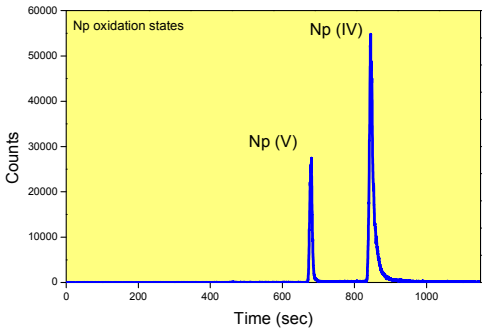

Fig. 3: *Electropherogram of Np oxidation states. Separation by CE-ICP-MS (1 M MeCOOH and 20 kV), [Np]= $3x10^{-07}$ M, 0.01 M $HClO_4$.*

In the supernatant filtrate solutions from the OPA and COx suspensions of the sorption experiments only Np(V) species could finally be confirmed. The shorter migration time (500 s) of Np(V) in OPA/COx measurements compared to the peak of Np(V) in Figure 4 is due to the higher voltage of 30 kV. The higher voltage was used for the clay solutions to get narrower peaks and higher intensities. CE-ICP-MS measurements at 30 kV have finally produced peak intensities of ~1.2 x 10^5 cps resulting in a calculated detection limit (DL) of ~5 x 10^{-11} mol/l.

The method so far demonstrates that Np redox species can be successfully separated and detected with very low backgrounds (i.e. 0.3 cps corresponding nearly to the dark noise of the detector) under optimal conditions. The detection limits can possibly be lowered once again by changing the rinse protocols for the capillary and to alter the tube system conveying the aerosol from the spray chamber to the SF-ICP-MS. The observation that no Np(IV) was detected in the supernatant solutions obtained from the sorption experiments, however, has to be interpreted with caution taking into account that the sample solution might have been oxidized during transport from the inert gas box to the ICP-MS or during injection of the sample and the passage through the capillary. Further technical improvements are necessary including a modified sample injection system by using Ar instead of air to avoid oxidation of the species. Impact of air and hence oxidation becomes particularly critical at low analyte concentrations.

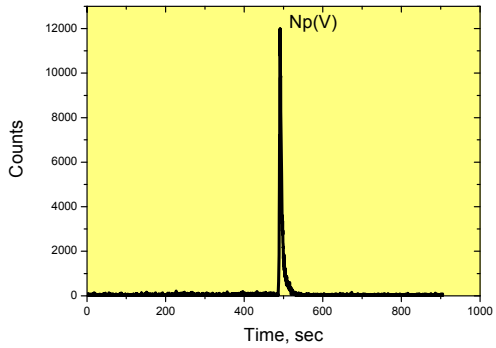

Fig. 4: *Electropherogram of Np speciation in filtrate COx clay rock, [Np] = $2x10^{-08}$ M, 0.1 M NaCl, S/L = 20, kinetic = 7 months, sample= filtrate supernatant solution, separation with 1 M MeCOOH at 30 kV.*

References

[1] P.L. Brown *et al.*, *Chemical Thermodynamics of Zirconium* (Elsevier, North-Holland, Amsterdam, 2005), Vol. 8.

[2] C. Walther *et al.*, Anal. Bioanal. Chem. 388, 409 (2007).

[3] A.J. Zielen, and R.E. Connick, J. Am. Chem. Soc. 78, 5785 (1956).

[4] V. Neck, M. Altmaier, and R. Müller, *unpublished results (*2003).

[5] S. Topin, J. Aupiais, N. Baglan, T. Vercouter, P. Vitorge, and P. Moisy, Anal. Chem. 81, 5354 (2009).

9.4 XPS and TEM study of neptunyl - green rust interaction

*D. Bach, D. Schild, E. Soballa, B.C. Christiansen**

**Nano-Science Center, Department of Chemistry, University of Copenhagen, Universitetsparkern, DK-2100 Copenhagen Ø*

Introduction

Nuclear waste will be disposed within steel canisters in deep underground repositories. Green rust (GR), a Fe(II)/Fe(III) layered double hydroxide mineral consisting of positively charged octahedral sheets of $Fe(II,III)(OH)_2$ and interlayers of H_2O and n-valent anions, may form as a product of steel corrosion after potential access of groundwater to the repository. Green rust may attenuate the migration of redox-sensitive radionuclides, e.g., Se(VI), Tc(VII), U(VI), and Pu(V,VI), by reduction to the tetravalent state exhibiting low solubility.

^{237}Np is a minor component (0.05 %) of spent nuclear fuel but has a long half-life, $T_{1/2}$ = 2.14 x10^6 years, and its concentration increases during the first 5000 years by α-decay of ^{241}Am, $T_{1/2}$ = 432.7 years. Np is expected to be leached from spent nuclear fuel as mobile neptunyl species, NpO_2^+, due to oxidizing conditions in the near-field caused by radiolysis.

In this study, GR of sodium sulfate form, $NaFe(II)_6Fe(III)_3(OH)_{18}(SO_4)_2{\cdot}12H_2O$ (thin hexagonal platelets), is reacted with an aqueous solution of neptunyl ions and analyzed by transmission electron microscopy (TEM) and XPS. The aim of the analyses is to achieve insight into the redox-reaction and potential immobilization mechanism.

Reaction of neptunyl with green rust

Green rust suspension is synthesized according to [1] and is contacted with neptunyl ions in aqueous solution to result in a molar ratio [Np]/[GR] of 1:2.7 with 1.55 mM/L Np in total. After 10 minutes reaction, the Np concentration in the supernatant (pH ~8, pe ~-6.7) is less than 1.7x10^{-8} M/L (LSC detection limit) indicating Np-GR formation.

XPS investigations

Np-GR samples are prepared and subsequently transferred into the x-ray photoelectron spectrometer, PHI model 5600ci, under permanent anoxic conditions.

In case of Np, the Np 4f main lines exhibit a similar chemical shift for both Np(V) and Np(IV). Due to low Np concentration, elemental lines other than 4f have no feasible intensities. However, satellites of the 4f main lines may be used for estimation of Np valency. The Np 4f spectrum of Np-GR shows a satellite at 6.5 eV higher binding energy than the 4f main lines, assigned to Np(IV) (Fig. 1). The observed

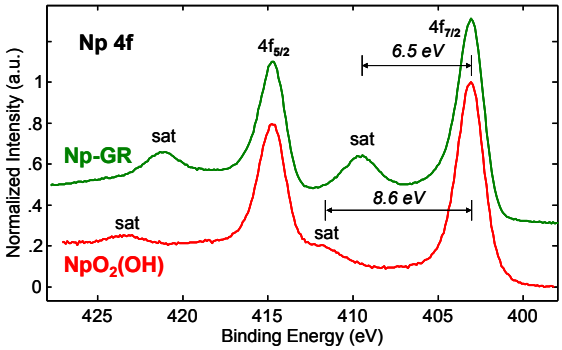

***Fig. 1:** XPS narrow scans of Np 4f elemental lines (stack plot): NpO_2^+ reacted with green rust compared to $NpO_2(OH)$ reference.*

satellite - 4f main line spacing is close to values observed for the pure An(IV)-oxides NpO_2 (6.8 eV), UO_2 (6.9 eV), and PuO_2 (6.9 eV). For comparison, neptunyl-hydroxide exhibits a less intense satellite at a spacing of 8.6 eV, similar to the 8.4 eV value observed for U(V) in the mineral ianthinite [2].

TEM investigations

TEM investigations are performed on Np-GR by means of a 200 keV FEI Tecnai G^2 F20 X-Twin microscope, located at IAM-WBM-FML (KIT Campus North). The instrument allows high-resolution TEM (HRTEM) and scanning TEM (STEM) and is equipped with various detectors enabling, e.g., high-angle annular dark-field (HAADF) imaging, energy-dispersive x-ray (EDX) spectroscopy, and electron energy-loss spectroscopy (EELS).

The first aim of the TEM analyses is the determination of the exact location where Np is immobilized on the GR particles. A few nm-wide bright rim is observed at the edge of Np-GR platelets by means of STEM-HAADF (Fig. 2), indicating the presence of an element with high atomic number. EDX investigations clearly demonstrate the presence of Np at the rim of GR platelets, whereas Np can not be detected inside the platelets [3]. Hence, the localization of Np at the edge of GR platelets suggests that NpO_2^+ does not enter the GR interlayers.

XPS analyses show that the interaction between NpO_2^+ and GR results in the reduction of Np(V) to Np(IV). The second aim of the TEM analyses is therefore to gather more information concerning the Np(IV)-containing phase formed. This phase could be, for instance, Np dioxide but the possibility of it

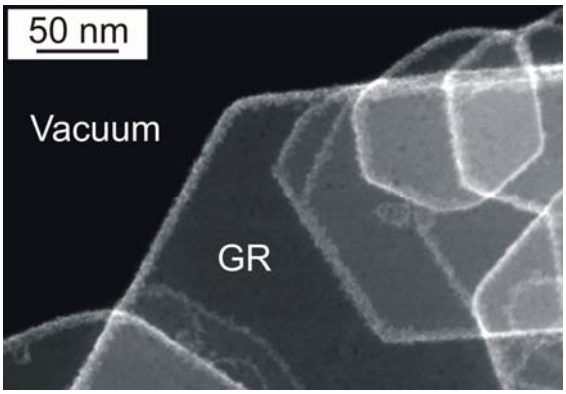

Fig. 2: *STEM-HAADF image of Np-GR.*

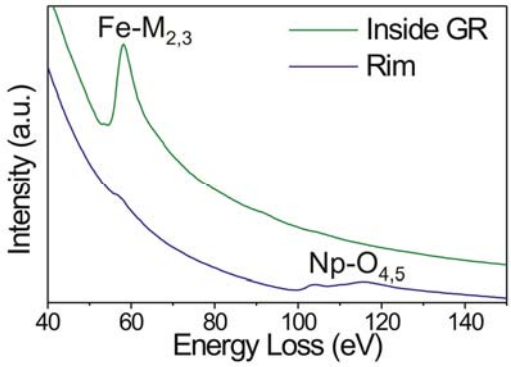

Fig. 3*: EEL spectra taken "inside" a Np-GR platelet and at its rim.*

being a Np-substituted iron oxide mineral cannot be excluded a priori. EELS spectra acquired under the same experimental conditions using an electron probe of around (1 - 2) nm in diameter are shown in Fig. 3 for the inside and for the rim of a Np-GR platelet. The spectrum acquired inside the platelet is characterized by strong Fe-$M_{2,3}$ edges. At the rim, Np-$O_{4,5}$ edges appear around 100 eV, whereas the intensity for the Fe edges almost completely vanishes. The residual Fe signal at the rim likely comes from the electron beam passing through the Np-containing rim and hitting some underlying or adjacent GR region, resulting in the weak signal. The EELS results strongly suggest that Fe is not present at the rim together with Np in one and the same phase, i.e. that the rim does not consist of a Np-substituted iron oxide phase.

HRTEM provides further insight into the Np-phase at the rim. The observed lattice fringe patterns indicate that the rim is composed of crystalline nanoparticles about (2 - 3.5) nm in size. Fig. 4 shows, for example, two distinct GR platelets (superposed on an amorphous background) and their associated rims comprised of nano-crystallites. The Fast Fourier Transform (FFT) of the HRTEM image of any crystalline material exhibits spots, whose position in reciprocal space is related to the orientation and spacing of lattice planes in real space. The position of some spots corresponding to the nanocrystallites at the rim is measured with respect to the center of the FFT (see Fig. 5). This is performed repeatedly for FFTs of different images resulting in an average lattice-plane spacing *d* of about (3.14 ± 0.05) Å. This value is in very good agreement with the *d*-spacing of 3.1370 Å determined from crystallographic data [4] for the (111) plane spacing in NpO_2. Further investigations are in progress to confirm this initial result via electron diffraction, which is a more accurate technique for phase identification.

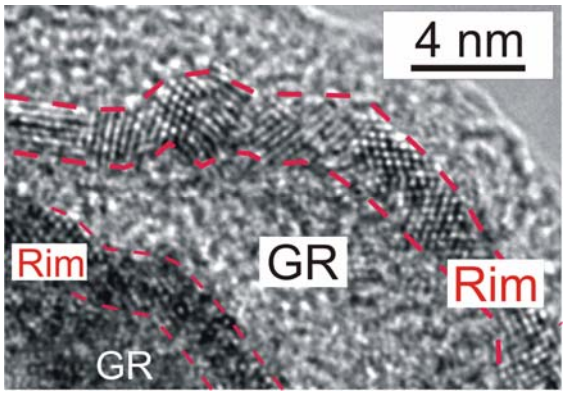

Fig. 4: *HRTEM image of Np-GR.*

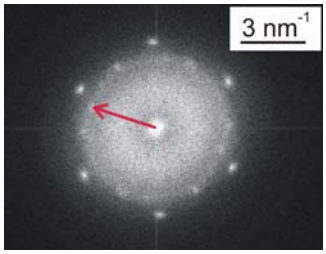

Fig. 5: *FFT of an HRTEM image of Np-GR. The arrow indicates the position of a spot resulting from the rim.*

These XPS and TEM findings suggest NpO_2^+ reduction at GR edges and subsequent growth of NpO_2 nanoparticles. Charge transfer as a sub-step of neptunyl reduction appears plausible, since GR is found to be conductive by XPS.

References

[1] B.C. Christiansen, T. Balic-Zunic, P.O. Petit, C. Frandsen, S. Mørup, H. Geckeis, A. Katerinopoulou, S.L.S Stipp, Geochim. Cosmochim. Acta, 73: 3579 (2009).

[2] M. Schindler, F.C. Hawthorne, M.S. Freund, P.C. Burns, Geochim. Cosmochim. Acta, 73: 2471 (2009).

[3] D. Bach, B.C. Christiansen, D. Schild, H. Geckeis, Microsc. Microanal., 16 Suppl. 2: 1630 (2010).

[4] J.A. Fahey, R.P. Turcotte, T.D. Chikalla, J. Inorg. Nucl. Chem., 38: 495 (1976).

9.5 NMR spectroscopy as a new tool for structural investigations on radioactive materials in solution

P. Kaden, M. Löble, A. Geist, F. Breher[a], I. Fernández[b], P. Oña-Burgos[a], M.A. Denecke

[a]Institut für Anorganische Chemie, Karlsruhe Institute of Technology, 76131 Karlsruhe, [b]Universidad de Almería, Laboratory of Organic Chemistry, E-04120 Almería, Spain.

Introduction

We have recently installed, commissioned and nuclearized a nuclear magnetic resonance (NMR) instrument in the INE controlled area. NMR spectroscopy applied to radioactive samples provides insight into the configuration, constitution and conformation of organic and inorganic compounds in solution relevant for safety assessment of a nuclear repository and for partitioning strategies. NMR is a versatile tool for structure elucidation on an atomic scale that makes use of the nuclear spin properties of certain nuclei in the molecules under investigation. NMR is a valuable extension of the INE portfolio of analytical tools, offering a broad range of techniques. Transferring magnetization along covalent bonds between scalar coupled spins and through space using dipolar coupling techniques provides access to topology and three-dimensional structure of molecules in solution. A key feature of NMR spectroscopy however is the facile access to important dynamic information for molecules in solution by probing magnetic relaxation and diffusion behavior. The principles of and opportunities offered by NMR spectroscopy and the experimental equipment that has been installed in our control area this year to analyze radioactive samples in solution are presented briefly in the following.

Nuclear Magnetic Resonance

NMR spectroscopy in general uses a strong magnetic field (here 9.4T) to align the spin of NMR-active nuclei along the magnetic field. Radio frequency pulses of distinct frequency (resonance frequency of the nuclei under investigation) disturb the resulting Gaussian distribution of nuclear spins by inducing transitions from favored to non-favored spin states. As the spins in the excited state relax back to their ground state, emitted energy is observed as a radiofrequency signal. While spins are in an excited state, additional sets of radiofrequency pulses are utilized to transfer magnetization onto other nuclei separated by chemical bonds or through space. An exhaustive compilation of available NMR techniques is found in [1]. Some of these techniques have been successfully used in initial investigations during commissioning of our new NMR instrument. As an example, some of our first results for a tripodal κ^6*N*-donor complex with ^{242}Pu(III) triflate are presented.

Experimental

In 2010 we installed a Bruker Avance III 400 MHz spectrometer for NMR investigations on radioactive solution samples in the INE controlled laboratory area. It is equipped with an inverse and an observe double channel ^{1}H/BB probe (BBI and BBFO^{plus}), both with z-gradients. Additionally, a DVT-CPMAS probe for investigation of non-radioactive samples in solid state is available. The spectrometer features a two channel setup with QNP equipment and is equipped for variable temperature measurements from -150° to 150°C. Safety precautions and protocol exist for measurements of radioactive samples in solution. A ventilation hood is installed on top of the spectrometer to ensure that exiting gas flow is drawn off, thereby preventing contamination release in any case of sample tube failure.

Radioactive samples are filled into NMR tubes in an inert and contamination-free environment inside of a dedicated glove box and then transferred out for subsequent NMR measurements. A set of different sample tubes is available for measurements under different sample concentrations and conditions. For example, the ^{242}Pu(III)-complex presented below, was measured in an air-tight J. Young tube to ensure oxygen-free sample conditions.

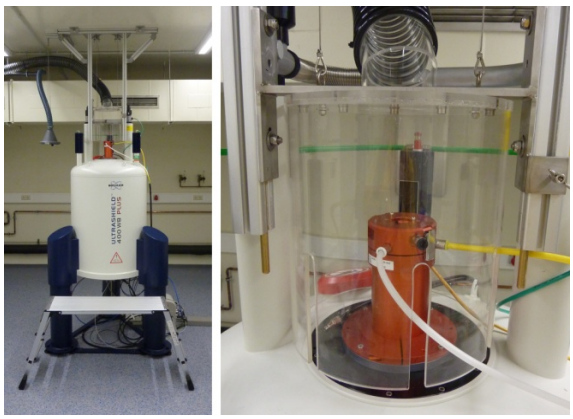

Fig. 1: *The new installed NMR spectrometer in the controlled area and the extractor hood on top of the i instrument.*

First results

We have developed a multidentate κ^6*N*-donor ligand (L), in order to study intrinsically well-defined 1:1 (ligand:metal) coordination compounds. Metal complexes of these ligands are used to systematically study the influence of counter anions on coordination and on liquid-liquid extraction behavior and to develop methods describing electronic properties and solution behavior of *f*-element coordination compounds. Several complexes of trivalent 4*f* metal cations of the form [Ln{PS(N^{Me}NC^{H}Py)$_3$}(OTf)$_3$] have been synthesized and fully characterized using various methods (XRD, TRLFS and XAS) and several advanced NMR techniques, including ^{1}H, ^{19}F HOESY, PGSE, low temperature ^{19}F NMR, ^{1}H, ^{15}N HMQC, ^{139}La NMR and ^{1}H, ^{89}Y gHMQC. We could show that, in the case of small metal cations (Y and Lu), a higher degree of dissociation and solvent separation in solution is predominant than for cations with larger ionic radii.

As plutonium shares similar magnetic properties as its lanthanide counterpart samarium (both with a relatively small magnetic moment of $\mu_{eff} \sim 0.85\ \mu_B$) [2], it is an ideally suited actinide for NMR investigations. The [^{242}Pu{PS(N^{Me}NC^{H}Py)$_3$}(OTf)$_3$] complex is isostructural as the Ln complexes, as confirmed by Pu L3 EXAFS, UV/Vis, P and S K edge NEXAFS. This complex showed chemical shifts in "diamagnetic regions" in its ^{1}H, ^{31}P and ^{19}F NMR spectra. To prove the constitution of the ligand in the complex, 2D correlations of proton resonances to the ^{13}C and ^{15}N spins were performed. Protons are observed via a ^{1}H, ^{13}C gHSQC to be correlated to carbon atoms, to which they are directly attached. Multi-bond correlations of protons to their neighboring ^{13}C and ^{15}N spins were identified by ^{1}H, ^{13}C gHMBC and ^{1}H, ^{15}N gHMBC, respectively. Only minor broadening of the resonances, compared to data of the free ligand in solution, is observed. To identify the binding of triflate counterions in the complex, ^{1}H- and ^{19}F PGSE [3] measurements were performed. Together with ^{1}H, ^{19}F HOESY and ^{19}F low temperature data, we aim to describe the dynamic behavior and characterize the positions of the three anions in the complex. In initial studies of the radiolytic behavior of this complex in solution, we could show via ^{1}H, ^{31}P gHMQC that the ligand framework is preserved.

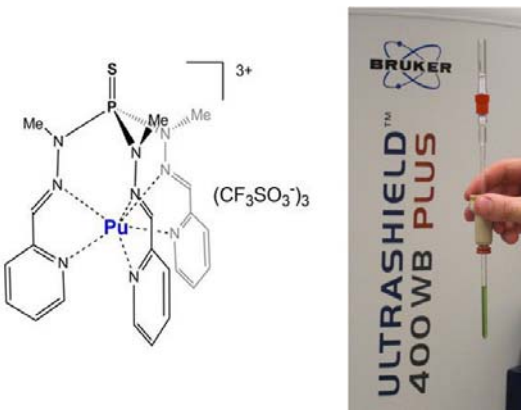

Fig. 2: *The tripodal κ^{6}N-donor complex with ^{242}Pu(III)-triflate. Right: NMR sample in an air-tight J. Young-tube prior to the nuclearisation of the NMR instrumentation.*

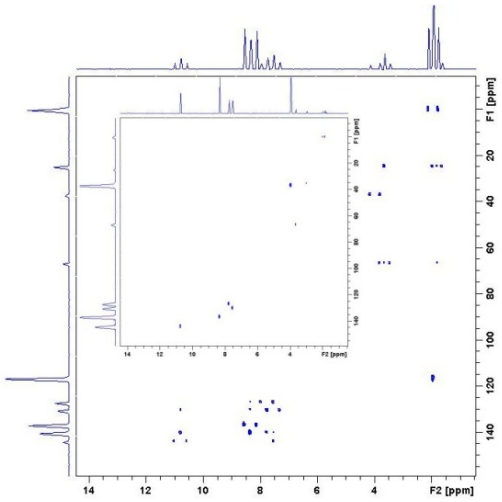

Fig. 3: *^{1}H, ^{13}C HSQC (small) and ^{1}H, ^{13}C HMBC (big correlation spectrum) probing the constitution of the ligand in the complex by correltating proton with carbon resonances over one and multiple covalent bonds, respectively.*

By comparative studies of Pu complexes with analogous samarium compounds, we hope to discriminate via NMR spectroscopy factors contributing to the selectivity of existing extracting agents for actinide cations over lanthanide cations such as:

- the nature of bonding between ligand and cation,
- ion pairing, aggregation and dynamic behavior in solution,
- steric effects.

Areas of applications

After installation, commissioning and nuclearization of the instrumentation, our new NMR has been used to give valuable insight into different fields of INE research program. In addition to actinide-lanthanide separation related studies, first results from investigations of colloids relevant to colloid-mediated contaminant transport and studies of glasses used for the vitrification of HAW were obtained. The NMR instrument is also already established as a key tool in routine analyses for the organic synthesis supporting INE's growing efforts in

the design of new extracting and complexing agents.

Actinide Center of Excellence Transnational Access

Substantial investment in advanced nuclear magnetic resonance facilities has been made in Karlsruhe to establish the “Actinide NMR Centre of Excellence”. The two instruments at INE and JRC-ITU (both Bruker Avance III 400 MHz) are operated in nuclear licensed facilities and commissioned for work on radioactive samples. The FP7 funded EURACT-NMR project (starting date: Feb. 2011) aims at providing access to these newly nuclearized modern instruments and associated laboratory infrastructure for European nuclear scientists. User access is provided through application, which will be judged for scientific excellence and merit by an expert scientific advisory committee.

NMR in general has made several very high profile contributions to actinide science over the last five years. The EURACT-NMR project will certainly help European scientists continue such studies of nuclear materials, including exotic actinide superconductors, oxide nuclear fuels, waste forms and complexes related to separation chemistry.

Acknowledgements:

We thank C. Apostolidis from the JRC-ITU for providing the $^{242}Pu(OTf)_3 \cdot 9H_2O$ used to make the complex studied. This work is supported by the German Federal Ministry of Education and Research (BMBF) under contract numbers 02NUK012A and 02NUK012D.

References

[1] (a) H. Günther, *NMR-Spektroskopie- Eine Einführung*. Georg Thieme Verlag: Stuttgart, 1973. (b) P.J. Hore, J.A. Jones, S. Wimperis, *NMR: The Toolkit*. Oxford University Press: Oxford, 2000.

[2] L.R. Morss, N.M. Edelstein, J. Fuger, J.J. Katz, (Eds.), *The Chemistry of the Actinide and Transactinide Elements.* 3rd ed. **2006**. Corr. 2nd printing, 2006, XVIII.

[3] (a) E. Clot, Eur. J. Inorg. Chem., 2009(16): 2319-2328 (2009). (b) A. Macchioni, Chem. Rev., 105: 2039-2074 (2005). (c) P.S. Pregosin, P.G.A. Kumar, I. Fernández, Chem. Rev., 105: 2977-2998 (2005).

9.6 Computational Chemistry

B. Schimmelpfennig, R. Polly, M. Trumm, M. Flörsheimer, T. Rabung, P. Lindqvist-Reis, D. Schild, N. Banik

Introduction

Methods of computational chemistry developed to powerful tool assisting and complementing experimental studies in modern science. Joint theoretical studies and experimental investigations provided significant improved knowledge and detailed understanding of the system under consideration due to synergetic effects.

Computational chemistry had been introduced and established at INE as a predicting and supporting tool in various different research areas, such as chemical and physical properties of mineral surfaces, extraction chemistry, oxo-hydroxo systems from small size in solution to nano particles or actinides in solution.

The theoretical description of actinides by means of quantum mechanics faces several severe challenges. In many cases we have to deal with open shell systems and multiconfigurational wave functions. When applying Density Functional Theory we assess the accuracy of the results with high quality ab initio calculations. The results are in turn compared with experimental data. Based on a good agreement we are able to provide important additional information, such as structural parameters or reaction energies, which are experimentally not accessible.

Computational chemistry at INE offers a wide spectrum of methods from ab initio and Density Functional Theory (DFT) methods based on quantum mechanics to classical Monte Carlo (MC) simulations and Molecular Dynamics (MD) based on classical mechanics.

The corundum (001) surface studied with MC simulations

MC simulations were applied to study the structure of water close to the surface [1]. We included 147 surface aluminol groups and 1800 water molecules in our simulation model.

The results are in excellent agreement with recent in situ high resolution specular X-ray reflectivity measurements [2] (see Fig.1). This warrants the high quality of the calculations.

MC simulations extend the information about the structure of water close to the surface and provide a number of important additional information which is otherwise not available by experiment:

(1) We were able to distinguish different water species according to their number of hydrogen bonds and the corresponding bonding partner at different distances from the surface (see Fig. 2).

(2) We determined the preferred orientation of different water species at different distances from the corundum (001) surface.

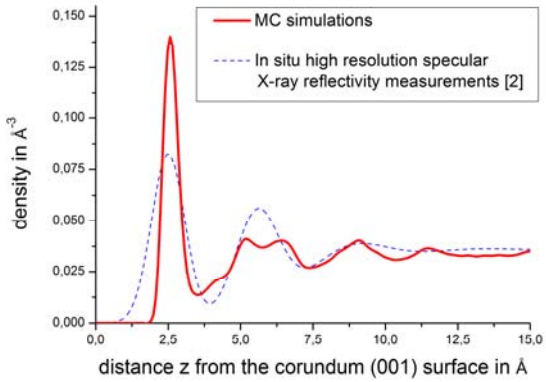

Fig. 1: *Oxygen density of the water molecules above the corundum (001) surface as a function of the distance z from the surface determined with MC simulations. The surface is located at z=0.*

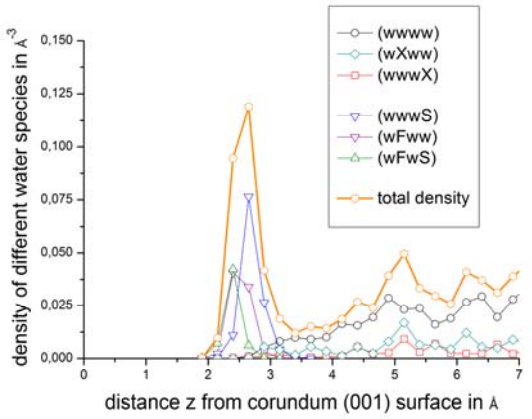

Fig. 2: *Density of different water species above the corundum (001) surface as a function of the distance z from the surface as determined by the MC simulations. The surface is located at z=0.*

With these results we verify that the water signal in the SF spectra of the mineral water interface around the point of zero charge comes mainly from a single layer of surface-bonded water species. The assignment of the bands at 3460 and 3700 cm^{-1} in the SF spectra to surface aluminol groups could be confirmed [3].

This project is a collaboration with J. Janeček (Institute of Physical and Applied Chemistry, Brno University of Technology, Czech

Republic) and R. R. Netz (Physik Department, Technische Universität München, Germany).

The corundum (001) surface studied with plane wave Density Functional Theory using periodic boundary conditions

We targeted this system with plane-wave DFT as implemented in VASP. This allowed us to obtain more theoretical information about the solvated corundum surface. DFT had the drawback that only smaller systems can be studied, but offered the advantage that the water molecules were not rigid and provided direct information about the structure of the water molecules close to the surface.

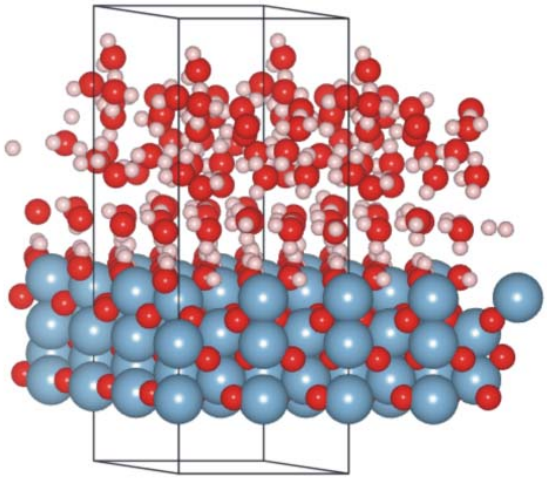

Fig. 3: *Unit cell used to study the solvated corundum (001) surface in contact with water used in the plane wave DFT calculations.*

The DFT model (see Fig. 3) contains only 26 water molecules. This is an extension of all available DFT studies on this topic until now. The model itself constituted a minimal model for the corundum (001) surface in the presence of bulk water. With this model we studied directly the influence of water on the aluminol groups of the surface and obtained very valuable information concerning the interaction of water with the corundum (001) surface. A crucial point is the interplay of the interaction of surface bond water with steep and flat aluminol groups. This explains the existence of one layer of surface bond water with distinct different properties compared to bulk water.

With both methods MC simulations and DFT calculations, we provide important information about the preferential orientation of the water molecules and the water species present in different layers above the surface. Hence our data complemented and augmented experimental information [2].

Sorption of trivalent metal ions at the corundum (110) surface studied with Density Functional Theory using the cluster model

Rabung et al. [4] studied the sorption of trivalent actinides at various corundum surfaces. We already carried out a theoretical study of sorption of these metal ions at the corundum (001) surface and found tri-dendate inner sphere complexes with six water molecules remaining in the first coordination shell of the metal ion.

At the (110) surface single-, double-, and triple-coordinated aluminol species coexisted at the surface. First we studied the properties of the plane surface. Our theoretical estimates for the deprotonation properties of the cluster are well in agreement with predictions by means of the one pK model. We found that deprotonation of triple-coordinated aluminol groups is more likely than deprotonation of aluminol groups with other coordinations.

The vibrational frequencies of these species were calculated and the measured Sum Frequency spectra were simulated with great success. Four peaks could be identified and assigned in both spectra.

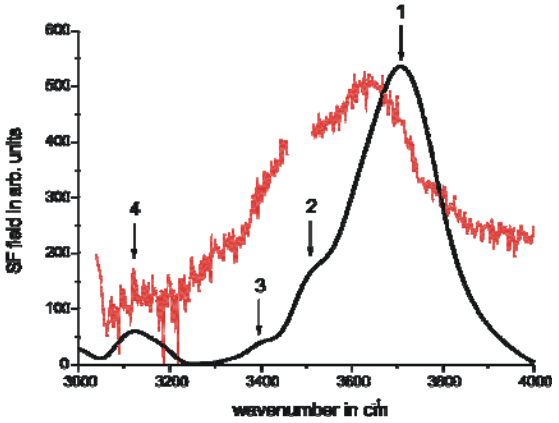

Fig. 4: *Simulation of the Sum Frequency spectra at the corundum (110)/water interface in excellent agreement with experimental data.*

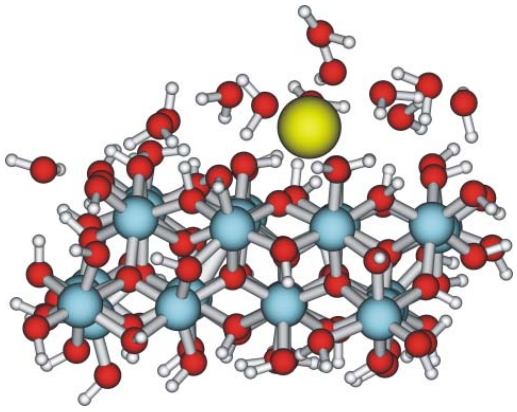

Fig. 5: *Tetra-dendate inner-sphere complex of trivalent f-elements at the corundum (110) surface.*

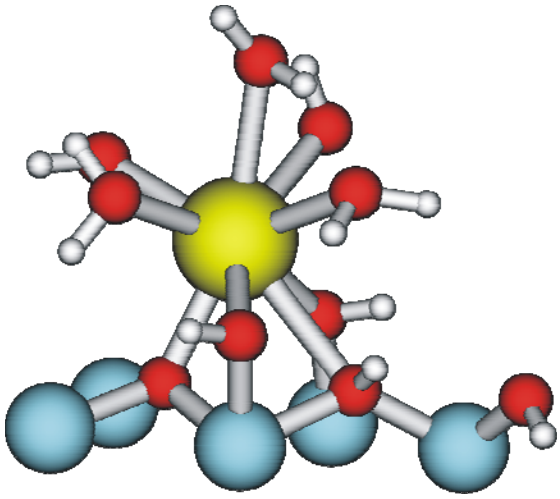

Fig. 6: *Zoomed details of Fig. 5 showing the tetra-dendate inner-sphere complex of trivalent f-elements at the corundum (110) surface. The metal ion is bonded to one deprotonated triple coordinated aluminol group and to two single- and one double-coordinated aluminol species.*

In a next step we extended our study of the sorption of trivalent f-elements at the (110) surface. At this surface we found tetra-dendate inner-sphere complexes at this surface with five water molecules remaining in the first coordination shell. This is in agreement with experimental results [4]. Thus we are able to confirm the trends observed in the experimental studies with our calculations and provide detailed knowledge about the sorption site at the surface. The most favorable sorption site has one triple-coordinated aluminol species deprotonated underneath the inner-sphere complex and two single- and one double-coordinated aluminol species (see Fig. 6).

Development of force fields for actinide ions and complexes in aqueous solution

With the help of quantum-chemical methods we were able to calculate binding energies and vibrational frequencies of complexes of about 30 water molecules around a given central ion in acceptable CPU-time. This was helpful when determining the coordination numbers or thermodynamically properties in the gas phase. For a proper description of the solvation effects about 1000 water molecules are needed to reach bulk behavior [5]. An alternative way of computing such big structures was provided by molecular dynamics. Therefore we started to employ the force-field TCPEp developed by Masella and Cuniasse [6]. The results will also deliver starting points for quantum-chemical calculations. As an example, Fig. 7 shows a Cm(III) ion surrounded by 1000 water molecules and three chloride anions as counter-ions.

With such a structure MD in the NVT or NPT ensemble was started and carried out on the nanosecond scale. Recording the trajectory of the central Cm(III) cation lead to a statistical coordination number. Exploring potentials of mean force at different temperatures gave rise to thermodynamical properties. The aim of these calculations in addition to finding coordination numbers or predict and verify thermodynamical data for solvated actinides was to achieve i.e. dipole-moments, structure analysis, transition mechanisms, exchange rates. To achieve a high accuracy, the parameters of the force-field were fitted to quantum-mechanical data obtained using large state-of-the-art basis sets and electron-correlation approaches like

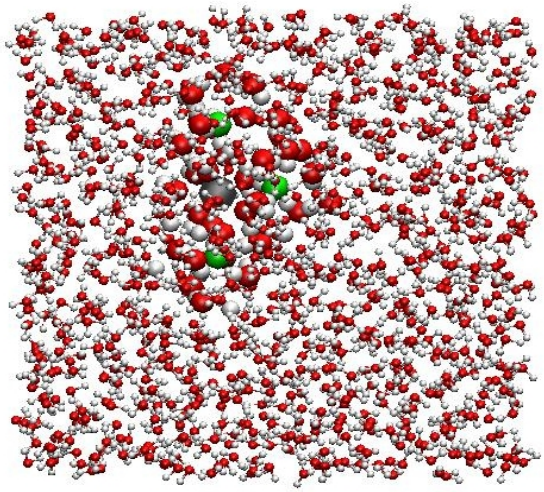

Fig. 7: *Cm(III) ion embedded in 1000 water molecules with three chloride counter-ions*.

MP2 or CCSD(T). Structures with up to 30 waters were geometry-optimized on the MP2 level with the MOLPRO software package, followed by single-point calculations at the CCSD(T) level including counterpoise corrections.

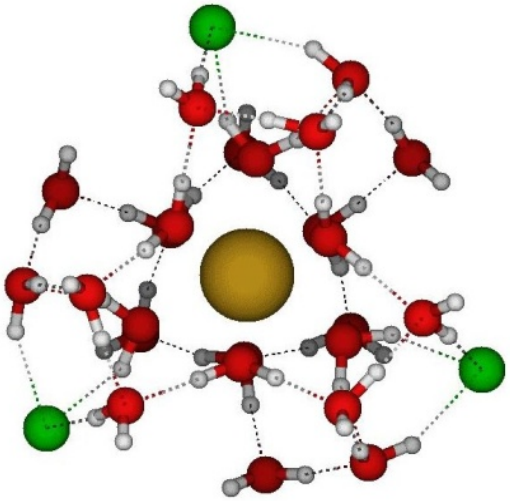

Fig. 8: *A structure with a Cm(III) ion, 27 surrounding water molecules and 3 chloride counter-ions optimized at the MP2 level*

The investigations focus on large-scale simulations of the Th(IV) [7] and Cm(III)-system including the counter-ions chloride, fluoride and bromide. As a result, the first hydration shell of Cm(III) at room temperature is found at an average distance of 249 pm to the central cation. The geometric structure of the first shell can be described by a ratio of 88% 9-fold and 12% 8-fold coordination, in good agreement with the experimental values in **[8]** stating a ratio of 90% to 10%. At a 0.1M Cl^- concentration no chloride ion enters the first hydration shell of the metal ion but the first shell distance is elongated to 253 pm and higher coordinated species are stabilized. The mean Cm-Cl distance is 412 pm for the second-shell chloride-ions. Further studies of many-body effects and their parameterization as well as transferring the developed techniques to other tri- and tetravalent actinides in solution and more complex counter ions will be carried out. This project was initiated as a collaboration within the ACTINET network and involves apart from the computational chemistry group at INE, V. Vallet, F. Real (former ACTINET-fellow) and J.P. Flament from Lille and M. Masella from CEA/Saclay.

Comparison of tri-capped-prismatic structures of trivalent actinides with isostructural lanthanides and quantum chemical calculations.

Systematic computational studies were carried out on molecular $[La(H_2O)_9]^{3+}[M(H_2O)_9(CF_3SO_3)_9]^{6-}[La(H_2O)_9]^{3+}$ (M = Ln (La, Nd, Gd, Er, Lu), An (Ac-Cf)) clusters in order to understand the trends in the M-O distances across the two series of isostructural salts $[M(H_2O)_9(CF_3SO_3)_3]$ (M = Ln, An (U-Cm, Cf) [9]. In the 'triflate' salts the $[M(H_2O)_9]^{3+}$ ions have a nine-fold, tricapped trigonal prismatic (TTP) coordination geometry, with six equidistant water oxygen atoms in the prismatic positions and three in the capping positions at markedly longer distances. Each of the nine waters donates two hydrogen bonds to the neighboring triflate ions. This hydrogen bond arrangement is the reason for the local C_{3h} symmetry, the large difference between the prismatic and capping M-O distances and the special orientation of the water ligands (Figure 9a). The structure of the $[M(H_2O)_9]^{3+}$ cations could be well-mimicked by DFT, by including a second sphere of triflate anions, hydrogen-bonded to two third spheres of $[La(H_2O)_9]^{3+}$ (Figure 9b). However, the f-in-core approach, despite it overestimates the Ln-O bond lengths, could describe the contraction of the bonds across the lanthanides series. Also the corresponding An-O bond lengths are notably overestimated with the corresponding f-in-core approach, which, in addition, gives the bonds a lanthanide character. Though, with the small-core approach the An-O bond distances fit better to the experimental ones (Figure 10a).

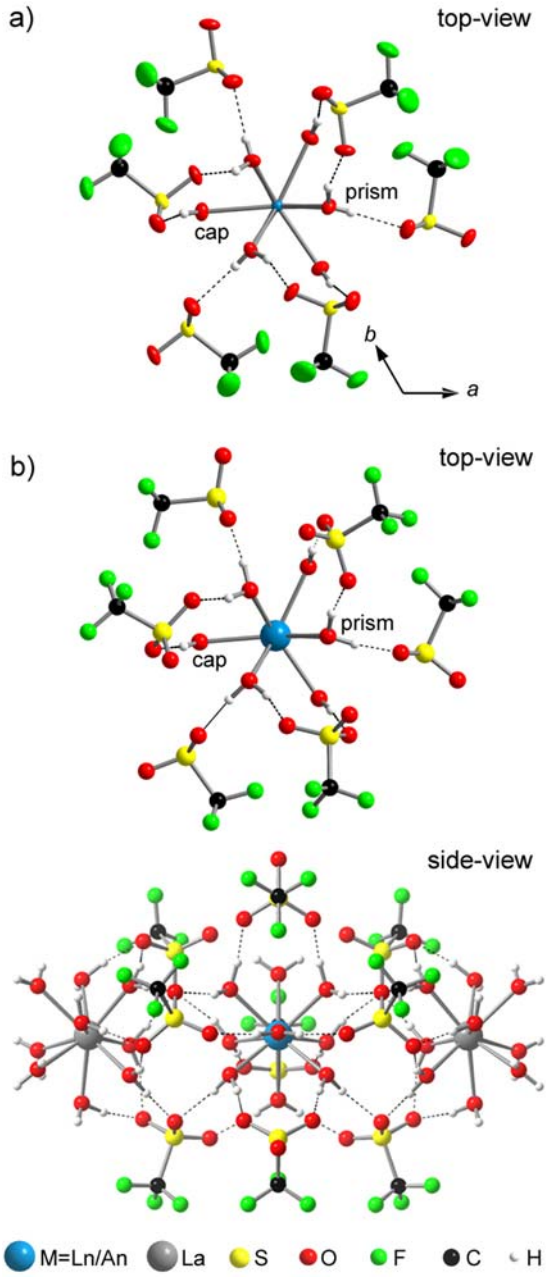

Fig. 9: *a) X-ray structure of the $[M(H_2O)_9\cdots(CF_3SO_3^-)_9]^{6-}$ entity in $[M(H_2O)_9(CF_3SO_3)_3]$ at 200 K (thermal ellipsoids are at 50% probability) and b) the DFT optimized cluster $[La(H_2O)_9]^{3+}\cdots[M(H_2O)_9\cdots(CF_3SO_3^-)_9]^{6-}\cdots[La(H_2O)_9]^{3+}$ (in the top view the $[La(H_2O)_9]^{3+}$ entities are omitted for clarity), M = U are depicted.*

Using the same methodology as for the triflate clusters, we compared the An-N bond lengths in the nine-fold (TTP) coordinated $[An(BTP)_3]^{3+}$ complexes as optimized using DFT with those derived from EXAFS of the same complexes in solution [10]. In this case, the f-in-core approach not only overestimated the An-N bond lengths, it also failed to mimic the general trend of the bond distances from Np to Cm, as it showed a contraction in the bonds while the

EXAFS data showed the bond distances to be more or less the same. Though with the small-core the An-N bonds fitted better to the experimental ones, in particular the overall trend was well mimicked. Despite this apparent lack of contraction in the An-N bonds from U to Cm, this fact may not be taken as an evidence for a contribution of the 5f electrons to the actinide-ligand bond. It is nevertheless a sign that these electrons have an impact on the bonding. Thus the combined experimental and theoretical data leads to the tentative conclusion that there is a trend of decreasing covalence in the An–N bonds in the $[An(BTP)_3]^{3+}$ complexes in the series from U to Cm. An analogous data base of information of a corresponding series of $[Ln(BTP)_3]^{3+}$ solution complexes is needed for comparison in order to judge if these trends indeed play a role in the selectivity of BTP for An(III) over Ln(III) in partitioning.

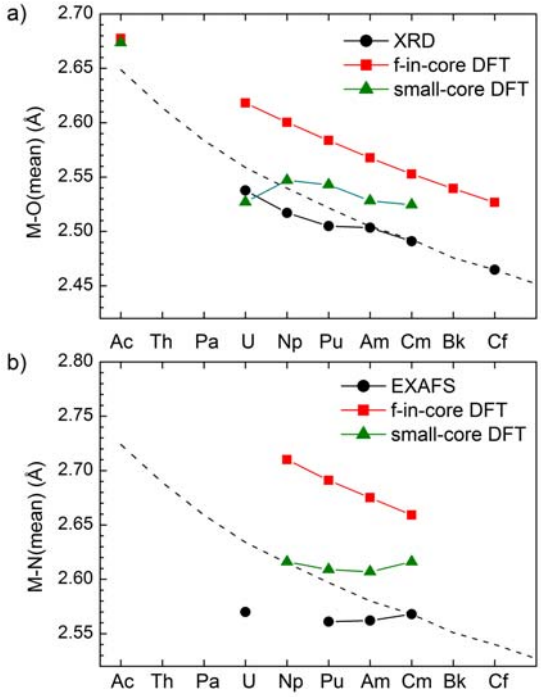

Fig. 10: *Comparison of mean actinide-ligand bond distances (d) from experiments (single-crystal X-ray diffraction and EXAFS) and theory (DFT) in the a) $[An(H_2O)_9]^{3+}$ ions of crystalline $[An(H_2O)_9](CF_3SO_3)_3$ and the clusters $[La(H_2O)_9]^{3+}\cdots[An(H_2O)_9\cdots(CF_3SO_3^-)_9]^{6-}\cdots[La(H_2O)_9]^{3+}$ and b) in the cation complexes of $[An(BTP)_3]^{3+}$.*

References

[1] J. Janeček, R. R. Netz, M. Flörsheimer, R. Klenze, B. Schimmelpfennig, R. Polly, (in preparation).

[2] J. Catalano, submitted to Geochimica et Cosmochimica Acta.

[3] R. Polly, B. Schimmelpfennig, M. Flörsheimer, K. Kruse, A. AbDelMonem, R. Klenze, G. Rauhut and T. Fanghänel, Journal of Chemical Physics 130(6), 064702 (2009).

[4] T. Rabung, D. Schild, H. Geckeis, R. Klenze, T. Fanghänel, J. Phys. Chem. B 108, 17160 (2004).

[5] D. Hagberg, E. Bednarz, N. M. Edelstein, L.Gagliardi, J. Am. Chem. Soc., 129, 14136 (2007).

[6] M. Masella, Ph. Cuniasse, J. Chem. Phys., 119, 1866, (2003).

[7] F. Real, M. Trumm, V. Vallet, B. Schimmelpfennig, M. Masella, J.P. Flament, J. Phys. Chem. B, 114(48) (2010).

[8] P. Lindqvist-Reis, R. Klenze, G. Schubert, T. Fanghänel, J. Phys. Chem. B, 109, 3077, (2005).

[9] C. Apostolidis, B. Schimmelpfennig, N. Magnani, P. Lindqvist-Reis, O. Walter, R. Sykora, A. Morgenstern, E. Colineau, R. Caciuffo, R. Klenze, R.G. Haire, J, Rebizant, T. Bruchertseifer, T. Fanghänel, Angewandte Chemie 122, 36, 6367 (2010).

[10] N.L. Banik, B. Schimmelpfennig, C.M. Marquardt, B. Brendebach, A. Geist, M.A. Denecke, *Dalton Trans.*, 39, 5117 (2010).

10 Publications

Papers in Books and Peer Reviewed Journals

APOSTOLIDIS, C., SCHIMMELPFENNIG, B., MAGNANI, N. , LINDQVIST-REIS, P., WALTER, O., SYKORA, R., MORGENSTERN, A., COLINEAU, E., CACIUFFO, R., KLENZE, R., HAIRE, R.G., REBIZANT, J., BRUCHERTSEIFER, F., FANGHÄNEL, T.
$[An(H_2O)_9](CF_3SO_3)_3$ (An=U-Cm, Cf): Exploring Their Stability, Structural Chemistry, and Magnetic Behavior by Experiment and Theory
Angew. Chem. Int. Ed., 49 (2010) 6343-47.

BANIK, N.L., SCHIMMELPFENNIG, B., MARQUARDT, C.M., BRENDEBACH, B., GEIST, A., DENECKE, M.A.
Characterization of redox sensitive plutonium(III) complexed with alkylated2,6-ditriazinylpyridine (BTP) in organic solution.
Dalton Trans 39 (2010) 5117–5122.

BANIK, N. L., GEIST, A., MARQUARDT, C. M., DENECKE, M. A., GECKEIS, H.
Characterization of Pu(III) extracted by Alkylated 2,6-ditriazinylpyridine (BTP).
European Nuclear Conference (2010), Barcelona, May 30 to June 2,
Transactions, ISBN 978-92-95064-09-6

BOUBY, M., LÜTZENKIRCHEN, J., DARDENNE, K., PREOCANIN, T., DENECKE, M.A., KLENZE, R., GECKEIS, H.
Sorption of Eu(III) onto titanium dioxide: Measurements and modelling
J. Colloid Interface. Sci. 350 (2010) 551-561

CACIUFFO, R., VAN DER LAAN, G., SIMONELLI, L., VITOVA, T., MAZZOLI, C., DENECKE, M. A., LANDER, G.H.
Uranium 5d-5f Electric-multipole Transitions Probed by Non-resonant Inelastic X-ray Scattering
Phys. Rev. B, 81:195104 (2010) 1-7

DARBHA, G.K., SCHÄFER, T., HEBERLING, F., LÜTTGE, A., FISCHER, C.
Retention of Latex Colloids on Calcite as a Function of Surface Roughness and Topography.
Langmuir 26 (7) (2010). 4743-4752.

DENECKE, M.A.
20th International Conference on X-Ray Optics and Microanalysis, Karlsruhe, Germany,
Sep 20-25, 2009, Editors Melissa A. Denecke and Clive T. Walker, Preface M.A. Denecke,
AIP Conference Proceedings Vol.: 1221 (2010)

FANGHÄNEL, T., GECKEIS, H.
MIGRATION 2009, Preface on the 12th International Conference on the Chemistry and Migration.
Behaviour of Actinides and Fission Products in the Geosphere.
Physics and Chemistry of the Earth 35 (6-8): 205-206 (2010)

FELLHAUER, D., NECK, V., ALTMAIER, M., LÜTZENKIRCHEN, J., FANGHÄNEL, TH.
Solubility of tetravalent actinides in alkaline CaCl2 solutions and formation of Ca4[An(OH)8]4+ complexes: A study of Np(IV) and Pu(IV) under reducing conditions and the systematic trend in the An(IV) series
Radiochim. Acta 98 (2010) 541–548

FISCHER, C., DHARBHA, G.K., MICHLER, A., SCHÄFER, T., LÜTTGE, A.
The impact of mineral and rock surface topography on colloid retention.
Mineral Surfaces - From Atomic Processes to Industrial Application.
Geotechnologien Science Report No.16, 47-64 (2010) ISSN: 1619-7399.

GEIST, A.
Extraction of nitric acid into alcohol:kerosene mixtures.
Solvent Extr. Ion Exch. 28 (5) (2010) 596–607.

GIRNT, D., ROESKY, P.W., GEIST, A., RUFF, C.M., PANAK, P.J., DENECKE, M.A.,
6-(3,5-Dimethyl-1H-pyrazol-1-yl)-2,2'-bipyridine as ligand for actinide(III)/lanthanide(III) separation.
Inorg. Chem. 49 (2010) 9627–9635

GOMPPER, K., GEIST, A., GECKEIS, H.
Actinides separation of highly radioactive waste.
Nachrichten aus der Chemie 58 (2010), 1015–1019

GRASSET, L., BREVET, J., SCHÄFER, T., CLARET, F., GAUCHER, E.C., ALBRECHT, A., AMBLÈS, A.
Sequential extraction and spectroscopic characterisation of organic matter from the Callovo-Oxfordian formation.
Organic Geochemistry 41(3) (2010) 221-233.

HEATHMAN, S., RUEFF, J.-P., SIMONELLI, L., DENECKE, M.A., GRIVEAU, J.-C., CACIUFFO, R.,LANDER, G.H.
Resonant x-ray emission spectroscopy at the L3 edge of americium up to 23 GPa
Phys. Rev. B 82, (2010) 201103(R)

HUITTINEN, N., RABUNG, Th., ANDRIEUX, P., LEHTO, J., GECKEIS, H.
A comparative batch sorption and time-resolved laser fluorescence spectroscopy study on the sorption of Eu(III) and Cm(III) on synthetic and natural kaolinite.
Radiochim. Acta, 98 (2010) 613-620

KALLAY, T. PREOCANIN, D. KOVACEVIC ,J., LÜTZENKIRCHEN, J., CHIBOWSKI,
Electrostatic Potentials at Solid/Liquid Interfaces - Review,
Croatica Chemica Acta, 83, (2010) 357-362

KIENZLER, B., METZ, V., BRENDEBACH, B., FINCK, N., PLASCHKE, M., RABUNG, T., ROTHE, J. SCHILD, D.
Chemical status of U(VI) in cemented waste forms under saline conditions.
Radiochimica Acta, 98 (2010) 675-684

KRATZ, J.V., FANGHÄNEL, T., GECKEIS, H.
MIGRATION 2009, Preface on the 12th International Conference on the Chemistry and Migration Behaviour of Actinides and Fission Products in the Geosphere.
Radiochim. Acta 98 (9-11): III-IV (2010)

LAW, G. T. W., GEISSLER, A., LLOYD, J. R., LIVENS, F. R., BOOTHMAN, Ch., BEGG, J. D. C., DENECKE, M. A., ROTHE, J., DARDENNE, K., BURKE, I. T., CHARNOCK, J. M., MORRIS, K.
Geomicrobiological Redox Cycling of the Transuranic Element Neptunium.
Conference: Conference on Goldschmidt 2010 - Earth, Energy, and the Environment Location: Knoxville, TN Date: JUN 13-18, 2010
Environ. Sci. Technol., 44 (2010) 8924–29

LEROUGE, C., CLARET, F., DENECKE, M.A., WILLE, G., FALKENBERG, G., RAMBOZ, C., BENY, C., GIFFAUT, E., SCHÄFER, T., GAUCHER, E.C., TOURNASSAT, C.
Comparative EPMA and μ-XRF methods for mapping micro-scale distribution of iodine in biocarbonates of the Callovian-Oxfordian clayey formation at Bure, Eastern part of the Paris Basin.
Physics and Chemistry of the Earth, Parts A/B/C 35(6-8) (2010) 271-277.

LÜTZENKIRCHEN, J., KUPCIK, T., FUSS, M., WALTHER, C., SARPOLA, A., SUNDMAN, O.
Adsorption of Al-13-Keggin clusters to sapphire c-plane single crystals: Kinetic observations by streaming current measurements
Applied Surface Science, 256 (2010) 5406-5411

LÜTZENKIRCHEN, J., RICHTER, C., BRANDENSTEIN, F.
Some data and simple models for the silanated glass-electrolyte Interface.
Adsorption. **16**, 2010, 249.

LÜTZENKIRCHEN, J., ZIMMERMANN, R., PREOCANIN, T., FILBY, A., KUPCIK, T., KUTTNER, D., ABDELMONEM, A., SCHILD, D., RABUNG, T., PLASCHKE, M., BRANDENSTEIN, F., WERNER, C., GECKEIS, H.
An attempt to explain bimodal behaviour of the sapphire c-plane electrolyte interface.
Advances in Colloid and Interface Science, 157, (2010), 61-74

MARQUES-FERNANDES, M., STUMPF, T.,BAEYENS, B.,WALTHER, C.,BRADBURY, M.H.
Spectroscopic Identification of Ternary Cm-Carbonate SurfaceComplexes
Env. Sci. Tec., 44 (2010) 921-927

MODOLO, G., KLUXEN, P., GEIST, A.
Demonstration of the LUCA process for the separation of americium(III) from curium(III), californium(III), and lanthanides(III) in acidic solution using a synergistic mixture of bis(chlorophenyl)dithiophosphinic acid and tris(2-ethylhexyl)phosphate.
Radiochim. Acta 98 (2010) 193–201.

PLASCHKE, M., ROTHE, J., ARMBRUSTER, M.K., DENECKE, M.A., NABER, A., GECKEIS, H.
Humic acid metal cation interaction studied by spectromicroscopy techniques in combination with quantumchemical calculations
Journal of Synchrotron Radiation 17 (2010) 158–165.

PLASCHKE, M., ROTHE, J., DENECKE, M.A. GECKEIS,H.
STXM/C 1s-NEXAFS study of Eu(III) and Uranyl humic acid aggregates at different pH
20th International Conference on X-Ray Optics and Microanalysis, Sep 20-25, 2009
AIP Conference Proceedings Vol.: 1221 (2010) p. 144-149

POLLY, R.,SCHIMMELPFENNIG, B., RABUNG, T., FLOERSHEIMER, M., KLENZE, R., GECKEIS, H.
Quantum chemical study of inner-sphere complexes of trivalent lanthanide and actinide ions on the corundum (0001) surface
Radiochimica Acta, 98, 9-11 (2010) 627-634

POLLY, R., SCHIMMELPFENNIG, B., FLÖRSHEIMER, M., KLENZE, R., GECKEIS, H.
Theoretical investigation of the solvated corundum surface
Geochimica et Cosmochimica Acta 74, 11 (2010), A824

POPA, K., WALLEZ, G., RAISON, P.E., BREGIROUX, D., APOSTOLIDIS, C., LINDQVIST-REIS, P. KONINGS, R.J.M.
SrNp(PO4)2: an Original Ordered Modification of Cheralite
Inorg. Chem. 49 (2010) 6904-6908.

SCHÄFER T., DENECKE M.A.
Nuclear waste repository research at the micro- to nanoscale
20th International Congress on X-Ray Optics and Microanalysis, Karlsruhe (G) SEP 20-25, 2009
Editors: Denecke MA, Walker CT, X-ray optics and microanalysis,
AIP Conference Proceedings Vol.: 1221 (2010) p. 181-187

SCHILD, D., ULRICH, S., YE, J., STÜBER, M.
XPS investigations of thick, oxygen-containing cubic boron nitride coatings.
Solid State Sciences 12 (2010) 1903-1906

SCHMIDT, M., STUMPF, T., WALTHER, C., GECKEIS, H., FANGHÄNEL, T.
Phase transformation in $CaCO_3$ polymorphs: a spectro-scopic, microscopic and diffraction study.
J. Coll. Interf. Sci., 351 (2010) 50-56

SKERENCAK, A., PANAK, P. J., NECK, V., TRUMM, M., SCHIMMELPFENNIG, B., LINDQVIST-REIS, P., KLENZE, R., FANGHÄNEL, TH.
Complexation of Cm(III) with Fluoride in Aqueous Solution in the Temperature Range from 20 to 90 °C. A joint TRLFS and Quantum Chemical Study,
J. Physical Chemistry B 114 (2010) 15626-15634.

STUMPF, S., SEIBERT, A., GOUDER, T., HUBER, F., WISS, T., BRENDEBACH, B., DENECKE, M.A.
Development of fuel-model interfaces: Characterization of Pd containing UO_2 thin films
J. NUCLEAR MATERIALS **397**, p. 19-26 (2010)

TERZANO, R., DENECKE, M.A., MEDICI, L.
Synchrotron Radiation in Soil and Geosciences
Journal of Synchrotron Radiation 17 (2010) 147–148

TERZANO, R., SANTORO, A., SPAGNUOLO, M., VEKEMANS, B., MEDICI, L., JANSSENS, K., GÖTTLICHER, J., DENECKE, M.A., MANGOLD, S. RUGGIERO, P.
Solving mercury (Hg) speciation in soil samples by synchrotron X-ray microspectroscopic techniques
Environmental Pollution 158 (2010) 2702-2709

TRUMM, S., LIESER, G., FOREMAN, M.R.S.J.., PANAK, P.J., GEIST, A., FANGHÄNEL, T.
A TRLFS study on the complexation of Cm(III) and Eu(III) with 4-t-butyl-6,6'-bis-(5,6-diethyl-1,2,4-triazin-3-yl)-2,2'-bipyridine in a water/2-propanol mixture.
Dalton Trans. **39** (2010) 923–29.

TRUMM, S., PANAK, P.J., GEIST, A., FANGHÄNEL, T.
A TRLFS study on the complexation of Cm(III) and Eu(III) with 2,6-bis(5,6-dipropyl-1,2,4-triazin-3-yl)pyridine in water/methanol mixture.
Eur. J. Inorg. Chem. 19 (2010) 3022–28

VILAS,.V., MATHIASCH, B., HUTH, J., KRATZ, J.V., DE LA ROSA, S.R., MICHEL, P., SCHÄFER, T.
Synthesis and Characterization of the Hybrid Clay-Based Material Montmorillonite–Melanoidin: A Potential Soil Model.
Soil Sci. Soc. Am. J. 74(6) (2010) 2239-2245.

VITOVA T., KVASHNINA K.O., NOCTON G., SUKHARINA G., DENECKE M.A., BUTORIN S.M., MAZZANTI M., CACIUFFO R., SOLDATOV A., BEHRENDS T., GECKEIS H.
High energy resolution x-ray absorption spectroscopy study of uranium in varying valence states.
Phys. Rev. B, 82:235118 (2010) S. 1-6

VITOVA, T., BRENDEBACH, B., DARDENNE, K, DENECKE, M.A., LEBID, A., .ROTHE, J., BATUK, O.N., HORMES, J., LIU, D., BREHER, F., GECKEIS, H.
High resolution X-ray emission spectroscopy: an advanced tool for actinide research.
ACTINIDES 2009, San Francisco, CA, JUL 12-17, 2009
IOP Conf. Series: Materials Science and Engineering **9** (2010) p. 012053 (1-6)
DOI: 10.1088/1757-899X/9/1/012053 Published: 2010

Proceedings of Workshops and Conferences

ALTMAIER, M., BUBE, C., BRENDLER, V., MARQUARDT, CH., MOOG, H., NECK, V., RICHTER, A., SCHARGE, T., VOIGT, W., WILHELM, S., WOLLMANN, G.
THEREDA: Thermodynamic Data for Waste Management Assessment – Focus on Actinide Data.
International Workshop on Actinide and Brine Chemistry in a Salt-Based Repository (ABC-SALT), Carlsbad, New Mexico, September 15-17, 2010. Book of Abstracts, 55-56.

ALTMAIER, M., NECK, V., BRENDEBACH, B., FANGHÄNEL, TH.
Actinide Carbonate Complexation and Solid Phase Stability in reducing MgCl2 Brine Systems
International Workshop on „Actinide and Brine Chemistry in a Salt-Based Repository"
Carlsbad, New Mexico, USA, September 15-17, 2010 Book of Abstracts, 43-44.

ALTMAIER, M., NECK, V.
Actinde Chemistry under High Salinity Conditions.
International Memorial Workshop "Aquatic Chemistry and Thermodynamics of Actinides and long-lived fission products"in honor of Dr. Volker Neck, 20th May 2010, Karlsruhe, Germany. Book of Abstracts, 25-26.

BACH, D., CHRISTIANSEN, B.C., SCHILD, D., GECKEIS, H.
TEM Investigations of Green Rust (GR_{Na2SO4}) Interacted with Neptunyl (NpO_2^+)
Proceedings Microscopy & Microanalysis 2010, Portland, Oregon, USA, August 1-5, 2010
Microsc. Microanal. 16 (Suppl 2), 2010, 1630-1631.

BUBE, C., METZ, V., KIENZLER, B.
Radionuclide behaviour in the near-field of a repository - building conference in simulations by experimental validation.
Jahrestagung Kerntechnik - Annual Meeting on Nuclear Technology. Berlin, 2010.
Berlin : INFORUM GmbH, 2010 , CD-ROM Paper 519

BANIK, N. L., GEIST, A., MARQUARDT, C. M., DENECKE, M. A., GECKEIS, H.
Characterization of Pu(III) extracted by Alkylated 2,6-ditriazinylpyridine (BTP)
ENC 2010 Transactions, ISBN 978-92-95064-09-6

BANIK, N. L, MARQUARDT, C. M., WALTHER, C., BRENDEBACH, B., ROTHE, J., KLENZE, R.
Speciation studies of tetravalent protactinium in aqueous solution.
Reports of user experiments at ANKA 2009/2010, Karlsruhe Institute of Technology, Oct 2010, S. 108

BANIK, N. L., MARQUARDT, C. M., WALTHER, C., ROTHE, J., DENECKE, M. A., KLENZE, R.
Speciation studies of tetravalent protactinium in aqueous solution
Plutonium Futures—The Science 2010, Keystone, Colorado, USA, Sept. 19-23, 2010, Book of Abstracts, p. 132-133.

BRENDLER, V., ALTMAIER, M., MARQUARDT, Ch., MOOG, H., RICHTER, A., SCHARGE, T., VOIGT, W., WILHELM, S., WOLLMANN, G.
THEREDA: Providing quality-assured thermodynamic data for waste management assessment.
International Memorial Workshop "Aquatic Chemistry and Thermodynamics of Actinides and long-lived fission products"in honor of Dr. Volker Neck, 20th May 2010, Karlsruhe, Germany. Book of Abstracts, 23-24.

BUTORIN, S. M., VITOVA, T., VEGELIUS, J., SEIBERT, A., CACIUFFO, R., DENECKE, M. A.
In-Situ RIXS studies of the possibilities of the existence of Pu(V) in plutonium
Dioxide.
Reports of user experiments at ANKA 2009/2010, Karlsruhe Institute of Technology, Oct 2010, S. 110

DENECKE, M. A., HEATHMAN, S., SURBLÉ, S., LANDER, G. H.
Electronic structure of Americium under high pressure from Am L3 XANES
investigations at the INE-Beamline.
Reports of user experiments at ANKA 2009/2010, Karlsruhe Institute of Technology, Oct 2010, S. 112

DENECKE, M.A., WALKER, C.T. (EDS.)
X-ray optics and microanalytics
Proceedingsof the 20th International Congress ICXCOM20, Karlsruhe Sept, 15-18 2009, (American Institute of Physics Conference Proceedings 1221)

FANGHÄNEL, TH., NECK, V., ALTMAIER, M.
Aqueous Plutonium Chemistry.
International Memorial Workshop ”Aquatic Chemistry and Thermodynamics of Actinides and long-lived fission products“in honor of Dr. Volker Neck, 20th May 2010, Karlsruhe, Germany. Book of Abstracts, 13-14.

FELLHAUER, D., ALTMAIER, M., NECK, V., RUNKE, J., FANGHÄNEL, TH.
Reduction Kinetics of Np(V) in Non-Complexing Aqueous Systems at pH 5 – 10
Plutonium Futures – The Science 2010,
Keystone, Colorado, USA, September 19-23, 2010. Book of Abstracts, 128-129.

FELLHAUER, D., KIRSCH, R., ALTMAIER, M., NECK, V., SCHEINOST, A. C., WISS, T., CHARLET, L., FANGHÄNEL, TH.
Plutonium Redox Behavior in Aqueous Solutions and on Nanocrystalline Iron Phases
Plutonium Futures – The Science 2010,
Keystone, Colorado, USA, September 19-23, 2010. Book of Abstracts, 37-38.

FELLHAUER, D., KIRSCH, R., ALTMAIER, M., NECK, V., SCHEINOST, A. C., WISS, T., CHARLET, L., FANGHÄNEL, TH.
Plutonium Redox Processes in Aqueous Systems
International Workshop on „Actinide and Brine Chemistry in a Salt-Based Repository”
Carlsbad, New Mexico, USA, September 15-17, 2010. Book of Abstracts, 39-40.

FINCK, N.
Selenite reduction by sulphide species.
ANKA Experimental Report, Annual Report 2010,114 -115.

FINCK, N.
Selenide binding to iron sulfides.
ANKA Experimental Report, Annual Report 2010,116 -118.

FLEISCH, J., GRUENEWALD, W., ROTH, G., TOBIE, W., WEISENBURGER. S., WEISHAUPT, M.
Radioactive Start-up of the German VEK Vitrification Plant ,
WM2010 Conference, March 7-11, 2010, Phoenix, AZ, Book of Abtracts on CD Nr. XXX

GAONA, X., ALTMAIER, M., GRIVÉ, M., MONTOYA, V., COLÀS, E., DURO, L.
Chemistry of An(III,IV)/Ln(III) eigencolloids: complexation reactions with inorganic and organic ligands
International Workshop on Actinide and Brine Chemistry in a Salt-Based Repository (ABC-SALT), Carlsbad, New Mexico, September 15-17, 2010. Book of Abstracts, 31-32.

GAONA, X., ALTMAIER, M., PETROV, V., FELLHAUER, D., TITS, J., WIELAND, E., DARDENNE, K., FANGHÄNEL, TH.
Aqueous speciation of Np(V/VI) in hyperalkaline systems
ANKA Experimental Report, Annual Report 2010,119 -121.

GAONA, X., ALTMAIER, M., PETROV, V., FELLHAUER, D., TITS, J., WIELAND, E., DARDENNE, K., FANGHÄNEL, TH.
Aqueous speciation and solubility of Np(V/VI) in hyperalkaline systems.
Plutonium Futures “The Science”, Keystone, Colorado, USA, September 19-23, 2010. Book of Abstracts, 123-124.

GAONA, X., GRIVÉ, M., MONTOYA, V., COLÀS, E., ALTMAIER, M., DURO, L.
Chemistry of An(III,IV)/Ln(III) eigencolloids: complexation reactions with inorganic and organic ligands
Plutonium Futures “The Science”, Keystone, Colorado, USA, September 19-23, 2010. Book of Abstracts, 79-80.

GRÜNEWALD, W., ROTH, G., TOBIE, W., WEISENBURGER, S., FLEISCH, J., SCHMITZ, F. J., WEISHAUPT, M.
"Verglasungsanlage VEK - Erfolgreiche Inbetriebnahme und erste Betriebserfahrungen",
Jahrestagung Kerntechnik, Berlin, 03.-06.05.2010, Abtractband auf CD Beitrag Nr. YYY

HUBER,F., ENZMANN, F., SCHÄEFER,T.
Bentonite nanoparticle mediated radionuclide migration under
simulated glacial melt-water intrusion in fractured rocks
Geochimica et Cosmochimica Acta, Volume 74, Issue 12, Supplement 1, Page A433 (20th Annual Goldschmidt Conference Absctracts June 2010)

ICKER, M.,WALTHER, C.,NECK, V.,GECKEIS, H.,
The redox potential of Pu containing acidic solutions and the fate of Pu(IV)-colloids - direct measurement versus optical absorption spectroscopy
IOP Conf. Ser.: Mater. Sci. Eng. , 9 (2010) S. 1-10

KUCZEWSKI, B., DITTRICH, H.T., DULLY, C., LAGOS, M., MAROSITS, E., MARQUARDT, C.M.
Development of a speciation method for iodine and uranium in environmental samples with special focus on the redox behaviour,
In Workshop Proceedings, 2nd Annual Workshop Proceedings of the Collaborative Project "Redox Phenomena Controlling Systems" (7th EC FP CP RECOSY),
(Ed.) BUCKAU, G., KIENZLER, B., DURO, L., GRIVÉ, M., MONTOYA, V., KIT, Karlsruhe, 2010, S. 171.

KUPCIK, T., HUITTINEN, N., RABUNG, T., LÜTZENKIRCHEN, J., GECKEIS, H., FANGHÄNEL, T.
Trivalent metal ion interaction with aluminium oxides/hydroxides
3rd EuCheMS Chemistry Congress Nürnberg, August 29 - September 2, 2010

LÖBLE, M., VITOVA, T., BRENDEBACH, B., ROTHE, J., DARDENNE, K., DENECKE, M. A., BREHER, F.
P and S K edge XANES investigations of lanthanide complexes consisting of a κ^6N-donor ligand with podand topology.
Reports of user experiments at ANKA 2009/2010, Karlsruhe Institute of Technology, Oct 2010, S. 122

LOIDA, A., GENS, R., METZ, V., LEMMENS, K., CACHOIR, C., MENNECART, T., KIENZLER, B.
Corrosion behavior of high burnup spent fuel in highly alkaline solutions.
Mat. Res. Soc. Symp. Proc. Vol 1193, pp.597-604 (2010)

METZ, V., KIENZLER, B., BUBE, C., BOHNERT, E.
Interactions of americium and uranium with cement alteration products under saline conditions.
International Workshop on Actinide and Brine Chemistry in a Salt-Based Repository (ABC-SALT)
Carlsbad, New Mexico, USA. Book of Abstracts, p. 49-50.

NECK, V., ALTMAIER, M., FELLHAUER, D., RUNKE, J., FANGHÄNEL, TH.
Quantification of the redox potential for the reduction of Np(V) in non-complexing aqueous solutions at pH 5-10.
1st Annual Workshop Proceedings, Collaborative Project "Redox Phenomena Controlling Systems" - Recosy , Barcelona, 10-12 Feb. 2009.
Wissenschaftliche Berichte FZKA 7466, Forschungszentrum Karlsruhe, Karlsruhe, Germany, Dec. 2009, pages 65-73.

PLASCHKE, M., ROTHE, J., DENECKE, M.A., GECKEIS, H.
STXM / C 1s-NEXAFS study of Eu(III) and Uranyl humic acid aggregates at different pH
in: Denecke, M.A. and Walker, C.T. (Eds.) "X-ray Optics and Microanalysis", Proceedings of the ICXOM20 Conference, September 13-18, 2009, Karlsruhe, Germany, American Institute of Physics, Melville, New York, AIP Conference Proceedings 1221 (2010), S. 144

ROTHE, J., DARDENNE, K., VITOVA, T., DENECKE, M. A., GECKEIS, H.
Actinidenforschung an der INE-Beamline – Status und Perspektiven.
SNI 2010, Deutsche Tagung für Forschung mit Synchrotronstrahlung, Neutronen und Ionenstrahlung an Großgeräten, FU Berlin, 24. – 26. Februar 2010
Book of abstracts, p…

ROSENBERG, Y.O., METZ, V., OREN, Y., VENGOSH, A., VOLKMAN, Y., GANOR, J.
Radium co-precipitation in evaporitic systems.
Third International Conference on Radium and Radon Isotopes as Environmental Tracers, Jerusalem, March 14-19, 2010. Book of Abstracts, page 53 (2010)

SCHÄFER, T., DENECKE, M.A.
Nuclear waste repository research at the micro- to nanoscale.
X-Ray Optics and Microanalysis
Proceedings. M. A. Denecke and C. T. Walker (eds.)
Amer. Inst. Physics Conference Proceedings (2010) 1221: 181-187.

SHARRAD, C., GOFF, G., MAY, I., RUNDE, W., BANIK, N.L., BRENDEBACH, B., DARDENNE, K., DENECKE, M.A., MARQUARDT, C.M.
U L3 edge XAFS investigation on U(VI) monomer species
ANKA Experimental Report, Annual Report 2010,130 -133.

SHARRAD, C., GOFF, G., MAY, I., RUNDE, W., BANIK, N.L., BRENDEBACH, B., DARDENNE, K., DENECKE, M.A., MARQUARDT, C.M.
U L3 edge XAFS investigation on U(VI) dimer species
ANKA Experimental Report, Annual Report 2010,134 -135.

SHARRAD, C., GOFF, G., MAY, I., RUNDE, W., BANIK, N.L., BRENDEBACH, B., DARDENNE, K., DENECKE, M.A., MARQUARDT, C.M.
Pu L3 edge XAFS investigation on Pu(IV) pentacarbonate species
ANKA Experimental Report, Annual Report 2010,136 -137.

SHCHERBINA, N.S., PERMINOVA, I.V., NOVIKOV, A.P., KALMYKOV, S.N., MARQUARDT, C.M., WALTHER, C., BUCKAU, G., KUMKE, M., EIDNER, S.
Redox properties of humic substances: identification of redox functional groups by TRLFS.
In Workshop Proceedings, 2nd Annual Workshop Proceedings of the Collaborative Project “Redox Phenomena Controlling Systems” (7th EC FP CP RECOSY), BUCKAU, G., KIENZLER, B., DURO, L.,

STUMPF, S., PETERSMANN, T., SEIBERT, A., GOUDER, T., HUBER, F., BRENDEBACH, B., DENECKE, M.A.
Comparative study of the structural and electrochemical properties of noble metal inclusions in a UO_2 matrix
Actinides Conference 2009 at San Francisco (CA) JUL 12-17, 2009
IOP Conference Series: Materials Science and Engineering. Article Number: 012014 (2010)

STUMPF, S., SEIBERT, A, GOUDER, T, DENECKE, M.A.
Spent Nuclear Fuel corrosion - The influence of Pd epsilon-particles on dissolution processes.
GEOCHIM. COSMOCHIM. ACTA **74** (2010) p. A1000-A1000

VITOVA T., BRENDEBACH B., DARDENNE K., DENECKE M.A., LEBID A., LÖBLE M., ROTHE J., BATUK O. N., HORMES J., LIU D., BREHER F., GECKEIS H.
High resolution x-ray emission spectroscopy: an advanced tool for actinide research.
IOP Conf. Ser.: Mater. Sci. Eng., 9: 012053 (2010) S. 1-6

VITOVA, T., DARDENNE, K., DENECKE, M. A., ERNST, H., ROTHE, J.
The latest development and optimization of the high-resolution X-ray emission spectrometer at the INE-Beamline.
Reports of user experiments at ANKA 2009/2010, Karlsruhe Institute of Technology, Oct 2010, S. 141

VITOVA T., DENECKE M.A., LÖBLE M., DARDENNE K., ROTHE J., GECKEIS H., KVASHNINA K.O., VEGELIUS J., BUTORIN S.M., NOCTON G., MAZZANTI M., SEIBERT A., CACIUFFO R., DENNING R.G.
Advanced X-ray absorption/emission spectroscopic tool for actinide speciation.
Plutonium Futures – The Science 2010, Keystone, Colorado, USA, September 19-23, 2010. Book of Abstracts, 220-221.

VITOVA T., DENECKE M.A., KVASHNINA K., LÖBLE M., DARDENNE K., ROTHE J., BUTORIN S.M., SEIBERT A., CACIUFFO R., GECKEIS H.
Actinide speciation with high-resolution X-ray absorption/emission spectroscopy.
7th International Conference on Inelastic X-ray Scattering, Grenoble, France, October 11-14, 2010, Book of Abstracts, 120.

VITOVA T., DENECKE M.A.
The potential of high-resolution X-ray absorption/emission spectroscopy for advanced studies of nano-materials.
Nanodesign: Physics, Chemistry, Computer Modeling
German-Russian Interdisciplinary Workshop, Rostov-on-Don, Russia, December 16-17, 2010, Book of Abstracts.

Reports

BOSBACH, D., BÖTTLE, M., METZ, V.
Experimental study on Ra2+ uptake by barite (BaSO4). Kinetics of solid solution formation via BaSO4 dissolution and Ra(x)Ba(1-x)SO4 (re)precipitation.
Svensk Kärnbränslehantering AB, SKB, Stockholm, Sweden. SKB TR-10-43 (2010)

BUCKAU, G, KIENZLER, B., DURO, L., GRIVE, M., MONTOYA, V. (EDS)
EURATOM EC 7th Framework Program Collaborative Project “Redox Phenomena Controlling Systems” – 1st Annual Workshop Proceedings
FZKA Report 7466, Forschungszentrum Karlsruhe GmbH, Karlsruhe, Germany.

BUCKAU, G, KIENZLER, B., DURO, L., GRIVE, M., MONTOYA, V. (EDS)
2nd Annual Workshop Proceedings of the Collaborative Project “Redox Phenomena Controlling Systems” (7th EC FP CP RECOSY)
KIT Scientific Reports 7557, Karlsruhe Institute of Technology, KIT Scientific Publishing, Karlsruhe, Germany.

GECKEIS, H., STUMPF, T., (EDS.)
Institute for Nuclear Waste Disposal. Annual Report 2009.
KIT Scientific Reports 7559, Karlsruhe Institute of Technology, KIT Scientific Publishing, Karlsruhe, Germany.

GRAMBOW, B., BRUNO, J., DURO, L., MERINO, J., TAMAYO, A., MARTIN, C., PEPIN, G. , SCHUMACHER, S., SMIDT, O., FERRY, C., JEGOU, C., QUIÑONES, J., IGLESIAS, E., RODRIGUEZ VILLAGRA, N., NIETO, J. M., MARTÍNEZ-ESPARZA A., LOIDA, A., METZ, V., KIENZLER B., BRACKE, G., PELLEGRINI, D., MATHIEU, G., WASSELIN-TRUPIN, V. , SERRES, C., WEGEN, D., JONSSON, M., JOHNSON, L., LEMMENS, K., LIU, J., SPAHIU, K., EKEROTH, E., CASAS, I., DE PABLO, J., WATSON, C., ROBINSON, P., HODGKINSON D.
MICADO, Model uncertainty for the mechanism of dissolution of spent fuel in nuclear waste repository. Final activity report.
European Commission, Brussels, Belgium. Priority No. NUWASTE-2005/6-3.2.1.1-2

HUBER, F., LÜTZENKIRCHEN, J., PFINGSTEN, W., TIFFREAU, C. (HRSG)
TRePro II 2009: Workshop on Modelling of Coupled Transport Reaction Processes
Proceedings of the Workshop TRePro II. Wissenschaftliche Berichte, FZKA-7482

SCHÄFER,TH., NOSECK,U (HRSG)
Colloid/Nanoparticle formation and mobility in the context of deep geological nuclear waste disposal (Project KOLLORADO-1 Final Report)
Wissenschaftliche Berichte, FZKA-7515 Oktober 2010

Internal Reports

LOIDA, A., MÜLLER,N., METZ, V., BUBE, C., KIENZLER, B.
Investigation of the Corrosion Behaviour of Irradiated Spent Fuel
in High pH Solutions – Intermediate Report, Working Period 2009 – 2010,
Contract No 350 150 65 with ONDRAF/NIRAS (B), September 2010.

Patent

GEIST, A., MÜLLICH, U., KARPOV, A., ZEVACO, T., MÜLLER, T.
Alkylierte Bis-Pyrazolylpyridine zur selektiven Extraktion von Actiniden(III).
DE 10 2009 003 783 A1 2010.10.21

Presentations

Invited oral presentations

ALTMAIER, M.
Actinide chemistry in aqueous systems at high ionic strength.
240th American Chemical Society National Meeting,
Boston, Massachusetts, USA, August 22 – 26, 2010.

ALTMAIER, M., BUBE, C., BRENDLER, V., MARQUARDT, CH., MOOG, H., NECK, V., RICHTER, A., SCHARGE, T., VOIGT, W., WILHELM, S., WOLLMANN, G.
THEREDA: Thermodynamic Data for Waste Management Assessment – Focus on Actinide Data.
International Workshop on Actinide and Brine Chemistry in a Salt-Based Repository (ABC-SALT), Carlsbad, New Mexico, September 15-17, 2010.

ALTMAIER, M., NECK, V.
Actinide Chemistry under High Salinity Conditions,
International Memorial Workshop in honor of Volker Neck, “Aquatic Chemistry and Thermodynamics of Actinides and long-lived fission products”, KIT Karlsruhe, Germany, May 20th, 2010

ALTMAIER, M., NECK, V., BRENDEBACH, B., FANGHÄNEL, TH.
Actinide Carbonate Complexation and Solid Phase Stability in reducing MgCl2 Brine Systems
International Workshop on „Actinide and Brine Chemistry in a Salt-Based Repository”
Carlsbad, New Mexico, USA, September 15-17, 2010.

DENECKE, M.A.,
Application of X-ray spectroscopy methods at ANKA to issues concerning nuclear waste disposal,
Workshop Nuclear Analytical Techniques and Applications (NAMA2010), Bukarest, RO, 3.-4. Nov. 2010

DENECKE, M.A.
Synchrotron-based X-ray spectroscopy on actinides
DAE-BRNS Workshop “EXAFS Studies on Actinides”, Raja Ramanna Centre for Advanced Technology, Indore, India, 8.-9. March 2010

DENECKE, M.A.
Facilities at synchrotron laboratories in Europe dedicated to work on radioactive samples
DAE-BRNS Workshop “EXAFS Studies on Actinides”, Raja Ramanna Centre for Advanced Technology, Indore, India, 8.-9. March 2010

FANGHÄNEL, TH., NECK, V., ALTMAIER, M.
Aqueous chemistry and thermodynamics of plutonium
240th American Chemical Society National Meeting,
Boston, Massachusetts, USA, August 22 – 26, 2010

FELLHAUER, D., KIRSCH, R., ALTMAIER, M., NECK, V., SCHEINOST, A. C., WISS, T., CHARLET, L., FANGHÄNEL, TH.
Plutonium Redox Processes in Aqueous Systems
International Workshop on „Actinide and Brine Chemistry in a Salt-Based Repository"
Carlsbad, New Mexico, USA, September 15-17, 2010.

BRENDLER,V., NECK, V., ALTMAIER, M., MARQUARDT, C., MOOG, H.C., RICHTER,A., SCHARGE, T., VOIGT, W., WILHELM, S., WOLLMANN, G.
THEREDA: Providing Quality Assured Thermodynamic Data for Waste Management Assessment.
International Memorial Workshop in honor of Volker Neck, "Aquatic Chemistry and Thermodynamics of Actinides and long-lived fission products", KIT Karlsruhe, Germany, May 20th, 2010

BRENDLER, V., ALTMAIER, M., MARQUARDT, Ch., MOOG, H., RICHTER, A., SCHARGE, T., VOIGT, W., WILHELM, S., WOLLMANN, G.
THEREDA: Providing quality-assured thermodynamic data for waste management assessment.
International Memorial Workshop "Aquatic Chemistry and Thermodynamics of Actinides and long-lived fission products"in honor of Dr. Volker Neck, 20th May 2010, Karlsruhe, Germany.

FANGHÄNEL, TH., NECK, V., ALTMAIER, M.
Aqueous Plutonium Chemistry.
International Memorial Workshop in honor of Volker Neck, "Aquatic Chemistry and Thermodynamics of Actinides and long-lived fission products", KIT Karlsruhe, Germany, May 20th, 2010

FLÖRSHEIMER, M.
Sum Frequency Spectroscopic Observation of Aluminol and Water Species,
Technical University of Munich, Physics Department I, Garching, March 4, 2010

GECKEIS H.
The back end of the nuclear fuel cycle: Chemical aspects of nuclear waste disposal,
2nd International Conference on Asian Nuclear Prospects 2010, 11.-13.October, Chennai, India

GECKEIS, H., GEIST, A., GOMPPER, K., MÜLLICH, U., PANAK, P., RUFF, C., TRUMM, S.
Partitioning and Transmutation : A Solution to the Nuclear Waste Problem?,
3rd EuCheMS Chemistry Congress, August 29 - September 2, 2010, Nürnberg / Germany

GECKEIS, H.,
Research on geochemical aspects of nuclear waste disposal,
US-German Workshop on Salt Repository Research, Design, and Operation, May 25-28, 2010, Jackson, Mississippi USA

GECKEIS, H., GOMPPER, K.
Nachhaltige Kernenergie – Wege zu einem geschlossenen Kernbrennstoffkreislauf ,
Wiss. Abendvortrag der Deutschen Physikalischen Gesellschaft (DPG), April 28, 2010, Berlin, Magnus Haus

GECKEIS, H.
Actinide solid/solution interface chemistry relevant to nuclear waste disposal,
2010 MRS (Materials Research Society) Spring Meeting, April 5-9, 2010, San Francisco, USA

GECKEIS, H.
Sichere Endlagerung radioaktiver Abfälle – ein Ding der Unmöglichkeit?
AWWK-Vortragsreihe, Kernenergie – vielleicht doch? 29.03.2010, Akademie für Wissenschaftliche Weiterbildung Karlsruhe e.V., Karlsruhe

GAONA, X., ALTMAIER, M., GRIVÉ, M., MONTOYA, V., COLÀS, E., DURO, L.
Chemistry of An(III,IV)/Ln(III) eigencolloids: complexation reactions with inorganic and organic ligands
International Workshop on Actinide and Brine Chemistry in a Salt-Based Repository (ABC-SALT), Carlsbad, New Mexico, September 15-17, 2010.

GAONA, X., DÄHN, R., TITS, J., SCHEINOST, A., WIELAND, E.
Chemistry of Np(IV/V/VI) in cementitious environments: an EXAFS study
ROBL Annual Workshop, Dresden, Germany, December 15, 2010

GEIST, A.
Investigating the An(III)/Ln(III) selectivity of N-donor extracting agents – the BTP case.
239th ACS National Meeting, San Francisco, CA, March 21–25, 2010

GOMPPER, K.
Sicherheitsforschung zur Nuklearen Entsorgung - Kompetenzerhalt und Perspektiven
Kolloquium „Kernenergie hat Zukunft“, 14. - 17. März 2010 in Frankfurt/M.

GOMPPER, K.
Stand der Nuklearen Entsorgung in Deutschland
Familienkreis, Pfarrei St. Paul, Bruchsal, 15. April 2010

GOMPPER, K., GECKEIS, H.
FuE-Arbeiten im INE zur Behandlung hochradioaktiver Abfälle: Partitioning und Verglasung
Kolloquium IKET, KIT, 22. Juni 2010

GOMPPER, K., GECKEIS, H., ROTH, G., WEISENBURGER, S.
Vitrification of High Level Liquid Waste from the WAK Reprocessing Plant
17th Japanese-German Meeting on Nuclear Energy 2010, Hirosaki, Aomori Prefecture, Japan,
October 28-29, 2010

KIENZLER, B.
Retention, retardation and reactive transport of radionuclides.
Nuclear Waste Management : Research Challenges for the Future, Cambridge, GB,
September 28-29, 2010

KALLAY, N., PREOČANIN, T., LÜTZENKIRCHEN, J.
Introduction of surface potential measurements in interpretation of equilibrium at electrical interfacial layer
Geochemistry, Session: The Need for Eclecticism in Modeling Adsorption at Mineral/Water Interfaces,
21.-25. März, 2010, San Francisco, California

KOBAYASHI, T, FELLHAUER, D., GAONA, X, ALTMAIER
Technetium redox and Tc(IV) solubility studies
Seminar Talk, 15. Oct 2010, Loughborough University, England.

LOIDA, A., METZ, V., KIENZLER, B.
Experimental Study of the Corrosion Behavior of Irradiated Spent Fuel in High
pH Solutions – Effect of hydrogen.
Seminar at ONDRAF-NIRAS, Bruxelles, (B) Sept. 6-7, 2010

LÜTZENKIRCHEN, J.
Low isoelectric points of „inert“ surfaces in electrolyte solutions.
University of Zagreb, Kroatien, 16/02/2010.

LÜTZENKIRCHEN, J.
Sapphire c and its relation to hydrophobic surfaces.
Max-Plack-Institut für Metallforschung, Stuttgart, 26/05/2010.

LÜTZENKIRCHEN, J.
Inert surfaces and a potential relation with sapphire c.
Oak Ridge National Laboratories. Oak Ridge, TN, USA. 24/06/2010.

LÜTZENKIRCHEN, J.
pH dependent charging of some exotic surfaces. Chemical Speciation in Solution and at Solid/Solution Interfaces
Symposium in honour of Staffan Sjöberg, Umea, Sweden, 23-24/09/2010.

LÜTZENKIRCHEN, J.
Some experimental results related to the Hofmeister series for aluminium minerals in aqueous solutions.
Hofmeisterfest (organisiert von Pavel Jungwirth), Prague, Czech Republic, 13-14/10/2010.

METZ, V., KIENZLER, B., BOHNERT, E., BUBE, C., SCHLIEKER, M.
Interactions of Am(III) and U(VI) with cement alteration products in brines.
Beer Sheva Workshop on Water-Rock Interactions and Environmental Remediation, Ben-Gurion University of the Negev, Beer Sheva, Israel, 21.-25. Feb. 2010.

METZ, V., LOIDA, A., KIENZLER, B., MÜLLER, N., BOHNERT, E.
Spent fuel corrosion under hydrogen.
International Workshop on “Hydrogen inhibiting UO2 dissolution”
Barcelona, Catalunya, Spain, 2. Nov. 2010.

MOOG, H., HERBERT, H-J., BRENDLER, V., RICHTER, A., ALTMAIER, M., MARQUARDT, Ch., VOIGT, W., WILHELM, S.
THEREDA: The thermodynamic reference database for nuclear waste disposal in Germany
240th American Chemical Society National Meeting, Boston, Massachusetts, USA, August 22 – 26, 2010.

PANAK, P.J., BANIK, N.L., DENECKE, M.A., FANGHÄNEL, T., GEIST, A., SCHIMMELPFENNIG, B., TRUMM, S.
Structural characterization of actinide(III)- and lanthanide(III)-complexes with “partitioning” relevant N-donor ligands,
2010 MRS Spring Meeting, San Francisco, USA, April 5-9, 2010

RABUNG, TH.
Time resolved laser fluorescence spectroscopy (TRLFS): A sensitive technique for metal ion speciation in aqueous, colloidal and solid samples.
SCK-CEN, Belgium, June 25, 2010

SCHÄFER, T.
The CFM (Colloid Formation and Migration) Project at the Grimsel Test Site (GTS, Switzerland): Results from the colloid/ nanoparticle tracer tests and model interpretations.
Lawrence Livermore National Laboratory, CA, USA December 10, 2010.

STUMPF, T.
Incorporation of trivalent actinides and lanthanides into Ca-carbonates: Process understanding on a molecular level
20th General Meeting of the International Mineralogical Association (IMA), Budapest, Hungaria, August 21 – 27, 2010

STUMPF, T.
Virtual Institute “Advanced Solid-Aqueous RadioGeochemistry”: TRLFS
Workshop "From atomistic calculations to thermodynamic modelling", Institute of Geosciences, University of Frankfurt, Germany, March 2nd, 2010

VITOVA T., DENECKE, M.A.
The potential of high-resolution X-ray absorption/emission spectroscopy for advanced studies of nano-materials.Nanodesign: Physics, Chemistry, Computer Modeling
German-Russian Interdisciplinary Workshop, Rostov-on-Don, Russia, December 16-17, 2010.

WALTHER, C.
ESI-MS for nuclear safety assessment: polymerization of plutonium.
Frühjahrstagung DPG, Fachverband Massenspektrometrie,Hannover, 8.-12.März 2010
Verhandlungen der Deutschen Physikalischen Gesellschaft, R.6, B.45(2010) MS 1.2

WALTHER, C.
Formation of Actinide (IV) colloids in saline solutions
Actinide and Brine Chemistry in a Salt Based Repository
Carlsbad, NM 15.-17. Sept. 2010

WALTHER, C.
Speciation of polynuclear An(IV) complexes by electrospray mass-spectrometry
Aqueous Chemistry and Thermodynamics of Actinides and Fission Products:
A tribute to Volker Neck ACS Symposium, Boston, MA 25. Aug. 2010

WALTHER, C.
ESI-MS for nuclear safety assessment: Polymerization of plutonium
DPG Frühjahrstagung Hannover 8.-12. März 2010

WALTHER, C., SCHÄFER, T., GECKEIS, H.
Colloid Size Determination by Laser Induced Breakdown Detection - Applications for Safety Assessment of Nuclear Waste
EAWAG Seminar Dübendorf, CH 12. Jan. 2010

WALTHER, C., SCHÄFER, T., GECKEIS, H.
Colloid Size Determination by Laser Induced Breakdown Detection - Applications for Safety Assessment of Nuclear Waste
International Workshop on Radionuclide Migration, Beijing, VR China 11.-14. Okt. 2010

WALTHER, C., STEPPERT, M., ROTHE, J., GECKEIS, H.
Formation of polynuclear plutonium complexes and their role in Pu redox chemistry
Plutonium Futures
Keystone, CO 19.-23. Sept 2010

Presentations at Conferences and Workshops

ALTMAIER, M., BUBE, C., BRENDLER, V., MARQUARDT, CH., MOOG, H., NECK, V., RICHTER, A., SCHARGE, T., VOIGT, W., WILHELM, S., WOLLLMANN, G.
THEREDA: Thermodynamic Data for Waste Management Assessment.
Plutonium Futures “The Science”, Keystone, Colorado, USA, September 19-23, 2010.

ALTMAIER, M., FELLHAUER, D., NECK, V., LÜTZENKIRCHEN, J., FANGHÄNEL, TH.
Actinide(IV) chemistry in reducing alkaline CaCl2 solutions and the formation of ternary Ca4[An(OH)8]4+ complexes.
2nd Annual Workshop of the Recosy Project Larnaca, Cyprus, March 16-19, 2010.

ALTMAIER, M., NECK, V., BRENDEBACH, B., FANGHÄNEL, TH.
Plutonium Solubility and Solid Phase Stability under Reducing Conditions in $MgCl_2$ Brines
Plutonium Futures – The Science 2010, Keystone, Colorado, USA, September 19-23, 2010.

BACH, D., CHRISTIANSEN, B.C., SCHILD, D., GECKEIS, H.
TEM Investigations of Green Rust (GR_{Na2SO4}) Interacted with Neptunyl (NpO_2^+)
Microscopy & Microanalysis 2010, Portland, Oregon, USA, August 1-5, 2010

BANIK, N. L., GEIST, A., MARQUARDT, C. M., DENECKE, M. A., GECKEIS, H.
Characterization of Pu(III) extracted by Alkylated 2,6-ditriazinylpyridine (BTP)
European Nuclear Conference (ENC) Barcelona, Spain, 30 May - 2 June, 2010.

BANIK, N. L., MARQUARDT, C. M., WALTHER, C., ROTHE, J., DENECKE, M. A., KLENZE, R.
Speciation studies of tetravalent protactinium in aqueous solution
Plutonium Futures—The Science 2010, Keystone, Colorado, USA, Sept. 19-23,

BUBE, C., METZ, V., KIENZLER, B.
Radionuclide behaviour in the near-field of a repository - building conference in simulations by experimental validation.
Jahrestagung Kerntechnik - Annual Meeting on Nuclear Technology. Berlin, 03.-06.05.2010

DARDENNE, K., DENECKE, M.A., ROTHE, J., VITOVA, T., GECKEIS, H.
Actinide Research at the INE-Beamline at ANKA - Status and Perspectives
ANKA User meeting, Karlsruhe 7-8 october 2010

FELLHAUER, D., ALTMAIER, M., NECK, V., RUNKE, J., FANGHÄNEL, TH.
Kinetic aspects of Np(V) redox chemistry
2nd Annual Workshop of the Recosy Project, Larnaca, Cyprus, March 16-19, 2010.

FELLHAUER, D., ALTMAIER, M., NECK, V., RUNKE, J., FANGHÄNEL, TH.
Reduction Kinetics of Np(V) in Non-Complexing Aqueous Systems at pH 5 - 10
Plutonium Futures – The Science 2010,
Keystone, Colorado, USA, September 19-23, 2010.

FELLHAUER, D., NECK, V., ALTMAIER, M., RUNKE, J., FANGHÄNEL, TH.
Np(V) Redox Chemistry
2nd Annual Workshop of the Recosy Project, Larnaca, Cyprus, March 16-19, 2010.

FELLHAUER, D., KIRSCH, R., ALTMAIER, M., NECK, V., SCHEINOST, A. C., WISS, T., CHARLET, L., FANGHÄNEL, TH.
Plutonium Redox Behavior in Aqueous Solutions and on Nanocrystalline Iron Phases
Plutonium Futures – The Science 2010,
Keystone, Colorado, USA, September 19-23, 2010.

FINCK, N., DARDENNE, K., BOSBACH, D.
Selenium retention by iron sulfides.
20th Annual V.M. Goldschmidt Conference, Knoxville (TN, USA), June 13-18, 2010.

FINCK, N., BOSBACH, D.
Selenium binding to iron sulfides
ANDRA meeting, Nantes (France), March 29th – April 1st 2010.

FINCK, N., DARDENNE, K.
Selenide binding to disordered mackinawite: a multi-edge XAS approach
2nd ANKA / KNMF Joint Users Meeting, Akademie-Hotel, Karlsruhe, October 07th – 08th, 2010.

FLEISCH, J., GRÜNEWALD, W., ROTH, G., TOBIE, W., WEISENBURGER. S., WEISHAUPT, M.
Radioactive Start-up of the German VEK Vitrification Plant",
WM2010 Conference, March 7-11, 2010, Phoenix, AZ

GAONA, X., ALTMAIER, M., PETROV, V., FELLHAUER, D., TITS, J., WIELAND, E., DARDENNE, K., FANGHÄNEL, TH.
Aqueous speciation and solubility of Np(V/VI) in hyperalkaline systems.
Plutonium Futures "The Science", Keystone, Colorado, USA, September 19-23, 2010

GAONA, X., ALTMAIER, M., PETROV, V., FELLHAUER, D., TITS, J., WIELAND, E., KALMYKOV, S., FANGHÄNEL, TH.
Aqueous speciation and solubility of Np(V/VI) in hyperalkaline systems: a KIT-INE / PSI-LES / JRC-ITU / MSU joint project.
ReCosy annual workshop, Larnaca, Cyprus, March 16-19, 2010.

GAONA, X., GRIVÉ, M., MONTOYA, V., COLÀS, E., ALTMAIER, M., DURO, L.
Chemistry of An(III,IV)/Ln(III) eigencolloids: complexation reactions with inorganic and organic ligands
Plutonium Futures "The Science", Keystone, Colorado, USA, September 19-23, 2010

GRÜNEWALD, W., ROTH, G., TOBIE, W., WEISENBURGER, S., FLEISCH, J., SCHMITZ, F. J., WEISHAUPT, M.
"Verglasungsanlage VEK - Erfolgreiche Inbetriebnahme und erste Betriebserfahrungen",
Jahrestagung Kerntechnik, Berlin, 03.-06.05.2010

HUBER, F., SCHÄFER, T., SCHILD, D., SMYREK, A., DARDENNE, K., ROTHE, J.
U(VI) sorptive reduction on magnetite nanoparticles
20th Annual V.M. Goldschmidt Conference, Knoxville (TN, USA), June 13-18, 2010.

HUBER, F., ENZMANN, F., WENKA, A., DENTZ, M., SCHÄFER, T.
CFD modeling of fluid flow and solute transport in a µXCT scanned natural fracture:
Impact of fracture geometry on solute transport
AGU FALL MEETING 2010, San Francisco, December 13.-17., 2010

KALLAY, N., PREOČANIN, T., KOVAČEVIĆ, D., ŠUPLJIKA, F., SELMANI, F., LÜTZENKIRCHEN, J.
Surface Potential and Equilibrium at Mineral-Water Interfaces, ,
Frontiers in Geochemistry Seminar Series, PNNL (Pacific Northwest National Laboratory), Richland, WA, USA 17/03/2010

KIENZLER, B., METZ, V., FINCK, N., PLASCHKE, M., RABUNG, TH., ROTHE, J.
Cs and U retention in cement during long-term corrosion tests in salt brines.
European Materials Research Society Spring Meeting, Strasbourg, F, June 7-11, 2010

KIRSCH, R., FELLHAUER, D., ALTMAIER, M., NECK, V., ROSSBERG, A., CHARLET, L., SCHEINOST, A.C.
Redox-reactions of plutonium with iron-(II)-minerals under anoxic conditions: a XANES and EXAFS study
Goldschmidt 2010, Earth, Energy, and the Environment, Knoxville, Tennessee, June 13-18, 2010

KULIK, D.A., LÜTZENKIRCHEN, J., PAYNE, T.
Consistent treatment of 'denticity' in surface complexation models.
20th Annual VM Goldschmidt Conference, Juni, 2010, Knoxville, Tennessee, USA.

LÖBLE, M., VITOVA, T., TRAPP, I., DENECKE, M.A., FERNANDEZ, I., BREHER, F.
Solution Behaviour of f-Element Coordination Compounds
ICCC39, Adelaide, Australia, July 25-30, 2010

LOIDA, A., METZ, V., KIENZLER, B., MÜLLER, N.
Spent Fuel Corrosion Behaviour in Highly Alkaline Solution – Effect of Hydrogen Overpressure
International „Spent Fuel Workshop" Barcelona, Catalunya, Spain, 3-5. Nov. 2010.

LÜTZENKIRCHEN, J., BRENDLER, V., PAYNE,T.
A simple case and a comprehensive data set
NEA Symposium – From Thermodynamics to the Safety Case, Akademie Hotel, Karlsruhe, 17.-19. Mai, 2010, Karlsruhe.

LÜTZENKIRCHEN, J., BRENDLER, V., PAYNE, T.
Choice of the form of experimental data in the fitting procedure and consequences.
NEA Symposium – From Thermodynamics to the Safety Case, Akademie Hotel, Karlsruhe, 17.-19. Mai, 2010, Karlsruhe.

LÜTZENKIRCHEN, J., KALLAY, N., PREOCANIN, T., SELMANI, A.
Protolytic equilibria at 'inert' - electrolyte interfaces
20th Annual VM Goldschmidt Conference, Juni, 2010, Knoxville, Tennessee, USA.

METZ, V., KELM, M., BOHNERT, E., BUBE, C.
Interaction of hydrogen with radiolysis products in NaCl solution – comparing pulse radiolysis experiments with simulations.
International „Spent Fuel Workshop" Barcelona, Catalunya, Spain, 3-5. Nov. 2010.

METZ, V., KIENZLER, B., BUBE, C., BOHNERT, E.
Interactions of americium and uranium with cement alteration products under saline conditions.
Actinide and Brine Chemistry in a Salt-Based Repository
(ABC-Salt : Internat.Workshop, Carlsbad, N.M., USA, September 15-17, 2010

METZ, V., KIENZLER, B., BOHNERT, E., BUBE, C., SCHLIEKER, M.
Interactions of Am(III) and U(VI) with cement alteration products in brines.
Beer Sheva Workshop on Water-Rock Interactions and Environmental Remediation, Beer Sheva, IL, Barcelona - February 21-25, 2010

MODOLO, G., BOSBACH, D., GEIST, A., MALMBECK, R.
Recovery of long-lived minor actinides from high active waste solutions using innovative partitioning processes.
CIMTEC 2010 Conference, Montecatini, Italien, 13.–18. Juni 2010

MODOLO, G., GEIST, A., MALMBECK, R.
Actinide(III) recovery from high active waste solutions using innovative partitioning processes.
238th ACS National Meeting, Washington, DC, August 16–20, 2009

MODOLO, G., GEIST, A., MALMBECK, R.
Separation of Am(III) from Cm(III) and Ln(III) using aromatic dithiophosphinic acid.
239th ACS National Meeting, San Francisco, CA, March 21–25, 2010

PETROV, V.G., KALMYKOV, S.N., ALTMAIER, M.
Solubility and hydrolytic behaviour of Np(V) in alkaline solutions with high salinity.
4th Russian school on Radiochemistry and Nuclear Technology, Ozersk, Chelyabinsk area, Russia, September 6-10, 2010.

PLASCHKE, M., BENDER, K., BÖTTLE, M., HECK, S., HILPP, S., KAUFMANN, A., KISELY, T., LAGOS, M., GÖRTZEN, A., GECKEIS, H. GEYER, F.W., GOMPPER, K., SEITHER, A., WALSCHBURGER, C.
Prozessbegleitende Analytik zum Nuklearen Betrieb der Verglasungseinrichtung Karlsruhe (VEK),
6. Workshop RCA & 23. SAAGAS Seminar, Dresden-Rossendorf, Germany, 6.-8.9.2010

POLLY, R., SCHIMMELPFENNIG, B., FLÖRSHEIMER, M., KLENZE, R., GECKEIS, H.
Theoretical investigation of the solvated corundum surface
Goldschmidt Conference 2010, Knoxville, Tennessee, June 13-18,

POLLY, R, SCHIMMELPFENNIG, B.
Theoretical investigation of the solvated corundum surface
Technical University of Munich, Physics Department I, Garching, March 4, 2010

ROSENBERG, Y.O., METZ, V., OREN, Y., VENGOSH, A., VOLKMAN, Y., GANOR, J.
Radium co-precipitation in evaporitic systems.
Third International Conference on Radium and Radon Isotopes as Environmental Tracers, Jerusalem, March 14-19, 2010.

ROTHE, J., DARDENNE, K., VITOVA, T., DENECKE, M. A., GECKEIS, H.
Actinidenforschung an der INE-Beamline – Status und Perspektiven.
SNI 2010, Deutsche Tagung für Forschung mit Synchrotronstrahlung, Neutronen und Ionenstrahlung an Großgeräten, FU Berlin, 24. – 26. Februar 2010

SCHILD, D.,
Surface analysis of air-sensitive and radioactive samples by XPS
PHI European Users Meeting, June 22-23, 2010, Ochsenfurt

STUMPF, T., SCHMIDT, M., WALTHER, C., GECKEIS, H., FANGHÄNEL, T.
Structural incorporation of Eu(III) into calcite, aragonite and vaterite: a comparative TRLFS study
XXIII. Terrae Rarae, Bayreuth, Germany, October 7-9, 2010

TRUMM, S., DENECKE, M.A., PANAK, P.J., FANGHÄNEL, T., GEIST, A.
Structural investigations on actinide(III)-BTBP and lanthanide(III)-BTBP 1:2 complexes in organic solution.
Actinides 2009, San Francisco, CA, July 12–17, 2009

VITOVA, T., DENECKE, M.A., LÖBLE, M., DARDENNE, K., ROTHE, J., GECKEIS, H., KVASHNINA, K.O., VEGELIUS, J., BUTORIN, S.M., NOCTON, G., MAZZANTI, M., SEIBERT, A., CACIUFFO, R., DENNING, R.G.
Advanced X-ray absorption/emission spectroscopic tool for actinide speciation.
Plutonium Futures – The Science 2010, Keystone, Colorado, USA, September 19-23, 2010.

VITOVA, T., DENECKE, M.A., KVASHNINA, K., LÖBLE, M., DARDENNE, K., ROTHE, J., BUTORIN, S.M., SEIBERT, A., CACIUFFO, R., GECKEIS, H.
Actinide speciation with high-resolution X-ray absorption/emission spectroscopy.
ANKA User meeting, Karlsruhe, 7-8 October, 2010.

VITOVA, T., DENECKE, M.A., KVASHNINA, K., LÖBLE, M., DARDENNE, K., ROTHE, J., BUTORIN, S.M., SEIBERT, A., CACIUFFO, R., GECKEIS, H.
Actinide speciation with high-resolution X-ray absorption/emission spectroscopy.
7th International Conference on Inelastic X-ray Scattering, Grenoble, France, October 11-14, 2010.

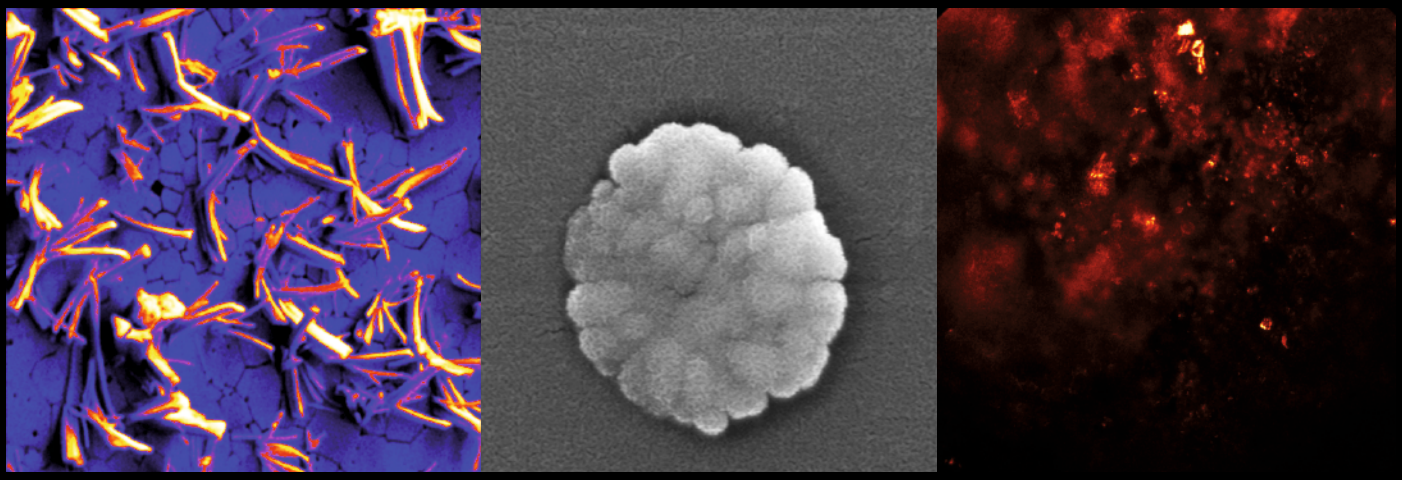

ISSN 1869-9669